RELATING STARCH STRUCTURE IN RICE TO ITS DIGESTIBILITY

Presented by:

Matthew Paul Van Leeuwen

BSc (Science – Chemistry)

Master of Philosophy (Science)

A thesis submitted in fulfilment of the requirement of

Doctor of Philosophy

Principal Supervisor: Dr Marianne Gaborieau[1]

Co-Supervisors: Dr Patrice Castignolles[1], Dr Gerald Muench[2], Dr Rachelle Ward[3], Prof. Elliot Paul Gilbert[4]

[1] Western Sydney University (WSU), School of Science, Australian Centre for Research On Separation Science (ACROSS)

[2] WSU, School of Medicine

[3] NSW Department of Primary Industries

[4] Australian Nuclear Science and Technology Organisation (ANSTO), Australian Centre for Neutron Science

Western Sydney University
2020

Acknowledgements

" The book of love is long and boring
No one can lift the damn thing
It's full of charts and facts and figures
And instructions for dancing"

- Stephen Merritt, "The Book of Love"

An apt description of my thesis and an appropriate theme song to signify the end of a journey. Follow link for dancing instructions here.

Welcome to one of the few times in my life I have attempted to make an emotional tribute. It has been a long, exhausting, frustrating and mentally challenging three years and I can honestly say I would not have finished on my own motivation alone (maybe on stubbornness though). So, there are quite a few people I need to acknowledge in getting me to this point.

First, I would like to acknowledge my supervisors, who all played a major role in guiding and motivating me throughout the failures and successes. To my primary supervisors, Dr Marion Gaborieau and Dr Patrice Castignolles, thank you for your extensive advice, discussions and support throughout my candidature. To Dr Rachelle Ward, thank you for your continued support, even when you always had to tell me the same thing over and over again "why is it so bloody analytical?, you need to focus on the broader industry", and for always going out of your way to check up on me. To Prof. Elliot Gilbert, thank you for your guidance on my research, and especially for your advice on shaping my research approach. To Prof. Gerald Muench, thank you for your support during my candidature. Thank you also to Dr Ric Wuhrer and Dr Laurel George as well as all the staff at Western Sydney University Advanced Materials Characterisation facility for equipment access, technical assistance and for valuable discussion on my research questions.

To my parents, Lee Anne and Leonard, I was certainly hoping to this degree from a better position in life, but when it came down to it you were there to support me and provide me a place to live…again. So really, this acknowledgement is the exact same as the one from my Masters. I cannot thank you enough for the supply of cooked, frozen and reheated food and along with so many other things.

Finally, to everyone else who collectively played the most important role of all. Keeping me sane. To the uni crew, I'd especially like to thank Joel and Kevin, you were both a big part of getting me through to the end. To Joel, thanks for being a great buddy always offering to help with my many problems and always offering valuable advice, you certainly helped me become a more efficient worker. But that efficiency dropped off pretty quickly after you left! Which brings in Kevin "Mustard" Dizon! Thank you Mustard for the plethora, yes plethora! of interesting and exciting

moments that we enjoyed during our confinement in that office, even if we did become the tiniest bit less efficient with our time. To the members of party car, Joel (again), Deandu, Charline, and Lola, thank you for all fun times even if tragically brief, it was definitely something I needed at that point in my life whether you knew it or not. And specifically, to Deandu, good work on becoming the new Kevin! Definitely helped me out a lot of the last 6 months mate. Thank you also to the MCT team crew and all of its rotating roster of members over the last 3 years.

Thank you to all the mates who didn't play a direct role in my thesis but gave me a life outside of it. Andrew, you showed me that 'rice is rice is rice, as is wild rice', truly words to live by. I opted not to use your suggested abstract; I didn't want to plagiarise your work. You also introduced me to a whole new group of mates! Though I think you did that just to get rid of me like you did with Joey. To Joey, my new buddy, I swear I never met you before, but I guess you're pretty good to have around. Regardless, you have been a strong advocate for my participation in the whole "social life" and "take a break" thing, and even came up with a great activity that combined them both, Shrek and Wings! Proud of you. To the boys, Danny, Pauly, Ethan, Julian, thanks for all the chills, the beers and the chicken. To the kind of Wenty leagues people? Neil, Matt Long, Panda, Phil, Julia, Alex and Renae, the midnight hangs were always a very important part of preparing for a productive day, especially when something ridiculous always seemed to happen every time. Finally, to Penny, we had that year, then that other year, now we have this year. I'm glad, that we still talk despite all we've gone through, it certainly helped to pull me out of a funk in the middle there, and I hope we can keep that going.

Statement of Authentication

The work presented in this thesis is, to the best of my knowledge and belief, original except as acknowledged in the text. I hereby declare that I have not submitted this material, either in full or in part, for a degree at this or any other institution.

……..

Matthew Paul Van Leeuwen

2020

Research Output of Thesis

Publications:

1. Characterisation of starch branching and lamellar structure in rice flours, MP Van Leeuwen, MR Toutounji, J Mata, R Ward, EP Gilbert, P Castignolles, M Gaborieau, submitted to Food Chemistry 2020
2. Separation of amylose and amylopectin using capillary electrophoresis, MP Van Leeuwen, JJ Thevarajah, R Ward, P Castignolles, M Gaborieau, in preparation for submission to Analytical and Bioanalytical Chemistry.
3. Starch structure in relation to rice digestibility, MP Van Leeuwen, R Ward, P Castignolles, M Gaborieau, 2019 AgriFutures Rice Extension R&D Update, 2019, p. 46-47
4. Rapid prediction of the glycaemic index of rice through starch structure, MP Van Leeuwen, G Barbosa, R Ward, P Castignolles, M Gaborieau, 2018 AgriFutures Rice Extension R&D Update, 2018, p. 52-53
5. Determination of the distributions of degrees of acetylation of chitosan. JJ Thevarajah, MP Van Leeuwen, H Cottet, P Castignolles, M Gaborieau, International Journal of Biological Macromolecules (IF 3.1, top 20 % in Polymer Science), 2017, **95**, p. 40-48

Oral presentations as presenter:

1. Relating starch structure in rice to its digestibility, **MP Van Leeuwen**, EP Gilbert, R Ward, P Castignolles, M Gaborieau, *AgriFutures Rice R&D Forum*, Yanco, Australia, August 2019
2. Supramolecular structure and Dynamics of starch in rice by SAXS, SEM and NMR relaxometry, **MP Van Leeuwen**, G Barbosa, EP Gilbert, R Wuhrer, P Castignolles, M Gaborieau, *Sydney Surfaces and Soft Stuff Symposium*, Sydney, Australia, May 2019
3. Exploring the supra(molecular) characterisation of starch in rice as a tool to predict digestibility, **MP Van Leeuwen**, G Barbosa, R Ward, P Castignolles, M Gaborieau, *Western Sydney University School of Science and Health research seminar*, March 2019
4. Characterisation of starch branching in rice by capillary electrophoresis, **MP Van Leeuwen**, G Barbosa, R Ward, P Castignolles, M Gaborieau, *9th International symposium on the separation and characterisation of natural and synthetic macromolecules*, Amsterdam, Netherlands January 2019
5. Supramolecular characterisation of starch in rice by NMR, SAXS and NMR, **MP Van Leeuwen**, J Mata, EP Gilbert, R Wuhrer, R Ward, P Castignolles, M Gaborieau, *Neutrons and Food 5*, Sydney, Australia, October 2018
6. Rapid prediction of the glycaemic index of rice through starch structure, **MP Van Leeuwen**, EP Gilbert, R Ward, P Castignolles, M Gaborieau, *AgriFutures Rice R&D Forum*, Yanco, Australia, August 2018
7. Nanostructural characterisation of starch in rice, **MP Van Leeuwen**, EP Gilbert, R Ward, G Muench, P Castignolles, M Gaborieau, *Australian Centre for Neutron Scattering Food Science Project meeting*, Sydney, Australia, October 2017
8. Relating starch structure in rice to its digestibility, **MP Van Leeuwen**, *Western Sydney University School of Science and Health 3-minute thesis*, Sydney, Australia, July 2017
9. Exploring the supra(molecular) characterisation of starch in rice as a tool to predict digestibility, **M Van Leeuwen**, M Toutounji, J Mata, E Gilbert, L Pallas, R Ward, J Coorssen, P Castignolles, M Gaborieau, *Australian Institute of Food Science and Technology (AIFST) Summer School*, Western Sydney University, Hawkesbury campus, NSW, February 2017.

Poster presentations as presenter:

1. Relating starch structure in rice to its digestibility using solid-state NMR spectroscopy, X-ray diffraction, small angle X-ray scattering**, MP Van Leeuwen**, G Barbosa, J Mata, EP Gilbert, R Wuhrer, R Ward, P Castignolles, M Gaborieau, *RACI Polymer Group ECR and postgraduate*

symposium: Synthesis and Application of Functional Polymers and Polymer Architecture, Sydney, July 2019

2. Relating starch structure in rice to its digestibility using solid-state NMR spectroscopy, X-ray diffraction and small angle X-ray scattering, **MP Van Leeuwen**, G Barbosa, J Mata, EP Gilbert, R Wuhrer, R Ward, P Castignolles, Marianne Gaborieau, *Royal Society of Chemistry Twitter Conference*, March 2019
3. Relating starch structure in rice to its digestibility using solid-state NMR spectroscopy, X-ray diffraction, small angle X-ray scattering, **MP Van Leeuwen**, G Barbosa, J Mata, EP Gilbert, R Wuhrer, R Ward, P Castignolles, M Gaborieau, *9th International symposium on the separation and characterisation of natural and synthetic macromolecules*, Amsterdam, Netherlands January 2019
4. Can microstructures and molecular dynamics help predict digestibility?, **MP Van Leeuwen**, G Barbosa, R Ward, EP Gilbert, J Mata, P Castignolles, M Gaborieau, *Sydney Surfaces and Soft Stuff Symposium*, Sydney, Australia, June 2018
5. Supramolecular characterization of starch in rice by NMR, SAXS and XRD, **M Van Leeuwen**, J Mata, E Gilbert, R Ward, P Castignolles, M Gaborieau, *Gordon Research Conference – Structure and Dynamics of Materials on Many Length and Time Scales*, Clear Water Bay, Hong Kong, August 2017.
6. Supramolecular characterization of starch in rice by NMR, SAXS and XRD, **M Van Leeuwen**, J Mata, E Gilbert, R Ward, P Castignolles, M Gaborieau, *Gordon Research Seminar – Neutron Scattering as a Cutting Edge Probe of Structure and Dynamics of Advanced Materials*, Clear Water Bay, Hong Kong, August 2017.
7. (Supra)molecular characterisation of starch in rice by NMR and SAXS, M Toutounji, **MP Van Leeuwen**, J Mata, EP Gilbert, L Pallas, R Ward, P Castignolles, M Gaborieau, *Sydney Surfaces and Soft Stuff Symposium*, Sydney, Australia, June 2017

Oral presentations presented by others:

1. Relation between polysaccharides structure and their properties, **P Castignolles**, M Van Leeuwen, S Delgado, O Fort, J Lee, D Water, C Blanchard, I Alric, V Durrieu, R Wuhrer, J Oliver, M Gaborieau, *16th Pacific Polymer Conference*, Singapore, December 2019
2. From food through adhesives to water purification: molecular insights into (industrial) polymers from solid-state NMR spectroscopy, **M Gaborieau**, M Van Leeuwen, K Bhullar, R Pedatte, K Dizon, G Johnston-Hall, R Wuhrer, P Castignolles, *12th Australian and New Zealand Society for Magnetic Resonance Conference*, Bunker Bay, Australia, November 2019
3. Polymers in foods: Insights into molecular structure, dynamics, digestibility with capillary electrophoresis, solid-state NMR, **M Gaborieau**, J Lee, D Waters, C Blanchard, M Van Leeuwen, R Ward, P Castignolles, *37th Australasian Polymer Symposium*, Sunshine Coast, Australia, November 2019
4. Free solution capillary electrophoresis to characterize proteins, drug carriers or rice, and to monitor drug loading and digestion, **P Castignolles**, J Oliver, A Maniego, N Delaunay , F Violleau, K Williams, M Van Leeuwen, R Ward, S Harrisson, M Destarac, V Durrieu, I Alric, M Du Plessis, A Grosas, J Carver, A Sutton, D Arrua, E Hilder, M Gaborieau, *26th International symposium on electro- and liquid phase separation techniques*, Toulouse, France, September 2019
5. NMR of Polymers: the Branched, the Non-Dissolved, and the Grafted, **M Gaborieau**, A Maniego, A Sutton, K Dizon, K Bhullar, M Van Leeuwen, P Castignolles, *9th International symposium on the separation and characterisation of natural and synthetic macromolecules*, Amsterdam, Netherlands January 2019
6. Germany-Australia: a solid (-state) NMR connection, **M Gaborieau**, K Dizon, M Van Leeuwen, K Bhullar, P Castignolles, R Wuhrer, R Ward, R Graf, HW Spiess, *World Polymer Congress*, Cairns, Australia, July 2018
7. Polymer characterisation beyond molar mass distributions: distributions of compositions, branching and distributions of electrophoretic mobilities. P Castignolles, A Maniego, M van

Leeuwen, C Lefay, Y Guillaneuf, C Fellows, R Ward, S Harrisson, M Destarac, J Oliver, M Gaborieau, *2018 IUPAC Word Polymer Congress (MACRO2018)*, Cairns (Australia), July 2018

8. Insights into the heterogeneity of polysaccharides with solid-state NMR spectroscopy. JJ Thevarajah, MP van Leeuwen, M Heuls, A Rouilly, R Ward, EP Gilbert, R Graf, P Castignolles, M Gaborieau, *255th American Chemical Society (ACS) National Meeting "Nexus of Food, Energy, and Water"*, New Orleans (USA), March 2018
9. Toward predicting starch food digestibility: characterisation of starch by capillary electrophoresis, NMR spectroscopy and more!, M Van Leeuwen, G Barbosa, R Ward, R Wuhrer, M Gaborieau, **P Castignolles**, *68th Australian Grain Science Conference*, Wagga Wagga, Australia, September 2017
10. Relating the (supra)molecular structure of starch in rice to its digestibility. M Van Leeuwen, J Mata, E Gilbert, R Ward, P Castignolles, M Gaborieau, *Australian Rice Quality Symposium*, Wagga Wagga (Australia), July 2017
11. Starch: molecular dynamics by solid-state NMR, M Van Leeuwen, R Ward, M Gidley, R Graf, HW Spiess, P Castignolles, **M Gaborieau**, 3rd *GDR Symbiose Seminar*, Paris, France, May 2017

Posters presented by others:

1. Relating starch structure in rice to digestibility, MP Van Leeuwen, EP Gilbert, R Ward, **P Castignolles**, Marianne Gaborieau, *Royal Society of Chemistry Twitter Conference*, March 2020
2. Relating starch structure in rice to digestibility, MP Van Leeuwen, EP Gilbert, **R Ward**, P Castignolles, Marianne Gaborieau, N*SW Department of Primary Industries Rice Field Day*, Yanco, Australia, March 2020
3. Separation and characterisation of starch by capillary electrophoresis, MP Van Leeuwen, JJ Thevarajah, R Ward, M Gaborieau, **P Castignolles,** *26th International symposium on electro- and liquid phase separation techniques*, Toulouse, France, September 2019
4. Towards predicting starchy food digestibility: characterisation of starch by capillary electrophoresis, NMR spectroscopy and more! M van Leeuwen, G Barbosa, R Ward, R Wuhrer, M Gaborieau, P Castignolles, *68th Australasian Grain Science Conference in Australia (AGSA 2018)*, Wagga Wagga (Australia), September 2018.
5. Relating starch structure in rice to digestibility, MP Van Leeuwen, EP Gilbert, **R Ward**, P Castignolles, Marianne Gaborieau, *NSW Department of Primary Industries Rice Field Day*, Yanco, Australia, March 2018

Professional Societies/Groups:

1. Golden Key International Honour Society, 2012 – Present
2. Royal Australian Chemical Institute – Member (2015 - present) and Western Sydney University student representative for NSW Analytical and Environmental chemistry group (2016 - 2018)
3. Molecular Medicine Research Group, Western Sydney University, 2013 - 2019
4. Australian Centre for Research on Separation Science (ACROSS), 2013 - Present

Attended Conferences/Meetings with no presentations:

1. Royal Australia Chemistry Institute Analytical division symposium, Sydney, Australia, April 2018
2. Master class hosted by the Food Structures, Digestion and Health International conference, Sydney, Australia October 2017
3. AgriFutures (Formerly RIRDC) Rice R&D forum, Yanco, Australia, August 2017

Awards/Competitive Grants:

1. 2018: Molecular Science Research Group Graduate student travel grant. AUD 1,000
2. 2018: RACI Polymer Division Student Travel Award. AUD 1,000

3. 2018: Molecular Science Research Group Seed Grant. AUD 7,000
4. 2018: Small-angle X-ray scattering equipment time grant from Australia Nuclear Science and Technology Organisation: Matthew Van Leeuwen, Marianne Gaborieau, Elliot Gilbert, Jitendra Mata. P6398, 6 days, AUD 11,310
5. 2017: Gordon Research Conference on Neutron Scattering Travel Award, USD 935
6. 2017 AINSE Top-up scholarship: AUD 11,250
7. 2017 AgriFutures top-up scholarship, AUD 60,000

Table of Contents

Table of Tables

Table of Figures

Table of Abbreviations

Abbreviation	Meaning
α	Power law exponent
β	Power law prefactor
δ	Chemical Shift
$\Delta \boldsymbol{q}$	SAXS Lamellar peak width
μ	Electrophoretic mobility
μ_m	Moment-average electrophoretic mobility
μ_w	Weight-average electrophoretic mobility
a.u.	Arbitrary Units
A_0	Pre-exponential factor for CPMG signal decay
AAC	Apparent amylose content
AACCI	American Association of Cereal Chemistry International
ACNS	Australian Centre for Neutron Scattering
ADPG	ADP-glucose pyrophosphorylase
AINSE	Australian Institute for Nuclear Science and Engineering
AMCF	Advanced Materials Characterisation Facility
ANSTO	Australian Nuclear Science and Technology Organisation
AsFlFFF	Asymmetric flow field flow fractionation
AUD	Australian Dollar
BE	Starch branching enzyme
*C**	Critical polymer concentration
CE	Free solution capillary electrophoresis
CE-CC	Free solution capillary electrophoresis in the critical conditions
CP/MAS NMR	Cross polarization / magic angle spinning nuclear magnetic resonance
CPMG	Car-Purcell-Meiboom-Gill sequence
D(*1,0*)	Dispersity calculated as the ratio of first and zeroth order moments divided by the ratio of zeroth and negative first order moments
D(*2,0*)	Dispersity calculated as the ratio of the second and first order moments divided by the ratio of first and zeroth order moments
D(*3,0*)	Dispersity calculated as the ratio of third and second order moments divided by the ratio of second and first order moments
D1	NMR recycle delay time
DAD	Diode Array Detector
DB	Degree of branching

DBE	Starch debranching enzyme
DMSO	Dimethyl sulfoxide
DMSO-d_6	Deuterated dimethyl sulfoxide
DNA	Deoxyribonucleic acid
DP	Degree of polymerisation
DPI	Department of Primary Industries
EOF	Electroosmotic flow
FFF	Field flow fractionation
FID	Free Induction Decay
FlFFF	Flow field flow fractionation
FTIR	Fourier transform infrared spectroscopy
FWHM	Full width at half maximum
GBSSI	Granule bound starch synthase
GI	Glycaemic index
GL	Glycaemic load
GPC	Gel permeation chromatography
HPLC	High performance liquid chromatography
HWHM	Half width at half maximum
HWI	Hot-water insoluble
HWS	Hot-water soluble
I.D.	Inner Diameter
IA-CE	Iodine affinity capillary electrophoresis
IL	Illinois
I_{max}	SAXS Lamellar peak intensity
IRRI	International Rice Research Institute
$I_{\alpha\ reducing}$	Integral of a reducing end signal
$I_{\alpha(1,4)}$	Integral of a(1,4) signal
$I_{\alpha(1,6)}$	Integral of a(1,6) signal
$I_{\beta\ reducing}$	Integral of b reducing end signal
LC-CC	Liquid chromatography in the critical conditions
l_d	Length to detector
LiBr	Lithium Bromide
l_t	Total length
MA	Massachusetts
MALS	Multi-angle light scattering
MAS	Magic angle spinning
MRI	Magnetic Resonance Imaging
NaOH	Sodium Hydroxide
NIST	National Institute of Standards and Technology
NMR	Nuclear magnetic resonance
NS	Number of scans
NS_{eff}	Effective scaled number of scans

NSW	New South Wales
O.D.	Outer diameter
$\boldsymbol{p}$	Angular momentum
PAA	Poly(acrylic acid)
PNaA	Poly(sodium acrylate)
ppm	Parts per million
$\boldsymbol{q}$	Scattering vector
$\boldsymbol{q}_{max}$	SAXS lamellar peak position
RDS	Rapidly digestible starch
rf	Radiofrequency
RH	Relative humidity
RI	Refractive index
rpm	Revolutions per minute
RS	Resistant starch
RSD	Relative standard deviation
SANS	Small angle neutron scattering
SAXS	Small angle X-ray scattering
SDev	Dispersity calculated as the standard deviation taking the weight average mobility as a reference
SDS	Slowly digestible starch
SEC	Size exclusion chromatography
SH-60	Percent starch hydrolysed after 60 min
SNR	Signal-to-noise ratio
SPE	Single pulse excitation
SS	Starch synthase
Std Error	Standard Error
Std. Dev.	Standard deviation
T	Temperature
t	Time
T_1	Spin-lattice relaxation time
T_2	Spin-spin relaxation time
T_2^*	Apparent spin-spin relaxation time
t_{eof}	Migration time of EOF
t_m	Migration time
USA	United States of America
UV	Ultraviolet
UV-Vis	Ultraviolet and visible light
V	Voltage
$W(\mu)$	Weight distribution of electrophoretic mobility
wt	Weight
XRD	X-ray diffraction

Abstract

Rice is a globally important crop and a major staple for over two-thirds of the world's population. Australian grown rice is renowned for its high and consistent quality and is the preferred choice in the domestic and many international rice markets. A long-established focus on quality in the Australian rice breeding program has led to a range of new varieties for different cuisines, for example sushi, long grain, medium grain and fragrant rice types. Development of new varieties takes up to 10 years from parental cross to a pure seed line that boasts sound agronomic, pest and disease resistance and the desired combination of quality traits. Selection techniques vary for each generation, and for each trait. This is a huge undertaking with upwards of 6500 breeding lines assessed for physical quality each year, and more than 3000 samples assessed for cooking qualities. As new consumer trends emerge, new market opportunities for rice are uncovered such as the recent shift toward more health-conscious consumer decisions. Development of more varieties with lower glycaemic index is one avenue to explore further. For this, additional, more well-understood tools are required to measure, predict and/or actively select for this trait at different stages of the breeding and quality program.

Apparent amylose content is currently the only published link available with which researchers can predict the digestibility characteristics of a given rice sample. While the correlation between these attributes is good ($r^2 = 0.73$), it is also indicative that there are other drivers at play. This is highlighted in instances where glycaemic index can vary by up to 20 points at a given apparent amylose content. There is a gap in the understanding of which levels of starch structure, if any, can account for the differences observed in digestibility where apparent amylose content is similar. To explore this, multiple levels of starch structure were assessed in different rice varieties using a combination of novel and well-established characterisation methods.

The starch structure was explored at 4 of the 6 levels of organisation at both the molecular and supramolecular levels. At the molecular level, the average degree of branching was determined using solution-state NMR spectroscopy, providing an accurate assessment of the overall frequency of starch branching within the rice samples. The average degree of branching was found to be proportional with apparent amylose content, a result of the bimodal branching distribution in starch, and was not intrinsically capable of individual assessments of the distributions of degrees of branching of amylose and amylopectin. As a result, it was determined that the average degree of branching did not provide significant additional value in comparison to the already well-established measurement of AAC.

The dynamics of the molecular structure was further characterised through the determination of T_2 relaxation times by solid-state NMR spectroscopy. A relationship between the T_2 relaxation

times of starch CH_x protons and the *in vitro* digestibility was observed with a correlation of r^2 = 0.93. The strength of this correlation was similar to what was found for apparent amylose content; however, the T_2 values were found to be attributed to structures independent of amylose chains. The determination of T_2 relaxation times was therefore determined to be a novel tool with which to predict digestibility characteristics in rice.

Finally, the branching structures of starch were characterised using iodine-affinity capillary electrophoresis. The methodology was adapted from literature and extensively modified to develop an optimised methodology for the accurate and precise characterisation of branching structures in starch. With this optimised methodology the bimodal distributions of electrophoretic mobilities of starch in rice were observed, and attributed to amylose and amylopectin but also a third mode in some cases. This hybrid third mode was found to behave more like amylopectin, while still retaining characteristics of amylose. Different rice varieties were found to exhibit different distributions related to branching through the differences in their electrophoretic mobility as well as in the heterogeneity of their branching. These outcomes highlighted the potential to broaden thinking around diversity of amylose and amylopectin structures and invites a revision of relationships between AAC and functional characteristics such as digestibility.

Preliminary work on the supramolecular structures in starch, including helix content, long range crystallinity and semi-crystalline lamellar structure was also performed to assess their impact on the digestibility characteristics of rice. No single level of supramolecular was found to be a sole driver for the digestibility characteristics, and it is rather a combination of factors at the supramolecular level that must be considered.

The determination of factors of starch structure relevant to digestibility in this study was intended to better understand the drivers of digestibility in rice grains. And through this, attempt to provide new tools with which to assess samples likely to exhibit a higher or lower digestibility, thus allowing for better selectivity in breeding where certain digestibility characteristics are a grain quality goal. This was achieved through the characterisation of multiple features of starch structure which were found to provide valuable input to refining the understanding of rice digestibility.

Declarations

I acknowledge the support I have received through the following:

- The provision of an Australian Government Research Training Program Scholarship
- The provision of an AgriFutures funded postgraduate scholarship top-up and research funding
- The provision of an AINSE funded postgraduate scholarship top-up
- The provision of breeding program rice samples by NSW DPI
- The provision of commercial rice samples by SunRice

Chapter 1 Background

1.1 The value of rice in our diet

1.1.1 A brief background of rice and rice breeding

A major staple for two-thirds of the world, rice is an important crop in the nutrition intake of the global population [1]. Milled rice grains are comprised primarily of starch along with water, proteins and lipids [1]. Rice belongs to the genus *Oryza*, containing 22 to 25 recognised species of which only *Oryza sativa* (Asian Rice) and *Oryza glaberrima* (African Rice) are cultivated [2]. *Oryza sativa* is grown worldwide, in contrast to *Oryza glaberrima* which is grown only in West Africa. The most common species consumed is *Oryza sativa*, comprised of 3 subspecies: *indica*, *japonica* and *javanica*. These subspecies evolved as a result of selective breeding for desired quality traits and adaptation to different ecological systems. There are hundreds of thousands of rice varieties worldwide, though only a very small proportion of these are widely cultivated [1].

In Australia almost all rice grown is classified as *japonica*, suited to subtropical and temperate climates. *Japonica* is also found in America, Egypt, Japan and China [3]. Many commercial rice varieties are the result of rice breeding and varietal diversity to maximise production from limited resources, be pest and disease resistant and to ensure the grain quality meet domestic and internal market preferences [4]. Selections for rice quality include combinations of chalkiness, colour, gelatinisation temperature, apparent amylose content (AAC) and many other traits [4]. Australian rice is renowned for its high and consistent quality and success in international markets [5]. This stems from the development and breeding efforts by Australian rice researchers, culminating in varieties such as *Opus* for Japanese markets, *Reiziq* for premium Middle East markets, as well as the low glycaemic index (GI) *Doongara* varieties, marketed as CleverRice™. This highlights the success of the Australian rice industry in creating a diverse portfolio of high quality and desirable rice products.

Development of new rice varieties is complex and time consuming, with rice breeders evaluating thousands of potential candidates every year, and a new variety taking 7 to 10 years to develop [6, 7]. There are many stages in the breeding and quality programs, each with their own analysis requirements and goals which are briefly summarised in Figure 1-1. Stability in local growing areas is also assessed, an important factor in assuring consistent quality. Thus, a suite of tools is necessary to inform selection of desired trait combinations. Evaluation in the F5-6 stage serves to confirm the marker assisted selection of earlier generations, with number of evaluated samples typically measuring in the thousands. It is only at this stage that enough sample is

available to conduct quality evaluation on additional quality traits. To build greater capacity and streamline the selection process, the scope of the Quality Evaluation Program is routinely reviewed.

Here, the focus is on further identifying the starch structure characteristics that play a role in the functional properties of a rice grain. A shift to a comprehensive characterisation of starch is even more desirable now that capacity for marker assisted selection is even more affordable and accessible. Similarly, a refined explanation of consumer observed traits such as texture and satiety may be afforded by the reconciliation of the contributions of protein [8] and lipids with a complete description of the starch structure. There are a broad range of abiotic and biotic stresses that can also influence grain quality, such as water management and growing temperatures [9-12], highlighting the complexity of rice breeding, agronomic practices with the variety of evaluation stages, and specific design goals paramount in creating novel varieties.

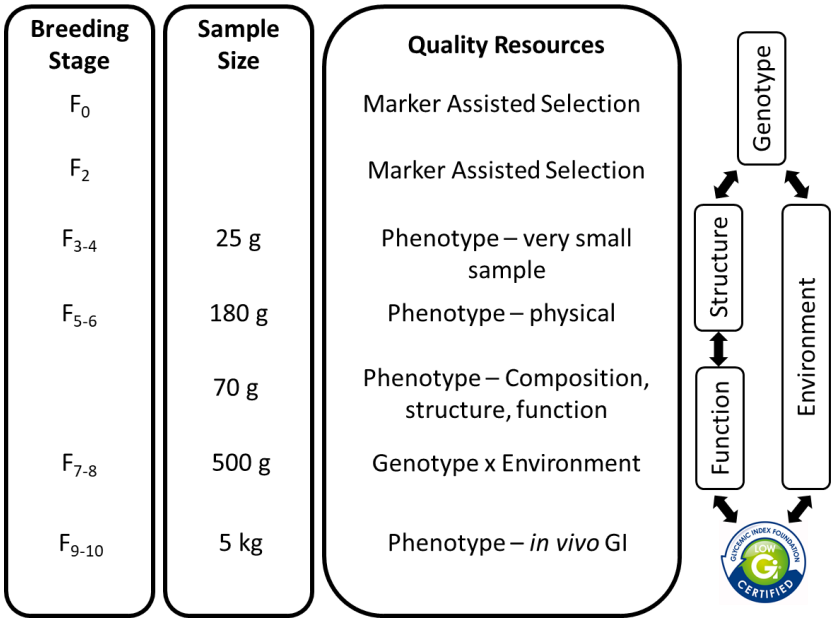

Figure 1-1 Generalisation of the rice breeding process (modified from [6])

1.1.2 The rice grain and its glycaemic properties

Grain based foods are a major component of the modern human diet and have been a dietary staple for thousands of years. Over the last 3 decades, shifts in consumer trends and the evolution of the food industry has resulted in increased levels of food processing in creating new grain-based products. This can range from low levels of processing seen in steam rolled oats, all the way to products such as breakfast cereals that can contain modified starches and added sugars. This shift has contributed to a greater availability of grain-based products, though primarily in the form of refined products [13]. While direct effects on population health cannot be confidently assigned, this shift in industrial practices has coincided with increased prevalence of malnutrition and

chronic health conditions linked to excess weight [14-16]. Carbohydrates and their influence on weight gain [17, 18], and insulin resistance [19, 20] has been widely studied and their impact on key health factors such as cardiovascular and digestive health has led consumers to take more notice of the amount and type of carbohydrate.

Milled rice is comprised primarily of starch (up to 91 % dry weight) [21] with lipids (1- 3 %) [22] and proteins (4-18 %) [8, 21] constituting the majority of the remaining dry mass. Despite the significant compositional contribution of starch, all of these components can impact the functional properties of milled rice grains [23-25].

Native starch, unmodified and measured directly in rice flour, plays an important role in grain quality [2]. AAC measured by iodine binding methods has routinely been linked with many grain quality traits such as digestibility and texture [26, 27]. This link between AAC and digestibility is currently the only such published link available with which researchers can predict the digestibility characteristics of a given rice sample. With an r^2 of 0.73, the linear correlation indicates some relationship of relative digestibility with *AAC* (Figure 1-2). However, it is interesting to note that differences of up to 20 in predicted GI could be observed in samples with similar *AAC*, highlighting that there are likely many other drivers in the digestibility of rice grains. Direct evaluation of other structural parameters of starch in rice to explain quality traits, such as digestibility, of milled rice grains has been limited. The digestion and intestinal absorption of starch from rice is near complete, and is higher than that of other cereals such as wheat flour and tubers [28], further pointing to additional factors intrinsic to the food itself facilitating the rate of digestion. And while AAC has been correlated with digestibility [26], factors such as cooking method [29-31] and preparative procedures [32, 33] have also been shown to have a significant influence on digestion.

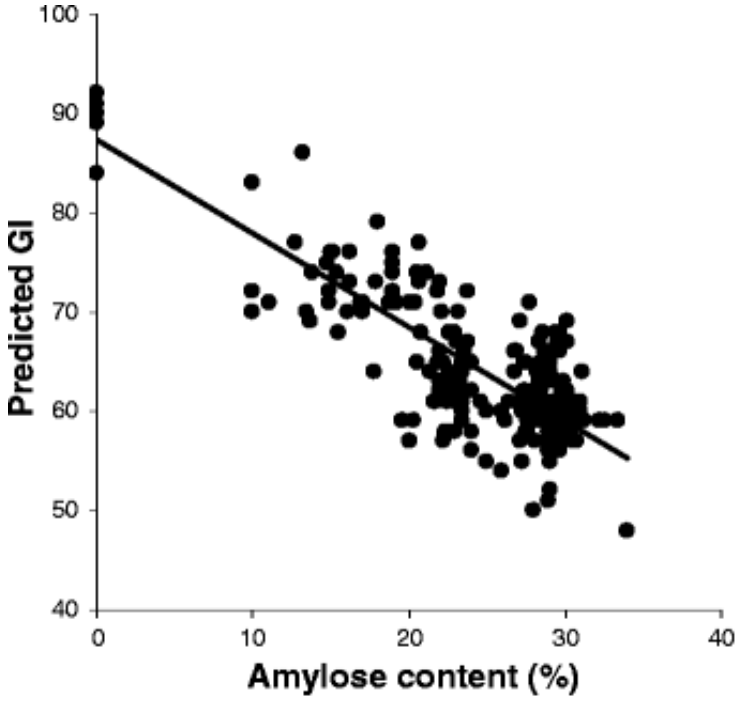

Figure 1-2 The relationship of predicted GI values against AAC for a number of rices (circles) and linear fit (r2 = 0.73) from Fitzgerald et al. [26]

The properties that consumers identify with are the driving force behind purchasing, and therefore a level of quality and consistency is expected [4]. This consistency is also an important factor in the context of labelling requirements. Rice varieties vary greatly in grain quality according to genetic background [24], growing conditions [34, 35], and processing [25, 36, 37]. As a result, routine quality analysis is an important component in the rice breeding process, maintaining consumer expectations while offering a broader range of products. A wide range of information is already integrated into the development process shown in Figure 1-1, though there are opportunities to identify additional markers that could assist in decision making during breeding. A more comprehensive characterisation of starch structure has potential in improving predictions of digestibility (and other traits), positioning such measures as possible future markers in rice breeding.

1.2 Starch structure and properties

1.2.1 (Supra)molecular structure of starch

Starch structure can be described as a multi-level hierarchical organisation (Figure 1-3). These interconnected levels can differ on the basis of botanical origins, genotype and growing conditions [22].

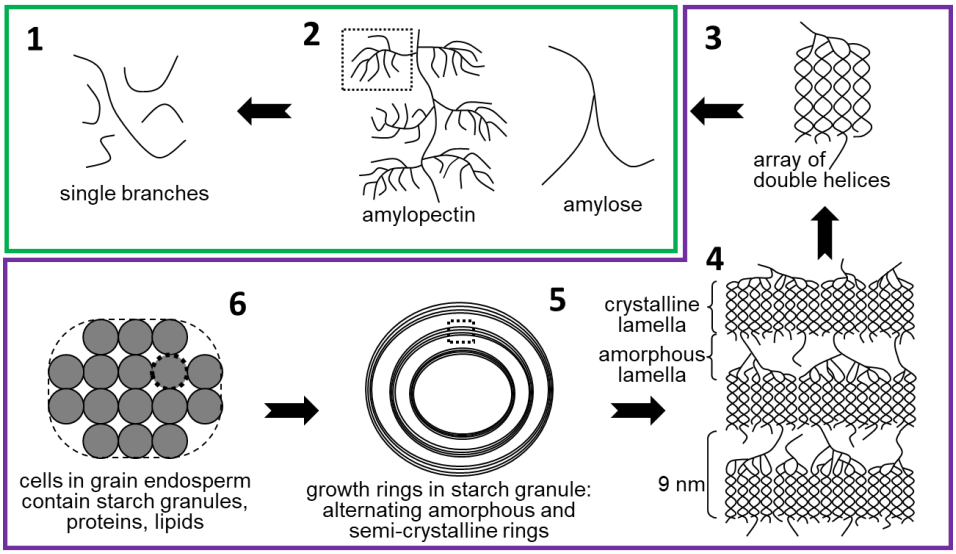

Figure 1-3 Molecular (green) and supramolecular (purple) structural levels of starch. Adapted from Castignolles and Gaborieau [38]

Starch macromolecules consist of glucose monomer units connected by linear α(1, 4) glycosidic bonds with branch points involving α(1, 6) linkages (Figure 1-3, Levels 1-2). Starch is comprised of two macromolecular components, amylopectin and amylose, which primarily differ in their degrees of branching and branch chain lengths. Amylopectin and amylose do not exist as single molecules, but rather as populations of molecules with different branching structures. These two populations of branching structures can be characterised as distributions, a term describing a series of possible values of a given parameter and the frequency of those values. A simple example of a frequency distribution is shown in Figure 1-4, where the y-axis is simply the frequency of the x-axis number (X).

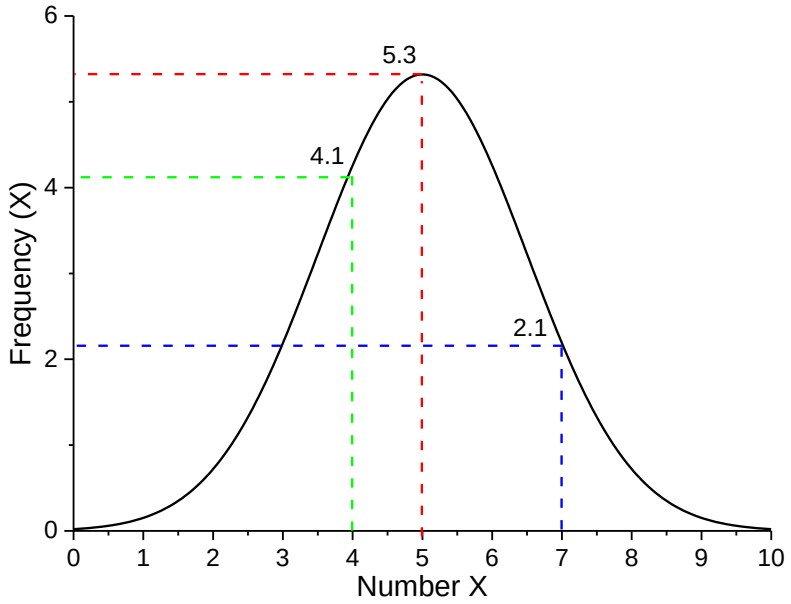

Figure 1-4 Frequency distribution of number values, highlighting frequencies for different values of x by dotted lines for x = 4 (green), x = 5 (red) and x = 7 (blue)

In the case of amylopectin and amylose, distributions of degrees of branching, of branch chain lengths, or of branch points can be defined. Amylopectin molecules account for one of the two populations of molecules in starch, characterised by a high average degree of branching (4 – 5 %) typically in the form of short to intermediate chain length branches (Figure 1-3, Level 2) [22]. Branching in amylopectin occurs not only on the initial chain, but also on the branches themselves, with different classes of branches named A-, B- and C- type chains [22]. A-type refer to outer chains linked by their reducing end to an inner chain, referred to as B-type and defined as a chain bearing other chains as branches. Finally, C-type chains are a single chain per molecule that carries all branches. These highly branched molecules are typically conformationally found in tightly packed clusters or double helix arrangement (Figure 1-3, Level 3) and are the building blocks of the crystalline regions with the semi-crystalline structure of starch granules (Figure 1-3, Levels 4-5) [22]. Amylose molecules represent the second of the two populations of molecules in starch, characterised as linear or slightly branched molecules, and usually in the form of long chain branching (Figure 1-3, Level 2). Given the low degree of branching, amylose is often associated with amorphous phases of starch structure; however, it is also capable of forming single helix structures in the presence of lipids or other suitable inclusions.

Due to the multiple levels of structural order present in starch, it is often referred to in terms of short- and long-range order. Short range order refers to the formation of helices by amylose and amylopectin both as individual molecules as well as with inclusions such as lipids (Figure 1-3, Level 3). Long-range order refers to the formation of larger scale crystalline lamellae in the semi-crystalline lamellar structure of starch, primarily arising from arrangements of double helices of amylopectin molecules. These crystalline structures are further defined depending on their specific packing arrangements, named A-type (primarily observed in cereal starches) and B-type (observed in tubers and high amylose starches) crystalline polymorphs. A- and B-type crystalline polymorphs differ in their packing arrangements of double helices within the starch granule (Figure 1-3, Level 4). A-type polymorphs consist of double helices packed with space group B2 in a monoclinic unit cell, and B-type polymorphs consist of double helices packed with space group $P6_1$ in a hexagonal unit cell [22]. A third C-type polymorph (found in legumes) is also observed, defined as a combination of A- and B-type polymorphs.

The packing of these starch crystallites forms the ordered and amorphous regions that make up the repeating semi-crystalline lamellar arrangement in starch [22]. At the highest level of this lamellar structure is a repeating concentric arrangement of semi-crystalline and amorphous lamellae (hundreds of nm). The semi-crystalline lamellae are then described as being composed of repeating ordered and amorphous lamellae units (≈9 nm). It is primarily in the ordered lamellae in which the crystalline polymorphs of starch exist.

1.2.2 The digestive properties of starch: Glycaemic response and satiety

At a basic level, the glycaemic response is the effect of carbohydrate consumption and subsequent digestion on blood sugar levels, influenced by both the rate and extent of digestion. The actions of insulin are also involved in this process, and as such the glycaemic response to different foods can have important physiological implications.

Starch digestion enzymes principally work by cleaving the starch chains into successively smaller chains until glucose monomer units are obtained. This process may be challenged by the molecular structures including branching and size, supported by the relation of AAC with digestibility [26]. Enzyme access to starch may also be a key factor in the digestibility between individual starches [39]. Access could be challenged by properties such as short- and long-range molecular order and the semi-crystalline lamellar structure. These structural characteristics often vary significantly between samples.

In the context of human digestion, starch is categorised into three fractions: rapidly digestible starch (RDS), slowly digestible starch (SDS) and resistant starch (RS) [40]. These fractions exhibit different rates of starch digestion as measured by the postprandial blood glucose level of an individual over time (blood glucose after food consumption) [41]. This postprandial effect on blood glucose is known as the glycaemic response. In the digestion of RDS and SDS, the monomer unit, glucose, is released into the bloodstream and, via insulin, the glucose is then mobilised into the cells for use. RS is generally considered to escape digestion in the small intestine, and is instead fermented later in the colon [42]. The rate of carbohydrate digestion is dependent on a number of factors such as gut mobility, food matrix, the nature of the starch and the quantity of available carbohydrates [43].

Measuring starch digestibility is a point of contention in the scientific community with pros and cons for both *in vivo* and *in vitro* methods [44]. The concept of glycaemic index (GI) was introduced as a way to classify carbohydrate-containing foods according to their postprandial impact on blood glucose levels [45]. The GI is defined as the total glycaemic response 2 hours immediately after intake of a test food (usually 50 g digestible carbohydrates, RDS and SDS) relative to a reference carbohydrate source. This reference carbohydrate is an equal carbohydrate quantity of a high digestibility carbohydrate source such as glucose or white bread. Currently, *in vivo* GI measurements are limited to 10 healthy individuals, likely incurring significant variability simply from individual biological factors of each participant. The initial costs for this small trial set are significant and the cost of scaling to a greater number of participants to assess the true statistical variance arising from an individual's biology (gut mobility, genetic dispositions, etc.) is prohibitive. Glycaemic load (GL) was introduced in 1997 in an attempt to quantify the overall

glycaemic response for a typical portion of food [46, 47] GL is calculated by multiplying the total available carbohydrate in a serving by the GI value.

The complexity of *in vivo* human digestion results in great difficulties in creating precise and accurate *in vitro* methods that can be used as a substitute to human testing. However, the number of repeats and high cost associated with obtaining a statistically relevant dataset by *in vivo* methods makes *in vitro* alternatives a more attractive option for the purpose of larger scale analysis [26, 43]. The control over the digestive process and mechanical factors with *in vitro* methods allows for greater repeatability [48], making them ideal for comparative analysis in investigating digestibility. The comparatively lower cost of *in vitro* methods not only lends to their accessibility but is also a boon to their scalability. Differences between *in vitro* methodologies likely make them incomparable to one another, and similarly, *in vitro* digestion processes do not directly parallel human digestion.

When assessing the role of digestibility in terms of weight management and general health, the benefits of satiety are often discussed due to its psychological relevance to self-managed nutrient intake [49]. The glucostatic theory of satiety states that satiety is regulated by the glycaemic and insulinaemic response from carbohydrates digestion [50], with continued support into recent decades [51, 52]. This theory states that a rise in blood glucose concentration would trigger satiety, while a drop would trigger hunger. In the context of GI, this theory would suggest that the high glycaemic response triggered by a high GI meal, and subsequent hypoglycaemic period will trigger hunger sooner than a low GI meal. In the long term, overeating can be detrimental to health, increasing the risk of developing type 2 diabetes, cardiovascular disease and hyperglycaemia in people living with type 1 diabetes [53]. A slower glucose release (SDS) increases satiety by reducing spikes in blood glucose and insulin levels [54]. This slower glucose release has also been associated with more stable blood glucose levels (lacking large spikes or drops), potentially beneficial in weight management through satiety management [55] and, in animals, shown to play a role in the prevention of type 2 diabetes [56, 57]. Consumption of foods with higher proportions of SDS is recommended across the entire population with studies showing counter-regulatory hormones and free fatty acids indicative of insulin resistance were reduced [58, 59]. It has been suggested that RS has a strong impact on satiety by adding bulk to the diet, producing viscosity and slowing mobility during digestion [60], likely factors in its relationship with GI [60, 61]. Further studies have shown that both short [62] and long-term satiety [63] are increased with the addition of a fibre source to a meal. Thus, the inclusion of a fibre source in a meal is predicted to be beneficial in weight management through better managed satiety, having potential in the reduction of overall energy intake. So, by studying what features of starch structures are responsible for the subsequent fractions of RDS, SDS and RS, a better understanding of the role of starch structure in digestibility may be gained.

1.2.3 Processing and cooking of rice

During manufacture of starchy food products, different types of treatment such as heat, mechanical stress or dehydration can significantly impact the starch structure. In rice products, the primary factors in processing before consumption include initial milling of the rice grains and the cooking method employed.

Most consumer rice varieties available are white polished grains, where the majority of the pericarp layer has been removed, leaving the starchy endosperm and rice germ as the primary components of the grain. In brown rice, this pericarp layer is left partially intact, with only minimal milling to remove the rice husk. Brown rice has been reported to contain higher levels of fibre and in some cases exhibit lower digestibility [64, 65]. However, direct comparisons of digestibility to white rice can be misleading due to different cooking behaviour of brown rice, often requiring longer cooking times [64]. In addition, the fibre and RS present in rice has not been shown to influence the digestibility of rice grains significantly [31]. As a result, the lower suggested digestibility of brown rice could solely arise from a difference in extent of gelatinisation, rather than the retention of the fibrous pericarp layer.

Various studies have reported on the effect of conventional cooking methods, such as boiling and steaming, on the digestibility of rice grains [64]. These studies noted differences in digestibility between different cooking methods; however, also noted differences in extent of gelatinisation between methods accounting for the differences in digestibility [64]. However, when extent of gelatinisation is consistent, difference in digestibility between cooking methods are not observed [29, 66]. Non-conventional processing and cooking methods such as explosion puffing, extrusion and instantization have been shown to increase the digestibility of rice products [64].

Factors arising from varietal differences can also play a major role in the resulting properties of the cooked rice grain, e.g. sticky rice, long/short grain, low GI [21]. The availability of different varieties allows for a catalogue of products that meet different consumer preferences for traits such as texture, appearance, and digestibility. These properties are typically influenced by the starch, proteins and lipids that comprise most of the dry weight of rice grains [67, 68].

1.3 Measuring the multiple levels of structure in starch

1.3.1 Molecular structure

1.3.1.1 Non-separative methods

In starch, it is the relative ratios of amylose and amylopectin and their associated distributions of degree of branching, branch chain lengths, molar mass etc. that define the molecular level of starch structure (Figure 1-3, level 2). The relative ratio of these molecules, referred to as *AAC*, is of great interest for starches due to its effect on properties such as digestibility [26], pasting [69] and texture [70] (1.1.1). *AAC* of starch has traditionally been measured by amperometric, potentiometric and spectrophotometric techniques after binding iodine to starch . The most popular of these approaches, spectrophotometric detection, makes use of the distinct absorption profiles of the two iodine bound amylose and amylopectin molecules to yield an *AAC*, with absorption maxima of 550 and 580 - 620 nm, respectively [71, 72]. The development of a method of analysis approved by AACCI (Cereals and Grains Association, formerly American Association of Cereal Chemists International) has resulted in a strong uptake in a better controlled methodology for this measurement on rice yielding high precision (<5 % RSD), while modification of methodology in each laboratory for local equipment, standards and purposes, results in poor reproducibility [73]. Due to the strong overlap of absorbance bands for iodine bound amylose and amylopectin, errors in quantification can occur, often leading to overestimation. The absorptivity of the amylopectin-iodine relative to the amylose-iodine complex is quite low even at the maximum of absorption of the amylopectin-iodine complex [71]. The determination of *AAC* is based on a linear calibration of known *AAC* samples against absorbance at a given wavelength (usually 620 nm) [74]. As a result, the calibration and measurement of AAC is influenced by the absorbance of both amylopectin- and amylose-iodine complexes, resulting in the introduction of uncontrolled and unaccounted interference from amylopectin-iodine absorbance. It has been suggested that this cohesive interference can be accounted for using multi-wavelength processing as a corrective procedure [75]. This highlights the potential value of separation techniques prior to detection using UV-Vis detectors, overcoming the issues of interference between components.

1.3.1.2 Industry standards of separation analysis of starch

A variety of separation principles and techniques exist, with the most ubiquitous in the analysis of starch and food typically high performance liquid chromatography (HPLC) methods [76], while other novel approaches such as field flow fractionation (FFF) and capillary electrophoresis (CE) also show promise. However, the use of these methods requires complete dissolution of starch samples, which is not always possible, and isolation of starch from the sample matrix which can

inadvertently alter the structure [77]. Dissolution of starch typically requires the use of polar organic solvents [78] as well as the addition of high concentrations of salts to act as hydrogen bond disruptors in ensuring complete dissolution [79]. The use of such solvent systems can be damaging to a number of components of separation instruments, such as mechanical pumps, which can limit the application of ideal dissolution conditions. Where complete dissolution is not possible, solubilisation and/or degradation [77, 80] of starches is often required to obtain a complete dissolution. This is an important factor in protecting the integrity of columns in HPLC methods [81]. The resulting analysis of these modified starches is thus no longer representative of the original sample [82]. Where adequate dissolution is achieved, limitations in terms of the high pressures and dense stationary phases can also pose potential risks of shear scission of large branched chains [83-86] and/or chain deformation [87], as well as likely fouling of the stationary phase. This is typically undesirable; thus, filtration is commonly employed to exclude molecules such as this prior to analysis.

The industry standards in food and starch analysis are HPLC, and in particular size-exclusion chromatography (SEC), which provide established methods to characterise food samples [76]. The most common application of SEC is in the determination of molar mass distributions [88], and in some cases the molar mass distributions of enzymatically debranched starch known as distributions of chain length [89]. HPLC methods can achieve separation of analytes by a number of factors. For example, in SEC separation occurs as a function of hydrodynamic radius of the analyte, which is typically linked to molar mass and branching [90, 91]. Another HPLC method, ion-exchange chromatography, achieves separation as a function of the affinity of ions and polar analytes to an ion exchanger which can be either cationic or anionic. High performance anion-exchange chromatography (HPAEC) has been employed in the analysis of chain length distributions of starch [92].

Choices of mobile phase and stationary phase are also factors that can influence the separation of analytes in any HPLC method, and forms an important component of experimental design. The choice of mobile phase is especially important as solubility of the starch is required, with chemical compatibility of instrumentation becoming a limitation. Post-separation, a variety of detectors are available for analysis of the separated molecules. In the analysis of starch, HPLC or SEC is often coupled with multi-angle light scattering (MALS), refractive index (RI) detectors [82, 93], ultraviolet (UV) detectors [82] or fluorescence detectors [94]. The nature of the stationary phase in HPLC and SEC raises inherent limitations in its application to the analysis of starch, even in cases where adequate dissolution is achieved, and requiring filtration of the analyte. As a result, in the analysis of starch by liquid chromatography, SEC often yields poor resolution between amylose and amylopectin [82, 95-97].

1.3.1.3 Novel separation techniques for the analysis of starch

Alternative separation techniques that do not require a stationary phase like HPLC and SEC include field flow fractionation (FFF) and free-solution capillary electrophoresis (CE), mitigating some of the issues associated with sample preparation and separation. FFF is family of techniques, that operate based on elution like chromatography, but separation of molecules is based on the application of a force field orthogonal to the direction of laminar flow in a narrow channel. A wide variety of applied forces are possible such as electrophoretic, thermal, magnetic and hydrodynamic flow. The most common of these approaches is using a crossflow, referred to as flow FFF (FlFFF). In FlFFF, a semi-permeable membrane is used as a channel and the combination of flow and differences in diffusion coefficients results in separation of analytes. FlFFF has been shown to improve the peak resolution between amylose and amylopectin compared to SEC [98]. Asymmetric flow field-flow fractionation (AsFlFFF) is one approach to FlFFF which has shown great potential in the characterisation of starch [99, 100]. AsFlFFF is attractive as a starch characterisation technique due to its large size range (2 to >800 nm), low shear forces and the fact that filtration is often not required [99]. By employing AsFlFFF with MALS and RI detectors, the molar mass and root-mean-square radius can be measured directly [100]. The determination of weight-average molar mass and molar mass distributions may also become possible. AsFlFFF has the potential to yield different types of sample information to the typical molar mass and chain length distributions obtained by SEC and HPAEC, and thus could serve as a complementary technique in obtaining a complete characterisation of amylose and amylopectin in starch. However, it should be noted that the use of mechanical pumps limits the chemical compatibility. Current research indicates that DMSO is a viable solvent for starch [78]; however, the compatibility of DMSO with membranes used for FFF of starch is limited, while the addition of salts required to increase solubility of starch [79] raises additional compatibility issues. Thus, dissolution may become an issue in analysis of starches, and especially of more complex matrixes such as rice flours by FFF techniques.

Free solution capillary electrophoresis (CE) is a high-resolution separation technique, with separation occurring in free solution, thus the limitations of stationary phases are avoided [82]. Separation of molecules is based on their charge-to-friction ratio and is achieved by injection of the analyte into a fused silica capillary tube filled with a background electrolyte followed by application of an electric field. Analytes are then separated according to their electrophoretic velocity relative to the electroosmotic flow (EOF) of the background electrolyte, yielding an apparent velocity within the capillary (Figure 1-5) [101]. Separation is limited to charged analytes; however, the separation of neutral analytes is still possible by complexation with charged species to induce a net charge, this is referred to as affinity CE.

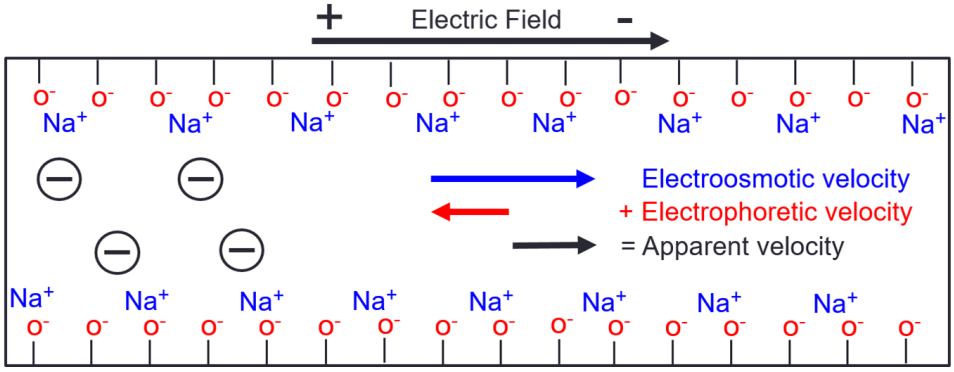

Figure 1-5 Electrophoretic migration of negatively charged analytes and of sodium from the background electrolyte in CE (counter-EOF mode); EOF – Electroosmotic flow (velocity)

CE has been shown to be a viable technique in food analysis, demonstrating the ability to separate sugars extracted from breakfast cereals [102], minerals in zucchini [103], and to separate carbohydrate and sugar components in complex fermentation matrices [104, 105]. With the use of calibration curves, CE can also be used for quantitative analysis of known components [81, 102]. Improved quantitative determination of carbohydrates in CE versus HPLC has been reported in fermentation mixtures, with CE showing a higher recovery of the separated analytes [81]. The robustness of CE is advantageous in the analysis of complex samples such as food products, allowing for direct analysis with minimal sample preparation (no filtration) in contrast to HPLC/SEC which often requires some form of sample pre-treatment that may result in undesirable modifications. Additionally, the background electrolyte employed for separation is not required to match the analyte solvent, contrary to the requirement of matching solvents and mobile phase in HPLC and FFF methods. This opens the door for a variety of solvents to be employed for starch dissolution, which would otherwise not be ideal background electrolytes such as DMSO with LiBr. CE also shows greater simplicity, versatility, lower operating costs than traditional gel electrophoresis and even the possibility of direct sample injection with no sample preparation [103, 106]. The resilience of fused-silica capillaries allows for the use of an extensive variety of buffers, cleaning solutions and samples which can be injected without negatively impacting the system. However, the use of high salt concentrations, such as those required for starch dissolution, can lead to excessive joule heating and affect CE performance. A variety of methods are also available that can improve sensitivity for dilute solutions such as electrophoretic pre-concentration, micelle based pre-concentration, and stacking [107, 108].

The determination of amylose content using capillary electrophoresis has been shown, taking advantage of the iodine binding nature of starch which imparts a net negative charge to the starch molecules necessary for separation. Detection is then achieved by employing simple ultraviolet and visible light (UV-Vis) detectors [109]. Some improvement of the methodology was previously undertaken [110] and then further work performed on method modifications during this work

(Chapter 3). This improved methodology addresses the issues reported in the literature with complete and stable dissolution of starch as well as modifications to the instrument setup to improve resolution and repeatability.

In addition to the determination of amylose content, further characterisation of the amylose and amylopectin can also be achieved. In CE when sufficiently large polyelectrolytes are separated, the separation becomes independent of molar mass. This is referred to as CE in the critical conditions (CE-CC), an analogy to liquid chromatography in the critical conditions (LC-CC) where conditions are sought in which a homopolymer is not separated by molar mass [104]. CE-CC has been demonstrated experimentally in DNA [111], poly(styrene sulfonates) [112], and poly(acrylic acid) [113]. In the separation by branching of poly(acrylic acid), greater branching was shown to yield lower electrophoretic mobility, while a reduction in the injected volume of linear polymer was found to increase resolution [114]. The same trend was noted in the separation of starch in which the less branched amylose had a higher electrophoretic mobility relative to the highly branched amylopectin [109, 110].

Polymers tend to manifest as distributions of molecular attributes such as molar mass, end groups, composition and branching characteristics. Currently, the most commonly assessed molecular attribute of polymers is the heterogeneity of molar mass [115]. This is typically determined by SEC; however, this approach cannot inform on the molecular attributes due to separation by hydrodynamic size [90]. In CE-CC the separation is sensitive to the structural features other than molar mass such as branching, composition and end groups. This yields associated distributions of mobility linked with the underlying separation mechanism from which heterogeneity can be assessed [116].

Several techniques and methods are available in the literature capable of probing the molecular structure of starch (Figure 1-3, Levels 1 and 2). *AAC* is one the most popular direct measures of molecular starch structure, especially in food related research as a result of its relationship with many important properties. In exploring the additional features of molecular starch structure, SEC is the most ubiquitous separation approach, though suffers from an inherent inability to provide a true characterisation of the native structure of amylose and amylopectin without pre-treatment or degradation. Of FFF and CE, CE offers a much simpler experimental design and operation in addition to the capabilities of analysis in structural heterogeneity by CE-CC. The complexity of FFF can make employment difficult; however, the possibility of different types of fields that can be applied also affords a diverse range of molecular features to be assessed. Given low running costs, simple experimental design and robust operation, CE exhibits valuable characteristics for use in routine measurements.

1.3.2 Supramolecular structure

At the supramolecular level of starch structure, the amylose and amylopectin molecules are arranged into increasingly larger forms of ordered structure including the helical, long-range crystalline and the semi-crystalline lamellar structures (Figure 1-3, Levels 3-5).

1.3.2.1 Helical structure and molecular dynamics

The helical structures, seen in the supramolecular structure of starch arises from the arrangement of double helices of amylopectin with an estimated diameter of ~20 nm [117] and forms the underlying unit of order that forms the higher levels of order seen in starch (Figure 1-3, Level 3). Amylose molecules can also form helices; however, these single helix structures require the presence of inclusions such as lipids. As such, these tend to represent a very low proportion of total helix content (<5 %) [118]. Amylopectin and amylose form the basis for the crystalline structures observed in starch, and as such their proportions, distributions and dynamics are important in describing higher level structure as well as explaining starch properties. There are very few techniques available capable of probing the size scale necessary for directly measuring helix content, with solid-state nuclear magnetic resonance (NMR) spectroscopy being one of them. NMR spectroscopy has been used extensively to study various starch systems, investigating attributes such as the starch structure, effects of processing, and the comparison of starches from different botanical origins [118-120].

NMR spectroscopy works on the principle of nuclear spin and resonance. Any nucleus which has a nuclear spin quantum number greater than zero exhibits nuclear magnetic resonance. This magnetic resonance arises from the angular momentum (***p***) of a spinning nucleus and its charge which result in a magnetic moment. In NMR spectroscopy, the nucleus is placed in a large magnetic field that induces different spin states. The nucleus is then irradiated by radiofrequency (rf) pulses that alter the spin state of the nuclei through energy absorption. The relaxation of nuclear spin magnetisation is then detected and recorded in the form of the free induction decay. The most commonly studied NMR active nuclei are ^{1}H, ^{13}C, ^{19}F and ^{31}P, all of which are crucial in the field of organic chemistry. The data obtained from simple NMR experiments can then be employed to identify chemical structures through well documented chemical shifts, allowing for elucidation of molecular structures and investigation of molecular dynamics [121].

A wide range of samples and sample forms can be analysed by NMR, with solution-state and solid-state measurements being most common. Solid-state NMR spectroscopy differentiates itself from solution-state NMR spectroscopy primarily in the resonance signal width, with solid-state signals broadened by dipolar couplings and motion. This broadness can be attributed to homogenous, inhomogeneous or heterogeneous broadening [122]. A homogenous signal is the

sum of signals exhibiting the same broadening, but no change in chemical shift. This type of broadening typically arises as a result of dipole-dipole couplings. An inhomogeneous signal is the sum of signals that are not overlapping with limited broadening. This type of broadening typically arises as a result of heterogeneity in local packing of the molecules within the sample. Heterogeneous broadening is the sum of signals that are coupled but have different chemical shifts. These molecular interactions then dictate how individual atoms behave within the magnetic field, yielding a certain degree of molecular mobility dictated by its local environment.

The dynamics of molecules is commonly investigated through the measurement of spin-lattice (T_1) and spin-spin (T_2) relaxation times of the nuclei within the sample and depend on the strength of the ^{1}H-^{1}H dipolar interactions (both intra- and intermolecular) and its time dependence [122, 123]. The T_1 relaxation time, or longitudinal relaxation time, represents the time it takes for the bulk magnetisation vector (M_0) of the nuclear spins to recover along the z-axis in a given magnetic field (B_0) after pulse excitation of nuclear spins [123]. However, this spin relaxation does not occur strictly along the z-axis and rather nuclear spins will precess with slightly different frequencies around the z-axis dependant on their local field [123]. The T_2 relaxation, or transverse relaxation time, refers to the time it takes for these precessing nuclear spins to be spread in the x-y plane in such a way that there is zero net transverse magnetisation (Figure 1-6).

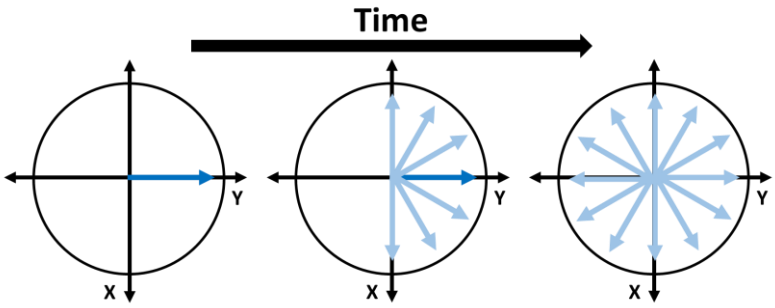

Figure 1-6 The transverse precession of M_0 in the x-y plane towards net zero magnetisation with time

The measurement of T_1 relaxation times is commonly achieved using the inversion recovery pulse sequence which involves applying a 180° pulse along the z-axis, then a 90° pulse after a suitable evolution time (τ) to place the vector back in the x-y plane where it can be detected [123]. When τ is zero, the magnetisation vector results in an inverted spectrum, so repeating the experiment with increasing values of τ allows for the monitoring of the relaxation of the spins. When τ is sufficiently long, complete relaxation occurs between the two pulses and maximum signal positive signal is recorded. This type of experiment is typically performed to either ensure maximum sensitivity, or to ensure recording of quantitative spectra.

There are two avenues in the assessment of T_2 relaxation times. Due to the influence of local intermolecular interactions on signal broadening, and its association with T_2 relaxation times, the width of the broadened signal can be used to interpret the molecular mobility of nuclei within a

sample, providing an estimate of spin-spin relaxation (T_2) referred to as apparent T_2 (T_2^*) [123]; however, this does not represent the true T_2 value. True T_2 values can be determined using the Car-Purcell-Meiboom-Gill spin-echo pulse sequence [124, 125]. Signal broadening by both dipolar couplings and/or local molecular heterogeneity can be attributed to the lack of motion of the molecules with respect to the experiment time scale [123]. Thus, it can be inferred that the faster the molecular motion, the narrower the resulting signal. This case is especially true in the case of ^{1}H NMR spectroscopy. However, this broadness can hinder other types of analysis by NMR. Improvements in the resolution of the broad signals obtained by solid-state NMR spectroscopy can be achieved by a technique known as magic-angle spinning (MAS) [126]. MAS involves spinning the sample rotor at a specific angle to the static magnetic field during measurement. Resolution is improved as a result of artificially inducing movement of the molecules to minimise dipolar coupling. Samples are typically spun between 1 and 111 kHz in commercial probes [127]. The magic-angle (54.74°) is calculated from the perturbation theory, introducing a factor of $3\cos^2\theta - 1$ to describe the evolution of the dipolar coupling. At the magic angle this expression is equal to 0, and the effects of the dipolar coupling reduced. Current limitations on MAS rotational speeds (up to 110 kHz) prevent complete neutralisation of dipolar coupling. These issues are not observed in solution-state NMR spectroscopy as the anisotropic interactions are usually averaged by Brownian motion, resulting in much narrower signal shapes [128].

Solid-state NMR spectroscopy has been employed extensively in the characterisation of starch structure. For example the determination of helix content in starch by ^{13}C NMR has been shown, with agreement between double helix content and X-ray diffraction experiments [118, 129-131]. Additionally, investigations probing the molecular dynamics of water and starch molecules in starch using ^{1}H NMR have shown the existence of different distributions and types of dynamics within starch [132]. Solution-state NMR spectroscopy has also provided valuable avenues to the analysis of starch structure, with ^{1}H NMR capable of resolving the resonances of the individual protons on the polymerised monomer units of starch. This has allowed the development of a method to quantify branching in starch [133]. The unique ability for molecules to only be visible in solution-state NMR when in solution enables the rate and extent of dissolution to be monitored for starches in organic solvents [78, 79]. While the starch structure and dynamics can be assessed by investigating the ^{13}C nuclei, other carbon-based components can also be assessed. In the analysis of rice this opens the door to investigation of the lipids and proteins naturally occurring in rice grains. Therefore, it is clear, that in the analysis of starch in rice, both solid- and solution-state NMR spectroscopy provide a sound platform for the characterisation of multiple structural features.

1.3.2.2 Long-range crystalline structure

The long-range molecular order in starch arises from the arrangement of helical structures into a repeating ordered structure (Figure 1-3, Level 4). Different types of crystal polymorphs have been observed in starch, named A- and B-type [22], including a combination of the two referred to as C-type. Another crystal polymorph arising from single helices of amylose complexing with lipids is also often observed, dubbed the V-type polymorph [134].

The size and presentation of defined unit cell crystalline units at this level of supramolecular starch structure lends itself well to the capabilities of X-ray diffraction (XRD) analysis. XRD is a ubiquitous technique in the analysis of crystalline structures, especially powerful for the determination of unit cells and by extension mineral classification [135]. XRD functions on the basis of Bragg's law, where sample bombardment with electrons results in X-ray emission by electrons that have been knocked out of inner energy shells. These X-rays are then detected, and when the geometry satisfies Bragg's equation a peak in intensity occurs. However, the quality of diffraction effects relies heavily on the strict and undisturbed periodicity of atoms. In minerals this is not an issue, and very sharp and unique diffraction patterns are observed [135]. In the case of sufficiently small crystals, or defective periodicity, constructive interference can occur, evidenced by diffraction peak broadening. The latter is typically the case for semi-crystalline polymers, where non-uniform and incomplete crystalline structure results in broad diffraction peaks. The same is true for amorphous and non-crystalline samples. Therefore, it is important in the analysis of semi-crystalline samples that both amorphous and crystalline contributions are described.

XRD has been extensively applied in the analysis of starch and starch systems, with investigations in the role of crystallinity in a range of starch properties including retrogradation [136, 137], digestion [138, 139] and cooking [140, 141]. In these studies, XRD has been shown to be capable of both differentiation between A- and B-type packing structures, while also quantifying the extent of long-range A/B type and V-type crystalline order [131]. There are a number of approaches in the quantification of crystallinity in starch by XRD. The majority of the approaches are subtractive or involve fitting, with both requiring identification of the amorphous and crystalline contributions independent of one another. Early approaches were subtractive, with the assumption of a two-phase system driving the calculation [142]. Despite the oversimplification of the crystalline structure with this approach it has remained a commonly used approach [131, 143]. More recently, curve fitting approaches have become increasingly popular [131, 144-147], attempting to account for the complex crystalline structures in starch using advanced modelling techniques. These fitting methods all rely on the accurate decomposition of the crystalline and amorphous contributions from the total intensity profile;

however, modern computing has allowed for high quality fitting analysis to be performed. As a result, curve fitting approaches have been shown to be a more accurate approach, capable of accounting for the imperfect crystalline structures observed in starch [131].

Therefore, XRD provides a valuable avenue for the determination of crystallinity in starches. Curve fitting approaches are capable of accounting for the imperfect long-range order in starch and has been confirmed by ^{13}C NMR spectroscopy [131]. Using this approach, the extent of A/B type and V-type crystallinity can be determined and the peak parameters such as peak width useful in exploring other aspects of the diffracting structure. The use of curve fitting approaches also lends itself well to analysis of complex multi-components systems, with the potential to identify and isolate potential interfering components. In the determination of starch crystallinity using peak fitting approaches, several factors need to be considered. A sufficiently thick sample is required (≈5 mm) to reduce the effects of background diffraction that can be significant compared to the relatively weak diffraction peaks given for semi-crystalline materials. The fitting software used is also an important factor to consider, with different software packages taking slightly different approaches in the fitting and refinement process [135].

1.3.2.3 The semi-crystalline lamellae

Finally, the semi-crystalline lamellar structure of starch is the culmination of the different levels of molecular order in starch (Figure 1-3, Levels 4 and 5). It arises from repeating lamellae of the long-range crystalline order and amorphous lamellae forming the semi-crystalline lamellae. Repeating lamellae of semi-crystalline and amorphous structure then describe the overall semi-crystalline lamellar structure. The features of this semi-crystalline structure manifest on the scale of 10 to 400 nm from the repeat unit d-spacing up to the thickness of repeating semi-crystalline and amorphous lamellae [148].

Small angle X-ray scattering techniques are powerful tools in the analysis of structures on the length scale of one to hundreds of nm, bridging the gap between crystallography and microscopy [148]. Scattering is characterised by a law of reciprocity giving an inverse relationship between the size or dimensions of the scattering object and the associated scattering angle. A variety of incident radiations can be employed in small angle scattering techniques, with two of the most common being X-rays and neutrons. For scattering to occur from a sample, a contrast difference between the atoms or molecules in the sample and its surroundings is required. This contrast is dependent on radiation source, with differences in scattering caused by chemical or physical differences within the sample. Small angle X-ray (SAXS) and neutron (SANS) scattering are complementary techniques that employ different types of radiation for scattering analysis.

SANS works on a similar principle to SAXS with incident radiation from a beam of neutrons rather than X-rays. Where X-rays are scattered by electrons, neutrons are scattered by atomic

nuclei, thus the scattering contrast is obtained through differences in neutron scattering length density between different nuclei. The difference in the extent of neutron scattering between deuterium (-0.3742 x 10^{-12} cm) and hydrogen (0.6671 x 10^{-12} cm) is extremely valuable for the study of hydrogen containing materials. From this "contrast variation" emerges, whereby structural features of different components can be distinguished by contrast matching one via differences in scattering length density. A commonly used approach to obtain contrast in starch is deuteration by suspension in deuterium oxide, exchanging the free water within the supramolecular starch structure [148].

These techniques are fundamental for the analysis of soft condensed matter and are especially powerful for the analysis of biological samples. While information such as size, shape, mass and scattering lengths densities may be obtained from scattering curves, relevant existing knowledge of the system is required. A model that adequately describes the scattering measured in reciprocal space is difficult due to the apparently infinite number of possible solutions. Therefore, a model based on parameters that are physically and chemically realistic, is necessary to allow for the analysis of the semi-crystalline lamellar structure of starch. The lamellar structure of starch can be detected in both hydrated and dry states by small angle scattering; however, with much less intensity in the dry state. One possible explanation for this phenomenon is provided by the liquid crystalline model for starch where amylopectin side chains align into a lamellar register upon plasticisation [117, 149, 150]. Thus, it is important to completely hydrate starch samples and in the comparison of samples to ensure a consistency in the degree of hydration. Additionally, in the analysis of the lamellar structure, care must be taken in the treatment of scattering data. In the case of isotropically scattering samples, the scattering data can be normalised to sample transmission, background subtracted, and then radially averaged to a 1-dimensional scattering curve. However, in orientated samples, sector averaging approaches are considered to be more appropriate [140].

The characteristic lamellar peak of starch ($\boldsymbol{q} \approx 0.06\text{-}0.07$ Å^{-1}, d-spacing ≈ 9-10.5 nm) has been well studied with SAXS in a diverse array of starches including rice starch [151, 152]. A second higher order diffraction peak ($\boldsymbol{q} \approx 0.13$ Å^{-1}) is also often observed in starch; however, is rarely reported in the literature and likely to have its origin as a second order reflection from the lamellar peak. Information on the size of lamellar repeat unit, the average amount of repeat units in each lamella, and the relative amount of sample with this semi-crystalline arrangement may be obtained from the resulting scattering profiles [148] (Figure 1-7).

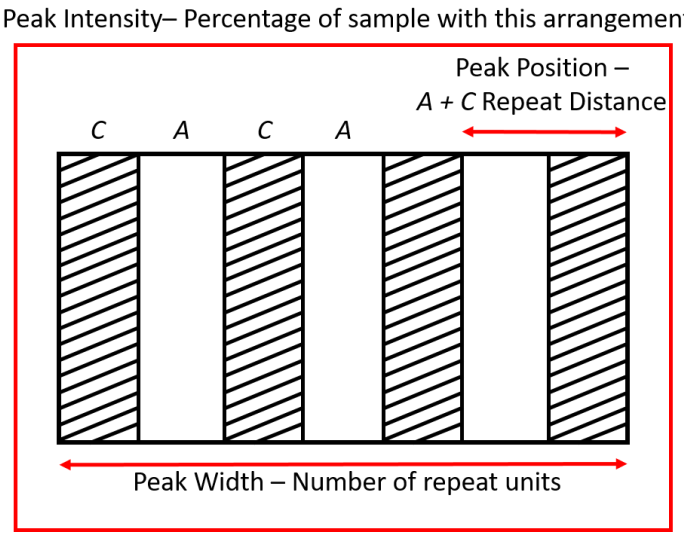

Figure 1-7 Relationship of SAXS peak parameters to lamellar structure of starch (C - crystalline, A – amorphous) [110]

The peak parameters of starch scattering profiles are typically extracted by two approaches. The first is through direct least-squares fitting of the scattering data, and the second through correlation and interface distribution functions using a Fourier transformed intensity profile. Direct least-squares fitting approaches have a long history in the analysis of starch scattering profiles. At the most simplistic end of the scale, the paracrystalline model assumes three different electron densities: crystalline and amorphous for the semi-crystalline lamellae, and a further amorphous background [149]. However, this is often considered too simplistic, leading to more complex models being proposed to account for structural imperfections [153, 154]. These more complex models seemingly enhance the ability to fit scattering data; however, the fitting parameters have significant uncertainty. Combining these more complex models with additional scattering information obtained through other scattering methods would provide a greater degree of confidence in the resulting fit.

The second approach, based on correlation and distribution functions, involves the Fourier transform of intensity data, and the resulting one-dimensional correlation function interpreted in terms of lamellar morphology. From this, structural parameters such as lamellar repeat distance and crystalline and amorphous lamellae thicknesses can be determined [155-157]. The lamellar thickness obtained by the intensity profile method was found to be consistently greater than that by the correlation function method [158]. This is a result of assumptions made about the scattering function in order to make meaningful determinations from the Fourier transform. However, with existing knowledge meaningful results can be obtained by this approach [158].

Peak parameters can also be determined by more empirical methods such as the graphical method [159] and by fitting equations that describe the SAXS peak and underlying interfacial scattering [39, 160, 161]. The latter fitting approaches employ a Gaussian/Lorentzian peak to fit the lamellar peak, a Gaussian peak for the second order reflection peak and a power-law function

to describe the underlying diffuse scattering, particularly at low $\boldsymbol{q}$ [39]. Recently, a refinement to this fitting equation has been developed that indicated an improved fitting of SAXS curves for starch [162].

In the analysis of the structure and properties of starch, the capability of controlling scattering contrast in SANS, in contrast to SAXS, has provided a platform with which to investigate how the lamellar structures behave when subjected to external stimuli. The scattering contrast between deuterium and hydrogen has allowed for extensive studies in defining starch structure [163, 164], and assessing the role of water in starch structure [150, 165]. SANS is a versatile instrument in the analysis of starch under different conditions and under different conditions such as during pasting [166] and during digestion [39].

1.4 Thesis Aims

With the background research above, it is clear that the no direct links between starch structure and digestibility apart from apparent amylose content (*AAC*) is available in the current literature. Given the variability seen in the correlation of AAC with digestibility, further analysis into starch structures, especially where *AAC* is similar, needs to be undertaken in explaining the differences in rice grain digestibility. This thesis aims to fill the gaps in the understanding of starch structures role in rice digestion and to refine methods in the characterisation of the complex multi-level starch structure. The specific aims of this thesis were to.

- Develop effective methods to provide a comprehensive characterisation of the molecular structure of starch to better define what is referred to as AAC
- Characterise multiple levels of the (supra)molecular of starch using a range of established and novel approaches
- Assess the value of these different levels of starch structure in differentiating rice samples and their relation to digestibility

1.5 Overarching statement

1.5.1 Publications and chapters overview

As identified in the background, AAC represent the only published method available to researchers in predicting digestibility. The strength of this correlation indicates that there are likely other drivers for digestibility. There is a gap in the understanding of which levels of starch structure, if any, can account for the differences observed where *AAC* is similar. The following publications and chapters allowed a deeper understanding in this area of research.

The manuscript of chapter 2 presents a study of multiple levels of starch structure in a rice variety x temperature glasshouse trial. Current routine measures of *AAC* were complemented by measures of average degree of branching (*DB*) by NMR spectroscopy and features of the semi-crystalline lamellar structure by small angle X-ray scattering. The performance of the measurement of average *DB* was determined in comparison to determination of *AAC* for the first time. The measurement of *AAC* is precise (<5 % RSD), indicating a high repeatability; however, reproducibility can suffer (4 – 40 % RSD) as a result of factors such as standards selection and instrumentation, bringing into question accuracy [73]. As a novel tool for the characterisation of starch in rice, average *DB* had comparable precision to the measurement *AAC*, and with the nature of the methodology, exhibits a greater accuracy, with higher reproducibility also supported by data. The features of the semi-crystalline lamellar structure were found to provide a valuable insight into the differences of large-scale structure between samples of similar *AAC*.

The manuscript of chapter 3 presents the optimisation and development of a capillary electrophoresis (CE) for the separation of starch. This manuscript forms its basis on published methodology [109, 167] and outlines an extensive process of improvements to the methodology. Key features include starch dissolution and dissolution stability in the context of separation science are highlighted, as well as the importance of the impact of different common preparative procedures such as filtration. This manuscript provides the optimal experimental conditions for the accurate characterisation of molecular structure discussed in chapter 4.

Chapter 4 explores the characterisation of amylose and amylopectin branching structures in rice flours by capillary electrophoresis. This was achieved through the novel analysis of the distributions of electrophoretic mobilities obtained and how these distributions are affected by branching structure. In addition to this was the application of dispersity calculations developed by our research team [116] to these distributions of electrophoretic mobility, allowing for assessment of the heterogeneity of branching structures present in the rice samples. The assessment of branching structures and heterogeneity of branching structures by CE of rice flour or of purified starches has, to the best of my knowledge, not been shown in the literature. This analysis represents a novel approach to the assessment of the distributions related to branching structures that exist in native starches. This raises many questions about the definition of amylose and amylopectin and what is measured by AAC. Molecular structure is discussed in context of weight-average mobilities, relating to type of branching, and the dispersity, relating to the heterogeneity of the branching structure such as degree of branching or branch chain lengths. It was found that different rice varieties could exhibit vastly different distributions, a potential factor in the differences in their functional properties.

Chapter 5 explores the application of NMR relaxometry to rice research in the context of digestibility. The simple yet often under-utilised aspect of NMR spectrometry, spin-lattice (T_1) and spin-spin (T_2) relaxation, are tied in with the molecular dynamics of the sample being analysed. These molecular dynamics allow for a unique local insight into the difference environments that can exist within a rice grain and between different rice samples. This work found multiple relaxation components in both raw and cooked rice grains, similar to reports in the literature for other starches [168]. However, most literature in this area focuses on the dynamics and distributions of water within the granules, while this study explored the apparent correlation with *in vitro* digestion. This relationship between molecular dynamics and starch digestion has not been shown in the literature prior and represents a novel finding of this work.

1.5.2 Contribution to personal, professional development and to the field of study

Throughout this project I have had a variety of experiences and opportunities that have contributed to both my personal and professional development. Working within a research team

of peers employing similar analysis techniques as well as sharing similar sample sets with one peer has allowed for me to experience working closely in team. This has brought with it an opportunity to both provide and benefit from valuable discussion between peers.

I was also involved in the writing of a successful AgriFutures research grant aimed to towards supporting my project and resulting in a strong link of my research with the agricultural industry. Through this research grant, I was involved in managing the finances of the project, while also being responsible for the timely delivery of progress reports and meeting of contracted milestones. As a result of the industry implications of this project, along with the industry funding support, I was invited annually to AgriFutures Rice R&D forums held in Yanco NSW to present an update on my research to the members of the rice industry. The audience included famers, breeders, cereal chemists, agricultural chemists, and industry representatives. During these trips I also had the opportunity to stay on site at the Yanco Agricultural Institute and discuss my research and progress in depth with my NSW DPI industry supervisor, Dr Rachelle Ward. These opportunities provided me a valuable opportunity to experience and understand my research from an industry perspective while I undertook the majority of my work in an academic setting.

1.5.2.1 Characterisation of starch branching and lamellar structure in rice flours – Submitted to Food Chemistry (Chapter 2)

The experience of writing this publication was beneficial in a number of ways. It allowed me to experience the preparation of a publication with guidance from co-authors both in industry and academia. This provided me with a perspective on how to approach this research from an industry perspective while still maintaining a fundamental foundation that fills a gap in current literature. In terms of contribution, I completed the first draft of the manuscript, and collected and processed the majority of data presented.

This experience contributed to my professional development in allowing me to prepare a manuscript for submission with co-authors covering a wide range of disciplines. This work also afforded me the opportunity to undertake experiments in two different professional facilities. The first included training and operation on new instrumentation within the Advanced Materials Characterisation Facility (AMCF) at Western Sydney University. During the experiments performed at the AMCF, I was involved in preparing a research case for the purchase of a new cold-stage FTIR sample stage, and as the first user, was also involved heavily in the instrument setup and optimisation as well as the development of the standard operating procedures. The second included training and operation of the small-angle X-ray scattering instrument at the ANSTO Lucas Heights facility, following a successful application to AINSE for a PhD scholarship top-up which also had provisions for access to ANSTO equipment. This work at ANSTO provided an opportunity to experience research in a high-pressure professional environment requiring

experiments to be completed in the allocated instrument time and involving repeated long days of intense work.

This publication has 7 authors including Dr Patrice Castignolles, Dr Marion Gaborieau, Prof. Elliot Gilbert, Dr Jitendra Mata, Dr Rachelle Ward and Michelle Toutounji. Dr Patrice Castignolles, Dr Marion Gaborieau and Dr Rachelle Ward provided guidance and direction of the paper. Dr Rachelle Ward was responsible for providing the samples measured, arising from her own research in a variety by temperature trial at NSW DPI, rice quality data, as well as contributions in analysis interpretation and experimental design. Prof. Elliot Gilbert and Dr Jitendra Mata provided training on the SAXS instrument, guidance and experimental design on SAXS experiments and general guidance on the publication. Dr Marion Gaborieau provided training for NMR experiments and analysis and Michelle Toutounji performed early work on the assessment of conditions for measurement of average *DB*.

1.5.2.2 Separation of amylose and amylopectin using capillary electrophoresis – Prepared for submission to Analytical and Bioanalytical Chemistry (Chapter 3)

This work began during my Masters degree, and carried over heavily into my PhD. The topic was a driver for a large proportion of my training and experience with capillary electrophoresis and NMR spectroscopy. The results of this work contribute to the field of separation science by providing important proofs and discussion on the topic of starch dissolution and separation methodology. The publication shows the impact of many common steps taken in separation analysis, while providing recommendations on ideal protocol. These results have been presented multiple times as the research evolved over my PhD including at international conferences in Amsterdam and Hawaii, presenting to analytical chemists and separation scientists, in regional Australia, presenting to agricultural researchers including farmers, breeders and cereal chemist, and within Sydney, presenting to a range of food and polymer scientists. Earlier work was previously submitted for review to Food Hydrocolloids before this PhD project started; however, it was deemed to be missing vital experiments and needed to be focused on the analytical chemistry side. Further work during my PhD has involved addressing these shortcomings to form a stronger evidence base for conclusions.

In terms of professional experience, this work involved the co-writing of a successful application for a grant to undertake reproducibility studies. This resulted in the opportunity to co-supervise a number of international students studying different degrees in different countries while they collected and analysed data based on my methodology. In addition to this I also had the opportunity to co-supervise a variety of smaller undergraduate student projects.

This manuscript for publication has 5 authors. Dr Patrice Castignolles and Dr Marion Gaborieau conceptualised the ideas on which this work was based and provided the direction of the paper

and helped formulate experiments. Dr Rachelle Ward contributed to the discussion and interpretation of results. Dr Joel Thevarajah contributed to experimental work as well as to the discussion and interpretation of results. James Lee, Giovanni Barbosa, Dylan Andres, Oceane Fort, Morgan Gray and Baanu Paul Remician provided technical assistance on broader aspects of the project, performing measurements which allowed for different directions of progress to be assessed. My contribution included the data acquisition for all experimental data, which included guidance on method development by Dr Marion Gaborieau and Dr Patrice Castignolles. I also wrote the first full draft of the manuscript which was reviewed by all co-authors. After presenting this work at the ITP conference in September 2019 in Toulouse, we realised that this manuscript for publication is in need of one more experiment for confirmation of the binding conditions before it can be resubmitted. Based on knowledge of the method, we expect that the binding conditions are occurring in the ideal conditions.

1.5.2.3 Characterisation of branching in rice flours using capillary electrophoresis – Chapter in preparation for publication (Chapter 4)

This work carries on from the work of chapter 3 and represents one of the most valuable aspects of the developed methodology in the field of separation analysis of starch. It allowed me to present the application of novel concepts developed by our research team [116] on rice samples. Through this I was able to contribute a novel avenue for the characterisation of heterogeneity in starch structure.

This work provided me the opportunity to learn and implement new concepts and theories in my own work. This was supported by a working knowledge of the application of this novel research through co-authorship a publication on its applications in chitosan during my Masters [169].

This chapter, and the resulting manuscript, will have a total of 5 co-authors including Dr Marion Gaborieau, Dr Patrice Castignolles Dr Rachelle Ward and Dr Joel Thevarajah. Dr Marion Gaborieau and Dr Patrice Castignolles conceptualised the ideas on which this work was based and provided guidance and direction of the study. Dr Rachelle Ward was responsible for the selection of two diverse sets of rice samples from the NSW DPI (breeding lines developed by Dr Peter Snell), rice quality data, as well as contributions in analysis interpretation, experimental design and writing guidance. Dr Joel Thevarajah provided discussion and guidance on data treatment. I collected all experimental data and performed all analysis. I wrote the first full draft of the chapter.

1.5.2.4 The link between molecular dynamics and digestibility in different rice varieties – Chapter in preparation for publication (Chapter 5)

This work afforded me the opportunity to expand my knowledge in a new field of NMR that I had no previous experience in. It was built on a refreshing but difficult investigation of the literature and textbook references to develop my own understanding so that I could better interpret the results and properly design experiments.

This publication contributes to the field by taking a well-known but often under-utilised aspect of NMR spectroscopy (relaxometry) and applying it to the area of cereal chemistry. This resulted in the novel observation of an apparent dependence of rice grain digestibility on the molecular dynamics of starch in rice.

This chapter and the resulting manuscript will have 5 total authors. Dr Patrice Castignolles and Dr Marion Gaborieau provided the direction of this study and the idea of initial experiments. Prof Chris Blanchard and Michelle Toutounji provided the digestibility data and samples (originally donated by SunRice), with the digestibility data formerly published [170] as well as discussion on the outcomes of the research. The NMR relaxometry experiments and first full draft of the manuscript were completed by me.

1.5.2.5 The supramolecular features of starch and how they relate to in vitro digestibility (Future work)

In addition to the chapters in this thesis, I also performed additional measurements on the supramolecular features of starch in a range of rice cultivars provided by NSW DPI with a preliminary discussion on the results in relation to digestibility, positioned as future work of this project. Features of starch structure characterised included helix content by solid-state NMR spectroscopy, long-range crystallinity by solid-state NMR spectroscopy and XRD, and semi-crystalline lamellar structure by SAXS.

These measurements allowed for me to develop my knowledge and skills on a variety of analytical instruments. Measurements of helix content and crystallinity by solid-state NMR spectroscopy allowed me to develop my skills in the analysis of starch by ^{13}C NMR spectroscopy, requiring me to develop a deeper understanding of NMR and starch analysis. Measurements of long-range crystallinity by XRD were performed within the WSU AMCF, allowing an opportunity to work in a professional laboratory with instrument technicians, troubleshooting measurements and developing experimental design. As a direct result of a requirement to control the temperature and humidity of the sample stage, discussions with the facility manager resulted in the purchase of special specimen holders for this purpose. I was among the first to use these specimen holders, and discussions of my experience was used to guide future users in their

applications. Measurements of lamellar structure by SAXS were performed in ANSTO facilities and was the second time I had performed measurements on this instrument, allowing me to further develop my skills, and discuss with instrument scientists.

These results were contributed to by a total of 8 authors, Dr Marion Gaborieau, Dr Patrice Castignolles, Dr Rachelle Ward, Dr Richard Wuhrer, Dr Laurel George, Prof. Elliot Gilbert, and Dr Jitendra Mata. Dr Marion Gaborieau and Dr Patrice Castignolles provided guidance and direction of the study. Dr Marion Gaborieau provided training on ^{13}C NMR experiments and data analysis. Dr Rachelle Ward was responsible for the selection of a diverse sets of rice samples from the NSW DPI (breeding lines developed by Dr Peter Snell), rice quality data, as well as contributions in analysis interpretation, experimental design and writing guidance. Prof. Elliot Gilbert and Dr Jitendra Mata provided training and support for SAXS measurements, as well as in depth discussion on SAXS results in addition to results of other aspects of starch structure. Dr Richard Wuhrer and Dr Laurel George provided training and discussion for XRD measurements and analysis.

1.5.3 Significance to Industry

The Australian rice industry is known for producing high quality products and has a strong commitment to research and development of all aspects of rice agriculture. Ongoing research is integral for the development of new rice varieties, with development of a single variety taking 7-10 years to have a pure line with the desired quality. Currently, most quality evaluation traits are characterised at the F5-6 stage (Figure 1-1). Starch is acknowledged as a strong driver of grain quality; however, only AAC and its association to functional traits are characterised in the F5-6 stage. A broader understanding of the role of starch structure in grain quality could uncover additional aspects of starch structure valuable for rice quality evaluation. in the breeding process. Similarly, a refined explanation of traits such as texture and satiety could be supported by a more sophisticated description of starch.

A description of starch to explain these traits requires multiple characterisation approaches to describe the many underlying levels of structures that exist in starch. At the molecular level, AAC is already an important quality trait that is assessed, though in a limited scope. Further characterising amylose content and structure will greatly contribute to the understanding of its relationship to functional traits and markers by assessing the branching structures present. The methodology employed is straightforward, with minimal sample preparation and relatively low cost (AUD 1/sample) compared to other separation approaches, with the bulk of cost arising from initial instrumentation purchase (AUD 50-70,000) and labour.

At the supramolecular level, more advanced instrumentation is required to characterise and define starch structure. Multiple levels of structural order exist in starch granules, and each has

the potential to impact quality in different ways. The formation of starch helices, the packing of molecules in crystalline arrangements, and the organisation of these structures within the starch granule are all contributing factors in the functional traits of rice including digestibility. The similar size scales of both the supramolecular structure of starch and the active enzymes in human digestion highlight the relevance of these structures in predicating digestibility. While accessibility to the required instrumentation is likely limited, the information obtained in this work may prove to be valuable in relating to genetic markers, and molecular structures. This would allow for informed decisions to be made that account for supramolecular structures, for example predicting heterogeneity in lamellar structure from the branching structures, thus forming a basis for the prediction of supramolecular structures and subsequent traits.

Developing such relationships will allow for molecular-assisted screening to be further developed in the breeding process, allowing either faster development cycles or enhanced development of specific attributes e.g. precise predictions of digestibility. With the current trends in dietary advice and guidelines, the development of greater choice of low GI commercial rice varieties would play an important role in public health. Such products would represent a value-add for the gross margins of growers and offer unique health related marketing opportunities.

Chapter 2 Characterisation of starch branching and lamellar structure in rice flours - Manuscript

Characterisation of starch branching and lamellar structure in rice flours – Submitted to Food Chemistry

Matthew Paul Van Leeuwen[a], Michelle Rosemarie Toutounji[a], Jitendra Mata[b], Rachelle Ward[c], Elliot Paul Gilbert[b,d], Patrice Castignolles[a], Marianne Gaborieau[a,e]*

[a] Western Sydney University, Australian Centre for Research On Separation Science (ACROSS), School of Science, Parramatta, NSW 2150, Australia
[b] Australian Centre for Neutron Scattering, Australian Nuclear Science and Technology Organisation (ANSTO), Lucas Heights, NSW 2234, Australia
[c] Yanco Agricultural Institute, NSW Department of Primary Industries, Yanco, NSW, Australia
[d] The Australian Institute for Bioengineering and Nanotechnology and Queensland Alliance for Agriculture and Food Innovation, The University of Queensland, Brisbane, QLD 4072, Australia
[e] The University of Queensland, Centre for Nutrition and Food Sciences, St Lucia QLD 4072, Australia

E-mail addresses: m.vanleeuwen@westernsydney.edu.au, mtoutounji@csu.edu.au, jtm@ansto.gov.au, rachelle.ward@dpi.nsw.gov.au, epg@ansto.gov.au, p.castignolles@westernsydney.edu.au, m.gaborieau@westernsydney.edu.au
* corresponding author: m.gaborieau@westernsydney.edu.au

Abstract

Apparent amylose content is one of the primary parameters used to describe the composition of rice grains. This spectrophotometric method is the only direct measurement of starch structure in routine quality analysis. However, starch exhibits 6 levels of known structure and characterisation at each level could allow explaining variations in other grain quality parameters, including texture and digestibility . We measured the (supra)molecular starch structure in rice flours complementary to apparent amylose content: average degree of branching by 1H NMR spectroscopy and semi-crystalline lamellar structure by small angle X-ray scattering (SAXS). The suitability of these methods in routine quality analysis was assessed. Determination of apparent amylose content exhibit high precision (ca 5 % error) but low accuracy. Determination of average degree of branching exhibits similar precision to determination of apparent amylose content; our reproducibly test indicates good accuracy. Sample preparation (dissolution) is the first source of error in 1H NMR spectroscopy and presumably also in spectrophotometry. Over narrow ranges of apparent amylose content (less than 2.5 % absolute difference) differences in apparent degree

of branching and lamellar structure could be observed. This shows that the difference between chemical structures of different amyloses/amylopectins within a sample is not negligible; it is important to consider this aspect , not just amylose/amylopectin content in rice. The ability of structural features to distinguish varieties and the impact of growing temperature was assessed. This opens a way to explore how finer details of molecular and supramolecular starch structure can play a role in understanding rice quality.

Keywords

Rice, starch, amylose, branching, SAXS, NMR

2.1 Introduction

Rice is an important crop providing the main nutritional intake of two-thirds of the global population [1]. Milled rice grains primarily comprise starch along with water, proteins and lipids [1]. Many commercial rice varieties are the result of rice breeding to maximise production efficiency, convey pest and disease resistance and to ensure the grain traits used to describe grain quality meet domestic and international market preferences [67]. Descriptors of rice quality include physical, compositional and functional properties such as chalkiness, colour, gelatinisation temperature, apparent amylose content (*AAC*), texture and digestibility [67]. Variation in some traits can primarily be explained by molecular markers [23, 171] and these are used in early generation breeding selections. Many descriptors of quality are also interdependent, for example, digestibility has generally been observed to decrease when *AAC* increases [26], but *AAC* values by themselves do not allow an accurate prediction of rice digestibility. Different factors can impact grain quality, for example growing conditions have been observed to affect *AAC*, gelatinisation and chalkiness [9, 11, 172]. Processing starch into foods can also strongly affect starch structure in some cases but not others, which in turn impacts nutritional and sensory properties (e.g. texture, visual aspect and flavour) [148]. From rice breeding to processing, there is a common need for a deeper understanding of drivers of rice quality traits [7], and characterising starch structure at each level of organisation is a novel approach to do that.

The properties measured in describing grain quality often do not include any direct measures of starch structure outside of *AAC* [67, 173]. Native starch structure is complex, exhibiting a multi-level hierarchical structure (Figure 2-1). Starch macromolecules consist of glucose monomer units connected by α(1, 4) glycosidic bonds with branch points involving α(1, 6) linkages. Branched chains are regularly arranged into tightly packed clusters of double helices that are the building blocks of crystalline regions within the repeating semi-crystalline lamellar structure of each starch granule [22].

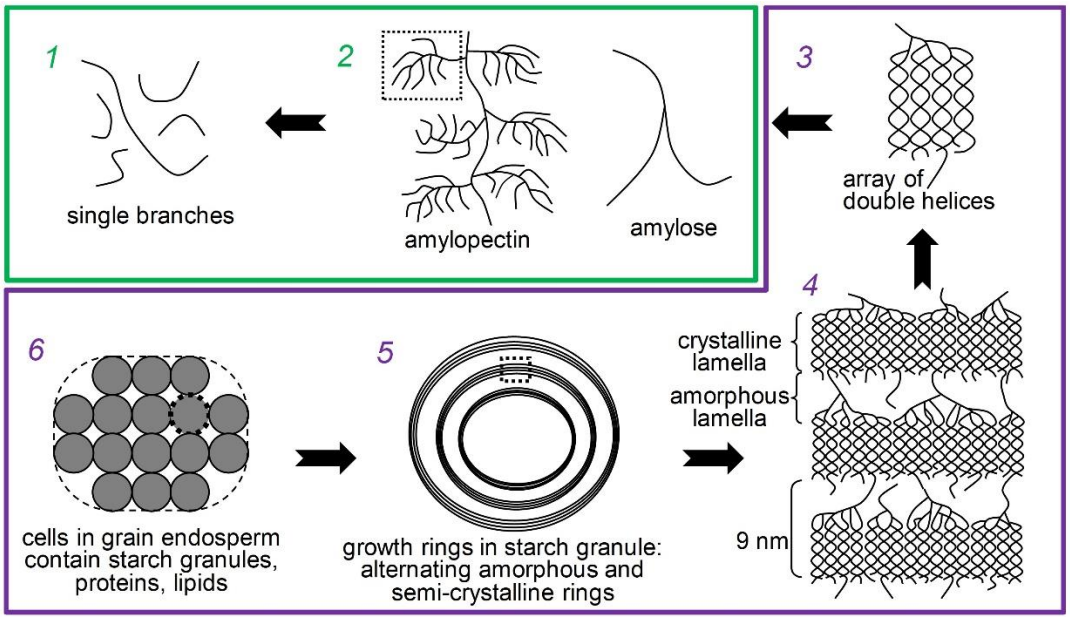

Figure 2-1 Molecular (green) and supramolecular (purple) structural levels of starch. Levels 1 to 6 start on the top left and follow the opposite order to that indicted by the arrows. Adapted from [38]

Native and modified starch structures have been characterised by a range of analytical techniques [148, 174, 175]. The molecular level of structure refers to the individual starch molecules and their branching structure (Figure 2-1, Levels 1 and 2). Amylose and amylopectin are respectively linear/slightly branched and highly branched starch. Starch has no chromophores, but *AAC* is most commonly determined by spectrophotometric methods after binding to iodine [73, 176]. Nuclear magnetic resonance (NMR) spectroscopy is one of the most versatile and informative spectroscopic techniques available for elucidation of molecular and supramolecular structure and dynamics (Figure 2-1, Levels 2 to 4) [123, 177]. ^{1}H NMR spectroscopy can differentiate between anomeric protons involved in α(1, 4) and α(1, 6) linkages and has been used to estimate the average degree of branching (*DB*) of D-glucans [178], oligosaccharides [38, 179, 180] and starches [133]. NMR is the preferred choice to determine the average *DB* [67] (Figure 2-1, Level 2). The measurement of average *DB* by ^{1}H NMR spectroscopy is one of the few established methods available for probing the branching structure of starch, with separation methods also available to probe other aspects of the branching structure such as the molar mass distribution of enzymatically debranched starch, commonly named "chain length distributions" [151, 181-183].

Characterisation of the multiple levels of crystalline structure in starch can be explored through a variety of techniques (Figure 2-1, Levels 3 to 5). X-ray diffraction (XRD) is capable of identifying and quantifying underlying A, B and C-type crystalline structures in starch [22, 131]. The proportions of single and double helices relative to the amorphous structure of starch can also be measured by ^{13}C solid-state NMR spectroscopy, allowing for insight into the short-range

molecular order [131]. Fourier transform infrared spectroscopy (FTIR) has been extensively used to characterise starch crystallinity, particularly in the range 1300-800 cm^{-1} where a crystalline index is often referenced. Crystalline index is defined as the ratio of 'crystalline' and 'amorphous' absorbance band intensities [184, 185]. However, strong overlap in absorbance bands and sensitivity to moisture limit the ability to obtain accurate data [144].

Lamellar starch structure can be measured by small angle X-ray scattering (SAXS) (Figure 2-1, Level 4 to 5) [148]. Chain length distribution (i.e., distribution of degree of polymerisation of the branches) and proportion of crystallinity correlate with the size and distribution of the lamellar structures in extracted starch [151]. This has important implications for understanding the activity of branching enzymes in starch synthesis, the resulting dynamic composition of amylose and amylopectin, and their unique branching characteristics [186]. These structural changes can consequently have significant impacts on the functional properties of the starch [138, 187]. SAXS can monitor starch processes including starch swelling [188], gelatinisation [189], retrogradation [190] and annealing [191].

AAC is known to be a valuable parameter in describing grain quality relevant to certain consumer preferences such as texture. However, there is scope to explore other structural features of starch. Here, the suitability of characterisation methods in differentiating rice flour samples based on starch structure is assessed. This is achieved by investigating *AAC* by the iodine binding spectrophotometric method, average *DB* by ^{1}H solution-state NMR spectroscopy and semi-crystalline lamellar structure by SAXS.

2.2 Materials and Methods

2.2.1 Rice samples

Seven varieties of rice were grown at the NSW Department of Primary Industries at Yanco, NSW, Australia. These varieties are examples of rice with different end-quality attributes, and different genetic backgrounds. Rice was grown in glasshouses using a two-phase randomised design. The first phase was from sowing to five days after anthesis whereby 24 pots per variety were grown in the same glasshouse. In the second phase, between five days after anthesis and harvest, pots (6 per variety) were placed into replicated growth rooms with temperatures of 26/17 °C and 36/27 °C day/night temperatures. All other growth input and conditions were consistent. Grain was harvested at physiological maturity, dehulled (THU35A 250V 50Hz Test Husker, Satake, Australia), milled (brush mill) and ground (Cyclotec 1093 Sample Mill, Tecator AB, Sweden) to pass through a 50 μm sieve.

Hot-water soluble (HWS) and hot-water insoluble (HWI) fractions from flours of the waxy rice varieties Hom, Makfay, Med Gnay, Laboun and Phae Savan were provided as freeze-dried powders by the International Rice Research Institute (Los Baños, Philippines). HWS and HWI fractions are specified as waxy varieties in the text.

2.2.2 Materials

Milli-Q® quality (Millipore, Bedford, MA, USA) water was used where specified, otherwise distilled water was used. Analytical grade sodium hydroxide pellets (NaOH), citric acid, potassium iodide and iodine were from Thermo Fisher Scientific (Scoresby, Victoria, Australia).

Deuterium oxide (D_2O) ≥99% (100 g bottles) and dimethyl sulfoxide-d_6 (DMSO-d_6) ≥99% were obtained from Cambridge Isotope Laboratories, Inc. (Andowver, MA, USA). Ethanol ≥99% and lithium bromide (LiBr) ≥99% were purchased from Sigma-Aldrich (Castle Hill, NSW, Australia). Ethylene glycol in DMSO-d_6 (80 %) standard was obtained in a sealed 5 mm NMR tube from Bruker (Bruker Biospin Ltd, Sydney). Quartz glass tubes: 80 mm length, 2 mm outer diameter, and 0.01 mm wall thickness were purchased from Hilgenberg GmbH (Malsfeld, Germany).

2.2.3 Methods

2.2.3.1 Apparent amylose content

AAC was determined using a modified AACC approved method 61-03.01 [176].

Rice flour was weighed (100 mg) and transferred quantitatively to 100 mL volumetric flasks. To this, 1 mL of 95 % ethanol (5 % H_2O) was added to wet the sample followed by vortexing, then 9 mL of 1 M aqueous NaOH added. Samples were then left at room temperature for 15-25 h to disperse. After dispersion, samples were made up to 100 mL with distilled water and vortexed.

For iodine colour measurements, 1 mL of dispersion was quantitatively transferred to a 20 mL test tube. To this, 2 mL of 0.1 M citric acid in water was added with mixing, followed by 1 mL of iodine solution (0.2 wt% aqueous I_2 and 2.0 wt% aqueous KI) then made up to 20 mL with distilled water. The dispersion was then mixed and left to stand for 20 min. Colour absorbance was recorded for 2 aliquots of each sample solution at 620 nm. Measurements were made on a Beckman Coulter DU800 Spec (Beckman Coulter Life Sciences, Indianapolis, United States).

Standard curve samples were prepared daily using water plus two in-house calibrated rice samples from NSW DPI. The absorbance at 620 nm was plotted against amylose content for each standard solution. The resulting standard curve was used to read amylose values for test samples.

The *AAC* of each variety and temperature is reported as the average of the replicate measurements and replicate glasshouse samples (n=4). Error bars are the standard error of the

mean. Groupings of *AAC* were based on a range of *AAC* independent of error bars (<2.5 % absolute difference).

2.2.3.2 Average DB

Rice flours (10 mg) were suspended in 2.24 g D_2O (5 g·L^{-1}) in round bottom flasks (50-250 mL), rinsed with D_2O prior to use. The flasks were sealed with Parafilm M®, mounted on an orbital shaker. Samples were continuously shaken (200 rpm) for 8 to 17 h at room temperature. Samples were then freeze-dried. This process was repeated once to ensure complete exchange of hydroxylic protons and minimise any resonance interference from residual solvent. The dried, selectively deuterated sample (4.5 mg) was dissolved in 0.45 mL of a 5 wt% LiBr DMSO-d_6 solution (made fresh from DMSO-d_6 with molecular sieves and LiBr powder stored in a desiccator) and heated in sealed glass vials at 80 °C overnight (approximately 15 h). 0.15 mL of D_2O was subsequently added to give a final sample concentration of 7.5 g·L^{-1} in DMSO-d_6/ D_2O (75/25). Samples were kept at 80 °C and measured immediately (less than 2 min).

The solution state ^1H NMR spectroscopy measurements were performed with a Bruker DRX300 spectrometer (Bruker BioSpin Ltd, Sydney) equipped with a 5 mm dual $^1H/^{13}C$ probe, at a Larmor frequency of 300.15 MHz. For older measurements in the reproducibility experiment (S 2.5.1.7), experiments were performed with the same setup but at a Larmor frequency of 300.13 MHz (due to decommissioning and recommissioning of spectrometer to new location). ^1H NMR spectra were recorded using a 10 000 Hz spectral width, 90° flip angle, and acquired at 90 °C (see section S 2.5.1.1 for temperature calibration).

The probe was tuned and the spectrometer was shimmed for each sample to ensure optimal signal-to-noise and resolution, respectively. Spectra were recorded and treated using Topspin software. Longitudinal relaxation times (T_1) of the signals of interest were estimated using the one-dimensional inversion recovery pulse sequence (S 2.5.1.3). Quantitative spectra were recorded with a 7.5 s repetition delay, which is longer than 5 times T_1 for the signals of interest. The chemical shift scales were calibrated with respect to the signal of DMSO at 90 °C (2.526 ppm) [193].

Average *DB* was calculated with equation 2 [194],

$$DB\ (\%) = \frac{I_{\alpha(1,6)} \times 100}{I_{\alpha(1,4)} + I_{\alpha\ \text{reducing}} + I_{\alpha(1,6)} + I_{\beta\ \text{reducing}}} \qquad \text{Equation 2-2}$$

where I_y is the integral of the ^1H NMR signal of the anomeric proton of type y, with observed y signals being α(1, 4) (5.13 ppm), α reducing end (5.00 ppm), α(1, 6) (4.80 ppm) and β reducing end (4.45 to 4.35 ppm) [133, 180, 194, 195]. An example of the partial spectra and integration regions is shown in Figure S 2-5. Reported values are the average of glasshouse replicates (n=2).

Error is reported as the standard error of the mean, and groupings of similar *DB* based on error bars.

For waxy rice flour fractions, the protocol above was slightly as detailed in section S 2.5.1.2.

2.2.3.3 Semi crystalline lamellar structure

Samples were packed into 2 mm quartz glass capillaries. Packed samples were hydrated with excess Milli-Q® quality water for at least 12 h prior to analysis and tubes sealed using paraffin wax.

Small–angle X-ray scattering experiments were performed on a Bruker NANOSTAR SAXS system, employing 3 pinhole collimation for focussing, Cu *K*α radiation with a wavelength of 1.541 Å and a VANTEC1000 2D detector (resolution 68 μm). The scattering vector, $\boldsymbol{q}$, in the range of 0.01 to 0.35 $Å^{-1}$ was used with optics and sample chamber under vacuum.

Scattering files were radially averaged using Bruker NANOSTAR software package, appropriately water background subtracted and scaled relative to a water filled capillary using the ATSAS software package [196]. Scattering curves were fitted using a power law function to represent large-scale structure combined with a combined Gaussian/Lorentzian function for the main starch peak ($\boldsymbol{q} \approx 0.067$ $Å^{-1}$) and a Gaussian function for the secondary peak ($\boldsymbol{q} \approx 0.13$ $Å^{-1}$) (Equation S 2-1). Fitting parameters were iteratively calculated to minimise chi-square using WaveMetrics Igor Pro software [197] and National Institute of Standards and Technology (NIST) Centre for Neutron Research macros [198]. An example curve and fit is shown in Figure S 2-7.

Reported values are the average of triplicate measurements of glasshouse duplicates (n=6). Error bars are reported as the standard error of the mean, and groupings of similar values based on error bars.

2.3 Results and discussion

2.3.1 Performance of determination of AAC by spectrophotometry and average DB by NMR spectroscopy in characterising molecular structure

The precision and accuracy of the determination of *AAC* and average *DB* are compared below. The reproducibility was also assessed through the measurement of the same samples by different operators on different instruments. Here a comparison between the two methods to characterise level 2 of the starch structure is provided, assessing three major points: 1) sample preparation, 2) the measurement itself and 3) the results obtained.

In the first point, the sample preparation is an important aspect of both methods, both sensitive only to starch that is solubilised at the molecular level. Full dissolution is sometimes assumed

when a transparent liquid is obtained or when no precipitation occurs upon centrifugation. Quantitative solution-state NMR spectroscopy showed that transparency, even upon centrifugation, can be obtained even if starch is not fully dissolved [79]. Conditions ensuring full dissolution at the molecular level have been implemented in this work for the determination of average *DB*. The NMR methodology published initially [133] was modified using dry DMSO-d_6 with the addition of 5 wt% LiBr instead of D_2O for dissolution of the samples (130:1 LiBr to glucose stoichiometry) [79, 82] to ensure complete dissolution at the molecular level. Lower LiBr concentrations (12.4:1 LiBr to glucose stoichiometry) were found to lower the precision of determined average *DB* (**Error! Reference source not found.**). This large molar excess of LiBr compared to glucose units is explained by the fact that LiBr does not just interact with the hydroxyl groups of the glucose unit (inhibiting hydrogen bonds) but it also interacts with and, in fact, modifies DMSO as a solvent [199]. Dry DMSO was used since even minute amounts of water in the DMSO have shown to slow down the dissolution [78]. D_2O was added after dissolution as it is reported to shift the residual H_2O solvent peak, yielding further improved resolution of starch signals [180]. The error associated with sample preparation was determined through 4 repeat preparations, yielding a relative standard deviation (*RSD*) of 2.6 % on the average *DB* of Doongara (S 2.5.1.6). In the spectrophotometric determination of *AAC,* the sample preparation requires quantitative solubilisation of the starch at the molecular level but also iodine binding to occur. Suspension of starch in 90 % DMSO/10 % water before iodine binding has been attempted a few times [72, 200]. Dissolution of starch with DMSO and LiBr has never been attempted for *AAC* determination. The AACCI method for *AAC* determination prescribes the use of aqueous sodium hydroxide for solubilisation, a protocol that is typically maintained even in modified *AAC* determination methods. However, the solubility of starch in aqueous sodium hydroxide at the molecular level has never been determined. The sample preparation in the accepted *AAC* determination methods could thus lead to low accuracy with especially some systematic errors.

For the second point, the measurements clearly differ between spectrophotometry and NMR spectroscopy, with differences in precision and accuracy. A typical limitation of NMR spectroscopy is its sensitivity. The error related the signal-to-noise ratio (*SNR*) can be determined from an empirical relation [201, 202]. In this work, spectra were collected until an *SNR* of at least 60 was obtained for the α(1, 6) signal (about 700 scans, in about 90 min), yielding an *RSD* of lower than 1 % based on the aforementioned empirical relation. The error due to data processing (phasing, baseline correction) was deemed negligible in the case of determination of chitosan composition by NMR when *SNR* was above 50 for the least intense signal of interest [203]. The resolution of the signals of interest in NMR of chitosan is similar to that observed in this work. The error due to processing is thus likely negligible for average *DB* of starch in this work. Measurements by ^{1}H NMR spectroscopy are not intrinsically quantitative contrary to common belief. To determine

quantitative conditions in this work, appropriate estimation of T_1 relaxation times was performed for all signals of interest, ensuring that signal intensities reflect the quantities of species dissolved in the sample (S 2.5.1.3). The T_1 assessment done in this work will apply to other instruments at the same magnetic field (300 MHz ^{1}H Larmor frequency). To ensure accurate integration of the signals of interest, resolution was improved by the addition of D_2O after dissolution [180] and high probe temperature (90 °C) (S 2.5.1.4). These conditions were then used to test long- and short-term sample aging to determine the stability of the samples (S 2.5.1.7) and the experimental impacts of waiting between sample preparation and measurement (S 2.5.1.9). A negligible effect of long-term aging (of the flour) was confirmed through repeat measurements 4 years after their initial measurement and storage at 4 °C in a refrigerator, with a change in operator and instrument giving an indication of the good reproducibility of the method. In contrast, short term aging (of the dispersion) was found to occur, with slow degradation after the addition of D_2O if the sample was left to evolve over several hours, therefore measurements were consistently performed immediately after addition of D_2O. Finally, the calculation of average *DB* is achieved by different equations in the literature, differing only in the inclusion/exclusion of α and β reducing ends [133, 194, 195]. Due to the detection of both α and β reducing ends in the non-waxy rice flours, they were included in the calculated of average *DB* as was also previously reported [194]. In contrast, α and β reducing ends were considered negligible in the waxy HWS and HWI fractions, so were not included in the calculation. In the rest of the work, the error bars are given based on precision values, which likely corresponds a reasonable estimate of the accuracy in this case. In the case of determination of *AAC* using spectrophotometry, sensitivity is not an issue. However, resolution is a limitation: amylose and amylopectin's UV absorption spectra are not fully resolved after iodine binding. Their bands are particularly broad due to branching affecting iodine binding. The absorbance assumed to be amylose includes some absorbance due to amylopectin [73] introducing some systematic error. Therefore, without corrective procedures, *AAC* determination is inherently semi-quantitative. The variability present in the methods of *AAC* determination has been assessed in a broad interlaboratory round-robin test (17 rice cultivars and 27 laboratories) [73]. The repeatability was found to be high, reflected in the repeat *AAC* measurements in this work (5 % *RSD*), and similar to that of the determination of average *DB* by NMR (6 % *RSD*). Reproducibility was however found to be low for *AAC* determination, identifying differences in standards and methodology as major sources of error. However, the use of rice cultivar standards instead of potato ones improved reproducibility. Here, an average relative difference in *AAC* of 6.8 % for this sample set was observed in reproducing measurements 4 years apart with different operators, instruments and methods (S 2.5.2.1). In the rest of the work, the error bars are given based on precision values, which likely corresponds an underestimate of the accuracy in this case.

Finally, the results of the two methods were compared to assess the consistency of the data between them (Figure 2-2). An apparent linear relationship between the average *DB* and *AAC* indicates, as expected, a decrease in average *DB* with increasing *AAC* due to amylose having a substantially lower *DB* than amylopectin. Boundary conditions were plotted to detect any potential variations in the linear relation for either measurement. These boundary conditions were created by taking the extreme values measured for average *DB* of waxy HWS and HWI rice flour fractions (assuming 0 % *AAC,* Table S 2-2) and linearly extrapolating to 100 % *AAC* and 0 % average *DB* (assuming negligible branching in amylose), shown as dashed lines. Boundaries were also plotted based on the highest and lowest average *DB* reported in literature for waxy starches in general, irrespective of botanical origin (Table S 2-3), shown as dotted line. The linear correlation between the average *DB* and *AAC*, as well as their confinement within the boundary conditions indicates that the data are consistent. However, with the adjusted r^2 of 0.93, it is possible that deviations as a result of different branching structures are occurring.

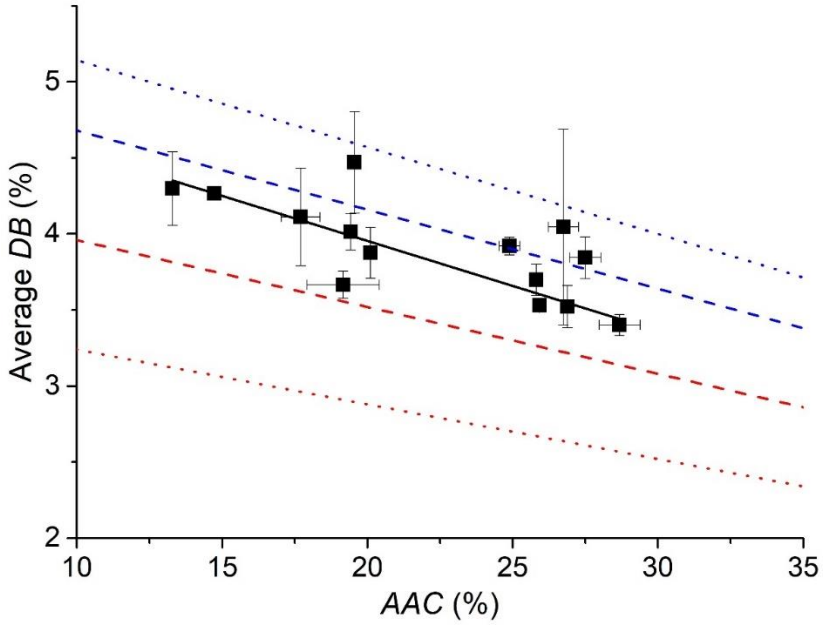

Figure 2-2 Average *DB* by ^{1}H NMR plotted against *AAC* for rice flours of different varieties grown at lower and higher temperature (black squares) showing a linear correlation (black line, adjusted r^2 = 0.93). Dashed lines are linear extrapolations of extreme values of average *DB* measured for HWS (blue) and HWI (red) fractions of waxy rice flours (Table S 2-2). Dotted lines are linear extrapolations from the highest (blue) and lowest (red) average *DB* values for waxy starches from literature (Table S 2-3). *AAC* error bars represent the standard error of 4 values (2 independent replicates of temperature and 2 instrument readings for each replicate). Average *DB* error bars represent the standard error of 2 values (2 independent replicates of temperature). See Table S 2-5 for individual *AAC* and average *DB* values

As a tool for rice quality assessment, the determination of *AAC* by iodine binding is a high-throughput, cost-effective method with standard methods strengthening its deployment [176, 204]. Spectrophotometry and NMR spectroscopy provide valuable data with which to assess the molecular structure of starch, with average *DB* expected to provide more accurate information. In contrast, while *AAC* and average *DB* methods are impacted by dissolution and branching

structures, the measurement of the semi-crystalline lamellar structure by SAXS is impacted primarily by the availability of, and competency in use of, instrumentation and the application of appropriate models. Given SAXS analysis is from solid samples, with excess hydration the only modification, sample preparation is simple and consistent. One exception is in the influence of sample packing density on relative intensity; however, this was observed to be adequately controlled in this work.

2.3.2 Assessing molecular structure through AAC and average DB

AAC is known to be influenced by temperature during different growth stages, with higher temperatures leading to a decrease in amylose synthesis for some varietals [205, 206]. Here, Cocodrie and I-Geo-Tze were shown to have a consistent *AAC* across temperature treatments whereas the remaining varieties had an observable decrease in *AAC* at higher growing temperatures (by 4.7 to 7.2 %) (Figure 2-3). Varieties could be grouped by their *AAC* values in each temperature treatments, displaying two groupings at the lower growing temperature, and three groupings at the higher temperature treatment. These observations have been explained by the expression of granule bound starch synthase (GBSSI) and the Waxy gene [205-208]. These groupings clearly indicates some similarity between certain varieties, but their responses to temperature also highlights their differences in other aspects. Thus, the determination of additional structural features here will serve to identify how the starch structure differs between temperature treatments and varieties.

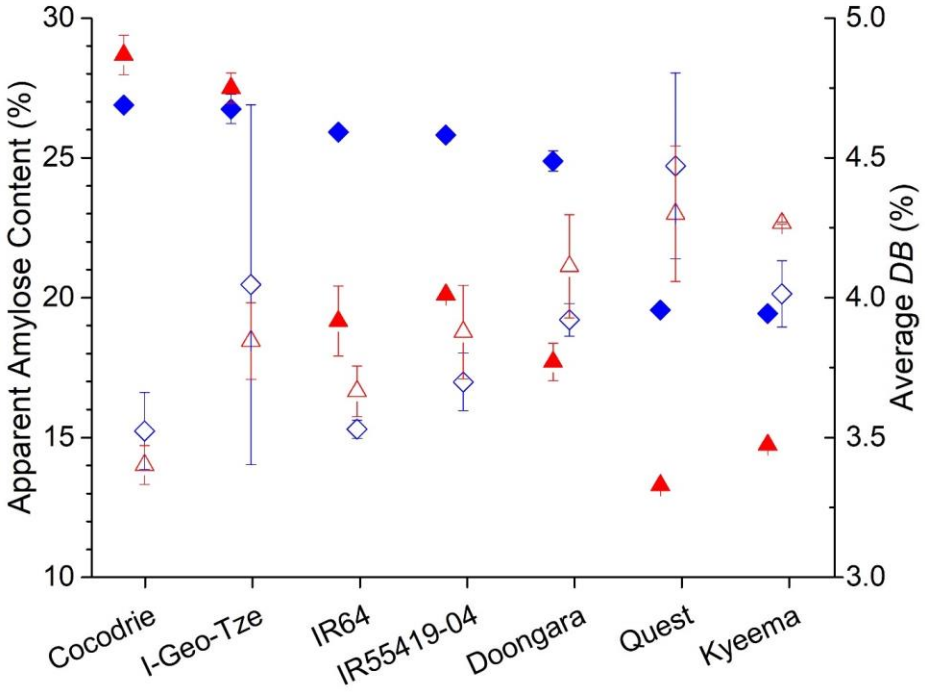

Figure 2-3 AAC measured by iodine binding (left axis, solid shapes) and average DB measured by 1H NMR spectroscopy (right axis, hollow shapes) for rice flours of different varieties grown at lower (blue diamonds) and higher (red triangles)

temperature. Error bars for AAC represent the standard error of 4 values (2 independent replicates of temperature, 2 instrument readings for each). Error bars for average DB represent the standard error of 2 values (2 independent replicates of temperature). See Figure 2 for data consistency check. See Table S 2-5 for individual values

Average *DB* is a metric related to *AAC*, with increasing proportions of less branched molecules generally expected to result in a decrease in the average *DB* (Figure 2-2). The average *DB* within the rice varieties grown at different temperatures is also shown in Figure 2-3. Average *DB* ranged from 3.4 to 4.5 % for all varieties and growing temperatures. Growing temperature did not influence average *DB* in any variety except Kyeema, where error bars indicated an apparent increase in average *DB* potentially arising from the coinciding decrease in *AAC* rather than a change in branching structure. All other varieties but Cocodrie and I-Geo-Tze displayed a reduction in *AAC* at the higher temperatures, but no significant change in average *DB*, counter to the observation in Kyeema and suggesting no direct association between *AAC* and average *DB* in these varieties. This is despite the general trend of decreasing average *DB* with increasing *AAC*, highlighting the need to report on a varietal basis (Figure 2-2). It is hypothesised that the reduction in the less branched amylose component had been counteracted by a decrease in *DB* primarily in the amylopectin component as a result of the higher growing temperature.

Differences in average *DB* could be noted between some varieties. At lower growing temperature, for the first grouping of varieties by *AAC* (24.9 to 26.9 %), the average *DB* was within the error bars, except for Doongara. For the second grouping (*AAC* of 19.4 to 19.6 %), a difference in their average *DB* was observed. At higher growing temperatures, two of the groupings by *AAC* (27.5 to 28.7 %, and 17.7 to 20.1 %) displayed a different average *DB* between varieties. For the third grouping, Kyeema and Quest (13.3 to 13.7 %), the average *DB* was within error.

While differences in average *DB* were observed between varieties, the average *DB* alone masks the distribution of α(1, 6) bonds between amylose and amylopectin. For example, the fine details of the branching structure such as short chain and long chain branches or the position of the branches, cannot be assessed. Given the multitude of possible combinations in branching and amylose content, it is expected that many of these can yield the same average *DB* despite displaying different branching distributions. Therefore, while the average *DB* may be a useful tool for general assessment of branching characteristics in some cases, it does not yield the fine details necessary to assess the potential relationships between branching structures and rice quality traits.

2.3.3 Assessing semi-crystalline lamellae with SAXS

The semi-crystalline lamellar structure of starch is the culmination of the amylose and amylopectin produced through starch synthesis and subsequent packing arrangements (Figure 2-1, Levels 3 to 5) as a function of their branching and size within each starch granule (Figure 2-1). The characteristic lamellar peak of starch ($\boldsymbol{q} \approx 0.06\text{-}0.07$ Å^{-1}, d-spacing ≈ 9-10.5 nm) has been well

studied with SAXS in a diverse array of starches including rice starch [151, 152]; however, to the best of our knowledge this is the first time it has been studied on native rice flours. This and a second higher $\boldsymbol{q}$ peak ($\boldsymbol{q} \approx 0.13$ Å^{-1}) were observed here for all varieties (Figure S 2-7). This second peak is rarely reported in the literature and likely to have its origin as a second order reflection from the lamellar peak. The extracted parameters of the primary lamellar peak are related to the features of the semi-crystalline lamellar structure of starch [148], providing an additional avenue in assessing the subtle differences in starch nanostructure beyond information on *AAC* and average *DB*.

2.3.3.1 Extent of semi-crystalline order

The relative intensity of the primary lamellar peak ($\boldsymbol{q} \approx 0.067$ Å^{-1}) relates to the extent of semi-crystalline order present in the sample. The peak intensity of rice grown in the two temperature treatments is shown in Figure 2-4. It is important to note that the relative intensity in SAXS is sensitive to sample thickness and packing density, and that care must be taken to minimise differences when comparing scattering intensity from different samples [148]. In this work, the sample thickness and packing density in preparation were not specifically controlled, so bias in relative scattering intensities may be introduced. However, a general decrease in relative intensity with increasing amylose content has been reported in the literature [148] and has also been observed in this study (Figure S 2-8). This trend indicates that packing densities were adequately controlled. This apparent relationship of *AAC* with relative peak intensity has been explained by the accumulation of defects within the lamellar architecture [148].

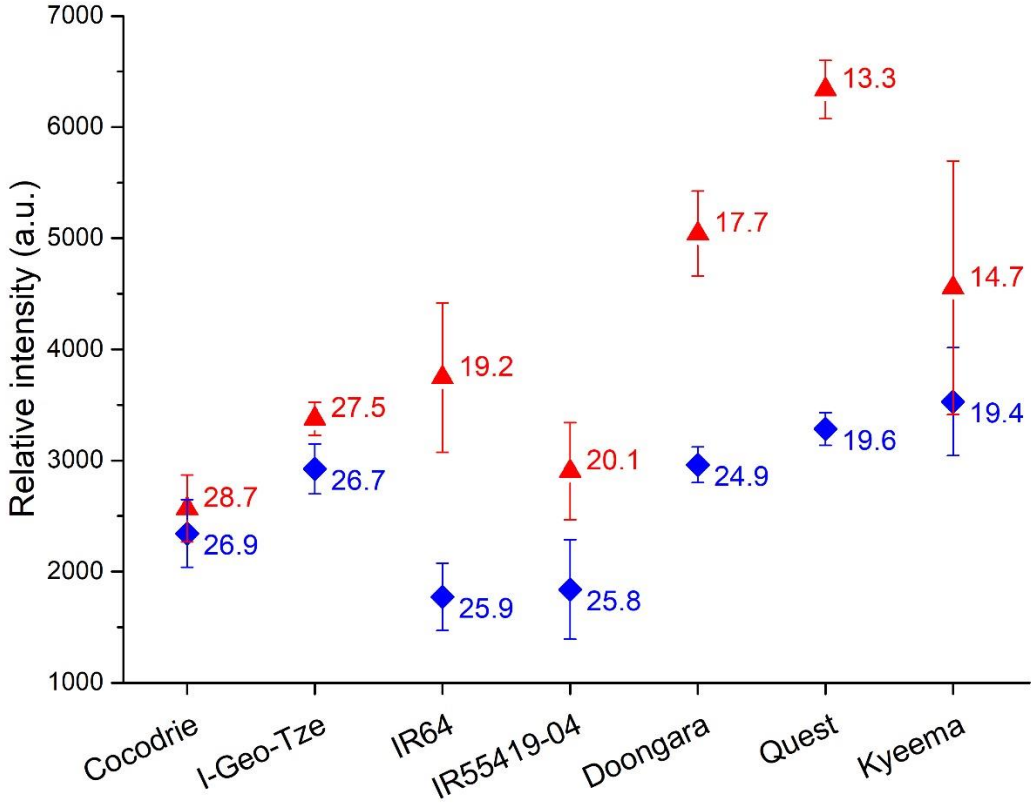

Figure 2-4 Relative peak intensity of main lamellar peak observed in SAXS for rice flours of different varieties grown at lower (blue diamonds) and higher (red triangles) temperature for each variety and temperature. Average AAC of samples is shown adjacent to data point. Error bars represent the standard error of 6 values (2 independent replicates of temperature, 3 preparations for each). See Table S 2-5 for individual mean peak intensity values

Differences in relative intensity between temperature treatments were within the error bars for Cocodrie and I-Geo-Tze, and given *AAC* and average *DB* were unchanged, this suggests no change in the extent of semi-crystalline order. IR64, IR55419-04, Doongara and Quest varieties exhibited a measurable increase in the relative intensity, a decrease in *AAC* and similar average *DB* at the higher growing temperature. These results agree with the consideration that the amylose component of starch contributes mainly to the amorphous regions of the semi-crystalline structure [209]. The extent of semi-crystalline order is thus expected to increase as a result of a decrease in the amorphous component. The consistency in average *DB* for all varieties except Kyeema indicates that the extent of semi-crystalline order in the semi-crystalline structure is independent of a change in branching frequency, reflected in the relationship of increasing relative intensity with increasing average *DB* (Figure S 2-9). At higher growing temperatures, Kyeema displayed no measurable increase in relative intensity despite an apparent decrease in *AAC* and increase in average *DB*. For Kyeema, this suggests the formation of crystalline structure has not been influenced by the reduced *AAC* and changes to branching structure. The large error in the relative intensity for Kyeema may indicate that intragranular packing density was significantly interrupted, especially at the higher temperature.

Differences in relative intensities could also distinguish varieties within each temperature treatment. The two groupings of varieties by AAC at lower growing temperatures (24.9 to 26.9 %, and 19.4 to 19.6 %), could be distinguished into three groups by their relative intensities. Of the higher *AAC* varieties, I-Geo-Tze and Doongara displayed the highest relative intensities and IR55419-04 and IR64 the lowest, while Cocodrie overlapped both. This highlights the difference in extent of semi-crystalline order that can occur between varieties despite a relatively narrow range of *AAC.* In contrast, the lower *AAC* Kyeema and Quest had both similar *AAC* and similar relative intensities. Interestingly, despite much lower *AAC*, the relative intensity of these varieties was similar to some of the higher AAC varieties at the lower growing temperature. At higher growing temperatures, the three groupings of varieties by *AAC* all displayed differences in relative intensity within the groupings, highlighting again how differences in the extent of semi-crystalline order can manifest independent of *AAC*. However, intergroup overlap of relative intensities was noted for the higher and intermediate *AAC* groupings, counter to the general observation of decreasing relative intensity with increasing *AAC* (Figure S 2-8).

At both lower and higher temperatures, varieties exhibiting similar average *DB* could not be further discriminated by their relative intensity. One exception was Doongara, displaying a substantially higher relative intensity at higher growing temperature than I-Geo-Tze and IR55419-04 despite similar average *DB;* however, due to the large error no conclusions can be drawn.

2.3.3.2 Thickness of semi-crystalline lamellae

The position of the primary lamellar peak relates to the thickness of the lamellar repeat unit, one crystalline plus one amorphous lamella, in real space (Figure 2-1 and Figure 2-5). The lamellar repeat thickness was typical of what has been reported for starch [163], with varieties exhibiting sizes between 8.9 and 9.7 nm.

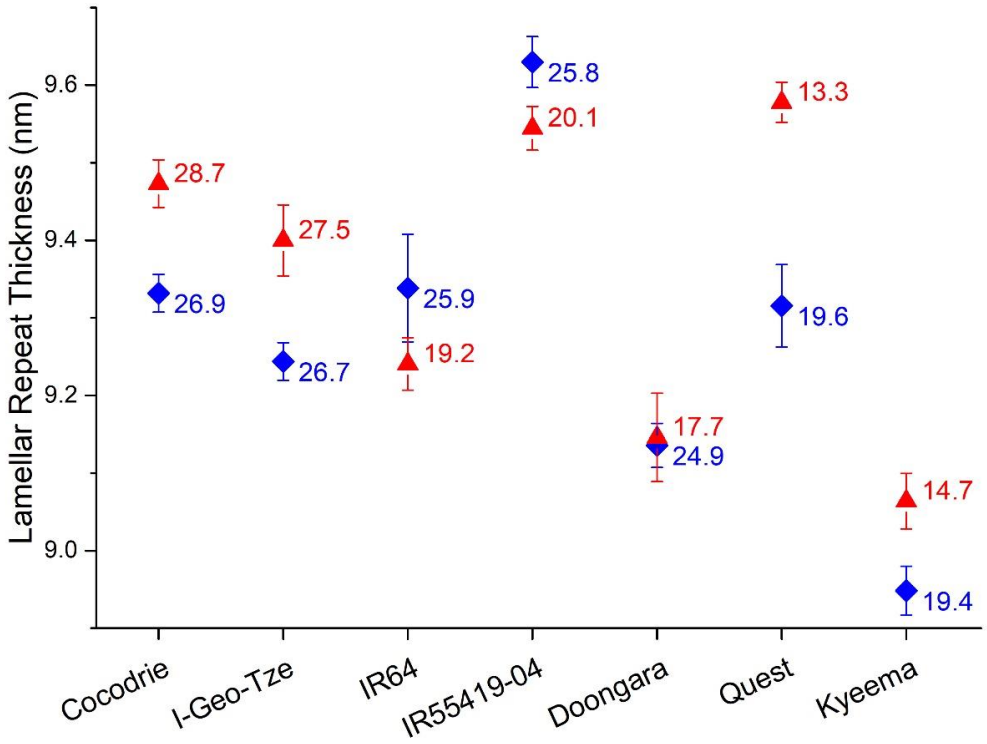

Figure 2-5 Lamellar repeat thickness measured with SAXS for rice flours of different varieties grown at lower (blue diamonds) and higher (red triangles) temperatures (Equation S 2-5). Average *AAC* of samples is shown adjacent to data point. Error bars represent the standard error of 6 values (2 independent replicates of temperature, 3 preparations for each). See Table S 2-5 for individual mean thickness values

All varieties displayed a change in the lamellar repeat thickness, within error, between temperature treatments except for IR64 and Doongara (Figure 2-5). Both IR64 and Doongara also displayed a decrease in *AAC*, similar average *DB* and an increase in extent of semi-crystalline order with the higher temperature treatment. This similarity in lamellar repeat thickness strongly indicates that the decrease in *AAC* is linked primarily with a decrease in the fraction of bulk amorphous regions rather than in the amorphous lamellae of the semi-crystalline regions. Of the varieties in which higher temperature treatment impacted the lamellar repeat thickness, Cocodrie and I-Geo-Tze had displayed no large difference in *AAC*, indicating again that *AAC* itself is not a primary driver of the lamellar repeat thickness, but may play a role. Variations in lamellar repeat thickness have indeed been reported to coincide with increased concentration of longer chain lengths of debranched starch (degree of polymerisation higher than 13), with either increased disordered chain ends contributing to amorphous regions or production of larger crystalline lamellae [151]. Kyeema was the only variety with a change in both lamellar repeat thickness and average *DB* between temperature treatments, potentially indicating a change in concentration of longer chain lengths. However, these suggestions cannot be confirmed by the average *DB* as it does not inform on such aspects of the branching structure.

The lamellar repeat thickness appeared to be independent of *AAC* between varieties within each temperature treatment. An exception to this was Cocodrie and I-Geo-Tze which displayed similar lamellar repeat thicknesses at the higher growing temperature, reflecting the consistency in other measured parameters. For the remaining varieties, grouped by *AAC* and exhibiting similar average *DB*, differences in lamellar repeat thickness were noted within groupings. At lower temperature treatment, this was observed for the grouping of Kyeema and Quest varieties, as well as for the grouping of IR55419-04 and Doongara varieties. At higher growing temperatures this was observed for the grouping of IR55419-04, IR64 and Doongara varieties. These observations confirm that *AAC* or average *DB* are not in themselves the primary drivers of the lamellar repeat thickness, though it is possible these differences arise from varietal differences in chain length distribution, similar to observations of the temperature treatments [151].

2.3.3.3 Heterogeneity of lamellae

The half width half maximum (HWHM) of the observed scattering peak for starch is related to the uniformity of the lamellar repeat thickness, with an increase in HWHM corresponding to a greater variation between the thickness of lamellae (Figure 2-1 and Figure 2-6). There is a positive relationship between HWHM and average lamellar repeat thickness (Figure S 2-10). This previously reported observation was explained by a minimum number of glucose units (degree of polymerisation of 10-12) required to form a helix [151].

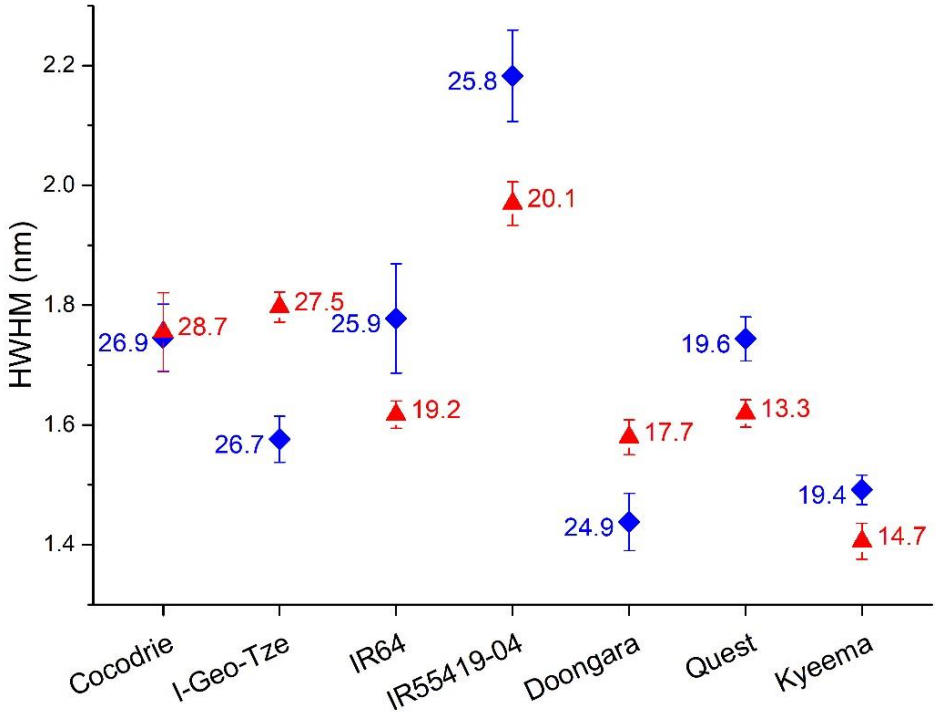

Figure 2-6 HWHM of the lamellar peak measured with SAXS for rice flours of different varieties grown at lower (blue diamonds) and higher (red triangles) temperatures (Equation S 2-6). Average AAC of samples is shown adjacent to data point. Error bars represent the standard error of 6 values (2 independent replicates of temperature, 3 preparations for each). See Table S 2-5 for individual mean HWHM values

All varieties displayed a change in lamellar heterogeneity between temperature treatments, except for Cocodrie (Figure 2-6). For Cocodrie this indicates a consistency in the lamellar repeat thickness between the lamellae, reflected in both the unchanged *AAC* and average *DB*, though an increase in the lamellar repeat thickness in the higher temperature treatment (Figure 2-5) indicates that some structural changes are still occurring. Of the other varieties where lamellar heterogeneity was different between temperature treatments, all except I-Geo-Tze recorded a decrease in *AAC* at higher growing temperature. Varieties displaying both positive and negative changes in HWHM were observed indicating an independence of lamellar heterogeneity from *AAC*. Kyeema was the only variety that exhibited a change in both the average *DB* between temperature treatments and in HWHM, which may again hint at some aspect of the branching structures playing a role; however, this cannot be confirmed.

Differences in lamellar heterogeneity were also observed between varieties within each temperature treatment. At lower growing temperature, the grouping of higher *AAC* varieties (24.9 to 26.9 %) exhibited a range of different HWHM values, indicating large differences in the lamellar heterogeneity between them. An exception to this was Cocodrie and IR64, for which along with HWHM both average *DB* and lamellar repeat thickness were similar. This could suggest that these varieties are exhibiting similar branching structures that account for the similarities observed, though similar HWHM of the lower *AAC* Kyeema suggests that *AAC* is not a major factor. This is further highlighted by the difference in HWHM between Kyeema and Quest at lower growing temperature despite similar *AAC* and average *DB*. At higher growing temperatures, similar observations were made for groupings of varieties by *AAC* exhibiting differences in lamellar heterogeneity. Where varieties also exhibited similar average *DB*, HWHM distinguished between them. An exception was Cocodrie and I-Geo-Tze, displaying similar HWHM and a narrow range of *AAC* (27.5 to 28.7 %), but an apparent difference in average *DB* suggests some similarity in branching structure that is independent of branching frequency.

2.3.3.4 General statements on semi-crystalline structure

When comparing groupings of varieties by *AAC*, the features of the semi-crystalline lamellar structure could be used to differentiate between varieties and the impact of growing temperature. Similarly, when comparing varieties of similar average *DB*, the lamellar features could be used to further differentiate samples. Drivers of such changes in the semi-crystalline structure could be explored at the molecular level, for example in terms of chain length distribution of debranched starch [151] or of distribution of branching structures [116]. FTIR may provide a more accessible approach to explore the crystalline structure. However, the complex non-linear relationship of the crystallinity index determined from FTIR with crystallinity measured by NMR or XRD [144] indicates that such an approach is not straightforward; this is principally associated with the

deconvolution of strongly overlapping signals biasing the intensity of the peaks of interest. Cryogenic temperatures have been suggested to improve resolution [210]; however, an adequate resolution could still not be obtained for starch in this work even at cryogenic temperatures (Figure S 2-11).

Tentative conclusions could be drawn from the SAXS peak intensity data. The lamellar repeat thickness and HWHM offer valuable information to characterise differences between samples. As far as its association with *AAC* and average *DB* is concerned, it is apparent that the lamellar structure is influenced by the *AAC*; however, within the range of samples studied, the average *DB* does not offer any more depth than *AAC* when examining the lamellar structure.

2.4 Conclusions

Determination of *AAC* by spectrophotometry is a standard measurement conducted on rice grains as part of the assessment of grain quality and providing a valuable parameter. However, there is a range of characteristics in starch structure that could play a role in grain quality. Whereas *AAC* has high precision and low accuracy, determination of the degree of branching using NMR offers a similar precision but the accuracy may be higher. There are intrinsic errors in NMR is due to sampling and dissolution; however, this can be largely addressed by dissolving the starch in dry DMSO and then measuring the sample as soon as D_2O has been added. The accuracy of *AAC* may be investigated by employing dissolution protocols shown to effectively solubilise starch; however, this would also require determination of the impact on the iodine binding. In terms of NMR, a round-robin test would give an important assessment of the accuracy of the average *DB*.

Average *DB* could distinguish varieties, showing groupings despite differences in other structural features. However, the subtle changes caused by a stressor to a single variety, in the current case temperature, are more challenging to detect if present. Groupings of varieties by *AAC* could be distinguished by their average *DB* within a grouping. However, the contributions of different branching structures and their distributions are averaged into this single value. As an alternative approach in the characterisation of molecular structure in starch, the separation of different branching structures using free-solution capillary electrophoresis shows promise as a complementary technique [109]. Evaluation of the lamellar structure similarly was able to distinguish different varieties and could also indicate differences in structure as a result of growing temperature. The ability of SAXS to investigate the semi-crystalline lamellar structure yields unique insights into the crystalline structure compared to the lateral long-range crystalline information that can be obtained by XRD; however, SAXS instrumentation is generally less accessible to food materials scientists.

Ultimately, features of starch structure other than *AAC* in rice flour are also capable of distinguishing samples, even in some cases where *AAC* was unchanged. However, the relevance of *AAC* to other quality parameters such as gelatinisation temperature, texture and digestibility is a major reason that it has cemented its importance as a quality parameter of rice flour. The use of more robust statistical approaches to explore the value of different measurements of starch structure in distinguishing between rice varieties or rice qualities would be a valuable approach.

While the focus of this study was on starch characteristics, it must also be acknowledged that proteins, lipids and other polysaccharides will contribute to rice grain quality. However, there is still an opportunity to explore how finer details of starch structure, including molecular (branching structures) and supramolecular (lamellar) structure, are linked to or can define other important quality traits of rice grains. Such a link would strengthen the case for inclusion of these alternative and complementary features of starch structure within routine rice quality analysis. Considering costs and accessibility, the characterisation of the lamellar structure (by SAXS) would be limited to selected samples, the measurement of average *DB* (by NMR) would be applicable to a larger range of samples to select the more promising ones, and the determination of the distribution of branching structures (with capillary electrophoresis) would be applicable as a high-throughput tool for the initial pre-selection.

Acknowledgements

This work was supported by the Australian Government [Research Training Program scholarship to MVL], AgriFutures [PRJ-010712 to MVL, MG, PC, RW, EG], and the Australian Institute of Nuclear Science and Engineering (AINSE) [Post-graduate Research Award to MVL], Western Sydney [Academic Development Plan to MG], and the Molecular Medicine Research Group at WSU [travel grant to MVL]. The Australian Nuclear Science and Technology Organisation (ANSTO) is acknowledged for granting access to the SAXS instrument (X4647 and P6398) and Robert Knott for training and technical assistance with the SAXS instrument. Tim Murphy and Richard Wuhrer (Advanced Materials Characterisation Facility, WSU) are thanked for training and general discussion. NSW DPI cereal chemistry team are thanked for rice samples, data and general discussion, IRRI for providing samples and Lorraine Spohr (NSW DPI) for biometric advice.

Declaration of Interest

None.

2.5 Supporting information

Supporting Information

for

Characterisation of starch branching and lamellar structure in rice flours

Matthew Paul Van Leeuwen, Michelle Rosemarie Toutounji, Jitendra Mata, Rachelle Ward, Elliot Paul Gilbert, Patrice Castignolles, Marianne Gaborieau

S 2.5.1 Determination of average DB

S 2.5.1.1 Calibration of probe temperature

The probe temperature was calibrated using ethylene glycol (80 % in DMSO-d_6) and equation S1 [211]:

$$T = \frac{(4.218 - \Delta\delta)}{0.009132} \quad \text{Equation S1}$$

where T is the sample temperature in Kelvin and $\Delta\delta$ is the difference in ppm between the CH_2 and OH singlets.

S 2.5.1.2 NMR measurement of waxy flour fractions

The protocol detailed in the main manuscript for rice flours was slightly modified as follows for the waxy rice flour fractions. The quantities were multiplied by 1.5 for the suspension in D_2O. DMSO-d_6 with 0.05 wt% LiBr was used for dissolution, as it yields complete dissolution of waxy rice flours [79]. NMR spectra were measured on a Bruker Avance NMR spectrometer operating at a Larmor frequency of 500.13 MHz for ^1H, equipped with a TXI5z probe (Bruker Biospin); the temperature calibration was carried out with a pure ethylene glycol standard (distilled, in a sealed tube) [79]. Quantitative ^1H NMR spectra were recorded at 90 °C using a 90° flip angle, and a repetition delay of 20 s. The signals of α and β reducing ends were negligible in the waxy rice flour fractions and not taken into account in the average DB calculation.

S 2.5.1.3 Estimation of T_1 for quantitative determination of average DB

Longitudinal relaxation times (T_1) of the signals of interest (in the range of 5.4 to 4.2 ppm) were estimated using the one-dimensional inversion recovery pulse sequence. In this experiment, a

signal is negative if the inversion recovery delay is shorter than T_1 *ln2, and positive if the inversion recovery delay is longer than T_1 *ln2. Signals in this range exhibited similar T_1, with T_1 determined to be between 0.5 and 1.5 s (Figure S 2-1).

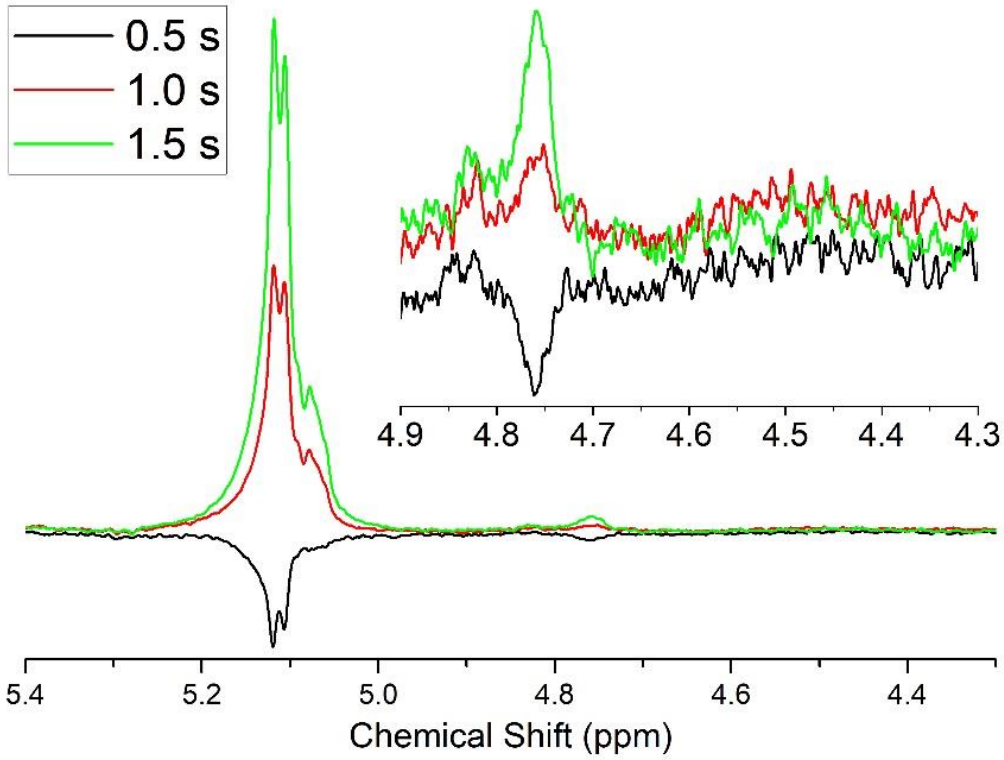

Figure S 2-1 Partial spectra of rice starch in DMSO-d_6 at 80 °C displaying measurements to assess whether T_1 values are shorter than 0.5 s (black), 1.0 s (red) and 1.5 s (green) seconds, with inversion recovery delay of 347 ms (black), 694 ms (red) and 1.042 s (green)

S 2.5.1.4 Effect of probe temperature on average DB measurement

The work of Gidley employed high probe temperatures in order to maintain favourable conditions for a stable starch dissolution [133]. The effect of temperature was tested to ensure optimal resolution and sample dissolution stability. With a dissolution temperature of 80 °C, probe temperatures of 70 °C and 90 °C were compared on rice samples to determine if there were any dramatic effects on the resulting spectra. The results indicate that similar spectra are obtained, with a slightly improved resolution of the reducing ends afforded by the 90 °C probe temperature (Figure S 2-2). This improved resolution was also noted in starch standard samples, leading to a lower calculated average *DB* (Figure S 2-3).

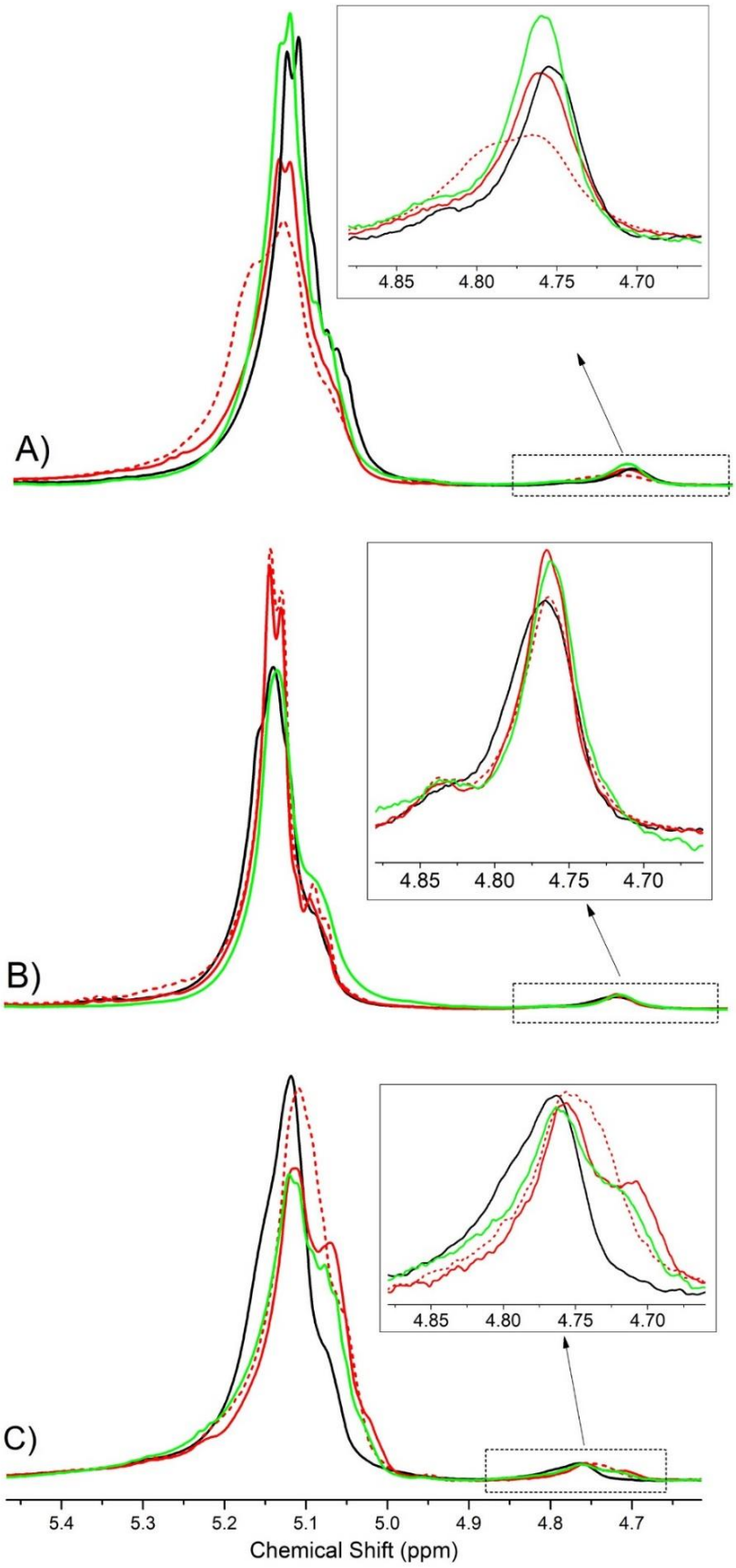

Figure S 2-2 Partial spectra of I-Geo-Tze (a), Doongara (b) and Quest (c) rice samples grown at lower (black) and higher temperatures (red and green). ^{1}H NMR spectroscopy measurement temperatures were 70 °C (dashed line) and 90 °C (solid line)

S 2.5.1.5 Solvent choice

The solvent was changed from pure D_2O [133] to DMSO-d_6 with the addition of LiBr for improved sample dissolution [79]. D_2O was also added. The amount of LiBr was tested on waxy maize, with 5 wt% found to give a more consistent average *DB* value regardless of probe temperature (Figure S 2-3). This likely arises from a more stable dissolution.

In terms of absolute value, the average *DB* in waxy maize (3.96 ± 0.1 %) was lower compared to earlier measurements of another waxy maize (4.76 %) [133].

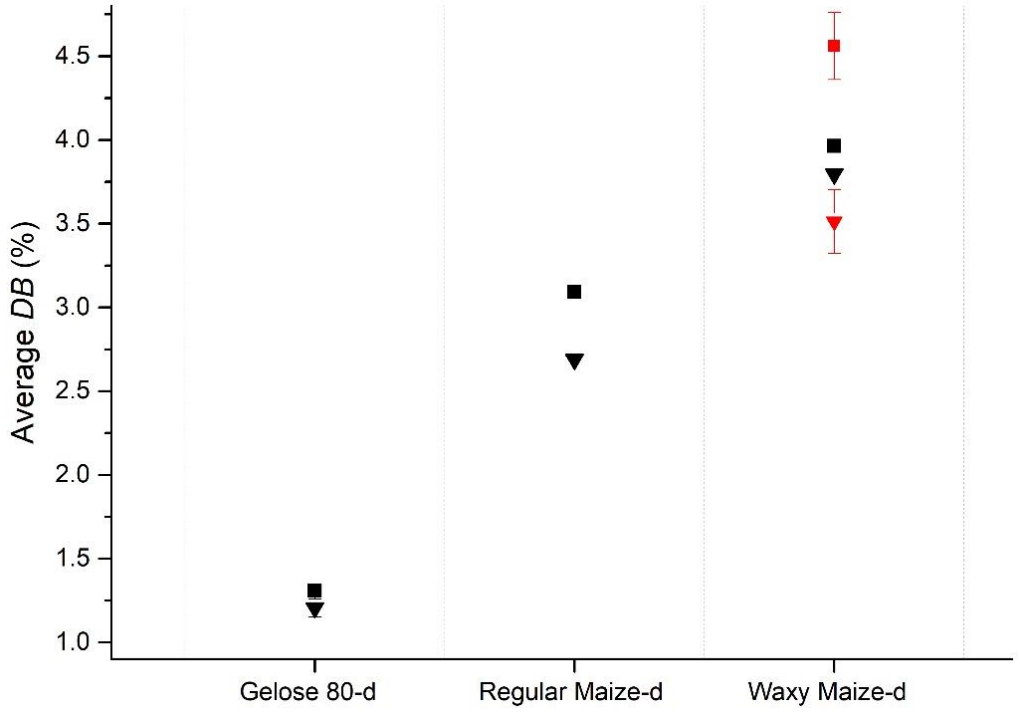

Figure S 2-3 Average degree of branching in standard starch samples, measured at 70 °C (square) and 90 °C (triangle) in 3:1 DMSO-d_6:D_2O with 5 wt% LiBr (black) or 0.05 wt% LiBr (red). Error bars were estimated from the signal-to-noise ratio of the α(1, 6) signal [201]

S 2.5.1.6 Repeatability of sample preparation

The error arising from the preparation of samples in the measurement of average *DB* was assessed using 5 repeat preparations of a single rice sample, from a single glass house (Table S 2-1). This was done to minimise the influence of sampling error arising from differences between samples grown in separate glass houses but at the same temperature. The first measurement was found to be significantly higher than later measurements. This has been attributed to the difference in freeze drying protocol, longer time in D_2O and shorter drying time, as well as the uncontrolled timing of measurement in regard to short term aging that was observed later (S 2.5.1.9). For this reason, the first experiment is considered to be an outlier and is not included in the assessment of repeatability. Given these results, the sample preparation was determined to contribute a relative standard deviation (*RSD*) of 2.6 %.

Table S 2-1 Average *DB* of Doongara rice flour for 5 repeat sample preparations, with freeze drying protocol timing and date of measurement of each preparation

Date	Average *DB (%)*	SNR	Shaking time in D_2O (h)	Freeze-drying (h)	Shaking time in D_2O (h)	Freeze-drying (h)
9/04/2019	4.49	61.9	16.75	7	16.75	5.5
30/04/2019	3.79	77.6	6	16	8	65
4/06/2019	3.72	76.8	8.5	19	6.5	17.5
4/06/2019	3.95	78.3	8.5	19	6.5	17.5
4/09/2019	3.87	75.8	8.5	19	6.5	17.5

S 2.5.1.7 Assessing reliability of average DB through long- and short-term sample aging

The reliability and reproducibility of the *DB* measurement were assessed to determine the robustness. A set of samples were prepared and measured 4 years apart by two different operators, in two separate laboratories due to the relocation of the spectrometer to a new campus, and the average degree of branching calculated from the resulting spectra (Figure S 2-4). The repeated experiments were in good agreement, indicating a high level of reproducibility, as well as a lack of any aging effect on the rice samples in the observed branching structure.

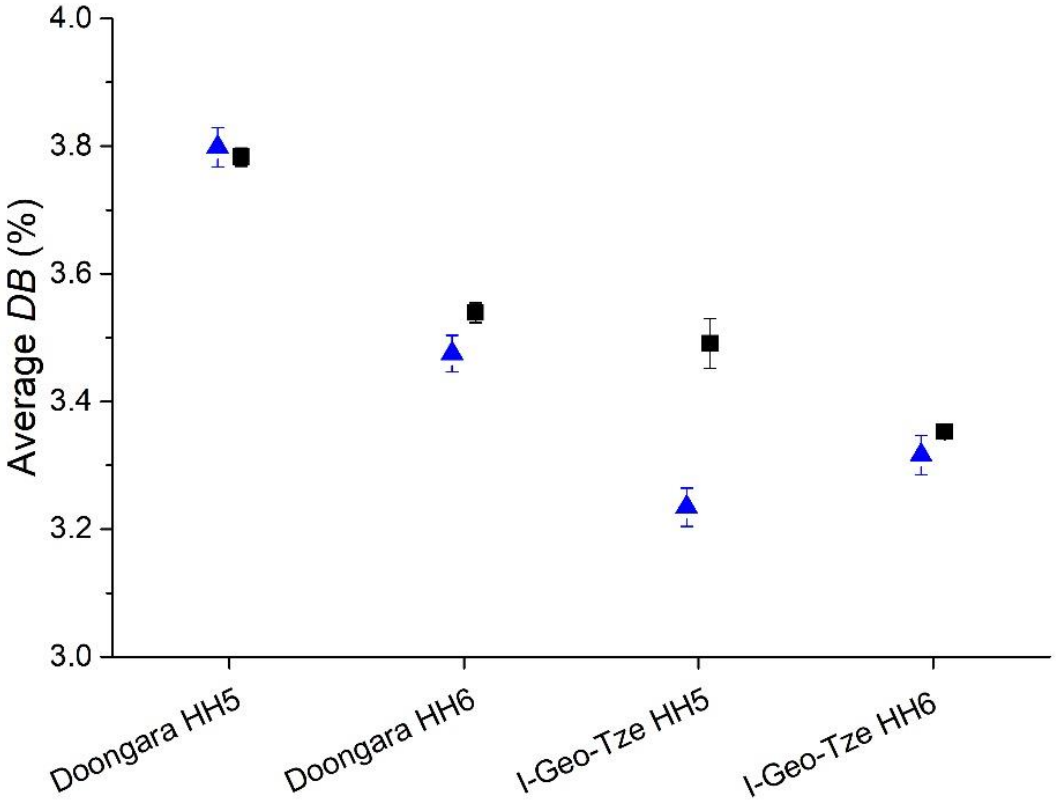

Figure S 2-4 Average degree of branching (%) of rice measured in 2015 (blue triangles) and 2019 (black squares). Error bars were estimated from the signal-to-noise ratio of the α(1, 6) signal [201]. Data points are offset along the x-axis for greater clarity. HHx refers to glasshouse x listed in Table S 2-4

Typically, this type of measurement is only performed on pure or modified starches while, in the current case, rice flours contain lipids and proteins. Thus, the potential for other components to interfere with analysis is an issue. Neither lipids nor proteins yield signals in the same regions as the starch signals used for *DB* quantification; however, other polysaccharides could. Rice flour displayed typical starch signals in the 6.0 to 4.0 ppm range indicating no additional components from other polysaccharides. However, any convoluted signals arising from other polysaccharides would be difficult to isolate and would result in a bias in average *DB* values. Despite this, direct analysis of rice flours is possible for comparative purposes.

S 2.5.1.8 Example spectrum of rice flour and integration regions for calculation of average DB

Figure S 2-5 shows partial spectra of the signals of interest for the calculation of average *DB*. Figure S 2-5A shows the full range of the spectrum with baseline correction for integration of α(1, 4) and α(1, 6) signals while Figure S 2-5B shows the zoomed and baseline corrected spectrum for integration of α and β reducing end signals.

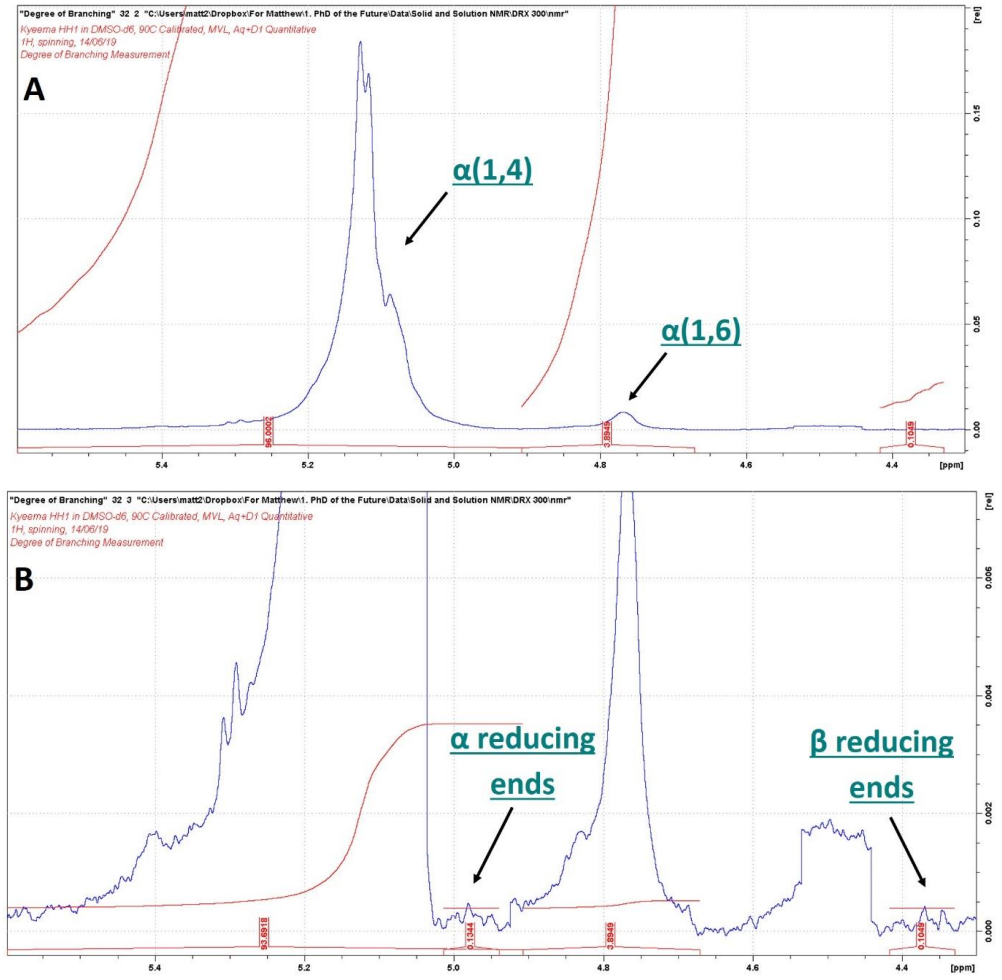

Figure S 2-5 Typical partial 1H NMR spectrum of rice flour with integration regions required for determination of average DB annotated with: A) baseline corrected for integration of α(1, 4) and α(1, 6) signals, and B) baseline corrected for integration of α and β reducing end signals

S 2.5.1.9 Assessing short-term aging contribution of reducing ends

The average *DB* was also monitored over a 24 h period after addition of D_2O and initial measurement (Figure S 2-6A). An immediate increase in the average *DB* was observed after the first hour, subsequently plateauing at ~0.3 % above the initial measurement. Further analysis of the α and β reducing ends revealed a proportional increase with time (Figure S 2-6B). This indicates that the average *DB* increase is likely not a result of chain aggregation, but rather of some degradation process. All data indicate that for measurements taken immediately after addition of D_2O, as done here, the effects of degradation are insignificant.

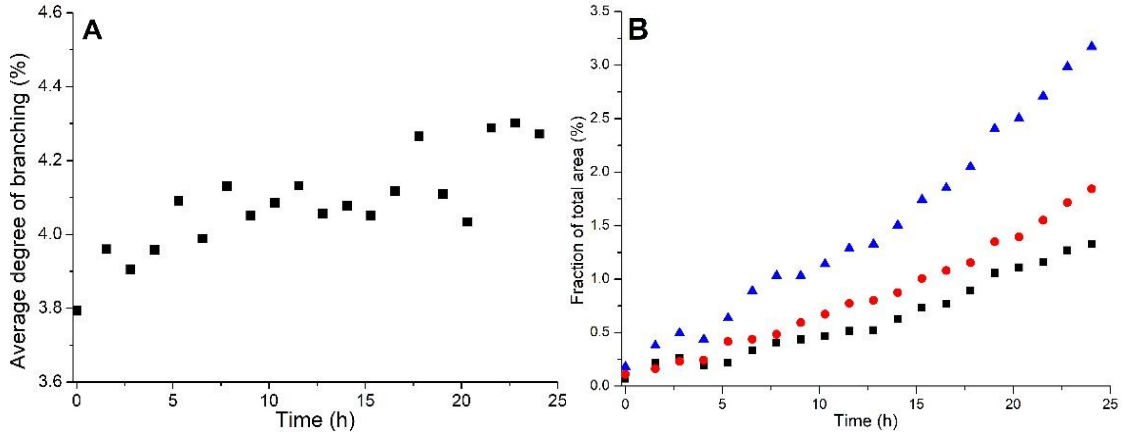

Figure S 2-6 Evolution with time spent in the spectrometer at 90 °C after D_2O addition of a) average *DB* (%) and b) percentage contribution to the total starch signal of α reducing ends (red circles), β reducing ends (black squares) and both α and β reducing ends (blue triangles)

S 2.5.1.10 Values of average DB for waxy flours

Table S 2-2 Values of average *DB* for waxy rice flours. Individual NMR measurements of the hot-water insoluble fraction (HWI) and hot-water soluble fraction (HWS) are reported; HWx-1 and HWx-2 refer to repeat fractionation of the flour. n.d. refers to 'not determined'

Variety	*Average DB (%), HWI-1*	*Average DB (%), HWI-2*	*Average DB (%), HWS-1*	*Average DB (%), HWS-2*
Phae Savan	4.80	4.93	4.75	5.10
Laboun	4.61	4.35	5.20	5.03, 4.98, 5.07, 4.98, 4.95
Med Gnay	4.40	4.42	n.d.	5.00
Makfay	4.59	4.44, 4.54, 4.52, 4.35, 4.52	4.83 (for mixed sample of HWS-1+HWS-2)	
Hom	4.42	4.43	n.d.	4.92, 4.94

Table S 2-3 Values of average *DB* by ^1H NMR for different types of waxy starch samples

Type of waxy starch	*Average DB (%)*
Waxy maize starch	5.00 [133], 3.80 [212], 5.26 [213]
Potato amylopectin	4.35 [133], 3.6 [214], 4.07 [195]
Tapioca amylopectin	5.71 [133]
Corn amylopectin	4.77 [195]

S 2.5.2 Apparent amylose content by iodine binding

S 2.5.2.1 Consistency of apparent amylose content (AAC) over time

The *AAC* of the samples in this work was originally measured in 2015 in the conditions cited in the methods section 2.2.3.1. To confirm samples had not aged at the molecular level, the *AAC* was remeasured 3 years later on 3 varieties, including four glasshouses each. Due to changes in instrument, methodology and operators, the 2018 measurements also give an indication of the reproducibility of the *AAC*. The original values (2015) and remeasured values (2018) are shown in Table S 2-4. One apparent outlier was the I-Geo-Tze variety in glasshouse 5, with a 19.1 % relative difference in *AAC*, the remaining samples had an average relative difference of 6.8 %.

Table S 2-4 *AAC* for different varieties grown in different glasshouses initially measured in 2015 then remeasured in 2018

Variety	Glasshouse	AAC (%) (2015)	AAC (%) (2018)	Difference (%)
Kyeema	Glasshouse 1 - Low Temp	19.63	20.61	4.9
Doongara	Glasshouse 1 - Low Temp	25.39	27.53	8.1
I-Geo-Tze	Glasshouse 1 - Low Temp	27.48	29.36	6.6
Kyeema	Glasshouse 3 - High Temp	14.58	15.70	7.4
Doongara	Glasshouse 3 - High Temp	16.76	17.79	6.0
I-Geo-Tze	Glasshouse 3 - High Temp	28.27	29.60	4.6
Kyeema	Glasshouse 5 - High Temp	14.89	15.92	6.7
Doongara	Glasshouse 5 - High Temp	18.64	19.87	6.4
I-Geo-Tze	Glasshouse 5 - High Temp	26.72	32.38	19.1
Kyeema	Glasshouse 6 - Low Temp	19.22	20.37	5.8
Doongara	Glasshouse 6 - Low Temp	24.38	26.31	7.6
I-Geo-Tze	Glasshouse 6 - Low Temp	26.01	28.96	10.7

S 2.5.3 Characterisation of lamellar structure by small angle X-ray scattering

S 2.5.3.1 Fitting of small angle X-ray scattering data

Scattering curves of rice flour samples were iteratively fitted with a power law function to describe the underlying small angle scattering (where β is the power law prefactor and α is the power law exponent) plus a Gaussian/Lorentzian function and a second Gaussian function to describe both the starch primary lamellar and secondary peaks (position, $q_{\max}$; Intensity, $I_{\max}$; full width at half maximum, Δq).

$$I(q) = (r(I_{\max 1}(1 + A_1)^{-1}) + (1 - r)I_{\max 1}A_2) + I_{\max 2}A_3 + (\beta q^{-\alpha}) \qquad \text{Equation S 2-1}$$

$$A_1 = \left[\frac{2(q - q_{\max 1})}{\Delta q_1}\right]^2 \qquad \text{Equation S 2-2}$$

$$A_2 = \left[e^{-\left(\frac{q-q_{max1}}{\Delta q_1}\right)^2}\right] \quad \text{Equation S 2-3}$$

$$A_3 = \left[e^{-\left(\frac{q-q_{max2}}{\Delta q_2}\right)^2}\right] \quad \text{Equation S 2-4}$$

Where, q is the modulus of the scattering vector equal to $(4\pi/\lambda)\sin\theta$ where λ is the X-ray wavelength (0.1542 nm) and 2θ is the scattering angle. r is the ratio of Lorentzian to Gaussian characteristics to the primary peak.

Figure S 2-7 shows an example scattering curve of a rice flour and its fit overlaid (red) after iterative calculation to minimise chi-squared.

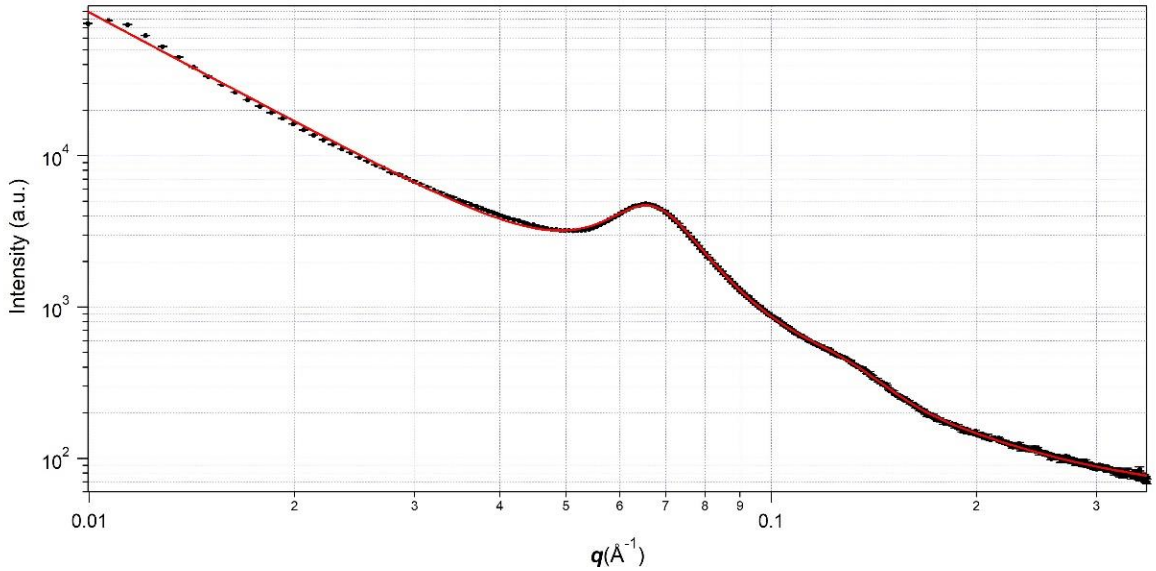

Figure S 2-7 Small angle X-ray scattering curve of Cocodrie rice flour grown at a higher temperature (black crosses) with an iteratively calculated fit with equation S1 (red line)

The real space lamellar repeat distance was calculated from the peak position by equation S 2-5. HWHM maximum was converted to real space units by equation S 2-6.

$$\text{Average repeat distance (real space)} = \frac{2\pi}{q_{max}} \quad \text{Equation S 2-5}$$

$$\text{HWHM (real space)} = \frac{2\pi}{{q_{max}}^2} \times \frac{\Delta q}{2} \quad \text{Equation S 2-6}$$

S 2.5.3.2 Relationship of peak intensity with AAC and average DB

A general trend of decreasing lamellar peak intensity with increasing amylose content has been reported in the literature [148]. This has been explained by the accumulation of defects within the lamellar structure. A similar trend was observed in the rice samples in this study, with the data shown in Figure S 2-8.

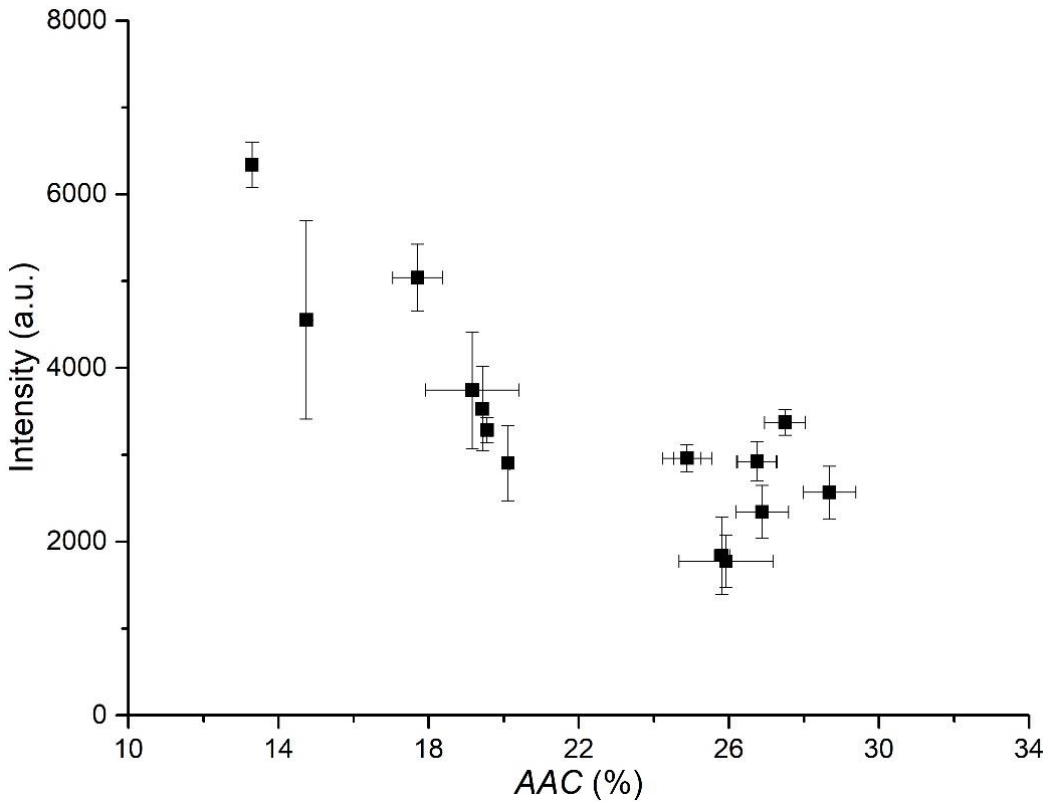

Figure S 2-8 Relation between SAXS peak intensity and *AAC* for rice flours of different varieties grown at lower or higher temperatures. SAXS peak intensity error bars represent the standard error of 6 values (2 independent replicates of temperature, 3 preparations for each replicate). *AAC* error bars represent the standard error of 4 values (2 independent replicates of temperature, 2 instrument readings for each). See Table S5 for individual *AAC* and average *DB* values

The peak intensity and average *DB* were loosely correlated, indicating an increased extent of semi-crystalline order with increasing average *DB* (Figure S 2-9). However, given the poor correlation, it is unlikely that the branching frequency is the primary driver for changes in the extent of semi-crystalline order. It is possible that other aspects of the branching structure such as chain length distribution play a larger role, thus peak intensity and average *DB* are both relevant in reporting on different aspects in the overall starch structure.

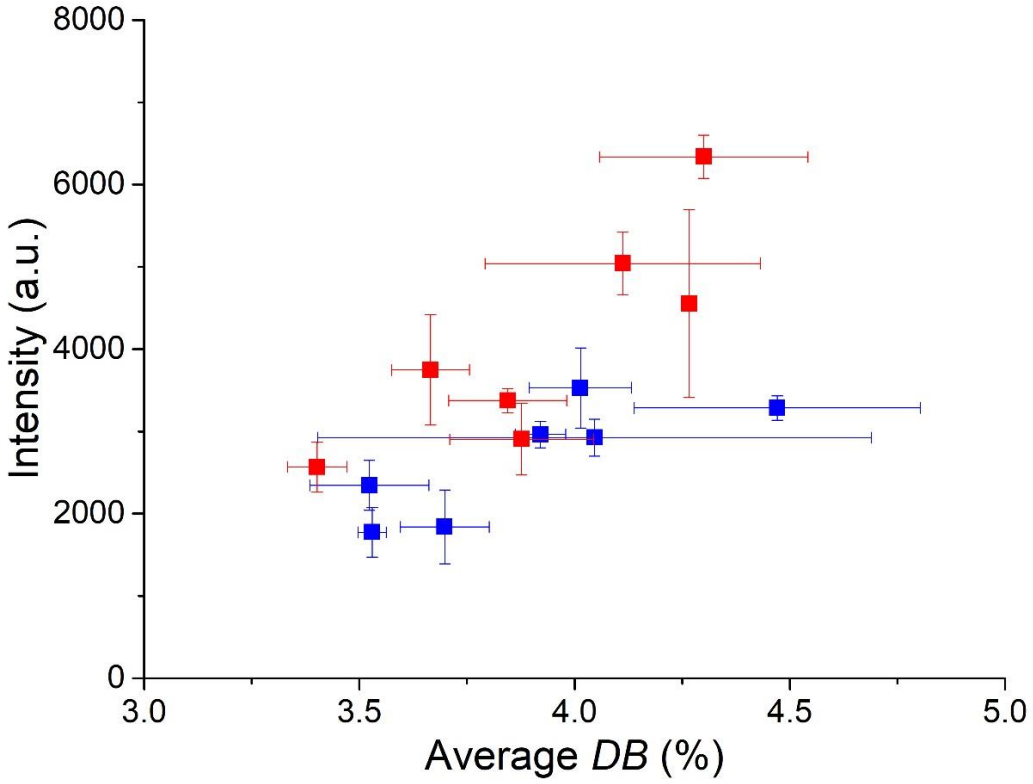

Figure S 2-9 Relation between SAXS peak intensity and average *DB* for rice flours of different varieties grown at lower (blue diamonds) or higher (red triangles) temperatures. SAXS peak intensity error bars represent the standard error of 6 values (2 independent replicates of temperature, 3 preparations for each replicate). Average *DB* error bars represent the standard error of 2 values (2 independent replicates of temperature). See Table S5 for individual *AAC* and average *DB* values

S 2.5.3.3 Relationship of repeat unit thickness with HWHM

The HWHM and lamellar repeat thickness are positively correlated (Figure S 2-10). This was previously observed on extracted starches of various botanical origin and thought to be due to a conserved distribution of lamellar sizes limited by the minimum number of glucose units (degree of polymerisation of 10-12) required to form a helix [151].

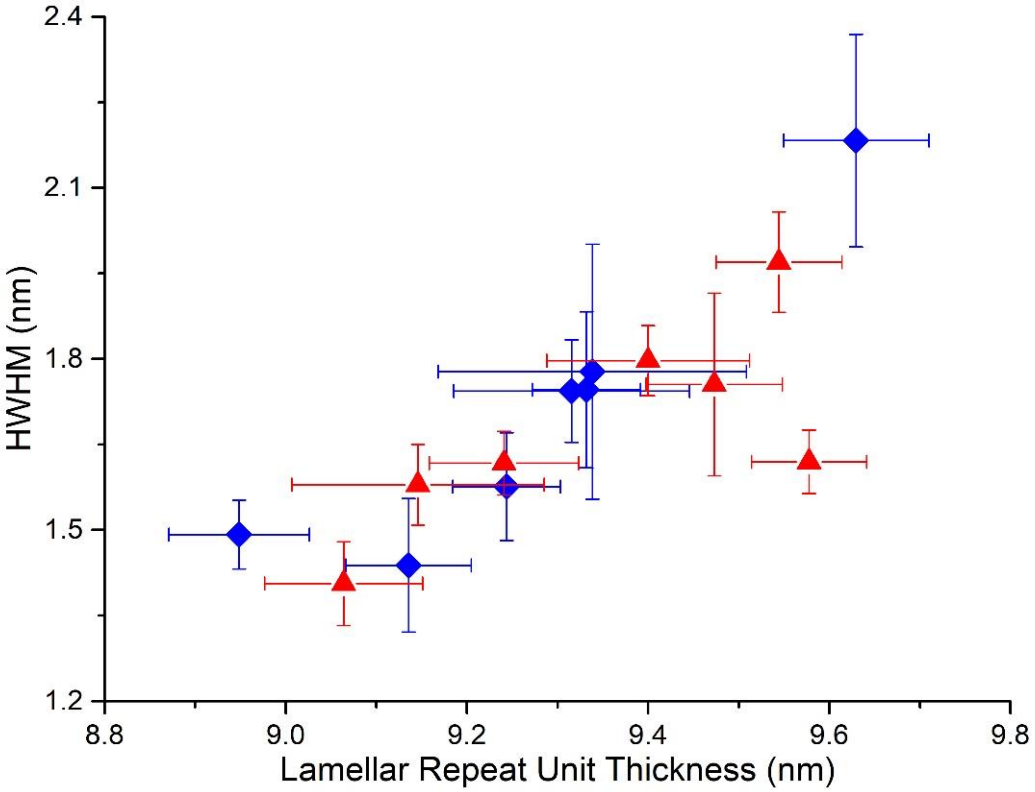

Figure S 2-10 Relation between HWHM and lamellar repeat unit thickness for rice flours of different varieties grown at lower (blue diamonds) or higher (red triangles) temperatures. Error bars represent the standard error of 6 values (2 independent replicates of temperature, 3 preparations for each replicate)

S 2.5.4 Mean values of AAC, average DB, SAXS intensity of main lamellar peak, SAXS lamellar repeat unit thickness, SAXS half-width half-maximum (HWHM) of main lamellar peak

Table S 2-5 Individual values of *AAC*, average *DB,* SAXS intensity of main lamellar peak, SAXS lamellar repeat unit thickness, SAXS half-width half-maximum (HWHM) of main lamellar peak. Mean values are reported for samples grown at lower and higher temperatures, with their standard error (Std error) for 4 measurements for *AAC* (2 independent replicates of temperature, 2 instrument readings for each), 2 measurements for average *DB* (2 independent replicates of temperature), 6 measurements for SAXS (2 independent replicates of temperature, 3 preparations for each)

Variety	*AAC (%)*		*Average DB (%)*		*SAXS peak intensity (a.u.)*		*SAXS thickness (nm)*		*SAXS HWHM (nm)*	
	Mean	*Std error*	*Mean*	*Std error*	*Mean*	*Std error*	*Mean*	*Std error*	*Mean*	*Std error*
Cocodrie, lower T	26.88	0.01	3.52	0.14	2344	305	9.33	0.02	1.75	0.06
Cocodrie, higher T	28.68	0.70	3.4	0.07	2568	302	9.47	0.03	1.70	0.06
I-Geo-Tze, lower T	26.75	0.52	4.05	0.64	2924	226	9.24	0.02	1.58	0.04
I-Geo-Tze, higher T	27.50	0.54	3.84	0.14	3376	148	9.4	0.05	1.74	0.02
IR64, lower T	25.92	0.06	3.53	0.03	1773	302	9.34	0.07	1.78	0.09
IR64, higher T	19.16	1.25	3.67	0.09	3746	671	9.24	0.03	1.65	0.02
IR55419-04, lower T	25.81	0.20	3.70	0.10	1840	449	9.63	0.03	2.18	0.08
IR55419-04, higher T	20.11	0.05	3.88	0.17	2904	436	9.54	0.03	2.01	0.04
Doongara, lower T	24.88	0.36	3.92	0.06	2961	160	9.14	0.03	1.44	0.05
Doongara, higher T	17.70	0.67	4.11	0.32	5041	382	9.15	0.06	1.58	0.03
Quest, lower T	19.56	0.13	4.47	0.33	3284	147	9.32	0.05	1.74	0.04
Quest, higher T	13.29	0.09	4.3	0.24	6338	262	9.58	0.03	1.53	0.02
Kyeema, lower T	19.43	0.14	4.01	0.12	3529	486	8.95	0.03	1.49	0.02
Kyeema, higher T	14.74	0.11	4.27	0	4552	1141	9.06	0.04	1.37	0.03

S 2.5.5 Fourier transform infrared spectroscopy at cryogenic temperatures

S 2.5.5.1 Materials and Methods

FTIR spectroscopy was performed on a Bruker Vertex 70 spectrometer. All spectra were acquired with 64 scans, at a resolution of 1 cm^{-1} in a transmission mode arrangement using a Specac variable temperature cell holder under vacuum. Samples were pressed into KBr pellets with a sample concentration of 2 wt% (200 mg total mass). Powder for pressing was prepared by combining sample and KBr powder and grinding together into a fine powder using an agate mortar and pestle. The powder was then transferred to the die and spread with light tapping. Pellets were pressed using a PIKE Technologies CrushIR digital hydraulic press. The pressure sequence was: 3 tonnes followed by immediate release, 7 tonnes for 30 s, then ramp from 7 to 10 tonnes and hold for 2 min. Pressed pellets were analysed on the day of pressing and stored in a desiccator until analysis.

Three types of commercial maize starches with different amylose contents: waxy maize (3.4 % amylose), regular maize (24 % amylose) and Gelose 80 (83 % amylose) [118] were from Penford Australia Limited (Lane Cove, NSE, 2066, Australia). All starch samples were conditioned to 44 % relative humidity for at least 1 week prior to analysis. Sample environments at 44 % relative humidity was created by placing a saturated solution of potassium carbonate (K_2CO_3) in a desiccator [215].

All spectra were processed with Bruker OPUS 7.5 [216]. All FTIR spectra were baseline corrected by 1 step (minimum amount) in the software's interactive mode using a rubber band based correction algorithm. All FTIR spectra were then normalised to an absorbance range of 0 to 2.0 based on min-max calculations.

S 2.5.5.2 Effects of cryogenic temperatures on FTIR spectra

Cryogenic temperatures have been used widely over the life of infrared technology, across an extremely broad range of applications, and leading to data exhibiting reduced peak width and improved resolution [210, 217]. This has been explained by weaker intermolecular interactions and lower intensity of bands corresponding to excited-state energy levels [218-220].

Figure S 2-11 displays the FTIR spectra of the three model starches at both 25 °C and -170 °C. Slight improvements in resolution were noted for all three starch samples; however, these improvements were minimal and still did not result in clearly resolved signals. As a result, the investigation of crystalline order by FTIR spectroscopy was not explored in this work.

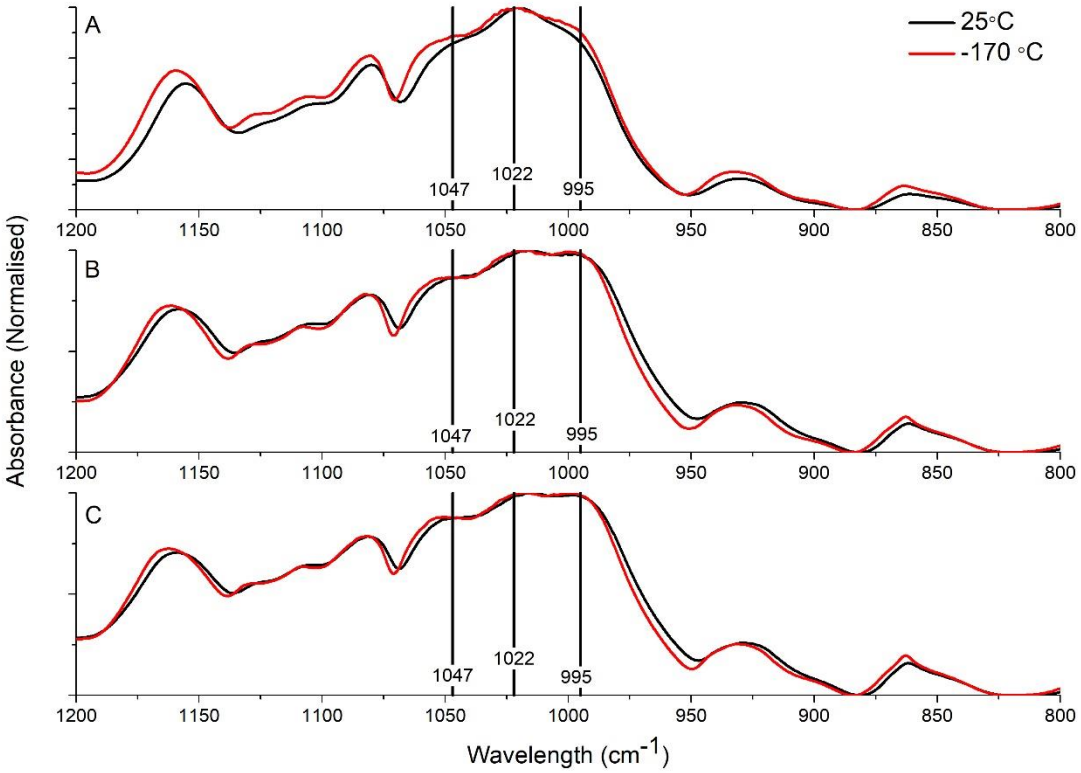

Figure S 2-11 Transmission mode FTIR spectra of A) Gelose 80, B) Regular maize and C) Waxy maize, conditioned at 44 % relative humidity and measured at different temperatures. Bands of interest are noted by vertical black lines and labelled with the wavelength

Chapter 3 Separation of amylose and amylopectin using capillary electrophoresis - Manuscript

Prepared for submission to Analytical and Bioanalytical Chemistry

Separation of amylose and amylopectin using capillary electrophoresis

Matthew P. Van Leeuwen [a,b], Joel J. Thevarajah [a], Rachelle Ward [c], Marianne Gaborieau [a*], Patrice Castignolles [a]

[a] Western Sydney University, Australian Centre for Research on Separation Science, School of Science, Parramatta Campus, Locked Bag 1797, Penrith, NSW 2751, Australia

[b] Western Sydney University, School of Medicine, Campbelltown Campus, Locked Bag 1797, Penrith, NSW 2751, Australia

[c] Yanco Agricultural Institute, NSW Department of Primary Industries, Yanco, Australia

*Corresponding Author – Dr Marianne Gaborieau, Western Sydney University, Australian Centre for Research on Separation Science, Parramatta Campus, Locked Bag 1797, Penrith, NSW 2751, Australia. Tel.: +61 2 9685 9905; Fax: +61 2 9685 9915; e-mail: m.gaborieau@westernsydney.edu.au

Abstract

Amylose content is recognized as a key molecular feature of starch and is commonly used in agriculture (breeding programs, grain quality), food and nutrition (relation with glycaemic index) or materials science (paper coating, bioplastics). There is, however, no method yet with high accuracy for the determination of amylose content, with reproducibility strongly dependant on standards and methodology and no established standards. Last but not least, amylose (and amylopectin) consist of thousands of different macromolecules. Iodine-affinity capillary electrophoresis (IA-CE) was shown in this work to separate amylose from amylopectin (in two populations) and also to separate the amyloses and amylopectins into continuous and broad distributions of electrophoretic mobilities. Distributions of electrophoretic mobilities were used rather than raw electropherograms as the former are more repeatable and reproducible. One key advantage of IA-CE is the minimal sample preparation. IA-CE does not require sample filtration, something typically required in liquid chromatography methods. Comparison of filtered and unfiltered samples showed that starch filtration can lead to massive sample loss and thus very poor accuracy of any measurement requiring filtration. Reducing sample concentrations also limits sample loss. Maximising starch dissolution requires the use of dimethyl sulfoxide with additional lithium bromide in more challenging cases such as high amylose starches. IA-CE was

shown to separate amylose and amylopectin even in these conditions. An *in-situ* incubation time with iodine was tested for the first time and is shown to be required to allow for complete starch-iodine binding. IA-CE shows a strong potential for alternative measurements of amylose content.

Keywords

starch, amylose, amylopectin, dissolution, iodine, capillary electrophoresis

3.1 Introduction

Starch is a highly abundant biopolymer, acting as the primary energy storage in plants and used widely in a variety of industrial applications other than food such as paper [221] and biodegradable plastics [222]. Starch is comprised of two macromolecular components: amylose and amylopectin. These glucose homopolymers are compositionally identical but differ in their branching structure and their role in the semi-crystalline structure of native starch. Amylose forms a minor component of starch in plants and exhibits only a few long branches [22]. Amylopectin represents the major component of most starches. Amylopectin differs from amylose primarily in the degree of branching and length of branches, with smaller branches occurring approximately every 24 glucose units [22].

The branching structure of starch and the relative proportions of amylose and amylopectin in starch play an important role in the supramolecular structure of starch and influence many of starch's physicochemical properties. The amylose content can influence properties [35] such as solubility [223], gel formation [224], digestibility [26] and texture [225, 226], all important measures in the quality of food products. Structural characteristics such as molar mass distribution and heterogeneity of branching can also have an impact on these physicochemical and mechanical properties [70, 224, 227]. This highlights the importance of accurate and robust methods for the characterisation of starch structure as tools for assessing the properties of starches and by extension starch containing products.

Colorimetric approaches are currently the most popular methods to quantify amylose content due to their simple methodology, high repeatability and availability of standard methods [74, 204, 228]. This relies on the well-documented ability of starch to form a complex with polyiodides in solution characterised by strong absorption of visible light. Amylose- and amylopectin-iodine complexes have different colorimetric profiles with absorption maxima at 620 and 540 nm, respectively [72]. The overlap of these broad absorption bands results in overlapping absorption bands which commonly causes interference in colorimetric methods [229], and thus can lead to overestimation of the amylose content. As a result, correction processes are required such as multi-wavelength processing [75]. Sample preparation for the colorimetric approaches always requires several steps and these steps differ between publications and standards [74, 75, 80].

After sample "dissolution" filtration or centrifugation are commonly used to avoid interferences due to light scattering by aggregates [84, 230], but the impact of the sample preparation is usually not discussed. The repeatability of apparent amylose content (*AAC*) in rice flours has been reported to be high, with reproducibility being poor and dependent on methodology and standards [73].

A major hurdle in the starch preparation is the complete dissolution of starch and flours without degradation. DMSO is the most frequently used polar aprotic solvent in the dissolution of starch [223, 224], with the both the kinetics and extent of dissolution quantified in the literature [78, 79]. Aqueous solvents such as NaOH are also popular, commonly employed in the determination of *AAC* for starches and flours. However, dissolution has not been quantified with this solvent, with dissolution typically assessed based on solution 'transparency'. Solution transparency for starch suspensions has been shown to not always be indicative of complete dissolution [79].

DMSO/water mixtures are commonly used (as in the pioneering work of Herrero-Martínez, Schoenmakers [109] on iodine-affinity capillary electrophoresis), with the addition of water thought to speed the dissolution of starch granules. It was shown by time-resolved NMR spectroscopy that the actual dissolution (rather than gelatinization of starch) occurs faster in anhydrous DMSO than in hydrated DMSO [78]. The use of water as a solvent, and its addition to other solvents is known to produce unstable solutions, with significant precipitation of the starch common [231]. To minimise this random precipitation, water as part of the solvent is avoided for reproducible dissolution in this study.

Temperature also plays an important role in the rate and extent of dissolution, with increasing temperatures improving the rate of dissolution in both anhydrous and 'wet' DMSO [78]. Addition of a hydrogen bond disruptor can further improve the dissolution of dense amylose structures in starch where hydrogen bonding and clustering [202] impedes dissolution. Lithium bromide is one such salt that has successfully been shown by quantitative NMR spectroscopy to improve the extent of dissolution of high amylose starches, increasing the extent of dissolution by up to 15 % [79].

The colorimetric (iodine binding) method is however, not performed in anhydrous DMSO with lithium bromide in the literature. For solubility reasons, it would be ideal to use only DMSO with lithium bromide. The formation of polyiodide ions (I_3^-) necessary for starch-iodine complexation has been shown in DMSO/water solutions [71] though the addition of lithium bromide is likely to inhibit starch-iodine complexation while water will likely impact dissolution.

Amylose is one of the two populations in starch; however, it still represents thousands of different molecules. This can be seen in molecular weight distributions of amylose, where the

ranges of molecular weight can already indicate >14,000 different amylose molecules based on just degree of polymerisation [232]. Thus, the physical separation of starch, both amylose and amylopectin, has been extensively attempted. Size-exclusion chromatography (SEC/GPC) can however, not fully resolve the amylose population from amylopectin [90], while field flow fractionation does [98]. Samples are commonly filtered prior to analysis, particularly in cases where light scattering may occur, interfering with light-based detection (ultraviolet, refractive index or light scattering) [230]. In the case of starch this presents a problem in terms of obtaining a filtered sample that is representative of the original one. A robust separation technique for which sample filtration is not required is free solution capillary electrophoresis (CE) [103, 105, 203]. The resilience of fused-silica capillaries also allows for a broad range of solvents and cleaning solutions to be used without negatively impacting the system.

The separation of amylose and amylopectin by iodine-affinity capillary electrophoresis (IA-CE) has been reported [109, 167]. In IA-CE the separation of amylose from amylopectin is due to differences in their iodine binding capacity which leads to a difference in the effective charge experienced, allowing separation by their charge-to-friction ratio. This method enables the complete separation of amylose from amylopectin, and thus quantification of the individual components, removing the absorbance interference seen in traditional colorimetric approaches.

In this work, separation of amylose and amylopectin in starches of different biological origins was achieved by IA-CE with careful consideration of sample preparation: dissolution conditions, concentration or filtration. Through optimisation of dissolution conditions, reproducible characterisation is possible thus providing more information with which to aid the development of quality traits in food processing.

3.2 Materials and Methods

3.2.1 Materials

Milli-Q® quality (Millipore, Bedford, MA, USA) water was used throughout the analysis. Sodium hydroxide (NaOH) pellets, glacial acetic acid, and anhydrous sodium acetate were sourced from Ajax Chemicals (Auburn, NSW, Australia). Boric acid (≥ 98 %) was purchased from BDH AnalaR, Merck Pty Limited. Analytical grade potassium iodide was obtained from Chem-Supply Pty Ltd (Gillman, SA, Australia). Analytical grade iodine was obtained from Univar (Downers Grove, IL, USA). Dimethyl sulfoxide (DMSO, ≥ 99.5 %), DMSO-d_6 (≥ 99.5 %), and lithium bromide (LiBr, ≥ 99 %) (all stored in a desiccator) were sourced from Sigma-Aldrich (Castle Hill, NSW, Australia). Millipore Millex-LCR hydrophilic poly(tetrafluoro ethylene) PTFE 0.45 μm filters (for sample filtration) and poly(ether sulfone), PES 0.22 μm filters (for buffer filtration) were sourced from Millipore (Bedford, MA, USA).

Two types of commercial maize starches were obtained in powder form from Penford Australia Limited (Lane Cove, NSW, Australia): waxy maize (3.4 % amylose) and Gelose 80 (83 % amylose) [118]. The apparent amylose content reported by Tan, Flanagan [118] was determined by a spectrophotometric iodine binding method. Waxy corn (S9679, batch: SLBJ1581V), potato amylose (A0512, batch: 070M7025V), potato amylopectin (A8515, batch: 049K3775V), corn (S4126, batch: MKBQ4397V) and rice starches (S7260, batch: BCBP5455V) were obtained from Sigma Aldrich in powder form (Castle Hill, NSW, Australia).

3.2.2 Sample preparation

Samples were stored at room temperature, 44 % relative humidity in a desiccator containing a saturated solution of potassium carbonate [215], and left for moisture content to equilibrate for at least a week prior to dissolution and analysis. Samples were prepared by one of two dissolution methods and modified as discussed in the results. The first employs the dissolution conditions of Herrero Martinez et al. [109], with samples prepared at a concentration of 10 $g \cdot L^{-1}$ in 90 % DMSO (10 % water by volume) and heated to 100 °C for 1 hour. This is referred to as the conditions of Herrero-Martinez et al. The second employs the dissolution conditions of Schmitz et al. [79] with a modified sample concentration. Samples were prepared at a concentration 1 $g \cdot L^{-1}$ in anhydrous DMSO containing 0.05 to 5.0 % w/v LiBr (where specified) and heated to 80°C with shaking at 300 rpm in an Eppendorf Thermomixer C (North Ryde, NSW, Australia) for at least 8 hours unless otherwise indicated. This is referred to as the conditions of Schmitz et al. All results shown in this manuscript are obtained from samples which gave clear and transparent "solutions".

3.2.3 Iodine-affinity capillary electrophoresis and pressure mobilisation

For CE separations, 20 mM acetic acid buffer (7.3 mM acetic acid and 12.7 mM sodium acetate, pH 5.0) with 7.2 mM potassium iodide and 1.2 mM iodine metal was prepared according to Herrero-Martínez, Schoenmakers [109] and 25 mM sodium borate buffer (pH 9.2) was prepared according [233]. The acetic acid buffer was prepared on the day of use, and sonicated for 5 min to ensure complete dissolution of iodine and degassing, and then filtered. The 1M NaOH was prepared and used within 24 h.

Experiments were performed on an Agilent 7100 (Agilent Technologies Waldbronn, Germany) with a Diode Array Detector (DAD) monitoring at 560 nm with a bandwidth of 20 nm. The total capillary length was 37.0 cm (28.5 cm effective length), using fused-silica capillaries including a standard capillary (75 μm i.d., Polymicro, Phoenix, AZ, USA) and an extended light-path capillary (75 μm i.d., bubble factor 2.7, Agilent Technologies Waldbronn, Germany). The capillary was preconditioned before use by flushing with 1 M NaOH (4 min), 0.1 M NaOH (4 min), water (4 min) and acetic acid buffer (12 min). All injections were preceded by flushing with 1 M NaOH for 24 s

(82 % capillary volume) and running buffer for 2 min. Samples were injected hydrodynamically by applying 17 mbar of pressure for 4 s (0.25 % capillary volume) followed by the injection of running buffer by applying 5 mbar of pressure for 5 s. All separations were performed at 20 kV (ramped from 0 kV over 1 min) and 25 °C, with samples kept at 80°C until placed in an autosampler at room temperature just before injection (<1 min), unless otherwise specified. All measurements had a total separation time of 15 min (applied electric field) and were performed in triplicate from a single sample preparation. Data was acquired using Chemstation A10.01 and data treatment conducted with OriginPro 9.0. Raw electropherograms were transformed into weight distributions of electrophoretic mobilities as shown in supplementary material (equations S 3-1 to S 3-6), with the electroosmotic flow determined at a wavelength of 560 nm. Average electrophoretic mobilities were calculated according to equations S 3-7 and S 3-8. The distributions were not normalised to allow for investigation into differences in peak areas in relation to concentration.

The CE hardware and capillary were validated before each experiment through the separation of a standard oligoacrylate solution in sodium borate buffer [113, 234]. The standard was qualitatively compared to previous separations for repeatability of electro-osmotic flow and mobility of oligoacrylate species (S 3.5.4).

Pressure mobilisation experiments were carried out in an identical fashion to CE separations up to the sample injection. After the sample injection, an internal pressure of 13 mbar was continuously applied, with initial mixing of the sample with the buffer through the application of voltage (ramping up to 20 kV over 1 min, then ramping down to -20 kV over 2 min then ramping up to 0 kV over 1 min) [203].

3.2.4 ^{1}H solution state nuclear magnetic resonance spectroscopy

Samples were prepared at a concentration of 1 $g \cdot L^{-1}$ in anhydrous DMSO-d_6 with 0.5 % w/w LiBr unless otherwise stated. A setup sample was prepared by dissolution in a glass vial using a thermomixer at 80 °C and 300 rpm for at least 8 hours. The sample was then inserted into the preheated NMR probe (80 °C) and allowed to equilibrate for 10 minutes before setup. Locking, shimming and tuning of the probe were performed on this setup sample.

Samples for dissolution kinetics were prepared by weighing sample directly into the NMR tube. Once the solvent was added, the tube was inserted into the preheated probe (80 °C) and recording of spectra immediately started. Samples for filtration experiments were prepared in the same way as the setup sample, followed by filtration of the sample with a 0.45 µm hydrophilic PTFE filter immediately prior to measurement. Lock, shim and tuning parameters from setup samples run the same day were in place for each test sample.

Measurements were performed with a Bruker DRX300 spectrometer (Bruker BioSpin Ltd, Sydney) equipped with a 5mm dual $^{1}H/^{13}C$ probe at Larmor frequency of 300.15 MHz. ^{1}H NMR spectra were recorded using a 5000 Hz spectral width, 90° flip angle and were acquired at a temperature of 80 °C. The probe temperature was calibrated using ethylene glycol (80 % in DMSO-d_6) and equation 3-1 [192],

$$T = \frac{(4.218 - \Delta\delta)}{0.009132} \qquad \text{Equation 3-1}$$

Where T is the sample temperature in Kelvin and $\Delta\delta$ is the difference in ppm between the CH_2 and OH singlets.

Spectra were recorded and treated using Topspin software. Longitudinal relaxation times (T_1) of the signals of interest were estimated using the one-dimensional inversion recovery pulse sequence (S 3.5.7). Quantitative spectra were recorded with a 20 s repetition delay, which is longer than 5 times T_1 for the signals of interest. Non-quantitative spectra were recorded with a 10 s repetition delay where specified (this provided enough relaxation between scans to observe more than 90 % of the total signal intensity). The chemical shift scales were calibrated with respect to the signal of DMSO at 90 °C (2.526 ppm) [193].

Dissolution kinetics and effects of filtration were assessed through the integration of starch signals in the range of 6 to 4 ppm, correlating to CH groups. These integrals are indicative of the amount of starch in solution and used here to qualitatively assess differences in the amount of starch present.

3.3 Results and Discussion

3.3.1 Impact of dissolution on separation of amylose and amylopectin

Complete dissolution of the sample is required for a meaningful and reproducible separation and characterisation of amylose and amylopectin in starch. Here the concentration, filtration and temperature conditions were explored, as well as a direct comparison of the dissolution conditions of Herrero-Martinez et al. [23] to Schmitz et al. [20]. While dissolution is discussed in this work, the extent of dissolution was not quantified.

3.3.1.1 Concentration

Aggregation is a major problem in solutions of very large polymers and is linked to their low 'critical concentration' (C^*). Below C^* the solution is dilute and individual macromolecules do not significantly interact [235]. Above C^* the domains occupied by polymer molecules in solution begin to overlap and macromolecules begin interacting with each other. In some cases, this overlap can result in aggregation or precipitation. In this study, the impact of sample concentration on the separation of amylose and amylopectin by the otherwise unmodified method

of Herrero-Martinez et al. [109] was explored, with a maximal reported concentration of 10 g·L^{-1}. This was compared to a concentration of 1 g·L^{-1}, a 10-fold decrease expected to have an observable impact.

Samples prepared at both 1 and 10 g·L^{-1} in 90 % aqueous DMSO exhibited large sharp peaks on the amylopectin peak (Figure 3-1A). In CE these large sharp peaks are typical of light scattering effects caused by large particles, and thus are likely due to the presence of aggregates [236]. This is typically a result of incomplete dissolution, thus may be a by-product of the dissolution conditions of Herrero-Martinez et al. [109]. An apparent shift of the amylose mobility at the peak maximum at 1 g·L^{-1} suggest a difference in amylose detected, indicative of some differences in the dissolution. This is supported by an apparent 23 % greater amylose peak area at 1 g·L^{-1} than at 10 g·L^{-1} despite the lower concentration of starch (Figure 3-1A). However, this shift may also arise due to other factors. The first is altered starch/iodine ratios leading to a change in the net charge of the iodine complexed amyloses, while the second is through possible differences in injection volume impacting on peak shapes. The experiments in this work cannot confirm or disprove these suggestions.

Y-axis of the electropherograms at 1 g·L^{-1} were multiplied by a factor of 10 to compare to the experimental 10 g·L^{-1} data (Figure 3-1B). The disparity in relative peak area of amylose and amylopectin was large, with larger peak areas for amylose and amylopectin in the scaled 1 g·L^{-1} results compared to 10 g·L^{-1} results. This disparity could be due to differences in injection volumes, differences in solubility or to non-linear relation between peak area and concentration. Herrero-Martinez et al. [109] obtained a linear calibration curve up to only 5 g·L^{-1}, therefore at higher concentrations it is possible that this relationship is non-linear. No significant differences in viscosity were observed in pressure mobilisation experiments, with 1 g·L^{-1} and 10 g·L^{-1} sample solutions yielding very similar migration times (see Figure 3-7, and the text associated to it later in the manuscript), thus injection volumes are likely very similar and no bias should be observed. Lower relative peak areas at 10 g·L^{-1} should then indicate a reduced concentration and thus an incomplete dissolution. Though a greater absolute peak area at 10 g·L^{-1} indicates improved sensitivity, incomplete dissolution significantly impacts on accuracy of the results. Therefore, a compromise is necessary, and given no issues of sensitivity, a concentration of 1 g·L^{-1} was deemed appropriate for sample preparation. While a series of experiments of additional concentrations between 1 and 10 g·L^{-1} could be performed, this would likely bring limited additional information and was therefore not explored.

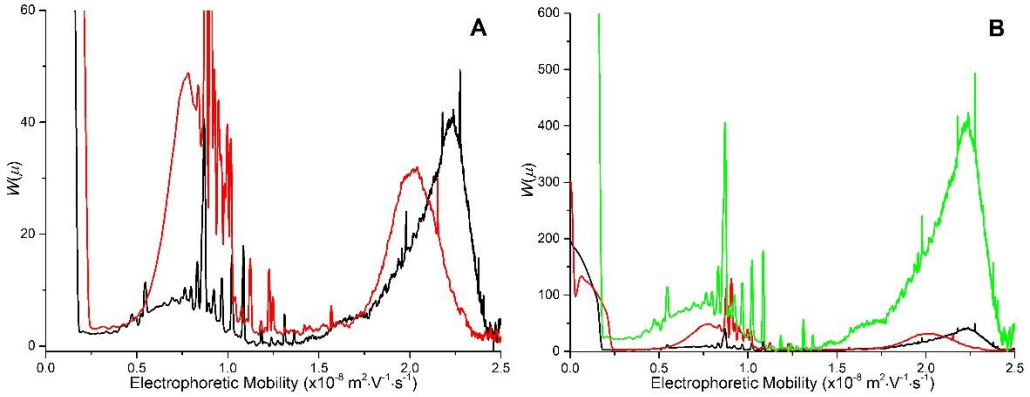

Figure 3-1 Weight distributions of electrophoretic mobilities of rice starch prepared according to Herrero-Martinez et al. [109] (90 % DMSO), at A) 1 g.L^{-1} (black) and 10 g.L^{-1} (red) and B) additionally showing the 1 g.L^{-1} with the y-axis multiplied by a factor of 10 (green). Amylopectin is in the range of 0.25 to 1.25 ×10^{-8} m^2·V^{-1}·s^{-1} and amylose is in the range of 1.5 to 2.5 ×10^{-8} m^2·V^{-1}·s^{-1}. Large sharp peaks in the range of 0.75 to 1.25×10^{-8} m^2·V^{-1}·s^{-1} correspond to aggregates

3.3.1.2 Filtration

Sample filtration prior to analysis with chromatography is often not mentioned in the literature but is common, particularly in cases where light scattering may occur [104, 230] and to prevent expensive maintenance and repair. Filtration has been shown to lead to poor recovery and sample degradation through shear stresses of large polymers leading to the analysis results not accurately representing the original sample [84, 237]. CE is a robust technique for which sample filtration is not needed [104, 203]. CE was especially shown to lead to the robust separation of carbohydrates in complex matrices [81, 102]. This provides an opportunity to confirm the effects of filtration on the starch structure by CE.

The effects of filtration were explored again with the conditions of Herrero-Martinez et al. [109] with sample concentration now decreased to 1 g·L^{-1}. A hydrophilic PTFE membrane filter was chosen for its chemical compatibility with the solvents used and its adequate interactions with the naturally hydrated starch samples. A significant impact of filtration was observed for all starch samples (Figure 3-2), with a complete or near-complete loss of the amylopectin peak in all samples and partial or complete loss of amylose after filtration. The weak broad signal of the corn starch (Figure 3-2B) may arise from the degradation of amylopectin by shear forces [83, 84, 237, 238]; however, the comparatively low peak area still indicates significant sample loss. These results thus support the suggestion that amylopectin cannot be filtered, and rather is retained on the filter, degraded [85] or deformed [87] and that amylose can be filtered in some cases [86]. Similar effects were observed at 10 g.L^{-1} (Figure S 3-4) It is possible that degradation of amylopectin and/or amylose could yield short chains unable to complex iodine, which would appear similar to sample loss; however, it this is unlikely.

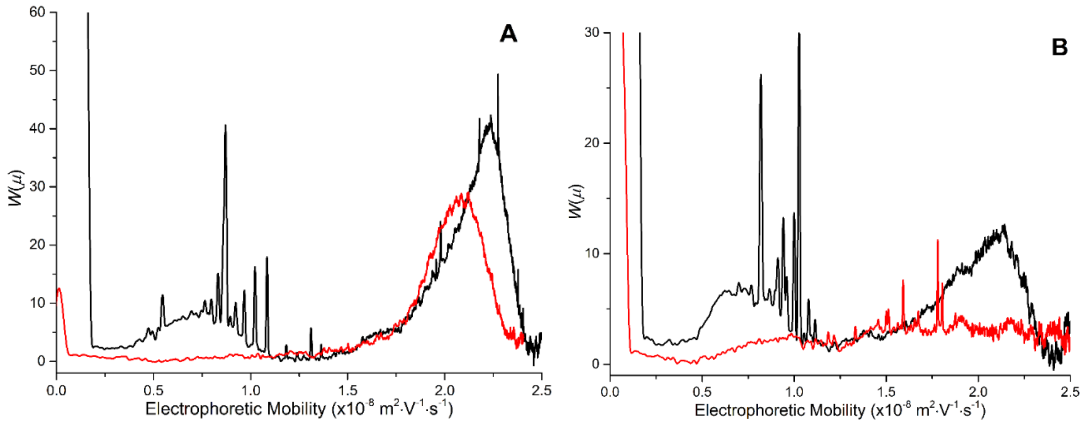

Figure 3-2 Weight-distributions of electrophoretic mobilities of both filtered (red) and unfiltered (black) A) rice starch at 1 g·L^{-1} and B) corn starch at 1 g·L^{-1} prepared following otherwise unmodified Herrero-Martinez [109]

The effect of filtration was also assessed by ^{1}H solution-state NMR, using the signals in the range of 4-6 ppm to assess the amount of dissolved starch present (Figure 3-3). An average decrease in signal area of 35 % over this range was observed as a result of starch filtration (Figure 3-3) The appearance of a small signal at 2 ppm and increasing signal areas at 1.4 and 0.9 ppm was also indicative of an increased concentration of short chain alkyl groups, possibly a result of the creation of short chain degradation products.

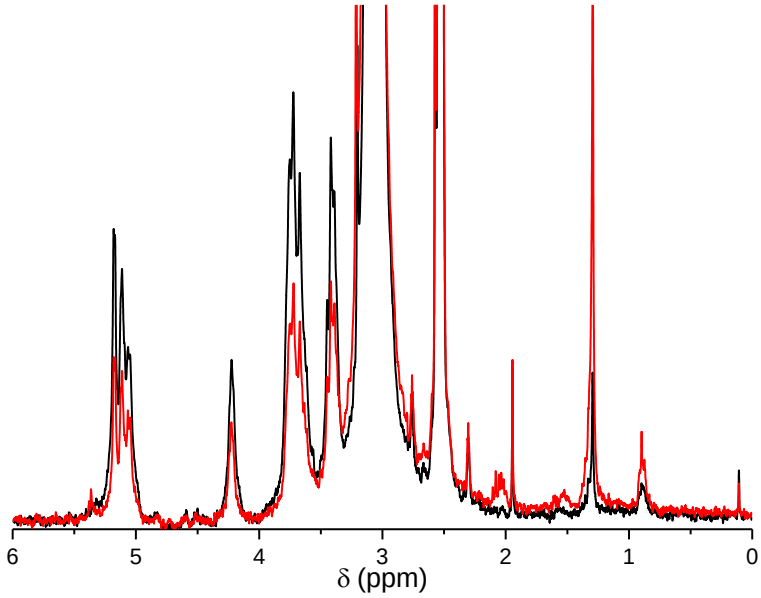

Figure 3-3 Solution-state ^{1}H NMR spectra of sigma rice flour without (black) and with (red) sample filtration prior to measurement (10 s repetition delay)

The stability of filtered starch solutions over time was also monitored to determine the aggregation kinetics of a filtered starch solution (see Figure 3-4 and Figure S 3-3). The potential for deformation of starch molecules due to filtration [87] may influence both iodine binding capacity as well as electrophoretic mobility but the effect should fade with time after filtration. The weight distributions of electrophoretic mobilities did not reveal any trend in peak area,

average mobility (Figure 3-4) and presence of aggregates (Figure S 3-2).

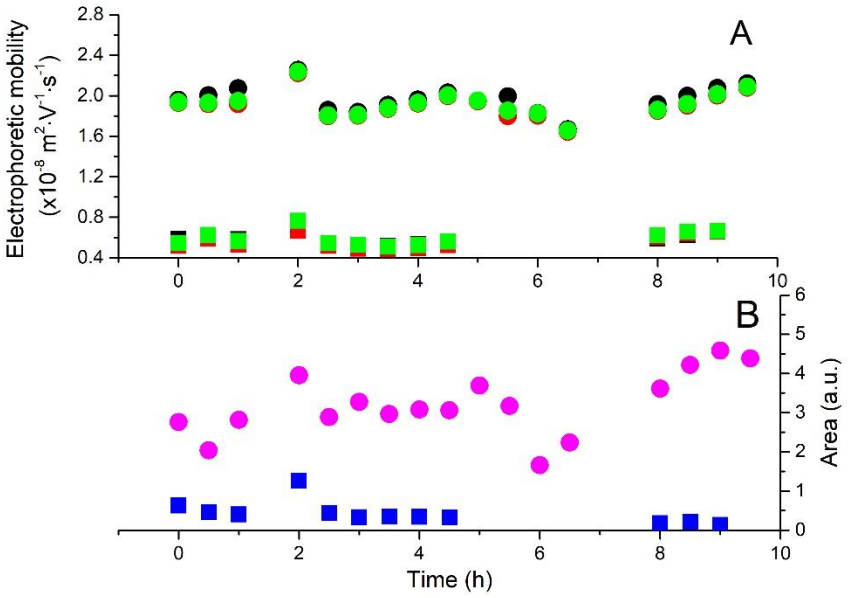

Figure 3-4 Change with time of peak parameters of amylose (circle) and amylopectin (square) from weight distributions of electrophoretic mobilities of rice starch: A) μ at the maximum (black), moment-average μ (red) and weight-average μ (green); B) peak area. Distributions are shown in Figure S 3-2. Moment-average and weight-average μ calculated by equations S 3-7 and S 3-8

Filtered samples exhibited less signs of aggregation as was noted by the sharp peaks in unfiltered samples; however, this was also accompanied by an apparent loss of most of the amylopectin (Figure S 3-2). Additionally, the effect of filtration on amylose content appeared to be more significant than is sometimes assumed. Filtration of amylose is believed to be possible; however, the results presented here suggested that its concentration is likely decreased through filtration (Figure 3-2). Therefore, it was concluded that filtration of starch samples should be avoided.

3.3.1.3 Comparing the dissolution conditions of Herrero-Martínez, Schoenmakers [109] and Schmitz, Dona [79]

Both the solvent and temperature play an important role in starch dissolution. High temperatures are essential in obtaining a complete dissolution and thus essential in quantitative analysis. However, heating starch can also initiate other processes such as gelatinization when water or water-containing solvents are used. The dissolution conditions employed by Herrero-Martinez et al. [109] and Schmitz et al. [79] were directly compared, with concentrations modified to 1 g·L^{-1} and no sample filtration. The conditions of Herrero-Martinez et al. [109] refers to dissolution of samples in 90 % DMSO at 100 °C for 1 hour. The conditions of Schmitz et al. [79] refers to dissolution of samples in anhydrous DMSO at 80 °C with shaking for at least 8 h (up to

16 h). The addition of 0.05 to 5 % w/v LiBr is suggested to improve dissolution of resisting starch components [79], with 0.05 % LiBr tested in this section.

For both corn and rice starch the conditions of Herrero-Martinez et al. [109] displayed a lower amylopectin peak area compared to the conditions of Schmitz et al. [79] (Figure 3-5), while amylose was only significantly affected in the rice starch (Figure 3-5B). However, Herrero-Martinez et al. [109] do not specify the injection temperature, while Schmitz et al. does indicate maintenance of high temperature for dissolution stability. Thus, this low recovery in 90 % DMSO may be a result of the unpredictable effects of sample cooling. These results also suggest a higher starch concentration and thus a more complete dissolution of starch in anhydrous DMSO, with the addition of LiBr further increasing the peak area of amylose and reducing the amount of aggregates. However, some level of aggregation, identified by apparently random sharp peaks, was still present in all samples prepared in anhydrous DMSO both with and without LiBr. This may be related to cooling during the time (<1 min) between dissolution and time of injection. Maintenance of high sample temperature was attempted by heating of the autosampler (60 °C); however, simultaneous heating of the buffer vials resulted in issues with buffer stability, discolouration and non-reproducible current values. The consistency of the amylose peak across preparation conditions in corn starch, in contrast to the rice starch, highlights that required dissolution conditions can vary between starches. This can arise from factors such as botanical origin and processing involved in commercial starch production that can play a role in the starch structure, and by extension the physicochemical properties.

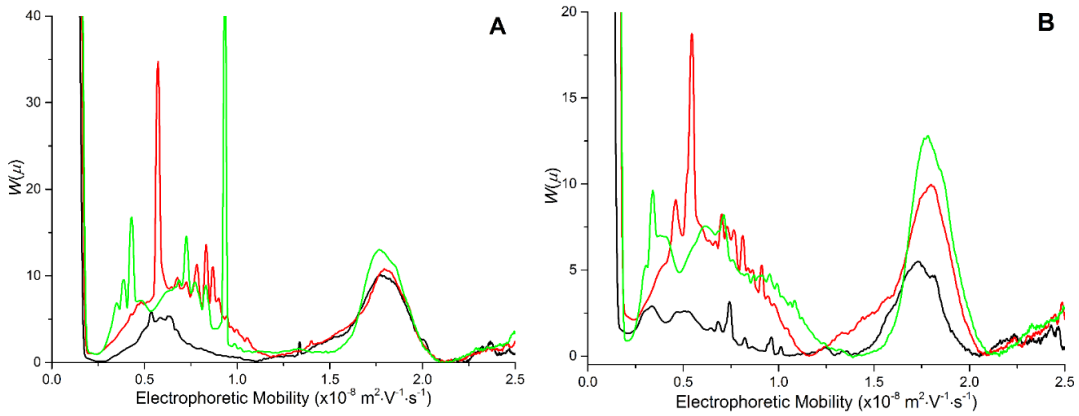

Figure 3-5 Weight distributions of electrophoretic mobilities of A) corn starch and B) rice starch prepared according to different methodologies modified to a sample concentration of 1 g·L^{-1} ; Herrero-Martinez et al. [109](black), Schmitz et al. [79] without LiBr (red) and with 0.05 % LiBr (green)

From the results discussed here, the dissolution conditions determined to provide the most accurate representation of the sample in IA-CE included a sample concentration of 1 g.L^{-1} and no filtration after dissolution. The dissolution in anhydrous DMSO at 80 °C with shaking for at least 8 hours was also deemed the most appropriate, shown in the literature to provide a complete dissolution of starch, with the addition of LiBr required in some cases [79], and reflected in the

results discussed here. These are referred to as the "optimal conditions" hereon, with concentration of LiBr specified as % LiBr.

3.3.1.4 Assessing dissolution kinetics

The optimal conditions were tested by solution-state NMR spectroscopy to validate the suitability of sample preparation for reliable and accurate characterisation by capillary electrophoresis. Initial experiments demonstrated a plateau after 150 minutes of dissolution; however, time resolution was not high enough to observe the initial dissolution (Figure 3-6, black squares). Measurement with a higher time resolution revealed similar kinetics, with a plateau reached after approximately 150 minutes of dissolution (Figure 3-6, red triangles). This plateau remained for at least 8 hours total dissolution time, suggesting the dissolution time of at least 8 hours employed for dissolution conditions in CE experiments is appropriate.

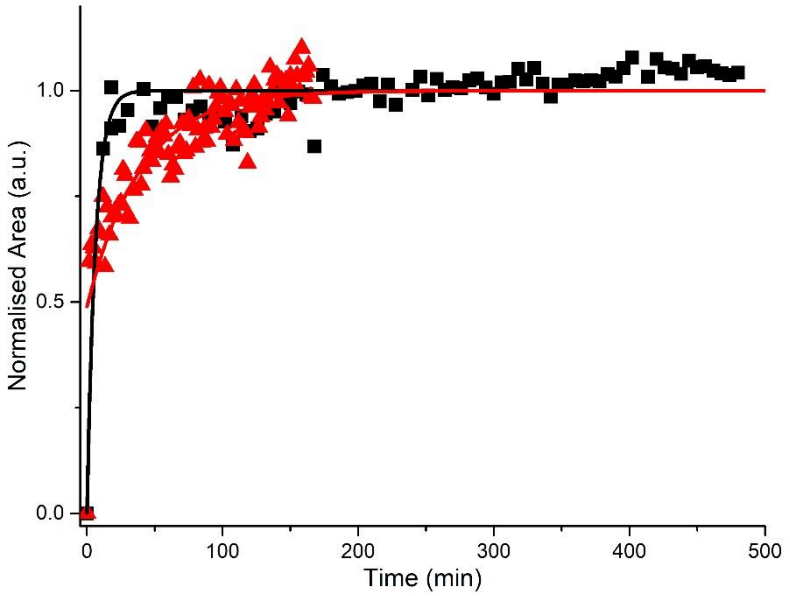

Figure 3-6 Integrals of ^{1}H NMR signals of starch from 6 to 4 ppm plotted against time and normalised to the asymptote of an exponential fit for series recorded with a repetition delay of 20 s, 16 scans (6 min 5 s per point) and r^2=0.86 (black squares) or a repetition delay of 10 s, 8 scans (1 min 45 s per point) and r^2=0.77 (red triangles). Both samples prepared at 1 g.L^{-1} in DMSO-d_6 with 0.5 % w/w LiBr

3.3.2 Separation of starch

In the separation of analytes by CE two properties are required: a net charge of the analytes and a way to detect the analytes. Amylose and amylopectin molecules are not natively charged; however, taking advantage of the well-studied and documented iodine binding phenomenon, both a charge and characteristic absorbance are obtained for starch [71]. The mechanism of complexation was not explored in this work, with the methodology being adapted from the work of Herrero-Martínez, Schoenmakers [109], modifying only the dissolution conditions to those determined in Section 3.1. This resulted in an effective change in the stoichiometry of available iodine to glucose monomer units from approximately 0.17:1 at 10 g·L^{-1} to 1.73:1 1 g·L^{-1}. This

method involves the complexation of both amylose and amylopectin with iodine, *in situ* rather than prior to injection. This is possible through a potassium iodide/iodine equilibrium within the acetic acid buffer producing polyiodide ions that allow complexation. The amylose content determination through spectrophotometric methods typically involves up to 20 minutes of 'reaction' time for complexation. Using the CE method employed in this study, the complexation time is reduced, thus its effect on the separation and detection of both amylose and amylopectin requires investigation. It is important to note that the detection occurs during the separation and not after it (post-column) as is the case in HPLC.

3.3.2.1 Pressure mobilisation

In CE, adsorption of the analyte onto the untreated silica capillary walls is common in the analysis of proteins, leading to peak tailing and loss of resolution [239]. This adsorption has a significant impact on the separation mechanism and the subsequent detection of analytes. The kinetics of this phenomenon has been successfully simulated [240], emphasising the importance of mitigating this effect through approaches such as capillary coatings [241, 242] or extreme pHs to invert the coulombic forces. In some cases, this adsorption can also result in tailing that never returns to the baseline [243], significantly complicating analysis. This effect is not limited to only proteins and can occur in any case where coulombic forces are strong enough to create significant interaction between the analytes and the capillary wall such as some polysaccharides [203]. In pressure mobilisation, the sample is pushed through the capillary using only pressure allowing for the interaction between the negatively charged capillary wall and the charged analytes to be investigated directly. It is important to note that without an electric field there is no separation of the analytes.

The complexation of amylose and amylopectin with iodine produces a negatively charged complex. Electrostatic repulsion may thus limit interactions with the silica capillary walls. Pressure mobilisation experiments were performed on samples prepared in optimal conditions (see section 3.1). No adsorption of the starch complex to the wall was observed, supported by the absence of tailing relative to a pure DMSO marker (Figure 3-7A). The broader, symmetric peak observed at 7.5 min is indicative of the presence of a larger component compared to the relatively sharp peak observed for pure DMSO and for starch samples dissolved in DMSO. There is an inverse relationship between the peak width and the diffusion coefficient [244]. The broad symmetrical peak was assigned to the iodine complexed starch components amylose and amylopectin. The sharp peaks observed before 6 min might be due to aggregates in a hydrodynamic chromatography separation mechanism and scattering light. The effects of increased viscosity and addition of LiBr were also assessed, finding no impact on adsorption (Figure S 3-5).

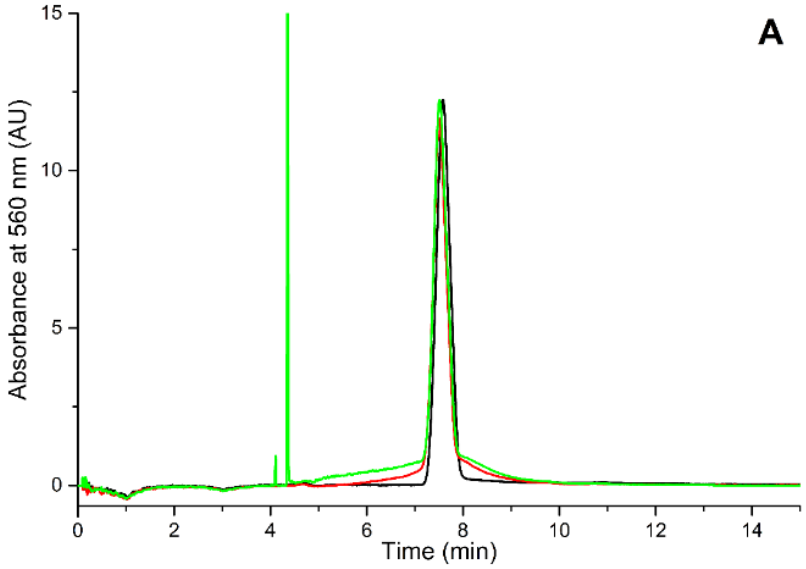

Figure 3-7 Pressure mobilisation elugrams of potato amylopectin (red) and amylose (green) prepared in optimal conditions at 1 g·L^{-1} and of DMSO (black)

In the CE separation of amylose and amylopectin the role of adsorption appeared to be insignificant, indicating that there is very little affinity between the iodine bound starch and glass, and thus recovery is likely high. This is in stark contrast to the characterisation of starch by SEC, where the methodology is often plagued by low recovery likely a result of adsorption to the organic stationary phases often employed [90].

3.3.2.2 Starch-iodine incubation and the effect of LiBr concentration

The nature of this method relies on the binding of amylose and amylopectin chains with iodine in solution to form starch-iodide complexes. Optimisation studies on the composition of the iodine solution were performed in the work of Herrero-Martínez, Schoenmakers [109], therefore only complexation incubation times and effect of LiBr concentration have been explored in this work.

This complexing reaction is often used in the determination of amylose content. Measurements are traditionally completed by simple colorimetric and spectrophotometric methods involving standing time for full complexation (typically 20 min). This approach is quick and simple, thus its high prevalence as an amylose determination technique. The extent of starch-iodine complexation was not reported in the work of Herrero-Martinez et al. [109]. The extent of complexation is likely to be a significant factor for the *in situ* complexation employed in this method. The impact of incubation time on *in situ* complexation was therefore assessed.

Samples were injected hydrodynamically (3.2.3) and a mixing procedure achieved in the acetic acid buffer by ramping the voltage up to 20 kV over 1 min, holding it for 30 sec and then setting it to 0 kV for the specified incubation time before setting back to 20 kV. The initial application of an electric field allows for the analyte to be mixed with the iodine-containing background electrolyte while also separating Li^+ and Br^- ions away from the analyte. The use of LiBr as a hydrogen bond

disruptor for dissolution impacts on the starch-iodine complexation. This was visually confirmed by lack of colourimetric reaction with addition of background electrolyte to starch in DMSO with LiBr (data not shown).

With 0.05 % w/w LiBr in the DMSO for dissolution, increasing incubation times generally resulted in an increase in peak area, as well as a reduction in presence of aggregates indicated by the lack of observed intense sharp peaks (Figure 3-8). Of note was the unexpected observation of an amylose peak ($2x10^{-8}$ $m^2 \cdot V^{-1} \cdot s^{-1}$) in waxy corn starch, with increasing incubation time yielding a significant increase in peak area, and additional populations appearing (Figure 3-8A). This effect was not observed to the same extent in the high amylose Gelose 80, with only an increase in total peak area observed (Figure 3-8B). This may arise from differences in the type of amylose present in each sample facilitating different iodine binding rates, or possibly a result of the incomplete dissolution of Gelose 80 only allowing for binding of certain populations of amylose.

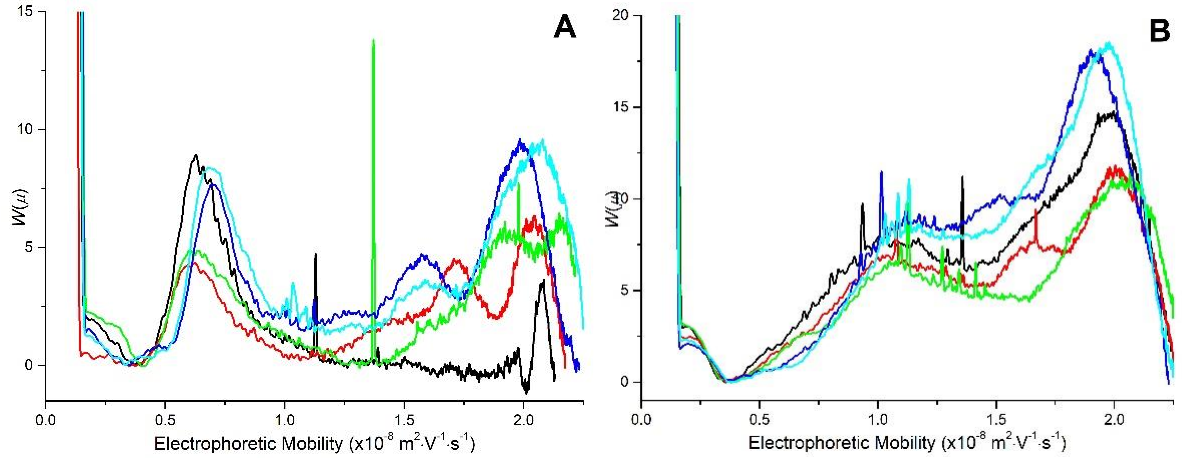

Figure 3-8 Weight distributions of electrophoretic mobilities at 0 min (black), 0.01 min (red), 1 min (green), 5 min (blue) and 10 min (light blue) incubation time in background electrolyte for A) Waxy corn starch and B) Gelose 80 prepared in the optimal conditions at 1 g·L^{-1} with 0.05 % LiBr

For high amylose starches, a higher salt content is typically required for dissolution. With a higher LiBr concentration (5 %) in the dissolution of Gelose 80, a significant loss in signal and increased signs of aggregation was observed where no incubation period was used (Figure 3-9A). Increasing the incubation time significantly increased peak area, with a reduction in the presence of sharp aggregate peaks observed. Notably, an improved separation of the populations was observed, closely aligning with the shoulder peaks observed in Gelose 80 samples with 0.05 % LiBr and 10 min incubations (Figure 3-8). This indicates that there is a need to balance the dissolution benefits of LiBr with the impact it has on iodine binding potential. Increasing incubation time further to 30 minutes yielded further changes to the separation with a reduction in observable sharp aggregate peaks as well as a shift in the distribution towards lower mobility. Due to the high salt content, it is suspected that interference of LiBr with iodine binding is so great that the resulting distributions are not truly reflective of the true distribution within the scope of

incubation times tested here. At 5 % LiBr, the molar concentration is in excess of the concentration of available iodine (666 mM LiBr to 7.2 mM KI and 1.2 mM I_2), indicating much longer incubation times would likely be required.

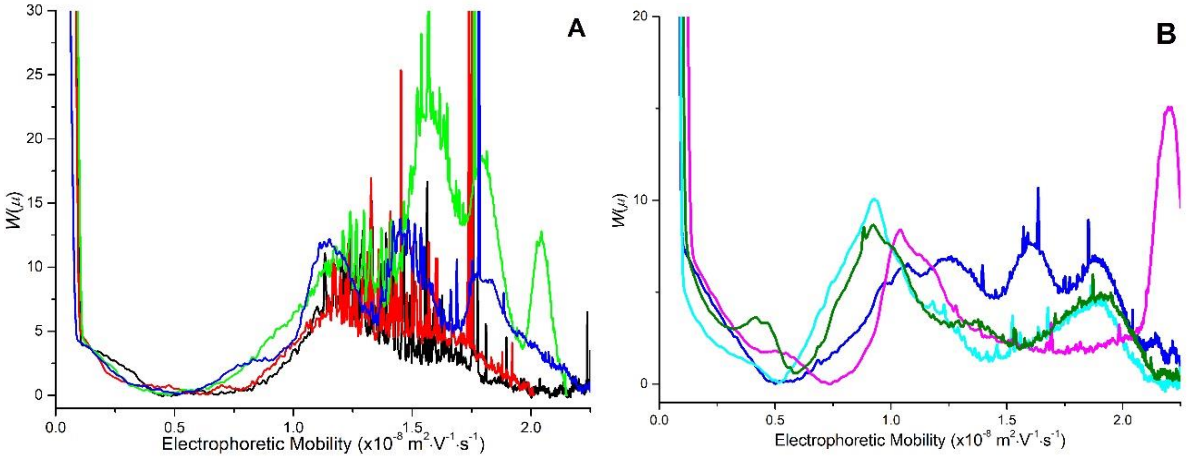

Figure 3-9 Weight distributions of electrophoretic mobilities at A) 0 min (black), 1 min (red), 5 min (green) and 10 min (blue) and B) 10 min (blue), 15 min (light blue), 20 min (purple) and 30 min (olive) incubation time in background electrolyte for Gelose 80 prepared in the optimal conditions at 1 g·L^{-1} with 5 % LiBr

Due to the binding issues associated with using very high salt contents, a middle ground of 0.5 % LiBr was assessed with an incubation time of 30 minutes to allow for more complete binding. At a concentration of 64 mM, the disruption of LiBr to the binding process should be significantly reduced. Interestingly, a waxy maize containing no amylose displayed increases in peak area with 0.5 % LiBr compared to both 0.05 % and 5 % LiBr with no observed changes in the distribution (Figure 3-10A). In Gelose 80, the change from 5 % to 0.5 % LiBr yielded a significant increase in the total peak area with minimal signs of aggregates (Figure 3-10B). However, while 0.05 % LiBr gave greater peak area, the aggregate peaks observed significantly contribute to these regions, indicating a poor dissolution.

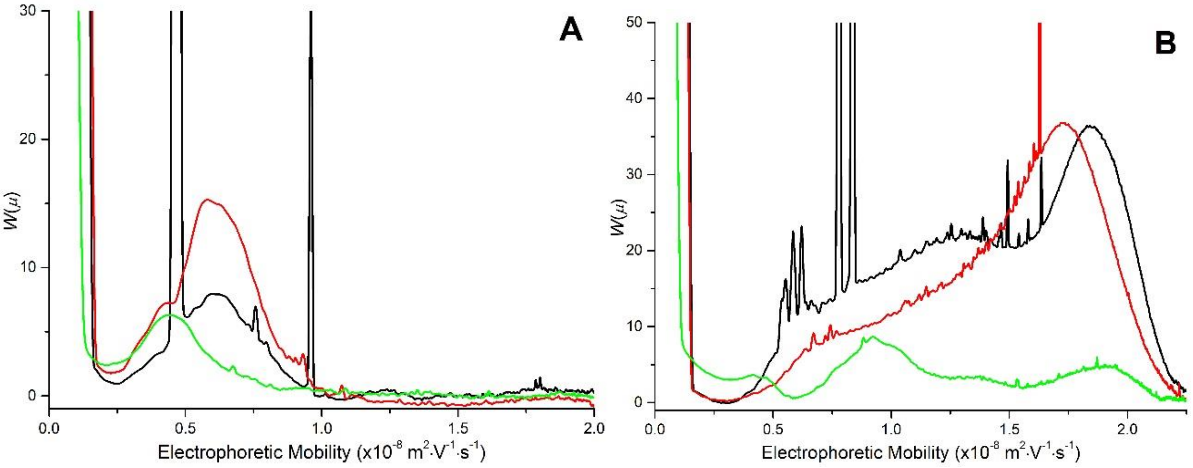

Figure 3-10 Weight distributions of electrophoretic mobilities with 30 min incubation time in background electrolyte and with 0.05 % (black), 0.5 % (red) and 5 % (green) LiBr for A) Gelose 80 prepared in optimal conditions at 1 g·L^{-1} and B) Waxy Maize prepared in optimal conditions at 1 g·L^{-1}

It is evident from this study that extended incubation times are important to allow for optimal iodine binding of starch for electrophoretic separation. Extended incubation times typically yielded increased peak areas, while also significantly decreasing the presence of starch aggregates. However, extended incubation times also resulted in significant baseline drift. To mitigate this, alternating pressure was applied during incubation to keep the sample plug mobile and mitigate adsorption and diffusion of the sample plug (S 3.5.6). Another important aspect of this incubation was the ability to offset the impact of increased LiBr content on iodine-starch binding; however, the best compromise was found here to be a LiBr concentration of 0.5 % w/w offering improved dissolution, minimised aggregation and negligible impact on iodine binding.

3.4 Conclusions

CE has been shown to separate amylose and amylopectin in starch samples by taking advantage of iodine complexation. Literature had shown that quantification is possible under these conditions, with a low limit of detection (0.1 $g \cdot L^{-1}$) [109]. However, obtaining a complete dissolution is essential in accurate quantitative analysis.

A number of parameters of dissolution were investigated in the dissolution conditions presented by Herrero-Martínez, Schoenmakers [109]. This assessment carried out by capillary electrophoresis was aided by ^{1}H solution-state NMR experiments. The most significant aspect of improvement to dissolution conditions was dissolution concentration, with lower concentrations resulting in an apparent greater extent of dissolution. This is supported by the knowledge of aggregation and poor dissolution in polysaccharide solutions at higher concentrations. Filtration of starch solutions was shown to result in significant signal loss for both amylose and amylopectin, suggesting a significant sample loss. Potential signs of degradation were also observed as a result of filtration. The high temperatures necessary for dissolution and dissolution stability should ideally be maintained up to and during sample injection. This could be achieved with equipment that allows for isolated sample temperature control, with the potential to greatly improve repeatability.

Improved dissolution conditions were found to yield a greater amylose peak area, indicative of a greater concentration. However, the presence of LiBr in the solution was shown to impact on the binding of iodine to amylose and amylopectin. This effect was significant at higher concentrations (5 %) but not at lower concentrations (0.05 %). These higher LiBr concentrations are essential for the complete dissolution of amylose in high amylose starches, thus modifications to the CE method were necessary to accommodate, with extended complexation time resulting in increased peak area and apparently greater extent of binding. Given a longer complexation time, a LiBr concentration of 0.5 % was found to be optimal. While optimal dissolution conditions are

likely to vary across samples, the use of samples covering a broad range of amylose contents allowed for confidence in dissolution conditions to be effective for similarly broad range of samples.

Further work will be required to assess the impact of joule heating on this binding reaction, as temperature fluctuations have been reported to influence binding constants in CE of proteins [240]. In addition to this, modification of the background electrolyte to an iodine containing DMSO/water mixture could reduce any interference of the buffer with solubility, with as little as 1 % DMSO likely to provide ample sensitivity [71].

The dissolution conditions tested in this work may also be applied to other types of characterisation of starch in solution such as field flow fractionation. It should also be used to investigate the effect of isolation of starch from grain and cereal flours (for plant breeding purposes for example) and the effect of cooking and how much change these important processes bring to starch content and structure. The dissolution and CE separation presented in this work may allow a more accurate determination of the amylose content of starches. The distributions of electrophoretic mobilities obtained by this method may also be explored to develop new ways to interpret amylose content and starch branching, as done in a recent study on chitosan's composition [169]. Through such characterisation a better understanding of the role of the components of starch and their structure in their physicochemical properties may be gained. This would prove to be especially useful in food, where a better understanding of amylose content and its role in starch digestibility could help to develop healthier products.

Acknowledgements

Dr Jose-Manuel Herrero-Martinez (University of Valencia), Prof. Peter Schoenmakers (University of Amsterdam) and Prof. Jens Coorssen (Brock University) for discussions. MVL acknowledges a Postgraduate Travel Award from the Molecular Medicine Research Group to present some of this work at the Pacifichem 2015 conference. This work was supported by Western Sydney University and the Australian Government (Research Training Program) and AgriFutures (PRJ-010712).

3.5 Supporting information

Supporting information

for

Separation of amylose and amylopectin using capillary electrophoresis

Matthew P. Van Leeuwen [a,b], Joel J. Thevarajah [a], Rachelle Ward [c], Marianne Gaborieau [a*], Patrice Castignolles [a]

[a] Western Sydney University, Australian Centre for Research on Separation Science, School of Science, Parramatta Campus, Locked Bag 1797, Penrith, NSW 2751, Australia

[b] Western Sydney University, School of Medicine, Campbelltown Campus, Locked Bag 1797, Penrith, NSW 2751, Australia

[c] Yanco Agricultural Institute, NSW Department of Primary Industries, Yanco, Australia

*Corresponding Author – Dr Marianne Gaborieau, Western Sydney University, Parramatta Campus, Locked Bag 1797, Penrith, NSW 2751, Australia. Tel.: +61 2 9685 9905; Fax: +61 2 9685 9915; e-mail: m.gaborieau@westernsydney.edu.au

S 3.5.1 Transformation of raw data

The raw data was transformed following the procedure of Chamieh, Martin [245]. Migration time of analytes is dependent on both the electrophoretic mobility (μ) of the analyte and the electroosmotic flow (EOF). Therefore, the migration time t_m was converted to the electrophoretic mobility μ so that it does not depend on the electroosmotic flow, using Equation S 3-1:

$$\mu = \frac{l_d l_t}{V}\left(\frac{1}{t_m} - \frac{1}{t_{eof}}\right) \qquad \text{Equation S 3-1}$$

where l_d is the capillary length to the detector, l_t is the total capillary length, V is the voltage, and t_{eof} is the migration time of the EOF marker.

The absorbance was corrected to account for the analyte velocity through the detection window, correcting absorbance as a function of time spent in the detection window and accounting for the transformation from time scale to mobility scale of the x-axis. It is important to note that the detection occurs during the separation and not after it (post-column) as is the case in HPLC. This is shown in Equations S 3-2 to S 3-6, where absorbance is first corrected for velocity,

$$UV\ Signal = \frac{Absorbance}{t_m} \qquad \text{Equation S 3-2}$$

Transformation to weight distribution of electrophoretic mobilities $W(\mu)$ is then completed,

$$W(\mu) = \frac{UV\ Signal}{\frac{d\mu}{dt_m}} \qquad \text{Equation S 3-3}$$

where $\frac{d\mu}{dt_m}$ is the derivative of μ with respect to t_m,

$$\frac{d\mu}{dt_m} = -\frac{l_d l_t}{V}\frac{1}{{t_m}^2} \qquad \text{Equation S 3-4}$$

Therefore,

$$\frac{d\mu}{dt_m} \propto \frac{1}{{t_m}^2} \qquad \text{Equation S 3-5}$$

Simplifying Equation S3 according to Equations S 3-2 and S 3-5,

$$W(\mu) = Absorbance * t_m \qquad \text{Equation S 3-6}$$

Using equation S 3-6, raw absorbance data was corrected according to analyte velocity and transformed from time-scale absorbance to mobility-scale absorbance. These corrections are essential in determining molecular property-based distributions. The transformation's effect on data is shown in Figure S 3-1, comparing the same data plotted in raw data form (Figure S 3-1A) and after corrective transformations (Figure S 3-1B).

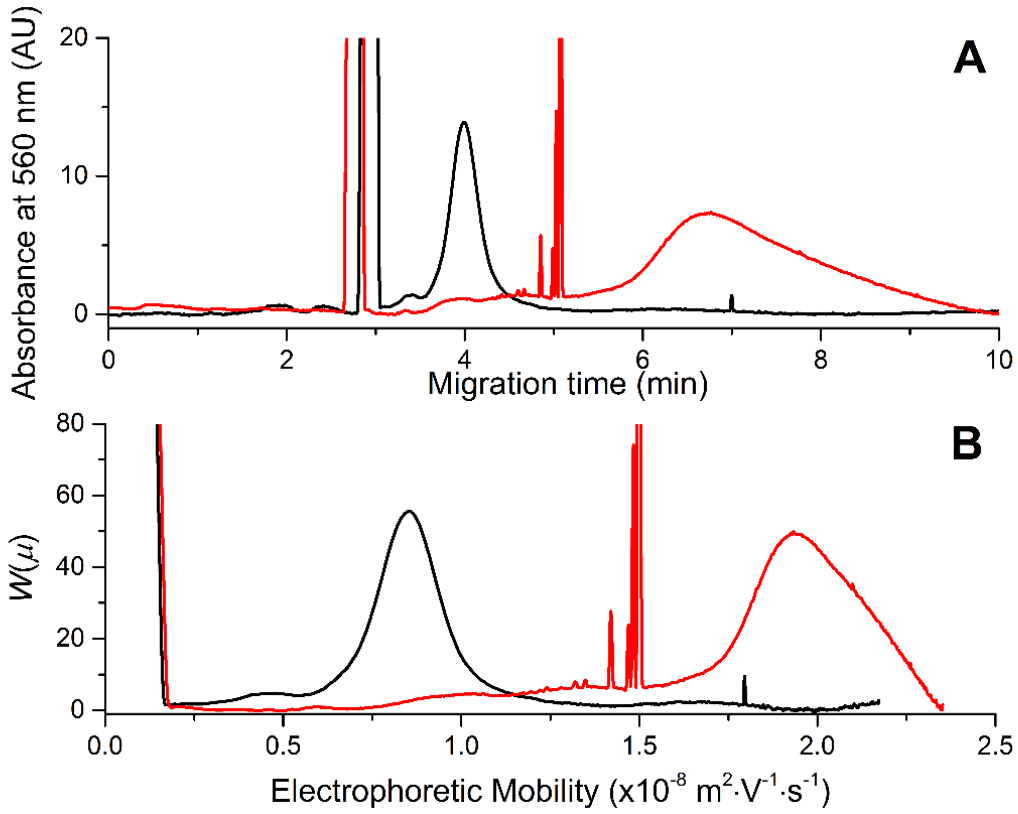

Figure S 3-1 A) Electropherograms and B) Weight-distributions of electrophoretic mobilities of amylose (red) and amylopectin (black) A) Before and B) After correction and transformation

S 3.5.2 Calculation of average mobilities

Weight-average electrophoretic mobility (μ_w) and moment-average electrophoretic mobility (μ_m) are calculated through Equation S 3-7 and S 3-8, respectively

$$\mu_w = \frac{[\sum_z W(\mu_z)\mu_z(\mu_{z+1}-\mu_z)]}{[\sum_z W(\mu_z)(\mu_{z+1}-\mu_z)]} \qquad \text{Equation S 3-7}$$

$$\mu_m = \frac{[\sum_z W(\mu_z)(\mu_{z+1}-\mu_z)]}{[\sum_z W(\mu_z){\mu_z}^{-1}(\mu_{z+1}-\mu_z)]} \qquad \text{Equation S 3-8}$$

where μ_z is the electrophoretic mobility of the z^{th} molecule.

S 3.5.3 Filtration – Aggregation kinetics

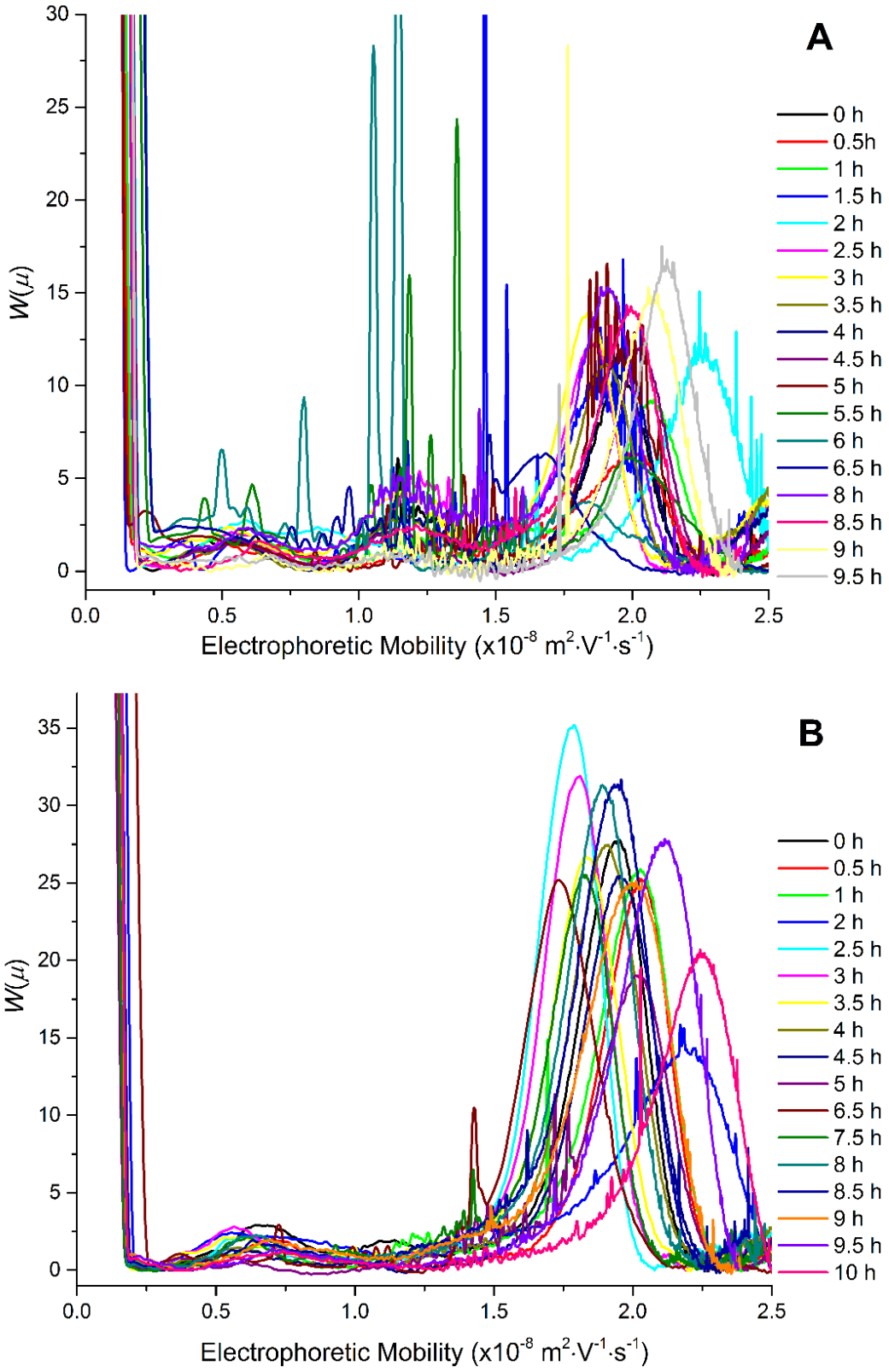

Figure S 3-2 Evolution with sample ageing of the weight-distributions of electrophoretic mobilities of A) filtered rice starch and B) filtered corn starch, prepared at 10 g·L^{-1} in 90 % DMSO by magnetic stirring at room temperature

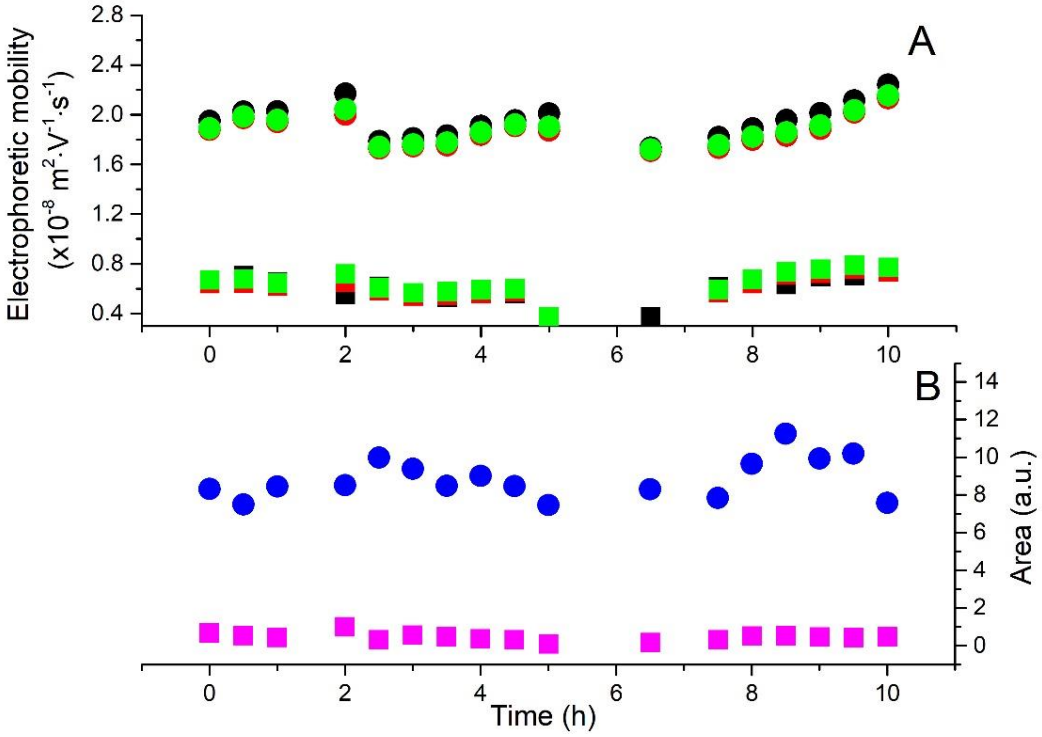

Figure S 3-3 Evolution with time of peak parameters of amylose (circles) and amylopectin (squares) from weight-distributions of electrophoretic mobilities of corn starch: the A) μ at the peak maximum (black), moment-average μ (red) and weight-average μ (green); B) peak area. Distributions are shown on Figure S 3-2B. Calculation of moment-average and weight-average μ is done through equations S 3-7 and S 3-8

Figure S 3-4 shows the effect of sample filtration prior to injection on the separation of starch by capillary electrophoresis. The sample was prepared at a concentration of 10 g·L^{-1} in the conditions of Herrero-Martinez et al. [109], and displayed very low signal for the amylopectin peak (Figure S 3-4, red). The separation is compared to the same sample prepared at 1 g·L^{-1} in the conditions of Schmitz et al. [79] with 0.05 % LiBr (Figure S 3-4, black), highlighting the clear loss of amylopectin signal in filtration even with 10-fold higher concentration.

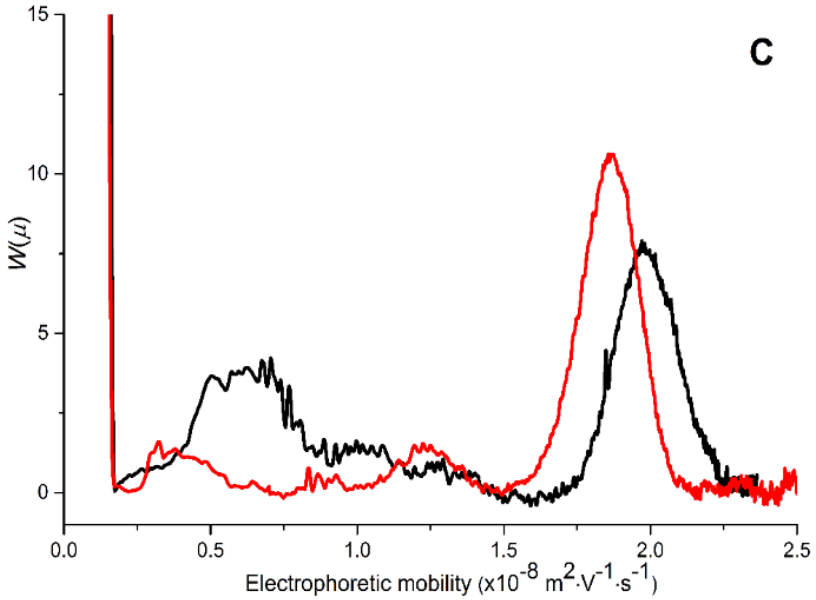

Figure S 3-4 Rice starch at 1 g·L^{-1} without filtration (black) (sample preparation of Schmitz et al. [79] with 0.05 % LiBr) and at 10 g·L^{-1} with filtration (red) (unmodified sample preparation of Herrero-Martinez et al. [109]

S 3.5.4 Validation of CE hardware

The standard was qualitatively compared to previous separations [233] for repeatability of electro-osmotic flow and electrophoretic mobility of oligoacrylate species. Initial assessment is based on visual reproducibility of the oligoacrylate solution with previous experiments, followed by determination of the repeatability of electro-osmotic flow, current and mobility of the AA1, RAFT and AA2 RAFT species present. Electrophoretic mobilities had a relative standard deviation (RSD) of 3.5 to 6.5 % for the species used to validate the capillaries and hardware used in this work (Table S 3-1). When EOF, current or electrophoretic mobilities were outside the range given in Table S 3-1 then the data was not used and the experiment repeated.

Table S 3-1 CE experiment data and calculated electrophoretic mobilities for separations of oligoacrylate solutions used to validate capillaries and hardware

Year	Month	Current (µA)	EOF (min)	Electrophoretic mobility (x10^{-8} $m^2 \cdot V^{-1} \cdot s^{-1}$)		
				PAA1	RAFT	PAA2 RAFT
2015	May	25	1.700	1.114	1.446	1.821
2015	May	23	1.696	1.105	1.447	1.783
2015	Sep	33	1.680	1.128	1.413	1.960
2016	Mar	24	1.648	1.116	1.301	2.000
2016	May	24	1.648	1.116	1.301	2.000
2016	Sep	25	1.700	0.993	1.195	1.916
2016	Sep	26	1.675	1.072	1.281	1.992
2017	Jun	24	1.640	1.072	1.281	1.894
2017	Oct	27	1.700	1.063	1.298	1.926
2017	Nov	28	1.600	1.043	1.226	1.886
2017	Nov	30	1.647	1.049	1.254	1.922
2017	Nov	30	1.653	1.085	1.294	2.008
2017	Nov	31	1.613	1.010	1.203	1.867
2018	Feb	33	1.630	1.019	1.187	1.936
2018	Mar	37	1.602	0.967	1.124	1.813
2018	Apr	27	1.630	1.052	1.226	1.918
2018	Nov	31	1.585	1.047	1.234	1.966
2018	Dec	28	1.681	1.043	1.262	2.006
2019	Jan	33	1.645	1.074	1.259	1.974
2019	Jan	34	1.632	1.112	1.312	2.009

S 3.5.5 Pressure mobilisation

Pressure mobilisation was evaluated at different concentrations and in different solvents in a comparative study to investigate whether the increased viscosity or addition of LiBr to the solvent had any significant effects on adsorption to the capillary wall. No significant signs of adsorption were observed related to either viscosity at higher concentration (Figure S 3-5, black and red) or addition of LiBr (Figure S 3-5, green) relative to a 50/50 volume DMSO/running buffer standard marker.

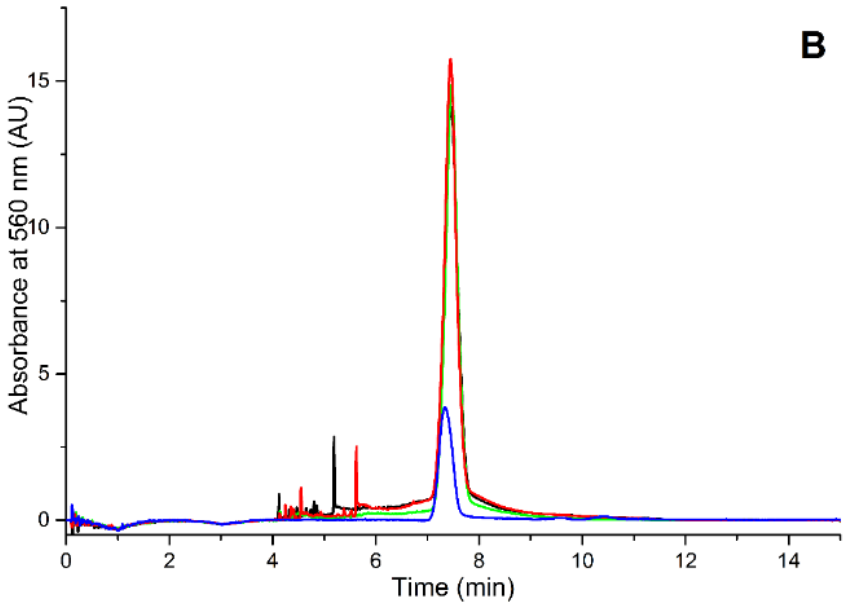

Figure S 3-5 Corn starch prepared at 10 g·L^{-1} in 90 % DMSO following Herrero-Martínez, Schoenmakers [109] (black), rice starch prepared at 1 g·L^{-1} in the optimal conditions (green), rice starch prepared at 10 g·L^{-1} following Herrero-Martínez, Schoenmakers [109] (red) and running buffer with 50 % v/v DMSO (blue)

S 3.5.6 Pressure mobilised incubation

Increasing incubation times was found to improve *in situ* binding of iodine with amylopectin and amylose molecules, resulting in both greater peak area as well as reduced incidence of large, sharp starch aggregate peaks. This was especially beneficial with the presence of LiBr in the anhydrous DMSO used for dissolution. However, longer incubation times resulted in significant baseline drift during the incubation period, which also affected the baseline in the region where starch migrates in some cases (Figure S 3-6). To mitigate this, a pressure mobilised incubation period was implemented, whereby upon initial injection of sample and electrokinetic mixing, the sample plug would be mobilised by low pressure of 5 mbar and -5 mbar alternating for 5 min each, for a total of 30 min incubation time (6 x forward/backward sample movements). This was done to minimise adsorption as well as diffusion of the sample plug. Figure S 3-6A demonstrates this effect in an electrophoresis experiment, as well as the effect of the method changes to mitigate this effect. Figure S 3-6B demonstrates this effect on pressure mobilisation experiments, as well as the impact of the method changes to mitigate this effect.

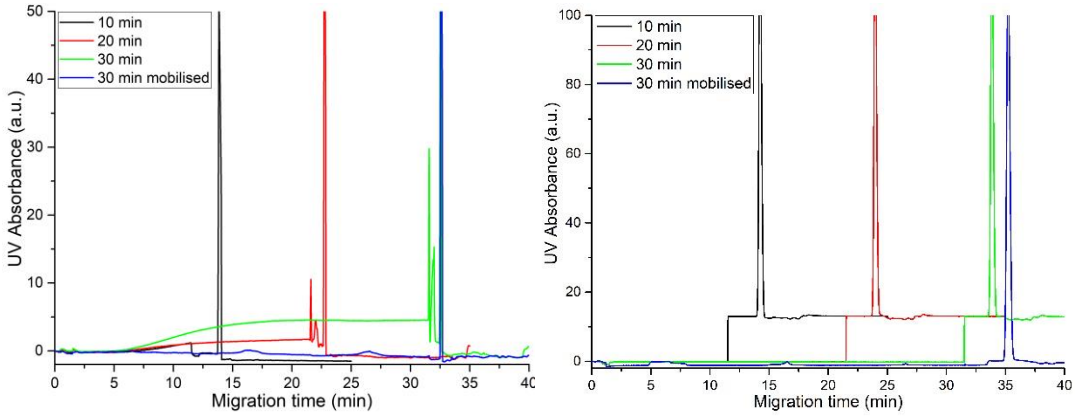

Figure S 3-6 A) A) Electropherograms of capillary electrophoresis experiments with incubation times of 10 min (black), 20 minutes (red), 30 minutes (green) and 30 minutes with mobilised incubation (blue) B) Elugrams of pressure mobilisation experiments with incubation times of 10 minutes (black), 20 minutes (red), 30 minutes (green) and 30 minutes with mobilised incubation (blue)

S 3.5.7 Estimation of T_1 for quantitative determination of average DB

Longitudinal relaxation times (T_1) of the signals of interest (in the range of 5.4 to 4.2 ppm) were estimated using the one-dimensional inversion recovery pulse sequence. In this experiment a signal is negative if the inversion recovery delay is shorter than T_1 * ln2 and positive if the inversion recovery delay is longer than T_1 * ln2. Signals in this range exhibited similar T_1, with T_1 determined to be between 3 and 4 s (Figure S 3-7).

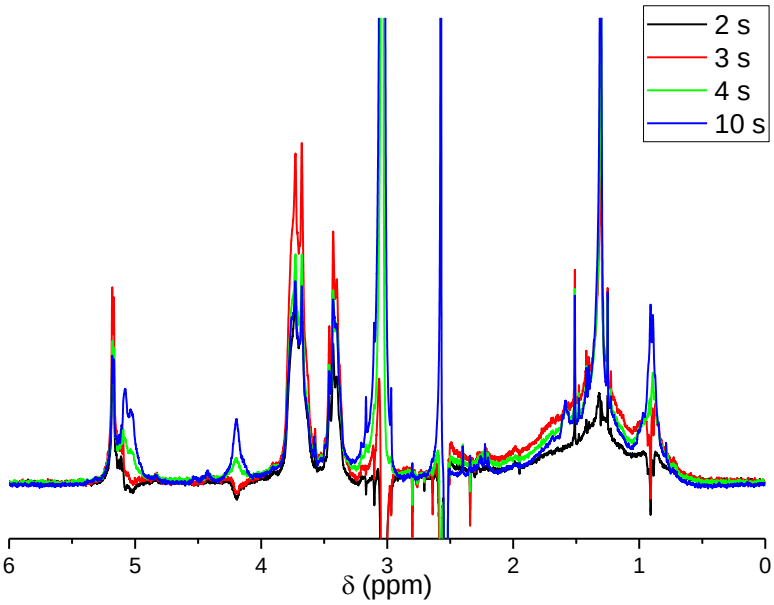

Figure S 3-7 Partial spectra of rice starch in DMSO-d_6 with 0.5 % w/w LiBr at 80 °C displaying measurements to assess whether T_1 values are shorter than 2 (black), 3 (red) and 4 (green) and 10 (blue) seconds, with inversion recovery delay of 1.386 s (black), 2.079 s (red), 2.773 s (green) and 6.931 s (blue)

Chapter 4 Characterisation of branching in rice flours using capillary electrophoresis

4.1 Introduction

Starch is a highly abundant biopolymer, acting as the primary energy storage in plants [222] and a major dietary source of energy for humans [246]. Modified forms of starch are also used widely in a variety of industrial applications such as food and adhesives [222]. At the simplest level, starch is comprised of two macromolecular components, amylose and amylopectin that differ in their role in the semi-crystalline structure of native starch. Amylose and amylopectin are both comprised of the same linear backbone of glucose monomers linked by α(1-4) glycosidic linkages, though differ in their degree of branching through α(1-6) glycosidic linkages [22]. Amylopectin exhibits a much greater degree of branching (5 – 6 %) and shorter branch chain lengths than amylose [22].

Within a granule, starch is synthesised by a concert of four classes of enzymes including ADP-glucose pyrophosphorylase (ADPG), starch synthase (SS), starch branching enzyme (BE) and starch debranching enzyme (DBE) [247]. With ADPG providing the substrate, ADP-glucose, SS, BE and DBE are then the architects defining the starch structure within the granule. SS acts to polymerise glucose through the formation of α(1, 4) glycosidic linkages, while BE catalyses the formation of the α(1, 6) linkages that form the branching structure of starch [247, 248]. However, multiple isomers of SS and BE exist across different cereals acting on different substrates and with different activity. In rice, there are 10 isomers of SS, divided into 5 types; SSI, SSII, SSIII, SSIV responsible for activity in the soluble fraction of the amyloplast, and granule bound SS (GBSS), with activity tightly bound to starch granules. Of these, three specific isomers; SSI, SSIII and SSIIIa, have been associated with amylopectin synthesis in rice [249], with their activities linked to amylopectin chain length distributions [250, 251] and accounting for major differences between indica and japonica varieties [251]. Meanwhile only one isomer, granule bound starch synthase (GBSSI) has been linked to the production of amylose, with its activity and presence correlating to amylose content [207, 247]. This has been theorised to arise from a number of factors including substrate availability [247] as well as steric hinderance [252]. Interestingly, while GBSSI appears to be the sole producer of amylose, it has also been observed to participate in elongation of amylopectin chains [250, 253, 254]. This is likely a contributing factor to the apparent “third” type

of starch that has been observed in rice [255], and also reported in Arabidopsis thaliana [256], which have been described as long-chain branched amylopectins.

The multiple isoforms of BE also impart different branching production behaviours such as in branches chain lengths, branching frequency and substrate preferences [247]. Typically, two isoforms are present in a given cereal, denoted A and B. In rice, the primary isoforms are BEIII(a) and BEI(b) [257], reported to preferentially branch amylose and amylopectin respectively [258, 259]. Thus have been suggested to participate preferentially in long- (degree of polymerisation (DP) > 36) or short-chain (DP < 10) branching [247, 259, 260].

Finally, DBE acts to cleave and relocate branches, suggested to work in concert with SS an BE to give rise to the organised supramolecular structure of starch [247]. The exact function of DBE is still unknown, however theories ranging from spatial management to allow for efficient packing [247] and chain elongation [261] as well as management of competing glucan substrates [247] have been suggested. It is clear then that while the basic molecular structure of starch can be viewed as quite simple, the various enzymatic pathways responsible for synthesis are very complex. As a result, the populations of different structures within a given starch granule can be similarly complex and diverse and the genetic drivers thus indirectly accountable for many of the resulting properties [262, 263].

The resulting compositional, structural and spatial arrangements within the starch granules (Figure 1-3) such as distributions of molar mass and branch chain length (discussed in 1.2.1), then play an important role in the functional properties of starch, ultimately impacting the properties of the starch containing grain [70, 224, 227]. For example, amylose content and structural heterogeneity have been shown to significantly impact properties such as solubility, viscosity and digestibility [26, 35, 223, 224, 264, 265].

Colorimetric approaches are currently the most popular high throughput methods for determining apparent amylose content [228], based on the formation of the dark blue starch-iodine complex that absorbs in the UV-VIS spectrum, and supported by the existence of standard methods of analysis [74, 204]. However, the complexation of amylose and amylopectin with iodine yields a colorimetric profile with a maximum absorption at 620 and 540 nm respectively [71, 72]. This results in overlapping absorption bands [229], and thus can lead to overestimation of amylose content, requiring correction processes such as multi-wavelength processing [75] or by appropriate selection of standards. The frequency of branches and distribution of branch points throughout the starch can interrupt iodine binding, and so any macromolecules that do not fit the ‘classic’ definition of amylose and amylopectin will further accentuate to this overlap [255, 256]. For this reason, the determination of amylose content by colourmetric approaches is appropriately referred to as apparent amylose content.

Although amylose is one of the two populations in starch, it still represents thousands of different molecules that have the potential to overlap with populations of amylopectin molecules in native starch. Many instruments have been used to separate amylose and amylopectin in starch with varying success. Size-exclusion chromatography (SEC/GPC) cannot fully resolve the populations of amyloses from amylopectins, [90] while field flow fractionation (FFF) [98], and free solution capillary electrophoresis (CE) can [109]. The complete separation of amylose and amylopectin populations was also shown for CE in Chapter 3. However, despite its limitations in whole starch analysis, SEC has been thoroughly employed in the analysis of enzymatically debranched starches [90], with subsequent correlations of apparent chain length distributions to different aspects of starch structure [151, 266]. However, the determination of these distributions has required important work into understanding the limitations of separation by SEC, most notably in the stationary phase which often requires debranching of starch prior to analysis. Enzymatic debranching of starch inherently results in an indirect assessment of the original branching structure, with information on the complete branching structures, such as the positions of the branches on the backbone lost as a result. and more information is available if separation of whole starch can be achieved. The current limitation for FFF is the limited chemical compatibility of the mechanical pump hardware, unsuitable for the high salt content, high temperature and organic solvents required to keep starch in solution. In contrast, CE does not employ a mechanical pump for injection, as there is no need for high pressures, and therefore has a much greater range of chemical compatibility. Additionally, due to the lack of a stationary phase, sample filtration is not required, increasing sample compatibility as well [267] as was shown in 3.3.1.2. The separation of amylose and amylopectin by iodine-affinity capillary electrophoresis (IA-CE) has been reported [109, 167] and an improved methodology developed (Chapter 3). By employing the IA-CE method, problems associated with overlap of absorption bands can be overcome. This allows for a more accurate characterisation and quantification of amylopectin and amylose individually to be performed.

While many studies have been performed on modified and/or extracted starches, altering the native starch structure [266, 268], they are rarely performed on whole grains or whole grain flours, which contain additional components including lipids (1 – 3 %) [22] and proteins (4 – 18 %) [269]. While phospholipids and fatty acids can form complexes with amylose chains [270], and proteins may undergo iodine binding [271], neither are likely to play a major role in the formation of the starch-iodine complex due to their low concentrations. A complete dissolution of starch would also prevent these starch-lipid complexes from forming.

In CE, when the DP of a polyelectrolyte is sufficiently high, the effects of DP on separation become negligible, in contrast to other structural factors such as branching or composition [104, 243]. As a result, the molar mass of polyelectrolytes for which critical conditions occurs will vary

greatly, dependant on the size of the monomer unit. CE of polyelectrolytes with a sufficiently high DP is thus referred to as "capillary electrophoresis in the critical conditions" (CE-CC) [116]. This is an analogy to liquid chromatography in the critical conditions (LC-CC) where conditions are sought in which a homopolymer is not separated by molar mass , for example in the characterisation of branching in poly(styrenes) [272]. CE-CC has been demonstrated experimentally in DNA [111], poly(sodium acrylates) [113, 234] and poly(styrene sulfonates) [112]. Most polymers are not simple and are composed of many molecules with different molar masses, end groups, composition distributions and branching characteristics. Currently the most commonly assessed molecular attribute of polymers is the average molar mass (M_n) with heterogeneity of molar mass also assessed, and calculated as the ratio of the weight-average molar mass and number-average molar mass. Typically these values are determined by size-exclusion chromatography [115]. Separation by CE-CC allows for separation by one or more of these characteristics with a negligible influence of DP, enabling the characterisation of complex polymers.

In CE-CC, the electrophoretic mobility is sensitive to structural and compositional features other than DP. The tendency of such features to exist as distributions related to possible structures yields an electrophoretic mobility distribution dependent on the separation factors. Recently it has been shown theoretically that in CE-CC a calculation of average mobilities, analogous to those used in SEC on molar mass distributions, can be made on distributions of electrophoretic mobility [104]. These mobilities include the weight-average electrophoretic mobility, analogous to weight-average molar mass, and moment-average electrophoretic mobility, analogous to number-average molar mass (though is not a number-average). The ability to calculate these average mobilities provides a wealth of knowledge on the polyelectrolytes being analysed, similar in scope to the importance of weight-average and number-average molar masses with regards to polymer properties. For example, the dependence of starch viscosity and resistant starch digestibility on molecular weight [273].

The calculation of dispersity and standard deviation for distributions of electrophoretic mobility has also been shown theoretically, analogous to those in SEC [116, 274]. As dispersity is calculated using a mobility of zero as a reference, two distributions could have identical dispersities, yet different absolute standard deviations. This is because standard deviation is calculated using the weight-average mobility as a reference. Thus, reliance on dispersity can result in the underestimation of variance, and in cases of narrow distributions where this is most pronounced the use of standard deviation is more appropriate [274].

Determinations of average mobilities and dispersity for distributions of electrophoretic mobility has been shown experimentally following the separation by branching in poly(acrylic acid) [116], degree of acetylation in chitosan [169] and composition in block copolymers [243]. In

the separation by branching of poly(acrylic acid), greater branching was shown to yield lower electrophoretic mobility [114]. The same trend was noted in the separation of starch in which the less branched amylose had a higher electrophoretic mobility relative to the highly branched amylopectin [109, 110], and was shown in Chapter 3.

The high DP of starch macromolecules results in the separation of amylose and amylopectin based on branching structure using the IA-CE methodology that was described in Chapter 3. The average mobilities of amylose and amylopectin were calculated to assess the differences in electrophoretic mobility distributions. Dispersity and standard deviation of the distributions of electrophoretic mobility was also calculated and used to assess the heterogeneity of starch molecules analysed.

4.2 Materials and Methods

4.2.1 Materials

Milli-Q® quality (Millipore, Bedford, MA, USA) water was used throughout the analysis unless stated otherwise. Sodium hydroxide (NaOH) pellets, glacial acetic acid, and anhydrous sodium acetate were sourced from Ajax Chemicals (Auburn, NSW, Australia). Boric acid (≥ 98 %) was purchased from BDH AnalaR, Merck Pty Limited. Analytical grade potassium iodide was obtained from Chem-Supply Pty Ltd (Gillman, SA, Australia). Analytical grade iodine was obtained from Univar (Downers Grove, IL, USA). Dimethyl sulfoxide (DMSO, ≥ 99.5 %), and lithium bromide (LiBr, ≥ 99 %) (both stored in a desiccator) were sourced from Sigma-Aldrich (Castle Hill, NSW, Australia). Deuterium oxide (D_2O) ≥99% and was obtained from Cambridge Isotope Laboratories, Inc. (Andowver, MA, USA).

Flours of different rice cultivars were provided by NSW DPI. Grain was harvested at physiological maturity, dehulled (THU35A 250V 50Hz Test Husker, Satake, Australia), milled (MacGill #2 mill) and ground (Cyclotec 1093 Sample Mill, Tecator AB, Sweden) to pass through a 50 μm sieve. Samples in flour form were stored in closed paper envelopes within a sealed plastic bag in a refrigerator (4 °C).

4.2.2 Iodine-affinity capillary electrophoresis and pressure mobilisation

4.2.2.1 Sample preparation

Samples were prepared at a concentration of 1 $g \cdot L^{-1}$ in anhydrous DMSO containing 0.05 % w/v LiBr at 80 °C with shaking at 300 rpm in an Eppendorf Thermomixer C (North Ryde, NSW, Australia) for at least 8 hours [79]. DMSO containing LiBr is referred to as 'DMSO with % LiBr', units are % w/v. All results were obtained from samples which gave clear and transparent

"solutions". The extent of dissolution is not quantified in this work. The sample preparation has been investigated and optimised previously (Chapter 3). Due to the chronology of experiments, 0.5 % w/w LiBr was not employed for dissolution in this work.

4.2.2.2 Methodology

For CE separations, 20 mM acetic acid buffer (7.3 mM acetic acid and 12.7 mM sodium acetate, pH 5.0) with 7.2 mM potassium iodide and 1.2 mM iodine metal was prepared according to Herrero Martinez et al. [109] and 25 mM sodium borate buffer (pH 9.2) was prepared according to Castignolles et al. [233]. The acetic acid buffer was sonicated for 5 min to ensure dissolution of iodine and degassing, and then filtered before use. Acetic acid buffer was stored in a foil wrapped glass bottle away from direct light when not in use. The 1 M NaOH was prepared fresh and used within 24h.

Experiments were performed on an Agilent 7100 CE instrument (Agilent Technologies Waldbronn, Germany) with a Diode Array Detector (DAD) monitoring at 560 nm with a bandwidth of 20 nm. The total capillary length was 37.0 cm (28.5 cm effective length), using an extended light-path fused-silica capillary (75 µm i.d., bubble factor 2.7, Agilent Technologies Waldbronn, Germany). The capillary was preconditioned before use by flushing with 1 M NaOH (4 min), 0.1 M NaOH (4 min), water (4 min) and running buffer (12 min). All injections were preceded by flushing with 1 M NaOH for 24 s and running buffer for 2 min. Samples were injected hydrodynamically by applying 17 mbar of pressure for 4 s (0.25 % capillary volume) followed by the injection of running buffer by applying 5 mbar of pressure for 5 s. Before separation a voltage of 20 kV is applied (ramped from 0 kV over 1 min), then set to 0 kV after 1.5 min. Following this, a period of active incubation is performed, with a pressure of 5 mbar and -5 mbar alternating for 5 min each, for a total of 30 min incubation time (6 x forward/backward sample movements) (see S 3.5.6). Following this, pressure was set to 0 mbar, and separation performed at 20 kV and 25 °C. The CE methodology was previously investigated and optimised (Chapter 3).

Data was acquired using Chemstation A10.01 and data treatment conducted with OriginPro 9.0. Raw electropherograms were transformed into weight distributions of electrophoretic mobilities as shown in supporting information of Chapter 3 (S 1), with the electroosmotic flow determined at a wavelength of 560 nm. For determination of peak areas with respect to concentration W(μ) was divided by μ (discussed in 4.3.2). Calculations of weight-average mobility (μ_w), dispersity (D(1,0)) and standard deviation were performed on the $W(\mu)$ of starch based on the work of Thevarajah et al. [116]. Calculations of μ_w, dispersity and standard deviation are shown in supporting information (S 4.6.1).

The CE hardware and capillary were validated before each experiment through the separation of a standard oligoacrylate solution in sodium borate buffer [113, 234]. The standard was

qualitatively compared to previous separations for repeatability of electro-osmotic flow and mobility of oligoacrylate species (Chapter 3).

4.2.3 Apparent amylose content

4.2.3.1 Sample preparation

Rice flour was weighed (100 mg) and transferred quantitatively to 100 mL volumetric flasks. To this, 1 mL of 95 % EtOH (5 % H_2O) was added to wet the sample followed by vortexing, then 9 mL of 1 M NaOH (in water) added. Samples were then left at room temperature for 15-25 h to disperse. After dispersion, solutions were made up to 100 mL with distilled water and vortexed.

4.2.3.2 Methodology

AAC was determined using a modified AACC approved method 61-03.01 [74].

For iodine colour measurement, 1 mL of solution was quantitatively transferred to a 20 mL test tube. To this, 2 mL of 0.1M citric acid in water was added with mixing, followed by 1 mL of iodine solution (0.2 % I_2 and 2.0 % KI by weight in distilled water) then made up to 20 mL with distilled water. The solution was then mixed and left to stand for 20 min. Colour absorbance was recorded for 2 aliquots of each sample solution at 620 nm. Measurements were made on a Mettler Toledo UV5 Bio (Mettler Toledo Ltd., Victoria, Australia)

Standard curve samples were prepared daily using water plus calibrated rice samples of known AAC from NSW DPI. The absorbance at 620 nm was plotted against amylose content for each standard solution. The resulting standard curve was used to read amylose values for test samples.

4.2.4 ^{13}C solid-state NMR spectroscopy

4.2.4.1 Sample preparation

Amorphous rice flour samples were obtained by heating 1 % w/v rice flour distilled water solution at 95 °C for 30 min. Dispersions were then freeze dried to remove the excess water. Dried samples were then stored at 44 % RH for at least 1 week to ensure consistent water content.

4.2.4.2 Methodology

The solid-state ^{13}C CP/MAS NMR spectroscopy experiments were performed at a ^{13}C frequency of 75.46 MHz on a Bruker DRX-300 spectrometer. Approximately 200-300 mg of starch samples were packed in a 4-mm diameter, cylindrical, partially stabilized zirconium oxide rotor with a KelF end cap. The rotor was spun at 6 kHz at the magic angle (54.7°). The 90° pulse was optimised each day by adjusting the pulse power at a constant pulse width (5 μs). A contact time of 1 ms was used

for all starch and rice samples with a recycle delay of 3 s. The spectral width was 20 kHz, acquisition time 50 ms, time domain points 2048, transform size 4096, and line broadening 50 Hz. The number of accumulated scans was dependant on the minimum number required for a signal-to-noise ratio of at least 30 for the C4 signal at ≈82 ppm. Spectra were referenced to external adamantane. The rate of cross-polarization was determined in a variable contact time experiment by Tan et al. [118] and confirmed here experimentally (S 4.6.2.1). The deconvolution of spectra for the determination of helix content is described in supporting information (S 4.6.2.2)

Peak fitting was performed using OriginPro 2016, with a least-squares Levenberg-Marquart algorithm to minimise chi squared.

4.3 Results and Discussion

4.3.1 The weight-distributions of electrophoretic mobilities of amylose and amylopectin in rice flour

The composition of starch is typically defined by two distinct populations of molecules, differentiated by their branching structures: amylose and amylopectin. These two populations of branching structure in starch exists as distributions of branch length, degree of branching and more, and can have a major impact on the subsequent properties of the starch, such as viscosity and swelling power. Yet there is also no absolute evidence that these molecules do not exists as a continuous, yet multimodal, population of branching structures.

In this chapter the CE method developed in Chapter 3 is employed to investigate the separation of amylose and amylopectin in rice flour, allowing for investigations into the populations of branching structure of starch. This is hypothesised to arise from the ability of the chains of amylose and amylopectin to bind with iodine, with the presence of branch points interrupting the binding, thus lowering the overall effective charge of the molecule. As a result, the mobility of amylopectin is observed to be lower ($< 1.5 \times 10^{-8}$ $m^2 \cdot V^{-1} \cdot s^{-1}$) than amylose ($> 1.5 \times 10^{-8}$ $m^2 \cdot V^{-1} \cdot s^{-1}$) (Figure 4-1).

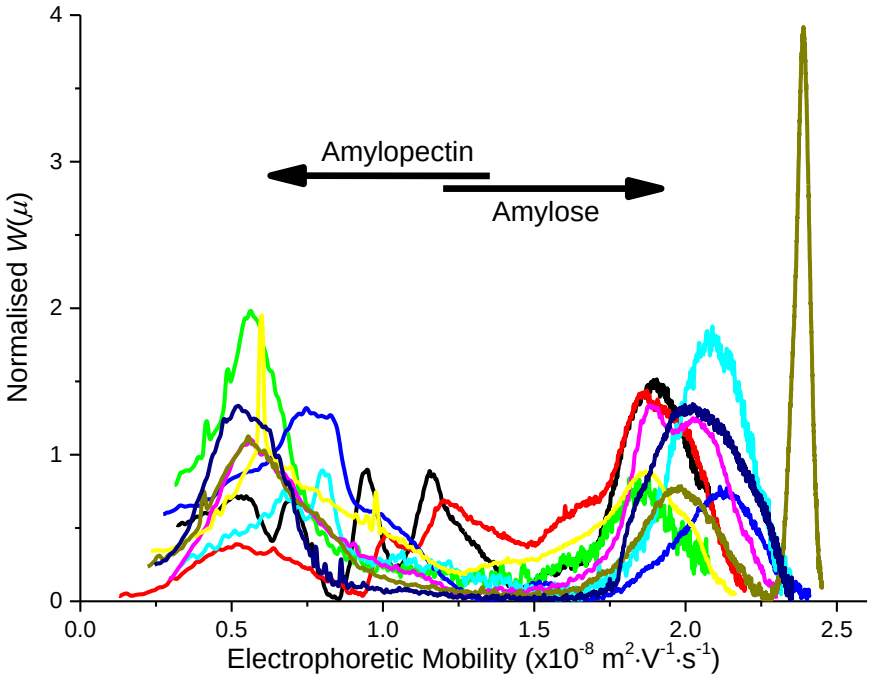

Figure 4-1 Weight distributions of electrophoretic mobilities for different rice samples

The electrophoretic mobility distributions of 9 different types of rice are shown in Figure 4-1. From these electrophoretic mobility distributions, it is clear that different rices exhibit different starch structures. This is highlighted by the difference in relative areas of the amylose and amylopectin peaks, width of the peaks, and most importantly, the presence of additional intermediate populations in the range of 1 to 1.75 x10^{-8} $m^2 \cdot V^{-1} \cdot s^{-1}$. These major compositional and structural differences are likely an important driver in some of the key properties of rice grains, while also providing scope to complement current understandings of correlations of AAC with rice properties.

4.3.2 Defining amylose and amylopectin by their electrophoretic mobilities

The electrophoretic mobility distributions shown in Figure 4-1, exhibit an intermediate population between amylose and amylopectin in some rice samples (≈1 to 1.5 x10^{-8} $m^2 \cdot V^{-1} \cdot s^{-1}$). There then arises a need to determine if this intermediate population of branched molecules is more amylopectin- or more amylose-like in its structure and function. In addition, clear ranges of mobility need to be defined and assigned if an accurate analysis of the electrophoretic mobility distributions is to be performed.

To determine an appropriate range of mobility to define both amylose and amylopectin, the mobility normalised electrophoretic distributions were integrated over two ranges, where the intermediate peak is included as either amylose or amylopectin. This corresponded to a mobility switching point of either 1 or 1.5 (x10^{-8} $m^2 \cdot V^{-1} \cdot s^{-1}$). The relationship of starch branching with iodine binding capacity and by extension, electrophoretic mobility (μ), suggests that the

absorbance of molecules at any given μ will be affected by the associated branching structure. This supported by the higher absorptivity of amylose-iodine complexes compared to amylopectin-iodine complexes [72]. So, if we assume a linear correlation between the Beer-Lambert coefficient and the mobility, we can account for this by dividing $W(\mu)$ by μ to account for the differences in branching structure of any given μ.

The obtained mobility normalised peak areas of the different ranges were then compared to other measured structural aspects of the rice samples to determine which most closely correlated. For the determination of the amylopectin range, the peak area was plotted against the double helix content determined by ^{13}C NMR spectroscopy (Figure 4-2), due to the exclusivity of amylopectins ability to form these double helices in starch. The relation of both integration ranges to double helix content was high, reporting r^2 values of 0.95 and 0.93 for the range ≤1.0 and ≤1.5 x10^{-8} $m^2 \cdot V^{-1} \cdot s^{-1}$, respectively. The similarity of these fits also indicates that the electrophoretic mobility distribution of amylopectin molecules that participate in the formation of double helices is quite broad in some cases.

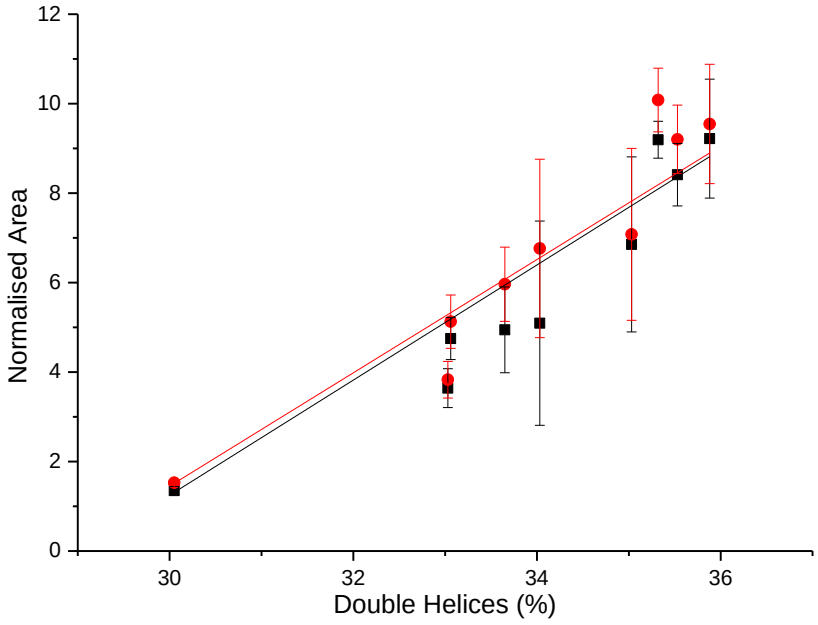

Figure 4-2 Electrophoretic mobility normalised peak areas of amylopectin peak integrated from the leading peak minimum to 1.0 (black) and 1.5 (red) x10^{-8} $m^2 \cdot V^{-1} \cdot s^{-1}$ plotted against the double helix content determined by ^{13}C solid-state NMR spectroscopy. Linear fits are shown for the 1.0 (black, r^2 = 0.95) and 1.5 (red, r^2 = 0.93) x10^{-8} $m^2 \cdot V^{-1} \cdot s^{-1}$ data. Normalised area error bars are the standard deviation of 3 instrumental repeats

The electrophoretic mobility range for the amylose molecules was then confirmed by relation of the mobility normalised peak areas against the apparent amylose content (*AAC*). Given the similarity of measurement protocols (absorbance of iodine-amylose complexes), this relationship is expected to be highly linear; however, this was not observed (Figure 4-3). In the choice between mobility ranges, only the turning point of 1.5 x10^{-8} $m^2 \cdot V^{-1} \cdot s^{-1}$ displayed an appropriate relationship with the *AAC*, though the correlation was poor, yielding an r^2 of 0.72. It is fairly well known that

AAC methods can both under- and overestimate true amylose content [73]; however, it is not yet clear if this arises from differences in branching structures, in size or from the presence of this third type of starch; commonly dubbed amylopectin-like-amylose. Conversely, this may also arise from incomplete dissolution of cultivars with high *AAC* in either the IA-CE or *AAC* methodologies, with higher amylose starches suggested to have reduced solubility [79].

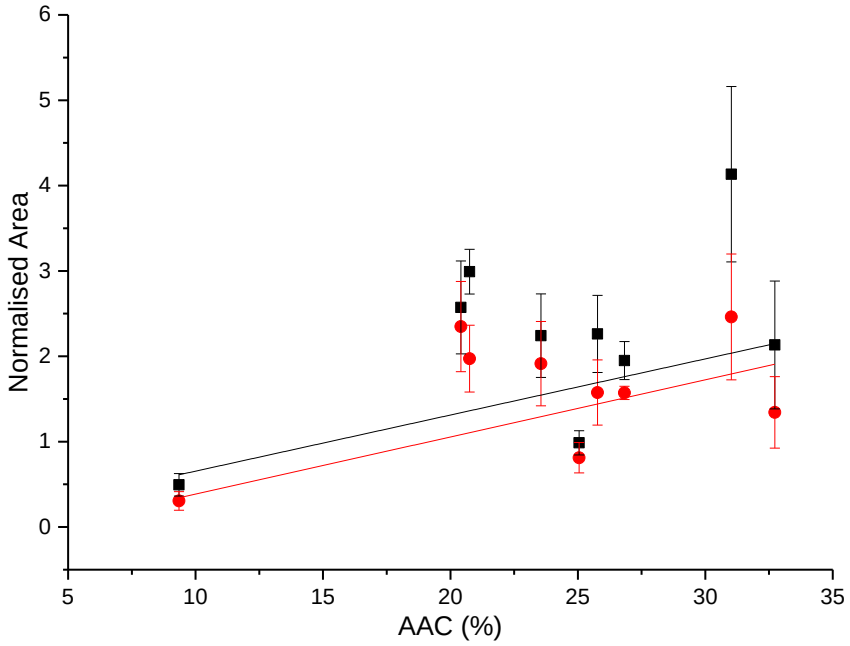

Figure 4-3 Electrophoretic mobility normalised peak areas of amylose peak integrated from 1.0 (black) and 1.5 (red) x10^{-8} m^2·V^{-1}·s^{-1} to the trailing peak minimum plotted against the AAC determined by spectrophotometry. Linear fits are shown for the 1.0 (black, r^2 = 0.25) and 1.5 (red, r^2 = 0.72) x10^{-8} m^2·V^{-1}·s^{-1} data. Normalised area error bars are the standard deviation of 3 instrumental repeats

Thus, this intermediate peak is assumed to behave more like an amylopectin, confirmed by both its lack of correlation with *AAC*, and its strong correlation with double helix content. As a result, the appropriate range delineation for amylopectin to amylose was determined to be 1.5 x 10^{-8} m^2·V^{-1}·s^{-1}. This delineation point was suitable for most rice samples, correlating to a point between baseline resolved peaks (Figure 4-1), though still intersected intermediate populations in some samples. This is an important observation in pointing to the presence of intermediate populations that may not exist in all rice samples. Therefore, to allow direct comparison in the case of these samples, a consistent delineation point was deemed appropriate, while future work should involve a direct assessment of these intermediate populations. Such intermediate starch structures have not been explicitly studied in the literature [229, 275]; however, there is some indirect evidence suggesting that such structures arise from long chain branching on amylopectins [255, 256]. This methodology then provides an evidence-based approach to define and characterise accepted definitions of amylose and amylopectin, providing confidence in the analysis and reporting of the weight distributions of electrophoretic mobilities.

4.3.3 Characterising the weight-distributions of electrophoretic mobility of rice flours

As shown here, and in Chapter 3, starch is separated in IA-CE based on branching structure. This yields a weight distribution of electrophoretic mobilities that allows for the assessment of branching structures in starch. Analysis of the weight-distribution of electrophoretic mobilities can describe two key features of starch.

The first is the sensitivity of the electrophoretic mobility to the degree of branching present as well as within each weight-distribution of electrophoretic mobilities (i.e. degree of branching above and below 1.5 x10^{-8} $m^2 \cdot V^{-1} \cdot s^{-1}$). A higher mobility indicates a lower amount of branching and/or longer average chain length. Thus, amylose has a higher weight-average mobility. The second feature describes the heterogeneity of branching structures. A broader electrophoretic mobility distribution is inclusive of a range of branching structures (more heterogeneous), whereas a narrow distribution suggests a limited range of branching structures (less heterogeneous). Here this is calculated and reported as dispersity.

4.3.3.1 The overall weight-average mobility and how it relates to AAC

The apparent amylose content (*AAC*) of rice covers a broad range of defined classes, including waxy (0 – 5 %), very low (5– 12 %), low (12 – 20 %), intermediate (20 – 25 %) and high (>25 %) [276]. The primary driver for differences of *AAC* arises from the genetic makeup of a given rice cultivar, with environmental influences also playing a minor role [67]. It is an important measure in rice grain quality, and thus a relevant parameter against which to explore further the structures of amylopectin and amylose.

The weight-average electrophoretic mobility (μ_w) for the total $W(\mu)$ of the starch (both amylopectin and amylose) was calculated for the rice samples (Figure 4-4). As a result of separation occurring as a function of branching structure, the μ_w of the total $W(\mu)$ can be stated to relate to the relative proportions of branching structures within the sample, for example a higher total μ_w would indicate a decreased amount of branching than a lower total μ_w. A simple interpretation of this would be a relative increase in amylose content corresponding with increasing total μ_w. Therefore, if we were to assume that each of the rice samples in Figure 4-1 had similar starch contents, then we could expect *AAC* to increase with increasing μ_w; however, this was not observed. The independence of total μ_w from *AAC* was highlighted by the observation of three clusters at 1.1, 1.3 and 1.5 x 10^{-8} $m^2.V^{-1}.s^{-1}$ for the non-waxy rice samples. This may arise from differences in total starch content, which was not quantified in this work, or from differing dissolution protocols for the *AAC* and IA-CE methods, especially for the higher amylose rice

samples. Despite this the implications of differences in the populations of branching structures are still quite clear for the intermediate *AAC* rice samples.

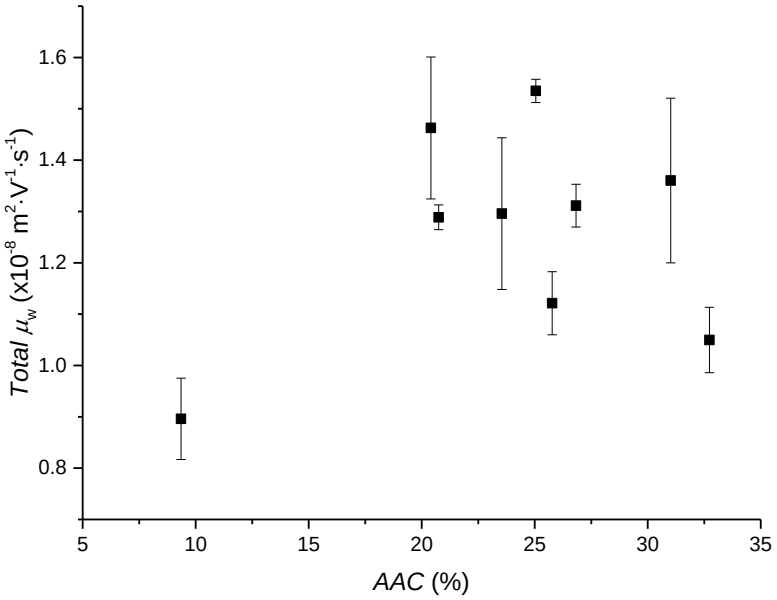

Figure 4-4 Calculated total weight average mobility (μ_w) of the weight distribution of electrophoretic mobility for different rices from the initial minimum of the amylopectin peak (~2.7 x 10^{-9} m^2·V^{-1}·s^{-1}) to the ending minimum of the amylose peak (~2.3 x 10^{-8} m^2·V^{-1}·s^{-1}) plotted against AAC. Error bars are the standard deviation of three instrumental repeats

Much research has related *AAC* to the functional properties of rice grains [26, 67, 69], allowing for the different *AAC* classes to be used as indicators of functional properties, with variation expected within each *AAC* class and even *AAC*. The apparent disconnect between total μ_w and *AAC* highlights the fact that a given measure of *AAC* is not strictly measuring one type of amylose but rather a wide range of amyloses, and this may be a driver for the variability of properties seen in rice grains of similar *AAC*. A key point is the spread of total μ_w reported for the three rice samples with *AAC* of 25-26 %, which indicates that while *AAC* was quite similar, the overall branching profile is broader than would be expected. For example, a greater proportion of more or less branched amylose would influence the total μ_w relative to samples of similar *AAC*. The same can be said of changing proportions of more or less branched amylopectins. A similar situation was also observed in the high amylose rices (Figure 4-4, > 30 % *AAC*), with a large apparent difference in total μ_w indicating that while both high amylose rices in terms of *AAC*, there is a difference in either actual amylose content or the amyloses and/or amylopectins simply exists as more or less branched populations of molecules. The only waxy rice variety measured (<10 % AAC), displayed the lowest total μ_w, clearly differentiating from the other cultivars as containing a larger proportion of highly branched structure, in agreeance with its low *AAC*, a characteristic of waxy rice grains.

4.3.4 Investigation of the weight-average mobilities of amylose and amylopectin

The synthesis of starch is complex, with multiple families of enzymes working in a concerted fashion to produce both amylopectin and amylose [250], resulting in multifaceted distributions of branching chain length, size and composition [22]. This is complexity is highlighted in the distinct μ_w of both amylopectin and amylose (Figure 4-5). The lack of linear correlation between the μ_w of amylose and amylopectin suggests that there is little influence of the branching of amylopectin and amylose on each other, strongly supporting the notion that amylose and amylopectin are produced by distinctly different pathways or experience different kinetics during action of SBE.

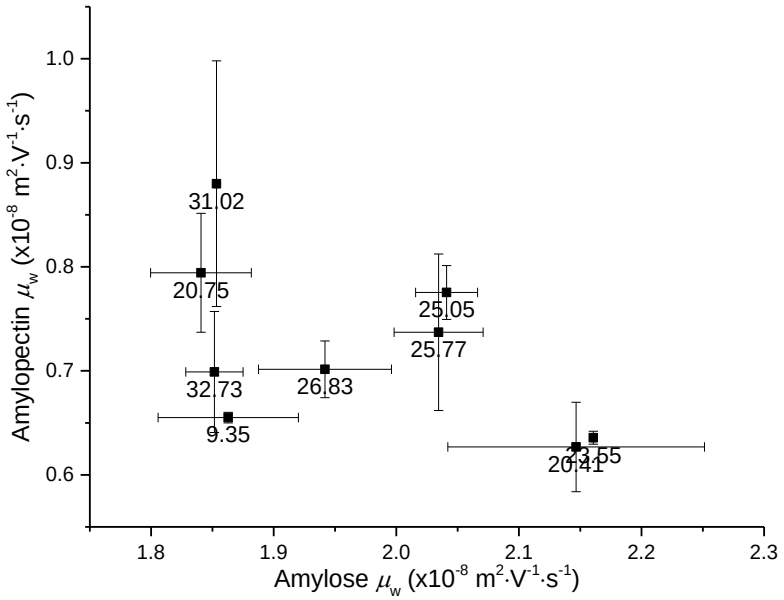

Figure 4-5 Calculated weight average mobilities (μ_w) of both amylopectin and amylose weight distributions of electrophoretic mobility for different rices where amylose and amylopectin are differentiated at 1.5 x10^{-8} m^2·V^{-1}·s^{-1}. Labels beneath each data point display the respective AAC. Error bars are the standard deviation of three instrumental repeats

By assessing the μ_w of both amylose and amylopectin with respect to one another, a unique identifying fingerprint can be obtained for each rice sample based on their branching structures. It was observed that significant differences in the branching structures of amylose and amylopectin could be identified between samples of similar AAC. For the two similar high AAC rice samples (>30 % AAC), the μ_w of the amylose peak was similar, indicating a similar branching structure of amyloses; however, a significant difference was observed in the μ_w of amylopectin indicating a significant shift in the branching structure. Interestingly, these high amylose cultivars also exhibited amylose μ_w values on the lower mobility end of the sample range indicating an increase in branching of amylose. Another outstanding case was the apparent difference in μ_w of both amylose and amylopectin in two of the intermediate AAC rice samples (20.75 and 20.41 %), showing opposite characteristics in both amylose and amylopectin branching. In this case, one rice (20.41 % AAC) was observed to have a high μ_w amylose (indicating low branching) and a low μ_w amylopectin (indicating high branching), while the other (20.75 % AAC) displayed a low μ_w

amylose and a high μ_w amylopectin. Groupings of rice cultivars with similar branching structures were also noted. Most interestingly, the similarity of amylopectin and amylose μ_w for the waxy (9.35 % *AAC*) and a high amylose (32.73 % *AAC*) rice, suggested the branching structures present are quite similar, despite a vast difference in proportions. Similarities of μ_w of amylopectin and amylose were also noted for two groupings of intermediate *AAC* rice cultivars, with both groupings having similar *AAC,* suggesting that these rices are likely to exhibit similar functional properties where molecular structure is key a driver.

These differences in branching characteristics of amylose and amylopectin, identified through analysis of the $W(\mu)$ distributions, have the potential to be a strong factor in further explaining the role of starch structure in some rice properties. The fact that branching populations differ for cultivars of similar *AAC* may in turn explain why different functional properties can arise from cultivars with the same AAC, for example the relationship of *AAC* with digestibility in rice [26].

4.3.4.1 The relationship of the individual weight-average mobilities of amylose and amylopectin to AAC

The determination of *AAC* in rice is one of the only direct measurements of starch structure employment in routine analysis of rice samples. The quantity of *AAC* is known to play a major role in many of the functional and sensory properties of rice grains [67]. However, *AAC* typically represents the minor compositional macromolecular component of the starch present within the rice grain (≈ < 35%) compared to the highly branched amylopectin molecules. Given this, it is no surprise that amylopectin and its branch chain length distributions also play a role in properties of rice such as gelatinisation temperature and pasting properties [69]. This represents an opportunity to potentially further discriminate rice samples where similar *AAC* has been reported by the individual branching structures of not just amylopectin, but also of amylose. An example of this is the apparent relationship of *in vitro* digestibility of rice grains with *AAC* [26]. This relationship yields a general trend of increasing amylose resulting in lower digestibility; however, at any point along the curve varieties of given *AAC* can be observed to exhibit significantly different digestibility. It is examples like this, where *AAC* does not give the complete picture, that additional characterisations of the different levels of starch structures can benefit our understanding of rice and starch properties.

The differences observed in amylopectin and amylose branching structures in rice samples were explored through the relationship of μ_w to *AAC* (Figure 4-6). This allowed for an investigation into both the range of values that may exists across rice samples as well as the ability to discriminate between cultivars of different and similar *AAC*. A broad range of μ_w were observable for amylopectins in rice, indicating differences in their branching structures towards higher branching/shorter chain lengths or lower branching/longer chain lengths at lower or higher μ_w,

respectively (Figure 4-6). However, this range was narrow (≈0.3 $m^2 \cdot V^{-1} \cdot s^{-1}$). Despite this, the extremes of the range could distinguish clearly differences in amylopectin branching structure between samples with a similar *AAC*, a potential insight to the differences in BE activity during synthesis between the different rice cultivars. This was most profound in two of the intermediate *AAC* cultivars (≈20 % *AAC*), where a significant difference in their amylopectin μ_w would indicate a significant difference in their amylopectin branching structure. A similar observation was also made for the high amylose rice samples (>≈ 30 % *AAC*). Interestingly, the only waxy variety measured (≈ 10 % *AAC*) displayed a μ_w on the low end of the range of μ_w observed (Figure 4-6). This would indicate a higher amount of branching/shorter chain lengths in general, something that has been noted for waxy varieties. However, the measurement of additional waxy varieties would be required to confirm if this low μ_w is a characteristic of waxy varieties. If it is, this may suggest that the action of amylose synthesis plays some role in the branching structure of amylopectin, more likely in chain elongation than in extent of branching based on current understandings in the literature [247].

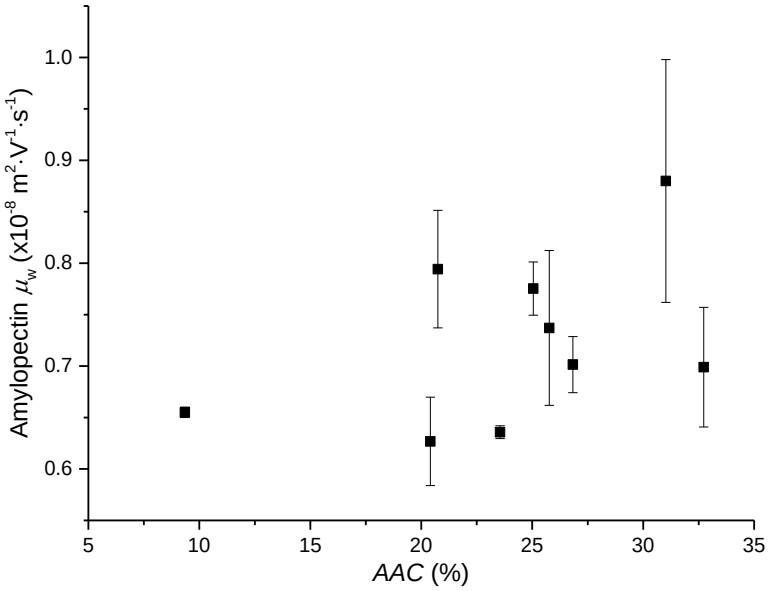

Figure 4-6 Calculated weight average mobilities (μ_w) of amylopectin weight distributions of electrophoretic mobility for different rices plotted against AAC. Error bars are the standard deviation of three instrumental repeats

The μ_w of amylose has an interesting relation to the *AAC*, as a given (unknown) mobility of amylose essentially represents the specific molecule measured by the colorimetric determination of *AAC* while μ_w identifies the weight average amylose that actually comprises the sample. These amyloses can be two very different molecules in theory. Standard methods for the determination of *AAC* employs calibration curves prepared from standards that can be of different or similar botanical sources to the analyte being measured, as well as from purified starches or starches from flour. This has the potential to introduce significant error relative to true amylose content. In the measurement of *AAC* in rice it has been shown that calibrations based on the use of

calibrated rice samples yields highly repeatable *AAC* values [73], which is the method employed in this work. However, a repeatable valuable may still contain a bias, and given that *AAC* can both under and overestimate amylose content, the bias is likely not systematic and thus it would be difficult to correct for a true amylose content.

By exploring the μ_w of amylose for different rice samples relative to their *AAC* it is clear that rice can contain a range of different amylose structures, even at similar amylose contents (Figure 4-7). The μ_w of the amylose molecules is a function of their iodine binding capacity, influenced by both their chain length and branching structures. Thus, it can be theorised that for any given μ_w the determination of a true amylose content for that molecule should be based on a calibration produced using samples of similar μ_w. This would yield a calibration curve that is based specifically off the iodine binding behaviour of a narrow range of molecules and should therefore allow for a closer approximation of the true amylose content.

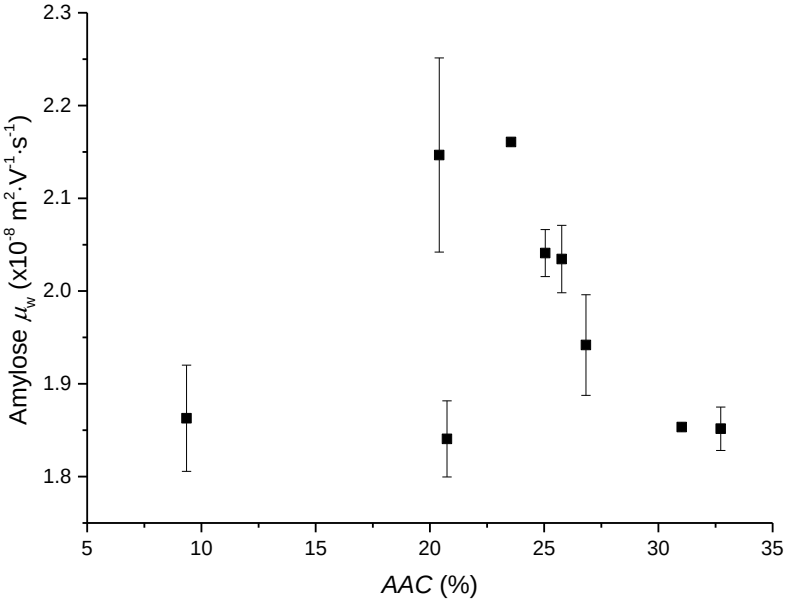

Figure 4-7 Calculated weight average mobilities (μ_w) of amylose weight distributions of electrophoretic mobility for different rices plotted against AAC. Error bars are the standard deviation of three instrumental repeats

The specific differences in the μ_w of amyloses for each rice samples covered a narrow mobility range (1.8 to 2.2 m^2·V^{-1}·s^{-1}, Figure 4-7); however, the differences between μ_w of different samples was typically larger than was seen in the μ_w of amylopectins (Figure 4-6). The rice samples of intermediate to high *AAC* (20 – 28 % *AAC*) displayed the greatest range of μ_w highlighting the difference in amylose structure that can exist even in a narrow range of *AAC*. The rice samples in this range also typically exhibited higher μ_w indicative of less branched structure, while higher and lower *AAC* rice samples display significantly lower μ_w, indicating an increase in branching structure. These differences may be a driver in differences in the properties of these rice samples,

especially those apparently linked to *AAC*. However, the lack of sample diversity at higher and lower *AAC* makes it difficult to make any inferences based on this apparent phenomenon.

4.3.5 Assessing the dispersity of starch in rice flours relative to AAC

The heterogeneity of branching structures was assessed through the calculation of dispersity and standard deviation values for the weight-distributions of electrophoretic mobilities. The calculated dispersity and standard deviation values for the amylopectin and amylose $W(\mu)$ are shown in Figure 4-8. In examining them against one another, it is immediate clear that the dispersity values for amylose were much lower than that of amylopectin (Figure 4-8A). However, this is a result of the dispersity calculation taking $\mu_w = 0$ as a reference resulting in decreasing dispersity values with increasing μ_w. However, the relative values of each can still be noted to display clear differences in the heterogeneity of both amylopectin and amylose branching structure (Figure 4-8A). Additionally, the heterogeneity of both amylopectin and amylose appeared to be independent of one another, indicated by the spread of data points showing no real correlation. For a more local assessment of the broadness of the $W(\mu)$ distributions of both amylopectin and amylose, the standard deviation of the $W(\mu)$ distributions was calculated as a measure of dispersity. The calculated standard deviation of amylopectin was observed to typically be higher than that of amylose (Figure 4-8B)[116]. Only one rice sample displayed an amylose standard deviation similar to that of the amylopectins of other rice samples, and interestingly was similar to the standard deviation of its own amylopectin. This lower standard deviation observed for the amylose $W(\mu)$ distribution is influenced by the selected ranges of electrophoretic mobility for analysis that were determined in 4.3.2, with the range of amylopectin determined to be quite broad (1.25 – 1.30 $m^2 \cdot V^{-1} \cdot s^{-1}$ wide) compared to amylose (<0.8 $m^2 \cdot V^{-1} \cdot s^{-1}$ wide). The higher standard deviations seen in the amylopectin is also counter to current understandings of branching of statistical polymers in the literature, where increased degree of branching has been correlated with decreasing dispersity, due to an apparent effect of saturation of heterogeneity [116]. Similar to the dispersity values, the standard deviation values of both amylopectin and amylose displayed no apparent correlation, indicating an apparent independence in the mechanisms of the heterogeneous branching. These findings highlight the complexity of starch synthesis, and lend support to the notion of differing pathways for branching in amylopectin and amylose as has been suggested in the literature [247, 250].

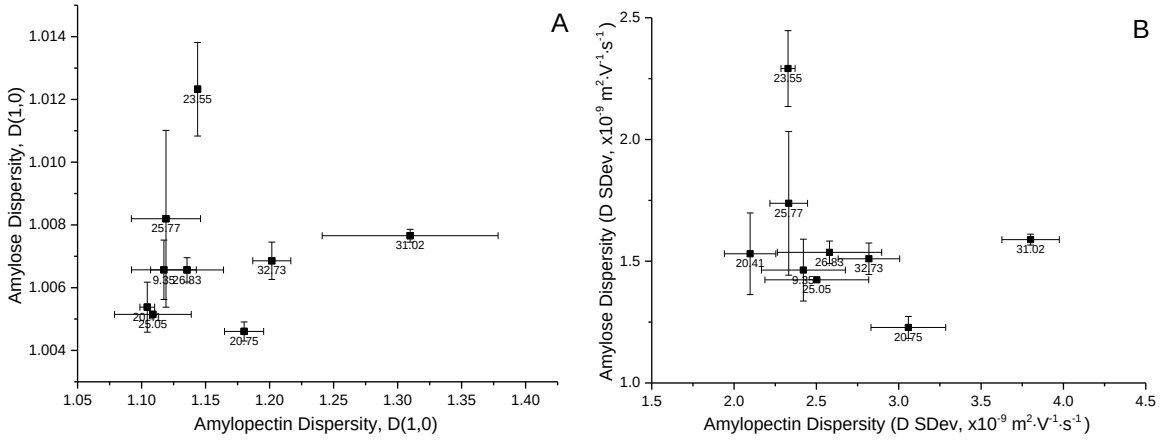

Figure 4-8 Calculated A) dispersity (D(1, 0)) and B) standard deviation of amylopectin and amylose weight distributions of electrophoretic mobility for different rices plotted against each other. Labels beneath each data point display the respective AAC. Error bars are the standard deviation of three instrumental repeats

In the assessment of heterogeneity, dispersity values of amylopectin and amylose were observed to be higher than for any other polymer reported using this methodology, while amylose displayed only slightly higher dispersities (Figure 4-8A) [116]. In the case of branching in poly(sodium acrylate acid)(PNaA), dispersity values reported range from ~1.0000 for linear to ~1.0015 for a 3-arm star, with *SDev* values an order of magnitude smaller than those reported here (Figure 4-8B) [116]. The calculated dispersity and standard deviation values for the entire $W(\mu)$were predictably much higher than the values of either amylopectin or amylose individually (S 4.6.3).

The heterogeneity of branching seen in the literature shows that as degree of branching increased in PNaA, dispersity increased [116]. However, when the degree of branching continues to increase, a point is reached where branching is so abundant that the heterogeneity of branching decreases [116]. This is essentially explained as a saturation in the degree of branching that results in a plateau or reduction in the possible branching arrangements. In contrast, less branched polymers have the potential to have a greater degree of randomness in their branching structures, dependant of course on the heterogeneity of the branching synthesis. This has been shown in the local dispersity values of poly(alkyl acrylates) by multiple detection SEC [90]. Therefore, it is theorised that amylose would display a higher dispersity than amylopectin, given its lower degree of branching. Of course, given that starch is a natural polymer, it is likely that the complex enzymatic pathways of starch biosynthesis exercise some degree of control of over how heterogenous branching can be; however, this would likely be on a per cultivar basis and so difficult to recognise.

4.3.5.1 Relation of dispersity of amylopectin and amylose to the AAC of starch

The heterogeneities of both the amylopectin and amylose individually was shown in the previous sections to vary substantially between different rice samples. Similar to the expectations

of different distributions of μ_w of amylopectins and amyloses, the heterogeneity of these distributions may also impact on their behaviour as polymers.

The heterogeneity of the $W(\mu)$ for amylopectin and amylose was explored in relation to the *AAC* of the rice samples through both dispersity (D(1,0)) and standard deviation (Figure 4-9). As mentioned in the previous section, dispersities of amylopectin were quite high and covered a broad range compared to what has been reported in the literature for synthetic polymers [116]. Dispersity values for amylopectin spanned the range of 1.10 to 1.30, indicating a significant range of heterogeneity within the branching structures of amylopectins in the different rice cultivars (Figure 4-9A). While most of the rice cultivars, including the waxy and intermediate *AAC* (< 27 % *AAC*) samples, occupied the range of 1.10 to 1.15 with overlapping error bars, the high amylose samples (> 30 % *AAC*) displayed dispersity values on the higher end of the range. This may be indicative of a contributing relationship of amylose to a more heterogenous amylopectin branching structure. Higher amylose contents are typically a result of increased GBSSI activity, and it may be possible that the increased activity has knock-on effects on amylopectin production. Such disruptions may be a factor in the amount of heterogeneity observed in the starch structure. The measurement of heterogeneity through the standard deviation (Figure 4-9B) did not display any significant differences in the observed heterogeneity of the $W(\mu)$ of amylopectin to those observed by dispersity (Figure 4-9A). This is likely a result of the low mobility of the amylopectin population, where the reference ($\mu_w = 0$) is not far enough from the μ_w of the amylopectin to show a significant difference in the apparent trends of relative heterogeneity.

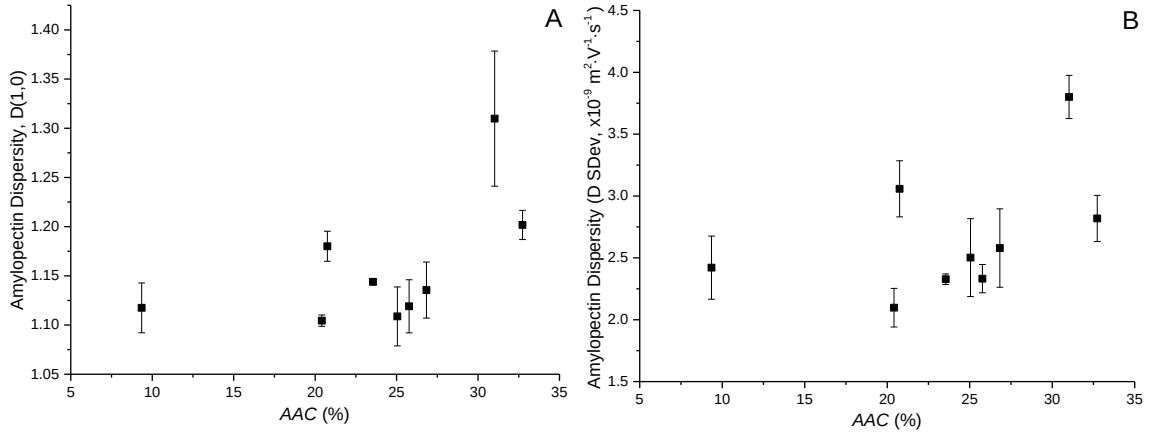

Figure 4-9 Calculated A) dispersity (D(1, 0)) and B) standard deviation of amylopectin weight distributions of electrophoretic mobility for different rices plotted against AAC. Error bars are the standard deviation of three instrumental repeats

Dispersities of amylose in the rice cultivars were lower than those reported for amylopectin (Figure 4-8), though were still high compared to literature [116]. Thus, even though amyloses are generally considered to exhibit a very low degree of branching, there appears to be a high degree of heterogeneity of branching structure (Figure 4-10). The amylose $W(\mu)$ dispersity values of the

rice samples covered a range of 1.004 to 1.012 (Figure 4-10A). This appears to represent narrow range; however, substantial differences in dispersity could still be noted between some samples with respect to their error bars. While most rice samples occupied a narrow range of dispersity values, one intermediate amylose sample (≈22.5 % *AAC*) displayed a significantly higher dispersity than the other samples. This is indicative of a much greater degree of heterogeneity of amylose structure and has the potential to be a property defining feature amidst samples of similar *AAC*. Smaller differences in heterogeneity could also be noted in the dispersity values of intermediate *AAC* samples (20 – 27 % *AAC*) which may also be an indicator for differences their molecular behaviour, and by extension rice sample properties. As a local determination of heterogeneity, the standard deviation of amylose allowed for a direct comparison of the heterogeneity of the amylose molecules, independent of branching structure (Figure 4-10B). Despite this, similar trends in standard deviation relative to *AAC* were observed as for dispersity. The exception to this were two intermediate *AAC* rice samples (≈20 % *AAC*) which displayed a significant different in their standard deviation (Figure 4-10B) in contrast to their dispersity (Figure 4-10A). This clearly indicates a difference in the heterogeneity of the amylose structures between these samples that could not be observed through dispersity, and with the addition of their large differences in mobility (Figure 4-7), both are likely to exhibit vastly different molecular behaviours. This highlights the usefulness of using multiple approaches in the investigation of heterogeneity.

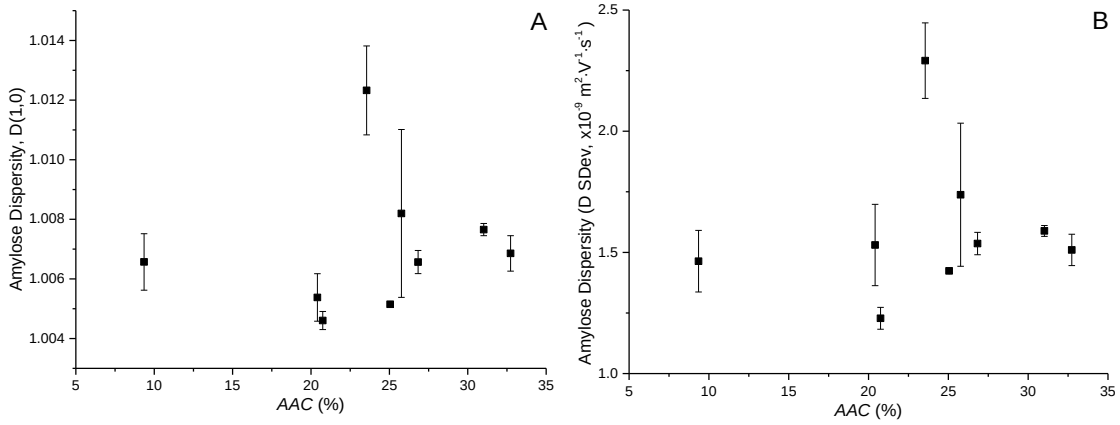

Figure 4-10 Calculated A) dispersity (D(1, 0)) and B) standard deviation of amylose weight distributions of electrophoretic mobility for different rices plotted against AAC. Error bars are the standard deviation of three instrumental repeats

The significance of differences in heterogeneity is analytically dependent on the error of dispersity and standard deviations values, closely linked to the repeatability of $W(\mu)$. The heterogeneity of structure distributions such as molar mass, branching or substitution could significantly affect physicochemical properties in synthetic and natural polymers [90]. However, it remains to be seen how the heterogeneity in starch structure impacts on the functional properties of the starch, and indeed the cereal it is contained in. Further to this, the existence of a well organised multi-level structure defined by a cocktail of overlapping and co-acting enzymes

further complicates how significant an amount of heterogeneity can be managed in this well-defined structure. Despite this, identifying differences in dispersity between samples can be used as indicator of consistency in branching structures seen in different rice samples, and indeed starch in general, while also serving to exemplifying the heterogeneous nature of starch structure. The determination of heterogeneity by CE is a powerful tool, that has the potential to further our understanding of how the structures of amylose and amylopectin can influence both higher levels of structure as well as overall starch properties.

4.4 Conclusion

The complete separation of starch by branching structures in rice flour was shown by capillary electrophoresis. The separation yielded two apparent populations of branching structure corresponding to amylopectin and amylose macromolecules. However, a third type of branching structure was also observed in some rice samples, indicating a macromolecule of intermediate branching structure. This third type of starch has been theorised in the literature to arise from the long chain branching on amylopectins [255, 256], and is especially relevant in the measurement of AAC, as it can lead to overestimation of the *AAC*. However, this third type of starch has not been explicitly observed or discussed [229, 275], typically assumed to co-elute with amylose in SEC. This work has shown for the first time, separation of starch in rice flour by capillary electrophoresis and successfully identified a third type of branching structure that may be linked to the long chain amylopectins theorised in the literature. For the purposes of this work, this intermediate starch structure was thus treated as an amylopectin, allowing for comparisons with samples that did not contain this type of starch. In future work this intermediate starch structure should be explored as an independent structural population of starch.

The distributions of electrophoretic mobility obtained by separation were then analysed further, employing methodology developed for the characterisation of the $W(\mu)$ of polymers obtained by capillary electrophoresis [116]. With this method, the weight-average mobility of the of the $W(\mu)$ for different rice flours revealed significant differences in the relative amounts of branching in different rice samples. This finding is similar to the physical basis of *AAC*; however, the μ_w is more closely representative of the ratio of each type of branching structure. For example, a higher μ_w would likely be indicative of a higher *AAC;* however, the difference in what these techniques measure means there is no real correlation.

The individual μ_w of the amylopectin and amylose populations were also observed to vary between rice samples. The differences observed in μ_w of amylopectin populations towards higher or lower μ_w are very likely closely linked to the differences in BE activity during starch synthesis, preferentially catalysing short, intermediate and long chain branching. This is a phenomenon that

has been seen to vary between different starches and indeed rice starch in molecular weight distributions of enzymatically debranched starches by SEC [90]; however, is shown here in native unmodified starch in whole rice flour. The differences in μ_w of amylose populations also highlighted the broad range of apparent branching structures of amylose that exists within and between rice samples. The function of branching during amylose synthesis is not clearly understood, and due to its low degree of branching is often referred to as functionally linear. However, it has been shown that the branching in amylose can vary significantly between rice samples. This could lend itself as an important property regarding *AAC*. Given the sensitivity of the iodine binding capacity of starch to the branching structures, the most ideal samples for calibration should be those exhibiting similar branching structures, and so μ_w could prove to be a means by which to identify appropriate standards.

The heterogeneity of the $W(\mu)$ of different rice samples was assessed through the dispersity and standard deviation. The total heterogeneity of the starch was observed to be very high compared to literature values for a number of synthetic and natural polymers [116]. This is likely due to the inherent multi-modal branching nature of the system, with between 2 and 3 distinct populations observed. The dispersity of the individual amylopectin and amylose $W(\mu)$ was also significantly higher than other polymers employing this method [116], highlighting the highly heterogenous nature of starch structure. This especially exemplifies the complexity of the synthesis pathways that lead to this heterogeneity. Within these high levels of heterogeneity, rice cultivars could still be noted to exhibit different levels of heterogeneity, which is likely to play a role in their individual functional properties.

This work has shown a new avenue to assess the differences in branching structure of starch in rice flours This contrasts with literature analysis of branching through molecular weight distributions of enzymatically debranched of starches by SEC. The analysis of unmodified starch directly in rice flour has allowed for insight into the native unmodified branching structures present, as opposed to typical analysis of starch fragments, where substantial information on the native structure is lost.

4.5 Future work

As the methodology currently stands, the data obtained by this unique characterisation method provides an interesting new approach in assessing differences in starch structure between different rice cultivars. Further analysis of a greater range of intermediate *AAC* class varieties (where most commercial varieties exist) would allow for an improved confidence in the existence of variability and groupings of mobilities (and by inference branching structures) that were observed for the small set of rice cultivars examined here. In addition, due to the small sample

volumes (≈< 10 nL), lower sensitivity can be an issue with dilute starch dissolutions; however, there are methods available that can improve sensitivity such as electrophoretic pre-concentration and stacking [107, 108].

Due to the chronology of experiments, dissolution in this chapter employed 0.05 % w/w LiBr rather than the 0.5 % w/w LiBr that was determined as optimal in Chapter 3. Therefore, the analysis of rice flours needs to be revisited to assess the role of improved dissolution conditions on the characterisation. This is especially important in the cases of the high amylose rice samples, as an incomplete dissolution will significantly bias the resulting $W(\mu)$. Subsequent confirmation of ideal dissolution conditions for rice flours would then allow for an analysis of a larger set of samples and subsequent investigations into potentially linking the role of the identified branching characteristics with both the functional properties of the rice grain, such as digestibility, and even other levels of starch structure. The application of sound correlations and robust methodology may then become a valuable tool for rice researchers in breeding for key rice grain characteristics through the identification of specific starch structures on the molecular level. This could be explored through a number of avenues, for example, the correlation of average mobilities of amylopectins and amyloses with digestibility parameters.

The availability of additional methodologies using capillary electrophoresis also allows for further analysis. Taylor dispersion analysis allows for an analysis of the size distribution using capillary electrophoresis instrumentation, eliminating many of the drawbacks of size analysis by SEC or FFF [277]. Additional separation mechanisms could also be explored, with the use of high pH buffers likely to allow for conditions such that separation of starch by other factors can occur [267].

4.6 Supporting information

S 4.6.1 Calculating average mobilities, dispersity and standard deviation values

Methodology for the determination of average mobilities, dispersity and standard deviation of distributions of mobilities in CE has recently been published by our research team [116]. Calculations in this work are based on the ratio of moments in a distribution, specifically the weight-distribution of electrophoretic mobilities with $W(\mu)$ representing the weight fraction of polyelectrolyte chains with electrophoretic mobility μ. A mass sensitive detection such as UV is required for this. The transformation of raw data to $W(\mu)$ is achieved using equations S 3-1 and S 3-6 in Chapter 3 S 3.5.1.

The specifics of these calculations will not be discussed here, and the reader is referred to [116] for further information. The equations used in the calculation of weight-average mobility (μ_w),

Dispersity (*D(1,0)*), and standard deviation (SDev) of electrophoretic mobility distributions are presented in equations S 4-1 to S4-3.

$$D(1,0) = D(W(\mu),1,0) = \frac{[\sum_z W(\mu_z)\mu_z(\mu_{z+1}-\mu_z)][\sum_z W(\mu_z)\mu_z{}^{-1}(\mu_{z+1}-\mu_z)]}{[\sum_z W(\mu_z)(\mu_{z+1}-\mu_z)]^2} \quad \text{Equation S 4-1}$$

$$SDev = D_\sigma = \left[\frac{\sum_z W(\mu_z)(\mu_z-\mu_w)^2(\mu_{z+1}-\mu_z)}{\sum_z W(\mu_z)(\mu_{z+1}-\mu_z)}\right]^{0.5} \quad \text{Equation S 4-2}$$

$$\mu_w = \frac{[\sum_z W(\mu_z)(\mu_z)(\mu_{z+1}-\mu_z)]}{[\sum_z W(\mu_z)(\mu_{z+1}-\mu_z)]} \quad \text{Equation S 4-3}$$

In the first approach ($D(1,0)$) an analogy with weight-average molar mass divided by number-average molar mass is employed. $D(1,0)$ is calculated as the ratio of the first and zeroth order moments divided by the ratio of zeroth and negative first order moments of the distribution. In the second approach (Equation S 4-2), the standard deviation is calculated as a measure of dispersity, taking the μ_w as a reference.

S 4.6.2 Determination of helix content by 13C solid-state NMR spectroscopy

S 4.6.2.1 Testing contact times

An appropriate rate of cross polarisation for determination of helix content by ^{13}C NMR spectroscopy has been reported by Tan et al. [118] to be approximately 0.5 to 2 ms. The rate of cross polarisation required for quantitative conditions was therefore confirmed for quantitative conditions through a variable contact time experiment (Figure S 4-1). 0.5 to 2 ms yielded similar intensities for the C1 peak (103 ppm), though both 0.5 and 2 ms yielded lower intensities for the C2, 3 and 5 (73 ppm), C4 (82 ppm) and C6 (61 ppm) signals. Therefore, it the optimal rate of cross polarisation was determined to be a contact time of 1 ms.

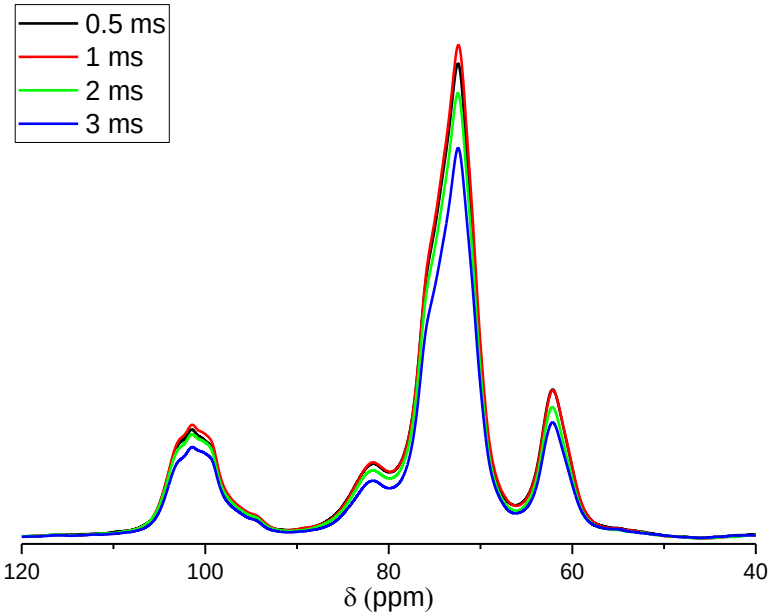

Figure S 4-1 Variable contact time experiment on Doongara rice flour testing contact times of 0.5 ms (black), 1 ms (red), 2 ms (green) and 3 ms (blue)

S 4.6.2.2 Peak fitting process for determination of helix content

For the determination of double helice and single helice content, the contribution from the amorphous component was determined by adjusting the intensity of a separately determined amorphous sub-spectrum (amorphous Doongara rice flour) with a scaling factor so that zero intensity was obtained at a chemical shift of 84 ppm (Figure S 4-2) [118].

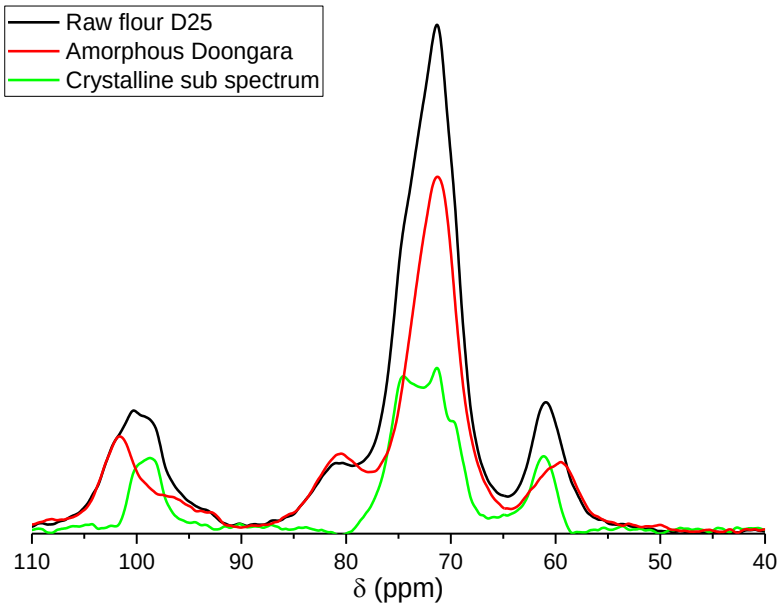

Figure S 4-2 Deconvolution of raw rice flour spectrum (black) by subtraction of the spectrum of a prepared amorphous Doongara flour (red) with the resulting crystalline sub spectrum for fitting in the region 90 to 110 ppm (green)

The C1 peak of resulting crystalline sub spectra (Figure S 4-3, red line) was then fitted with three Gaussian/Lorentzian (50/50) peaks at ~98, 99 and 100 ppm corresponding to the triplet

signal of the A-type polymorph (Figure S 4-3, blue dashed lines) in addition to a fourth broad underlying peak at ~95 ppm (Figure S 4-3, green dashed line). A fifth Gaussian/Lorentzian peak (50/50) is also fitted at approximately 102 ppm corresponding to the V-type polymorph (Figure S 4-3, pink dashed line). The relative ratio of the A-type triplet and V-type signal area to the original C1 peak area (Figure S 4-3, black solid line) is then used to calculate the proportions of single and double helix content in the samples.

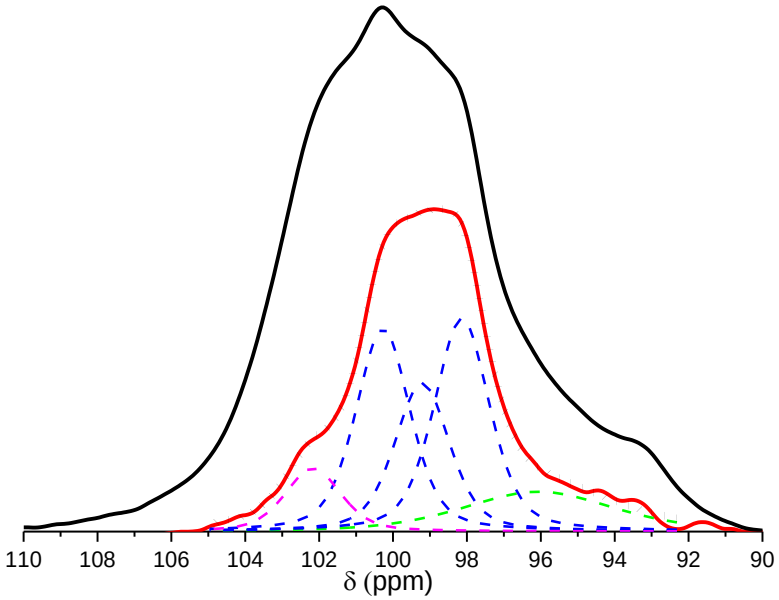

Figure S 4-3 Example of the peak fitting process of a ^{13}C spectrum of rice flour, displaying the original C_1 signal (solid black line), the crystalline sub spectra (solid red line), the fitted A-type (dashed blue lines) and V-type (dashed pink line) polymorph signals, as well as a fifth underlying signal (dashed green line). The combined fit of all signals is shown as a black dotted line

S 4.6.3 The measurement of total dispersity for the entire W(μ) of rice flour samples

Calculated dispersities values for the entire range of the $W(\mu)$ of rice flours were between 1.3 and 1.6, a significantly higher dispersity of branching than has been seen in any other polymers using this capillary electrophoresis method (Figure S 4-4A). This high dispersity is heavily influenced by the sample composition in the case of starch, generally comprising of two very different branching populations. The presence of significant proportions of both highly branched amylopectin and slightly branched amylose, each with their own high dispersities, results in an understandably highly disperse branching distribution. However, the calculation of dispersity used here is referenced to a μ_w of 0 inherently minimises the weighting of higher mobility dispersity in the dispersity value. Therefore, a measure of dispersity through standard deviation can also be employed to assess the overall heterogeneity. The standard deviation of the total $W(\mu)$

was predictably high, displaying values 2-4x higher than amylopectin or amylose alone (Figure S 4-4B). These results highlight the extremely high dispersity of branching structures within native unmodified starch, a result of seemingly non-random branching as a result of the highly complex *in vivo* synthesis of starch.

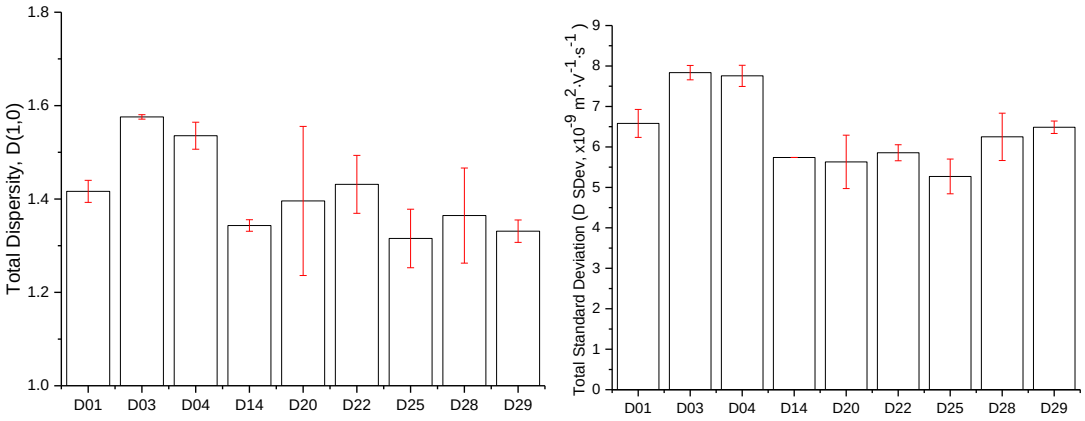

Figure S 4-4 Calculated by A) Dispersity D(1,0) and B) standard deviation of the total weigh distribution of electrophoretic mobility for different rices from the initial minimum of the amylopectin peak (~2.7 x 10^{-9} $m^2 \cdot V^{-1} \cdot s^{-1}$) to the ending minimum of the amylose peak (~2.3 x 10^{-8} $m^2 \cdot V^{-1} \cdot s^{-1}$). Error bars are the standard deviation of at least two instrumental repeats

Chapter 5 The link between molecular dynamics and digestibility in different rice varieties

5.1 Introduction

Starch, a highly abundant biopolymer, is the major component of rice (~90 %) and its structure is known to affect rice digestibility [26]. However, starch is one of the most complex materials found in nature with six known hierarchical levels of structure [22]. The supra(molecular) structure of starch has been extensively researched for many years using a variety of techniques such as X-ray diffraction, small angle scattering and NMR spectroscopy. This has resulted in a deep understanding of the various features of the complex multiscale structure of starch [22, 174, 227]. As a result, there has been a wide range of research into the role of different structural levels in functional properties such as gelatinisation [278, 279], retrogradation [280], texture [225] and digestion [145, 161]. However, these models rarely mention the role of the dynamics and distribution of water or the dynamics of amylose and amylopectin molecules within the starch granule. Given the major role of water in many common starch processing treatments such as cooking, retrogradation and chemical processing, investigating these dynamic features has the potential to allow a better understanding of how their variation relates to changes in starch properties.

The unique ability of NMR spectroscopy to explore the molecular mobility of nuclei within a magnetic field has been an invaluable tool in the research of many materials [281, 282]. The dynamics are commonly investigated through the measurement of spin-lattice (T_1) and spin-spin (T_2) relaxation times of the nuclei within the sample and depend on the strength of the ^{1}H-^{1}H dipolar interactions (both intra- and intermolecular) and its time dependence [122, 123]. Thus, in the case of starches, the heterogeneity of the (supra)molecular structure would give rise to a distribution of dipolar interaction strengths, internal motions and tumbling motions resulting in multiple types of relaxation for the nuclei present [122]. The resulting spin-spin relaxation times along with magnetic field inhomogeneity are responsible for the majority of broadening observed in solid-state NMR spectra. This allows for an estimation of spin-spin relaxation (T_2^*) from resonance full width at half maximum (FWHM) in ^{1}H NMR [283]. However, significant signal broadening due to dipolar coupling effects, even whilst undertaking magic angle spinning, can still

convolute the resonances of interest. As a result, the majority of investigations into molecular dynamics will make use of variations of spin-echo pulse sequences to determine relaxation parameters. One of the most common is the Carr-Purcell-Meiboom-Gill (CPMG) pulse sequence [124, 125], a now fundamental component of many pulse programs that are aimed at investigations of dynamics processes. The primary advantages of this approach are the suppression of the effects of diffusion, a major issue in early NMR magnet, as well as its ability to obtain a complete set of T_2 data for individual resonances in a single experiment [132, 284]. This approach is common, with decays in the range of 1 ms to 1 s reported [132, 168] and measurement of faster decays limited by ability to shorten pulse widths. For investigation into faster decays, a wide range of studies have reported the relaxation times determined from the free induction decay (FID) (4 to 1000 μs) [132, 285, 286], possible due to the dependence of the decay on spin-spin relaxation and yielding an apparent T_2 as with estimations from FWHM.

The dynamics of starch biopolymers and water is an established area of the application of NMR spectroscopy to starch-based foods. Recent research in this field can be categorised into studies on the effects of gelatinisation, and retrogradation on dynamics and the specifics of starch-water interactions. Studies into the investigation of gelatinisation through time domain NMR date as far back as the 1960s [287]. These early studies investigated the gelatinisation through the signal widths of ^{1}H NMR spectra [287, 288], while later studies began reporting on CPMG measurements through the 1970s [289-291]. These early studies typically measured a single T_2, implying that water behaves as a single phase during gelatinisation [289, 291, 292], especially at low moisture contents [290], though the presence of multiple components was acknowledged [292]. More recent studies have also explored the gelatinisation behaviour of potato starches, with the work of Tang et al. [168] providing a comprehensive investigation and analysis of the relaxation distributions from both FID and CPMG decays. Signal assignments based on measurements of amylopectin allowed for assessments of the independent relaxation behaviour of both the OH and CH_x groups using D_2O exchange . The authors reported the presence of three relaxation times for water using CPMG assigned to 1) water in the semi-crystalline lamellae, 2) water inside the starch granule and 3) free water outside the starch granule [168, 293]. For the non-exchangeable protons, CH_x groups, T_2 relaxation times were reported from both FID and CPMG decays. The faster decays of the FID were assigned to the CH_x of crystalline (10 μs) and amorphous (500 to 700 μs) amylopectin. Three decays observed by CPMG were attributed to amorphous amylopectin (1 ms), mobile amylopectin CH protons (20 ms) and amylose CH_x protons (80 ms). However, the mobilities of amylopectin and amylose protons in the native granule are unlikely to be significantly different within a semi-crystalline packed arrangement. Thus, the assignment of specific signals to amylopectin based on observations in waxy maize is a major weakness in this study. Despite this, this study found significant changes to the relaxation distributions that could

be attributed to the gelatinisation and its resulting impact on molecular mobility. Comparable CPMG relaxation decays were noted in a later study [294], with assignment of the 32 and 85 ms T_2 values to non-exchangeable hydrogens, while the presence of bound and trapped water was also reported. Other studies using the CPMG decay had similar findings on water mobility [295, 296] and the interactions of water with starch [297, 298], where the assignments of T_2 distributions and the dynamics of water are comparable with the work of Tang et al. [168, 293]. Further studies on hydrations states in other polysaccharide materials including paper [286], rayon fibres [285] and saturated wood fibers [299] have similarly reported rapid FID derived T_2 values attributed to solid polymer, while slower decays are attributed to water.

Retrogradation is also an area of great industrial significance for starch products with a wide array of studies involving the use of NMR spectroscopy to monitor the molecular dynamics of starch and water during this process [132, 295, 300, 301]. The outcomes of these studies have significantly exposed the impact of retrogradation on molecular dynamics, with increases in starch rigidity, decrease in water mobility and increases in dipolar coupling reported.

Magnetic resonance imaging (MRI) [302], commonly employed for medical imaging has also been employed in studies of unique relaxation behaviours of water in polysaccharides. Many of these studies employ spin-echo imaging sequences combined with the determination of per pixel spin-spin relaxation time and the relationship of T_2 with moisture content [303, 304]. This allows for quantitative spatial investigations into water distribution in a variety of polysaccharide systems including rice [303], wheat [304, 305] and wood [299]. In general these studies attributed very fast decays determined from the FID to the non-exchangeable protons of the polysaccharide and bound water [285, 299], while the slower decays observed through CPMG or spin-echo decays were attributed exclusively to a single [303, 305] or multiple [299] water components. It is interesting to note that while multiple types of bound and unbound water are generally accepted to exist within starch granules [293], many MRI studies commonly assume a single type of water in biological systems, and do not typically investigate the other types of water present in the sample matrix [306-308]. This is likely a result of the longer echo times (~10 ms) in MRI experiments, and so faster relaxing components may not be observed.

Typical MRI scanners operate at magnetic field strengths from 0.15 to 3.0 T (8.5 to 128 MHz for ^{1}H Larmor frequency) with research grade MRI (11.7 to 17.2 T, 500 to 730 MHz ^{1}H Larmor frequency) and analytical NMR spectrometers (up to 28.2 T, 1.2 GHz ^{1}H Larmor frequency) capable of much higher field strengths; however, this comes at a high cost, and smaller bore size, thus limiting sample sizes. The relatively low field strength of MRI instruments typically results in decreased sensitivity and resonance resolution. In the analysis of relaxation times, this can hinder the resolution of different types of water that may exhibit different relaxation behaviours.

This lack of resolution may be a possible reason for the relatively low number of studies that explore water distributions by MRI.

It is clear then from the different populations of water reported in the literature that the effects of supramolecular structure leading to confining geometries or motion bound states results in a reduction of T_2 of water protons from their bulk state in polymer systems [309]. It is also well accepted that the OH groups of polysaccharides tend to have very short T_2 relaxation times (< 1 ms), attributed to the strong hydrogen bonding network present. What is less clear, is the assignment of the different populations of non-exchanging protons, with a variety of literature reporting both similar and dissimilar assignments of various T_2 relaxation times.

The molecular dynamics was assessed in different rice varieties through NMR relaxometry. Multiple transverse relaxation times were measured, reporting on the hydroxyl groups as well as the non-exchangeable protons (CH_x). The interpretation of relaxation times was discussed in the context of starch structure and moisture content. The samples had been selected to have a known digestibility [170], and the relaxation results were related to digestibility.

5.2 Materials and Methods

Materials

Six commercial rice varieties and one waxy rice cultivar were obtained from the NSW Department of Primary Industries at Yanco, NSW, Australia. Grain was harvested at physiological maturity, dehulled (THU35A 250V 50Hz Test Husker, Satake, Australia), milled (brush mill) and ground (Cyclotec 1093 Sample Mill, Tecator AB, Sweden) to pass through a 50 μm sieve. Both milled and ground rice samples were received.

Samples were conditioned at 44 % relative humidity and 20 °C for at least 2 weeks prior to analysis. Sample environment at 44 % relative humidity was created by placing a saturated aqueous solution of potassium carbonate (K_2CO_3) in a desiccator and adequately sealing [215].

Methods

Digestibility data in the form of percent starch hydrolysed after 60 min of digestion (SH-60) is reported from the work of Toutounji et al.[170], with measurements reported here made on the same samples. One exception is the 'waxy' variety, which has been substituted in this work with another waxy variety due to sample unavailability.

^{1}H single pulse excitation (SPE) and T_2 experiments were performed on a Bruker DRX300 (Bruker Biospin Ltd, Sydney) operating at a Larmor frequency of 300.15 MHz. ^{1}H SPE experiments were also performed on a Bruker DPX200 (Bruker Biospin Ltd, Sydney) operating at a Larmor

frequency of 200.13 MHz. A commercial double resonance probe supporting zirconia rotors with 4 mm O.D. and 3 mm I.D. was used. ^{1}H SPE NMR spectra were recorded using a 50 000 Hz spectral width, 3.50 (DRX300) or 3.55 (DPX200) μs 90° pulse length, 5 s repetition delay and 8 scans. Measurements were performed on raw or cooked whole rice grains where specified, with at least 3 full grains packed in the rotor for each measurement.

^{1}H transversal relaxation times (T_2) were determined with a 2D-CPMG experiment [124, 125] at 25 °C. The spectra were recorded with no spin (static) at the magic angle (54.8°) with a 5.95-6.20 μs 90° pulse, a 11.95-12.35 μs 180° pulse, a 595-620 μs delay between pulses, a time-domain size of 64,000, a 5 s repetition delay, and 32 scans. The number of loops (of inter-pulse delay + 180° pulse) was incremented in the indirect dimension as follows: 1, 2, 3, 4, 5, 6, 10, 20, 30, 40, 60, 80, 120, 200, 400, 600, 1000, 2000 and the signal was fully decayed by the end of it. The data set was then phase-corrected, and baseline-corrected in TopSpin 4.0.1 software. The data (signal integral vs relaxation period) was then linearized and fitted using a multiple-step Levenberg-Marquardt linear fit to a multicomponent, single-exponential decay in Origin 2016 software (discussed in 5.3.2). Temperature was not controlled due to probe limitations with static measurements; however, it was determined that small variations of temperature would not affect the sample due to the typically high enthalpy of major structure transitions in starch.

For cooked rice samples, rice grains were cooked using the excess water method with a minimum of 200 mL of deionised water per rice grain. A maximum of 30 rice grains was placed in a stainless-steel mesh tea ball and suspended in boiling water (97-100 °C) until the minimum cooking time had elapsed. Five grains were then tested using a “squash” test to confirm that the rice was cooked. The minimum cooking times and specifics of the squash test are shown in supporting information (S 5.5.1).

Moisture was assessed on some samples, with moisture contents of 10-13 % for raw rice and 67 – 75 % for cooked rice (S 5.5.4).

5.3 Results and Discussion

5.3.1 The component of the ^1H NMR spectrum of cooked rice grains

Typical solid-state ^1H spectra of uncooked rice grains exhibited a broad featureless signal between chemical shifts of 0 to 10 ppm (Figure 5-1, brown). Measurements were taken on static samples, and as a result, broadening from dipolar coupling was strong. However, this was a conscious choice, ensuring that the methodology employed was transferable to benchtop NMR instrumentation that would be more accessible to industry researchers. The broad signal of rice grains contains contributions of all the proton containing components present within the rice grain including water, starch, proteins and lipids; however, a high level of convolution makes signal assignment impossible. When the rice grain is cooked, the starch within the rice grain is swelled with water, resulting in an increase in the water content of the grain, approximately ≈70 % w/w (

Table S 5-3) compared to 10 to 13 % w/w in raw grains (Table S 5-2). This results in a significant increase in intensity of the OH signal from water (≈5.0 ppm), a result of the water now accounting for approximately 93 % of the total OH in the sample (Figure 5-1). Shoulders became observable on the broad signal after cooking, attributed to different components within the sample; however, were still highly convoluted (Figure 5-1, Black trace). Suspending the cooked rice grain in water for an additional 30 minutes after cooking resulted in further absorption of water, though the resulting increase in the OH signal (5.0 ppm) almost entirely masked the contributions of other signals (Figure 5-1, Green). Therefore, in order to investigate the underlying non water components, the cooked rice grains were suspended in D_2O to mitigate the contributions of the free water OH signal at ≈5.0 ppm. After suspension for both 30 and 120 minutes, the intensity of the OH signal (≈5.0 ppm) was significantly reduced, with a residual OH signal still apparent, and the observation of an underlying signal at ≈3.5 ppm (Figure 5-1, red and blue). Due to the chemical shift of this signal, this signal was attributed to the non-exchangeable CH_x protons of the starch; however, due to the broadness, it is likely a convolution of signals from the C_2 to C_6 protons, while anomeric protons of C_1 for the α(1,4) and α(1,6) linkages come at 5.4 and 5.0 ppm, respectively [133, 195]. Interestingly, after 120 minutes of suspension in D_2O, an additional signal was observed at a chemical shift of ≈1.0 ppm, assigned to lipids based on prior solid-state ^1H MAS NMR experiments (Figure 5-1, blue) and also shown in solution-state NMR of starch [79]. While the partial exchange of protons using D_2O was intended to minimise the water OH peak only, starch bound water, and starch hydroxyl groups likely also experienced some degree of exchange. This effect was most noticeable after 48 hours of suspension, with a significant decrease in signal intensity for all observed signals (Figure 5-1, pink). From these

results the signal <4.0 ppm was assigned as corresponding to most CHs, except for CH on the C_1 (anomeric) at ≈5.5 ppm, and both water and starch OH groups assigned to the signal at ≈5.0 ppm. The signal assignments of CH_x and OH signals for the spectra of cooked rice grains were also supported by findings on raw waxy maize starch samples (S 5.5.6).

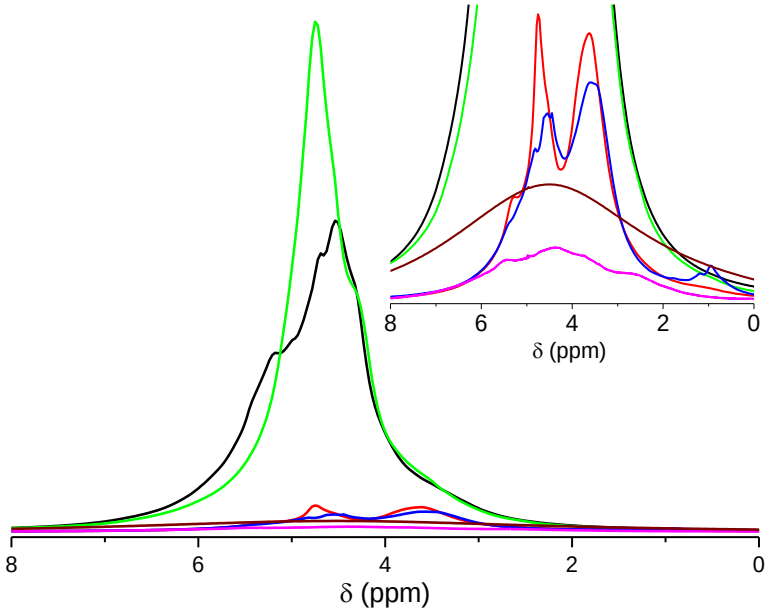

Figure 5-1 Static ^{1}H NMR spectra of raw (brown) and cooked Doongara grains, recorded immediately after cooking (black) followed by suspension in H_2O for 0.5 h (green) or in D_2O for 0.5, 2 or 48 h (red, blue and pink, respectively)

5.3.2 Extracting T_2 relaxation times for multiple components from a single peak using the CPMG pulse sequence

Over the first 4 spectra of the CPMG sequence, corresponding to a range of ≈1.5 to 5.0 ms, the OH signal (5.0 ppm) was observed to decrease significantly in intensity (shorter T_2), with the main CH_x signal (3.5 ppm) decreasing at a slower rate (longer T_2) (Figure 5-2). Additional populations were also observed at higher chemical shifts (8.0, 11.0 and 14.0 ppm). These may arise from populations of hydroxyls that are experiencing higher levels of dipolar coupling through stronger hydrogen bonding [310] relative to the water and starch hydroxyls identified at 5.0 ppm. However, higher levels of dipolar coupling should also result in much shorter relaxation, so it is unlikely that these are hydroxyls and these signals likely arise from carboxylic groups of the proteins present. Other functional groups of the proteins would likely be present in a similar region to the starch CH_x groups, and unlikely to be resolved. (Figure 5-2). Additionally, the CH_x signal is likely dominated by the CH_x groups of the starch, rather than the proteins (3-9 %), which would typically be at higher field, or lipids (1-3 %) given their negligible concentration in rice grains. Thus, the two major components observed in this decay were assumed to be attributed to both the combined OH of both water and starch (5.0 ppm) and to the starch CH_x protons (3.5 ppm), while the remaining signals were not explored. Due to almost equal ratios of OH protons from

water and starch in the raw rice grain (49/51), given 13 % moisture and 78 % starch, as well as a similar chemical shift, it cannot be determined by the CPMG sequence if the two OH sources exhibit different relaxation behaviours. This may arise from the time scale limitations of the CPMG approach, in which case determinations of relaxation parameters from the FID may be relevant, or it may arise from exchange of protons between the two groups resulting in similar average relaxation times. Due to the broadness of the signal at 3.5 ppm, the resolution of the CH_x signal for specific carbons was not possible. Additionally, the apparently slower decay of the CH_x relative to the OH indicates a higher mobility and likely lower degree of dipolar coupling. Therefore, the CH_x signal is expected to arise from starch molecules that are not participating in helical confirmations that involve strong hydrogen bonding networks. Literature studies have suggested that the relaxation of these CH protons in these arrangements can only be measured on the time scale of the FID (4 to 1000 μs), with relaxation times in the order of tens of μs reported in the literature [168, 293]. Due to its high degree of short chain branching, amylopectin primarily exists in a double helix conformation, while the formation of amylose single helices is typically less common (<5 % total order), due to the necessity of inclusions to form. Thus, it is likely that the CH_x signal being observed arises from the unordered or amorphous chains or regions of chains of both amylose and amylopectin.

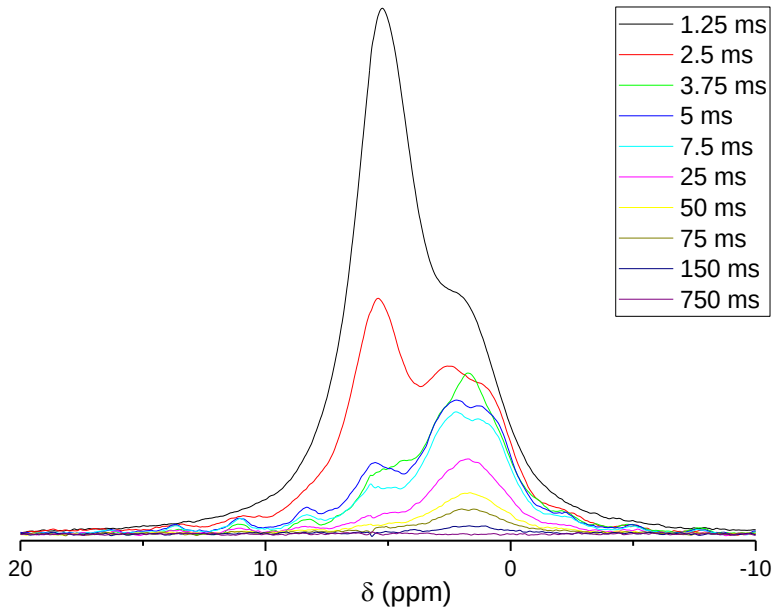

Figure 5-2 Spectra with increasing echo delays from Carr-Purcell-Meiboom-Gill experiment on raw rice grain showing the evolution of the signal with increasing number of repeat cycles. Echo delay lengths are as follows 1.25 (black), 2.5 (red), 3.75 (green), 5 (dark blue), 7.5 (light blue), 25 (pink), 50 (yellow), 75 (olive), 150 (navy) and 750 (maroon) ms

5.3.2.1 Fitting the CPMG decay to obtain T_2 parameters

From the exponential decay of signal area obtained by the CPMG sequence, the T_2 relaxation time of the signal can be determined from the rate constant of the decay. Built-in processing in the TopSpin software allows for the determination of T_2 relaxation times; however, the fitting options

available were found to have some limitations in determining T_2 values in systems with multiple relaxing components. First, the most typical fitting function, "uxnmrt2", allows for only one component to be fitted and therefore did not yield a good fit of the relaxation decay (S 5.5.7). The second likely candidate was "expdec", a simple function fitting the sum of exponential decays and allowing multiple T_2 values to be determined at once. However, this proved to be an inconsistent approach with little control over the fitting process sometimes resulting in unrealistic values. Therefore, to better control the fitting process, the concept of the "expdec" function was employed in an iterative manual extraction approach.

T_2 relaxation times were determined in this work through linear fits of the log transformed exponential decay, allowing for an assessment of the overall decay profile of the signal and the multiple components present. This similar to the built-in "expdec" function but is iterative rather than cumulative which allowed for greater consistency in fitting across all samples. The procedure for this determination is outlined in this section, with the exponential decay obtained by the CPMG sequence defined as,

$$y = A_0 e^{\frac{-t}{T_2}} \qquad \text{Equation 5-1}$$

Where A_0 is the pre-exponential factor, t is the delay time in ms, and T_2 is the relaxation time in ms. In a single relaxation component system, the T_2 can be determined from the inverse relationship of the rate coefficient ($\frac{-t}{T_2}$) with T_2 by plotting the natural log of y, yielding the linear equation,

$$\ln y = \frac{-t}{T_2} + \ln A_0 \qquad \text{Equation 5-2}$$

And determining the slope ($\frac{-1}{T_2}$).

However, in a system where multiple components are present, multiple exponential decays are additively observed in the form,

$$y = \sum_{k=1}^{n} A_{0_k} e^{\frac{-t}{T_{2k}}} \qquad \text{Equation 5-3}$$

where n is the number of unique components in the exponential decay.

An example experimental exponential decay of peak area for a raw rice grain is shown in Figure 5-3A, where the majority of protons can be seen to have completely relaxed by the 250 ms echo delay stage of the sequence. It is not clear from this decay that there are multiple relaxing components present, so the plot is transformed to $\ln y$ (Figure 5-3B). This transformation reveals the presence of three unique linear slopes underlying the initial function at an echo delay of less than 300 ms. At higher echo delays the integrals are more affected by background noise due to low signal area and were not included in fitting. In this case only two components were fitted for both raw (Figure 5-3) and cooked (Figure S 5-3) rice grains.

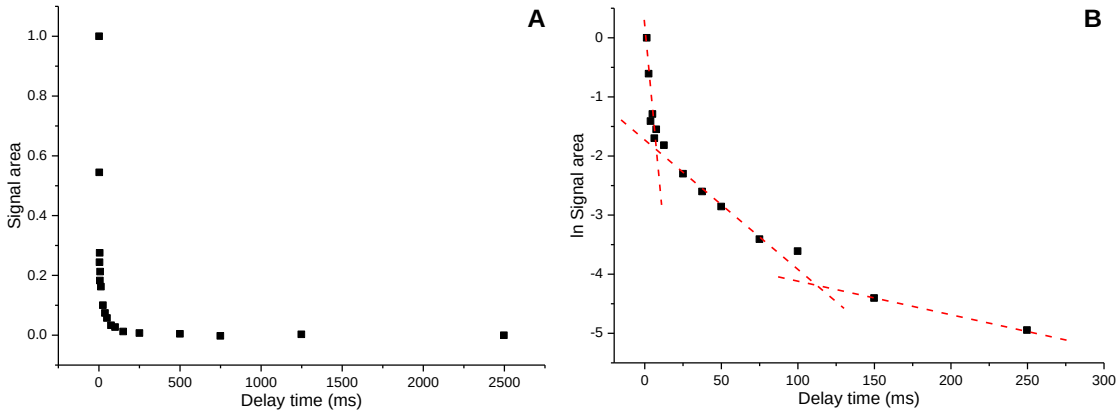

Figure 5-3 Decrease of signal area with increasing echo delay in CPMG experiment on a raw rice grain, plotted as the peak area (A) or its natural logarithm (B). Dotted red lines show the presence of multiple slopes, representing multiple T_2 relaxation times in the decay profile

In order to determine the T_2 of these components, each linear segment is fitted to determine the regression equation parameters (Figure 5-4A and 5-4B). First, the faster decaying initial linear segment, referred to as component 1 (OH signal), is fitted and the determined linear equation of the form of Equation 5-2,

is transformed back to an exponential form,

$$y = e^{\frac{-t}{T_2}} + e^{A_0} \qquad \text{Equation 5-4}$$

then subtracted from the initial exponential decay to yield an exponential decay unbiased by the first component. The natural logarithm of the resulting exponential is then fitted with a linear fit of the slower decaying second linear section, referred to as component 2 (CH_x signal).

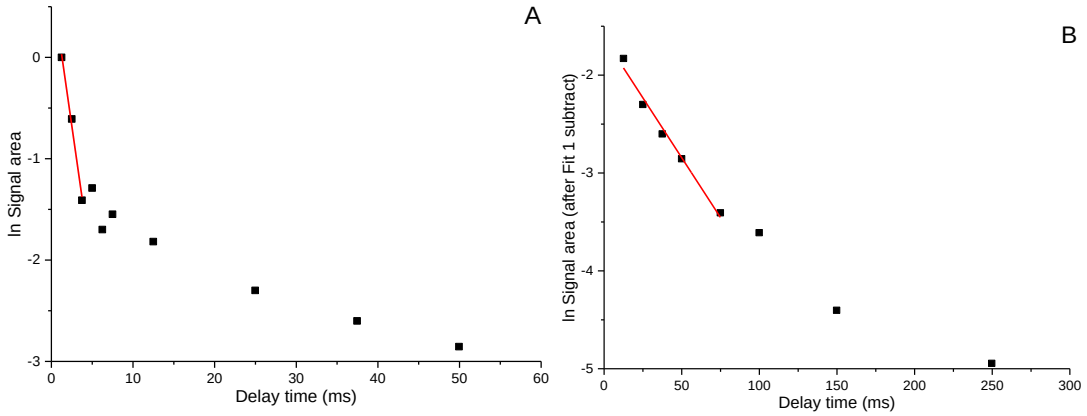

Figure 5-4 Linear fits of transformed data in Figure 5-3B for a) the first component (number of points (n) = 3 and r^2 = 0.98) then b) the second component of after subtraction of the initial linear fit (n = 5 and r^2 = 0.98)

With the linear regressions of both components of the linearized exponential, the T_2 can be determined as the absolute value of the inverse of the slopes. The above methodology was applied for all raw rice samples. For cooked rice grain samples, methodology differed only in the range of

echo delays included in the fits for each component. The T_2 values and linear regressions for each component are shown in supporting information (S 5.5.5).

5.3.2.2 The determination of pre-exponential factors of individual T2 decays

From the determined T_2 values of relaxing components the pre-exponential factors of the two exponential decays were also calculated through an iterative fitting approach. With a known set T_2 for both the fast decaying OH (T_{2_1}) and slower decaying CH_x (T_{2_2}) components, equation 5-3 was employed as a bi-exponential decay fitting function. Given A_0 represents the pre-exponential factor of the OH component; the pre-exponential factor of the CH_x component was then defined as $(1 - A_0)$ yielding the fitting equation,

$$y = A_0 e^{\frac{-t}{T_{2_1}}} + (1 - A_0) e^{\frac{-t}{T_{2_2}}} \qquad \text{Equation 5-5}$$

Equation 5-5 was then applied to the exponential decays of all samples, iteratively fitting A_0 using a Levenberg–Marquardt approach to minimise chi squared, with adjusted r^2 values in the range of 0.84 to 0.94. WithA_0 determined, the relative contributions of the OH and CH_x components to the total signal area of the initial CPMG echo spectrum could be assessed.

5.3.3 The link between molecular dynamics and digestibility

5.3.3.1 The relation of apparent amylose content with digestibility

The literature has shown a correlation between the *in vitro* digestibility of rice and the apparent amylose content on a diverse range of samples [26] and along with its importance as a marker for other rice properties integral to rice quality, this cements *AAC* as a valuable attribute in rice quality analysis. However, the statistical significance of the relationship of *AAC* with digestibility (r^2 = 0.73) indicates that there are likely additional drivers of digestibility. This is highlighted where predicted GI was observed to differ significantly at a similar *AAC* [26].

The digestibility of the rice varieties analysed in this study have been previously published [170], with a negative correlation observed between *AAC* and the *in vitro* digestibility, as expected (Figure 5-5). The correlation was good given the small sample size, yielding an adjusted r^2 of 0.92. Values of starch hydrolysed after 60 minutes of digestion (SH-60), determined by glucose concentration relative to the initial starch amount, are those reported by Toutounji et al. [170]. SH-60 values have been reported to be manifesting on a similar scale to glycaemic index (GI, 0-100), with the reference point, Doongara, at an SH-60 value of ~50 % lining up with its commercially published GI value of 55.

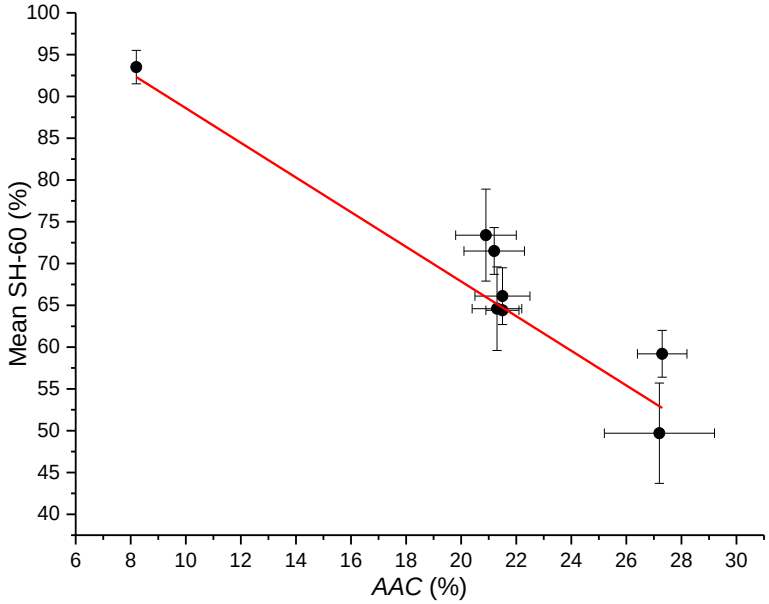

Figure 5-5 Mean SH-60 plotted against *AAC* adapted from Toutounji et al. [170]. Red line represents a linear fit of the data (n = 8 and r^2 = 0.92). Error in SH-60 is reported as the standard deviation of 6 repeats, and type of error and n is not reported for AAC

While an apparent link between the AAC and SH-60 is reported, the similarity of *AAC* for some varieties exhibiting small differences in their digestibility is an indicator that other factors are at play. This may arise simply from the possibility that *AAC* is not the only driver of digestibility, with other features of starch structure potentially also playing a role such as the molecular dynamics and spatial distribution. Thus, there are multiple avenues to explore in refining the understanding of the role of starch structure in digestibility. It should be noted that starch digestion is a complex multi-enzyme system, and while digestibility is often reported in the form of extent of digestion, the kinetics can also play a role. However, given the lack of an appropriate model for starch digestion, the kinetics is often not reported on, and as a result a reliable determination could not be made on the samples in this study.

5.3.3.2 The link of CPMG decay components in raw rice grains with digestibility

5.3.3.2.1 Relating T_2 relaxation times to digestibility

In the discussion of T_2 and its relation to digestibility, the relaxation time is displayed on the x-axis as the independent variable. This was deemed to be appropriate as this work was intended to employ any T_2-digestibility relationship as a screening tool for the digestibility of unknown rice samples. The T_2 relaxation of the first component in the CPMG decay of raw rice grains, assigned to OH protons, is shown against the respective SH-60 in Figure 5-6. The relaxation time of the first component of the CPMG decay is short, on the scale of ≈1.5 to 2.5 ms, and is associated with a convoluted combination of hydroxyls of both water and starch molecules within the rice grain. Thus, it may be influenced by the local availability of hydrogen bonding networks within the

starch and relating to either amorphous or ordered regions of the supramolecular structure. Despite the short T_2 times, a difference could still be noted between the T_2 of different varieties. For varieties with an SH-60 of 75 or lower, the SH-60 displayed an apparent relationship with the T_2; however, the highly digestible waxy variety (SH-60 = 90) did not follow this trend (Figure 5-6). Given the limitations of the CPMG sequence in terms of effective range (1 to 1000 ms), the closeness of the OH signal T_2 to the lower limit of the CPMG sequence may introduce significant limitations in the calculation of the T_2. Thus, it is possible that inaccuracies in the calculation of T_2 from experimental limitations could be the drivers for the apparent differences observed. If in fact these T_2 values are accurate, then they may be assigned to differences in structural features between the varieties. As the contributions of both water and starch to the OH T_2 are unknown, it is possible that this T_2 is arising from small differences in the distributions of either water and starch (or both) throughout the starch granules within the rice grains.

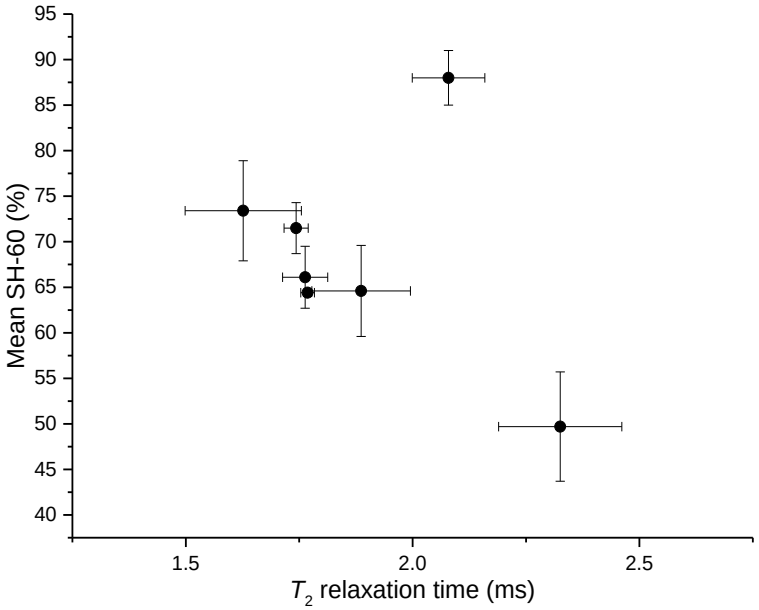

Figure 5-6 Mean SH-60 (n=6) as reported by Toutounji et al. [170] plotted against T_2 of OH signal . Error in SH-60 is reported as the standard deviation of 6 repeats, and error in T_2 is reported as the standard error of n=3 repeats

The relaxation of the second component of the CPMG decay is an order of magnitude slower than that the OH signal and is attributed to the relaxation of the CH protons (except for anomeric protons) of the starch molecules. A negative correlation was observed between the T_2 relaxation of the main CH_x signal in the CPMG experiment of raw rice grains and the respective SH-60 [170] (Figure 5-7). T_2 values in the range 40 to 60 ms as reported here have been assigned in the literature to the more mobile CH protons of amylose molecules and amylopectin branches existing in amorphous regions where dipolar coupling should be minimised. It is apparent that the structures represented by the CH_x signal exist in unique environments between the different rice varieties, displaying a range of T_2 relaxation times even where *AAC* was similar (Figure 5-7). The linear relationship between the CH_x T_2 and SH-60 (adjusted $r^2 = 0.93$) indicates that the underlying

structures being measured are likely important factors in digestibility. Given the assignment of the CH_x signal of the CPMG decay to amorphous regions, it appears that these amorphous regions have some role in digestibility. In the context of *AAC*, it may then be the link between *AAC* and amorphous structure that enables it to serve as a proxy for digestibility. Therefore, it may be possible that a more direct assessment of these amorphous regions through the T_2 could allow for an improved prediction of digestibility, and possibly also in cases where *AAC* is similar.

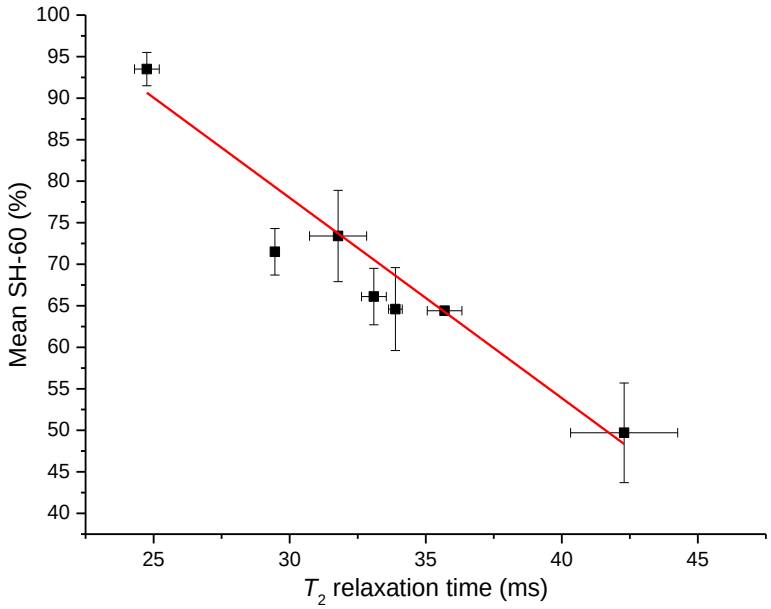

Figure 5-7 Mean SH-60 (n=6) as reported by Toutounji et al. [170] plotted against T_2 of main CH_x signal. Red line represents a linear fit of the data (n = 6 and adjusted R^2 = 0.93). Error in SH-60 is reported as the standard deviation of 6 repeats, and error in T_2 is reported as the standard error of n=3 repeats

5.3.3.2.2 Assessing the contributions of relaxing components

The pre-exponential factors of the CPMG decays of each component were calculated for the raw rice grains to investigate the contributions of the two decaying components to the total signal observed (Table 5-1, as described in Section 5.3.2.2). The pre-exponential factors displayed a significant contribution of the faster relaxing OH component to the total peak area (≈ 70 %) compared to the slower relaxing CH_x component (≈ 30 %).

Table 5-1 Pre-exponential factors for the bi-exponential decay function defining the T_2 decay for raw rice grains

Variety	Average A_0	Std. Dev.	RSD (%)	Average (1-A_0)
Doongara	0.661	0.051	7.66	0.329
Koshihikari	0.698	0.015	2.13	0.294
Topaz	0.673	0.011	1.53	0.304
Opus	0.677	0.011	1.51	0.301
Reiziq	0.711	0.033	4.55	0.265
Sherpa	0.707	0.028	3.93	0.279
Waxy (D25)	0.646	0.001	0.09	0.354

If the entire sample was present within the first spectrum of the CPMG sequence, almost equal ratios of ^{1}H from the OH and CH_x groups of the starch and water components would be expected for the raw rice grains (49/51) given 13 % moisture and 78 % starch. However, this was not observed, with the pre-exponential factors of the OH indicating a much higher contribution to the signal than the CH_x signal (Table 5-1). This is consistent with observations from the first spectrum of the CPMG sequence (Figure 5-2), and highlights the fact that different relaxation times can represent very different regions of starch structure in varying proportions. Due to the nature of the CPMG sequence, the first recorded spectrum is only representative of molecules with a T_2 greater than 1 ms. Therefore, the total contribution of the OH and CH_x signals with T_2 > 1 ms can be assessed with respect to the total protons in the sample by the corresponding ^{1}H SPE spectrum with the same acquisition parameters (Figure 5-8). The first spectrum of the CPMG sequence was found to represent a small percentage of the total protons present in the sample, an interesting observation given the differences in T_2 between varieties even for such a small structural component (Figure 5-8). With a typical starch content of 78 % at a moisture content of 13 %, the remaining mass of the sample (9 %) consists primarily of proteins and lipids. This means that some percentage of the ^{1}H SPE signal arises from proteins and lipids; however, these were not observed and/or resolved in the CPMG sequence. This suggests that the ratio of the two areas is inadvertently biased by the proteins and lipids present in each variety, which cannot be determined in a static ^{1}H SPE experiment.

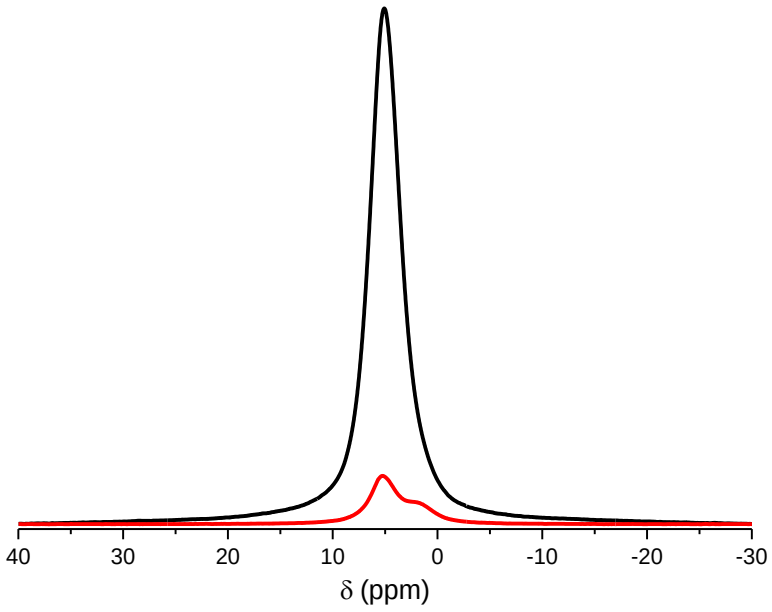

Figure 5-8 The ^{1}H SPE spectrum (black) and first spectrum of the CPMG sequence (red) for raw Doongara rice grains. The ^{1}H SPE spectrum has been scaled by a factor 4 to account for difference in number of scans (NS=8 to NS_{eff}=32)

Despite the uncertainty of the exact composition of the ^{1}H SPE spectrum, the relative proportions of the CPMG sequence were related to the total area of the ^{1}H SPE spectrum (Table 5-2). The first spectrum of the CPMG was found to represent between 8 and 14 % of the total ^{1}H

present in the samples, indicating that the components with a T_2 > 1 ms account for a small fraction of the composition in raw rice grains. Comparing the individual contributions of both OH and CH signals in the CPMG sequence displays the same trends, with the OH dominating the contribution. However, given the relatively large errors in these calculations, differences between these values were deemed insignificant. This is an interesting observation, given that the CH_x component represents such a small percentage of the total structure, yet the T_2 relaxation time yields a relationship with the digestibility. This then leads to two possible explanations: 1) the relationship with digestibility arises purely from those specific CH_x structures, or 2) the specific CH_x structures are a function of the surrounding structure which is much more abundant, and the CH_x component simply serves as a proxy in this situation.

Table 5-2 Percentage contributions of the first spectrum of the CPMG sequence for raw rice grains to the corresponding total area of a ^{1}H SPE spectrum

Variety	Area of CPMG relative to SPE		OH relative to total SPE		CH relative to total SPE	
	Average (%)	Std. Dev. (%)	Average (%)	Std. Dev. (%)	Average (%)	Std. Dev. (%)
Doongara	9.99	0.36	6.78	0.33	3.36	0.63
Koshihikari	10.45	0.67	7.86	0.24	3.17	0.43
Topaz	9.21	0.06	6.43	0.12	3.07	0.06
Opus	10.91	1.51	7.28	0.98	3.61	0.54
Reiziq	13.62	0.81	10.04	0.49	4.24	0.32
Sherpa	9.91	1.29	7.48	1.33	2.92	0.04
Waxy (D25)	7.80	0.12	5.03	0.33	2.77	0.23

T_2 relaxation times of 20 – 80 ms in starch have been suggested in the literature as arising from the mobile CH_x protons of amylopectin and amylose. In this work, only one clear CH_x relaxation was observed for rice samples with a T_2 of 30 to 50 ms, within the range observed in literature. Therefore, it is not immediately clear if these protons can be attributed to amylose or amylopectin. Amylose molecules have generally been noted to exist in and contribute to the amorphous regions of starch structure. Therefore, to assess this, the relative proportions of the CH_x CPMG signal to the total area of the corresponding ^{1}H SPE were compared to the *AAC* of the sample (Figure 5-9). No clear correlation was observed between the CH_x signal area and the AAC, indicating that the observed CH_x signal does not solely arise from amylose. This is especially evident for varieties with an AAC of 20-22.5 % where different relative areas were observed despite similar AAC. In addition, the relative contribution of the CH_x represents a significantly smaller proportion of the sample than what would be expected if solely driven by *AAC.* This indicates that even if the CH_x signal is linked to amylose molecules, it is not influenced by the amount of amylose present but rather other factors. Based on literature this may then arise from a combination amylose and

amylopectin CH_x with similar T_2 relaxation times, possibly a result of their location within similar regions. Additionally, it should be noted these differences in relative area may also be a bias introduced by different protein and lipid concentrations which were not measured for these samples.

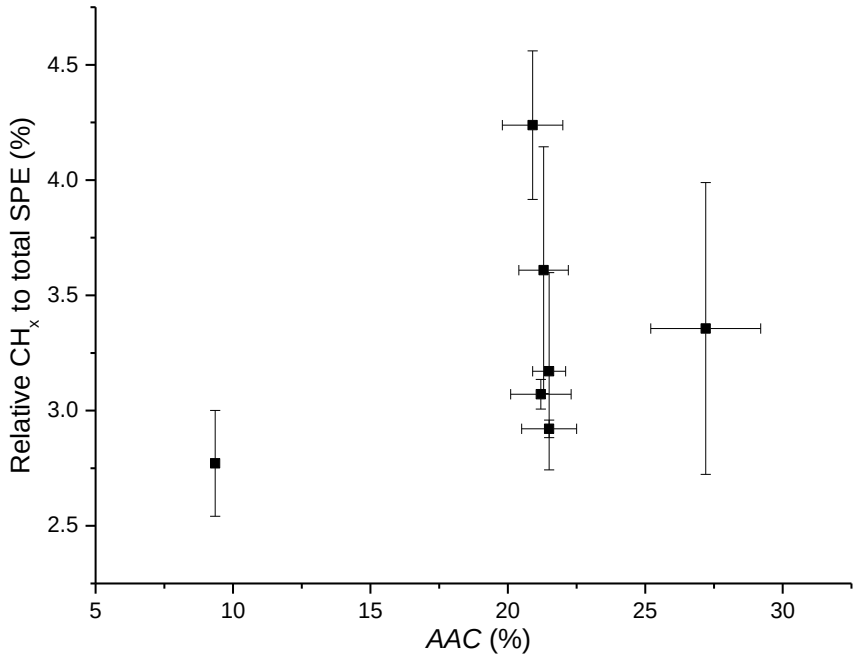

Figure 5-9 The average area of the CH_x in the first spectrum of CPMG sequence relative to the total area of the corresponding ^1H SPE spectrum. Error bars are the standard deviation of 3 repeat samples and instrument setups

It is evident that the observation of the OH and CH_x signal in the CPMG decay, and the associated relaxation times, correspond to a minor proportion of the total starch present within the sample. Relaxation times of 20 – 80 ms for the CH_x in starch have been reported in the literature to amylose chains and mobile amylopectin, due to their higher mobility relative to the typically highly coordinated CH_x of amylopectin in the form of double helices within crystalline lamellae. In this work, the CH_x was observed not to arise solely from amylose, and so is assumed to be a combination of both amylose and mobile regions of amylopectin. These results may then indicate that this CH_x decay component is a result of defects in the crystalline structure due to amylose molecules or a concentration of chain ends and branching points resulting in defects that allow more local mobility within the semi-crystalline structure. With this in mind, it is clear that different varieties of uncooked rice grains manifest these structures in unique ways, with a range of T_2 relaxation times highlighting difference in the local arrangements, as well as differences in the amount of the sample present in this arrangement.

5.3.3.3 The link of CPMG decay components in cooked rice grains with digestibility

5.3.3.3.1 Relating T_2 *relaxation times to digestibility*

2D CPMG experiments were also performed on cooked rice grains, with the T_2 relaxation time determined for the two observed components in the CPMG decay (S 5.5.2). Based on visual observations of the decay, neither the OH or CH_x signal could be assigned to either the faster or slower decay and therefore are discussed as component 1 and component 2. The T_2 relaxation times of the both components measured in the cooked rice grains were in the range of 20 – 100 ms, indicating a similar degree of mobility for both the OH and CH_x being measured (Figure 5-10). This was in contrast to raw rice grains, where the T_2 two components differed by an order of magnitude (Figure 5-6 and Figure 5-7).

The cooking rice grains in water results in the gelatinisation of the starch component, a process that swells the starch granules with water, disrupting the helical structures of starch. This gelatinised state is typically assumed to be highly amorphous as opposed to the semi-crystalline structure observed in raw starch. With respect to the T_2 relaxation times, this is likely to result in longer decays and higher T_2 relaxation times as a result of increased molecular mobility in the absence of ordered structure. The T_2 relaxation times of component 1 in the CPMG decay of the cooked rice grains (20 – 40 ms, Figure 5-10A) were found to be in the same range as the T_2 values reported for the CH_x signal in the raw rice grains (20 – 50 ms, Figure 5-7). This similarity supports the notion that the CH_x signal of the raw rice grains likely arises from some form of amorphous structure. The second component of the CPMG decay for the cooked rice (Figure 5-10B) displayed relaxation times slightly higher than was observed for the CH_x signal in the raw rice grain (Figure 5-7), indicating a higher degree of mobility. The higher T_2 relaxation times in cooked rice grains compared to the raw rice grain agrees with the notion that the helical structures of starch have become unwound, therefore previously strongly bound OH and CH groups of starch and OH groups of water are allowed less restricted mobility. However, it should be noted that the much higher moisture content of cooked rice grains (≈70 %) means that the majority of the OH signal likely arises from water rather than starch OH groups. Therefore, from the data here, it is impossible to conclude if the observed increase in the T_2 value with cooking is a result of gelatinisation, the increased water content, or both.

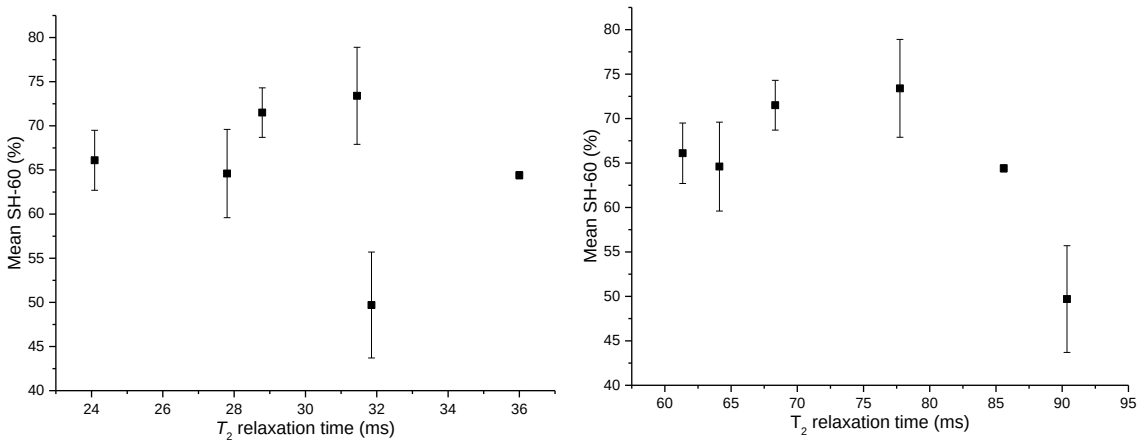

Figure 5-10 Mean SH-60 (n=6) as reported by Toutounji et al. [170] plotted against T_2 of A) component 1 T_2 and B) component 2 of cooked rice grains. Error in SH-60 is reported as the standard deviation of 6 repeats

No correlations of the T_2 relaxation times in cooked rice grains with the SH-60 were observed (Figure 5-10). In the case of one of these components, the T_2 likely primarily represents a distribution of water OH throughout the cooked rice grain rather than starch itself, a result of the high moisture content. The T_2 of the other component would then likely represent the distribution of starch CH_x throughout the grain, expected to represent contributions of both amylose and amylopectin as a result of gelatinisation essentially most chains into a similar amorphous state.

It is apparent that the driver for the differences in digestibility of cooked rice grains cannot be observed in the CPMG decay of cooked rice grains. This may be a result of an inappropriate relaxation time range of the CPMG sequence, with relevant structures potentially having much shorter T_2, for example tightly bound resistant starch. It may also be a result of relevant structures being masked by the major contributions of gelatinised starch and water, making it difficult to assess these structures in cooked rice.

5.3.3.3.2 Assessing the contributions of relaxing components

The pre-exponential factors of the CPMG decays of each component were calculated for the cooked rice grains to investigate the contributions of the two decaying components to the total signal observed (Table 5-3, as described in Section 5.3.2.2). The pre-exponential factors displayed a significantly greater contribution of the first relaxing component to the total peak area (≈ 90 %) compared to the second component (≈ 10 %).

Table 5-3 Calculated pre-exponential factors for the bio-exponential decay function defining the T_2 decay for cooked rice grains

	A_0	A_0 -1
Doongara	0.908	0.092
Koshihikari	0.922	0.078
Topaz	0.851	0.149
Opus	0.880	0.120
Reiziq	0.885	0.115
Sherpa	0.888	0.112

Given the high moisture content, it was determined that the first component (faster decaying) is likely attributed to the OH signal, visually confirmed by greater signal intensity at 5.0 ppm in compared to the CH_x shoulder at 3.5 ppm (Figure 5-11, red line). Therefore, the second component was assigned to the CH_x signal (slower decaying).

Given this assignment, the relative contribution of the OH and CH_x signals were then compared to the total ^1H in the sample (Figure 5-11). In contrast to the raw rice grains (Figure 5-8), the majority of the total ^1H in the cooked rice grain was present in the first spectrum of the CPMG sequence (Figure 5-11). This finding indicates that the mobility of the majority of the ^1H in the sample has increased significantly, with T_2 values of >1.5 ms apparently characterising the majority of structure present. This is logical given the disruption of order as result of gelatinisation significantly altering the degree of dipolar coupling compared to ungelatinized starch and its helical structures As a result of the high moisture content of the cooked rice grains (70 % w/w), result the majority of protons in the sample are solely from water. The higher relative contribution of OH than CH_x to the intensity of CPMG spectrum, and the subsequent relative contribution to the total ^1H observed in the SPE, indicates that the majority of the water present is accounted for in the OH signal of the CPMG sequence (Figure 5-11). Thus, the majority of the water molecules has likely become bound to some degree within the gelatinised starch matrix, hence its relatively low T_2 relaxation time compared to what would be expected for unbound or free water. The fact that this is occurring for the majority of the OH signal further indicates that the process of gelatinisation has created a largely homologated distribution of bound water within the starch structure, as opposed to the different types of bound water that are typically reported in raw starches. Free water in these samples would likely be highly mobile, and therefore not

expected to be well resolved in the solid state ^{1}H spectrum, and so given its apparently low contribution has not been discussed.

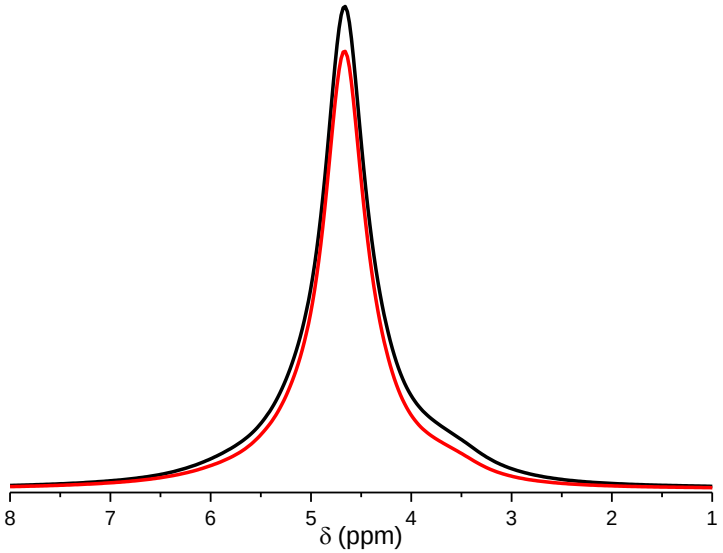

Figure 5-11 The ^{1}H SPE spectrum (black) and first spectrum of the CPMG sequence (red) for cooked Doongara rice grains. The ^{1}H SPE spectrum has been scaled by a factor 4 to account for difference in number of scans (NS=8 to NS_{eff} = 32)

These findings were then confirmed by the calculation of the relative contributions of the CPMG sequence to total area of the ^{1}H SPE spectrum (Table 5-4). The first spectrum of the CPMG sequence was found to represent ≈80 % of the total ^{1}H present in the samples, confirming that much of the sample has become increasingly mobile as a result of gelatinisation. Comparing the individual contributions of both OH and CH_x signals in the CPMG sequence, the OH dominates the contribution, making up approximately 68-75 % of the total ^{1}H, supported by the high moisture content, while the CH_x contributes 6 to 12 %. The calculated contribution of the CH_x signal (6- 12 %) is similar to the expected contribution (≈12 %) given starch concentration of 27 % w/w (given 70 % moisture content); however, the range of values observed indicate that varying levels of starch CH_x are not experiencing the same effects due to gelatinisation in different varieties. This variation may also be indicative of different concentrations of proteins or lipids, though these only represent a small fraction of the sample after cooking (3 % given 70 % moisture content). The differences in contributions of CH_x with T_2 measurable by the CPMG sequence maybe a factor in some differences between the varieties; however, was not found to correlate with either SH-60 or *AAC*. This lack of relationship of the CH_x signal with *AAC* shows that the observed CH_x signal in cooked rice grains likely arises from the contributions of both amylose and amylopectin, rather than just either individually.

The contribution of the starch OH is expected to be convoluted with water, likely dominated by exchange between the two and so is not expected to be a defining feature. However, the disparity between the total expected contribution of OH from water (≈80 %) and starch (≈5 %) to the total ^{1}H content and the contribution of OH in the CPMG spectrum (≈70 %, Table 5-4) indicates

that some combination of starch or water molecules are not detected in the CPMG sequence, potentially exhibiting much shorter or longer T_2 relaxations. These unaccounted molecules components may relate to structures such as resistant starch structures or helices that either escaped gelatinisation or were formed as a result of gelatinisation. Such tightly bound starch structures could also be responsible for unaccounted regions of trapped water with very low mobility; however, water in unbound form could also account for the unaccounted OH signal. Despite the potential for the disparity in the contribution of OH to be attributed to resistant starch formations, no correlation was observed with the SH-60 or *AAC*. This may indicate that the unaccounted signal area is in fact very slowly relaxing unbound water (> 1000 ms); however, investigation of the relaxation components of the FID may allow for assessment of faster relaxing components that can also account for this.

Table 5-4 Percentage contributions of the first CPMG spectra of cooked rice grains to the corresponding total area of a ^{1}H SPE spectrum

Variety	Area of CPMG relative to SPE (%)	OH to relative total SPE (%)	CH relative to total SPE (%)
Doongara	82.01	74.49	7.52
Koshihikari	82.21	75.83	6.37
Topaz	80.55	68.58	11.97
Opus	81.95	72.08	9.87
Reiziq	81.93	72.54	9.38
Sherpa	79.51	70.58	8.93

5.4 Conclusions and Future Work

The molecular dynamics of starch in raw rice grains were found to be an indicator of the *in vitro* digestibility of cooked rice grains. This was specifically attributed to the T_2 relaxation time of the CH_x signal in the CPMG sequence, a component which represented only ≈3 % of the total sample. It was hypothesised that while the contribution of these arrangements to the total sample is low, it is possible that it is the spatial distribution in conjunction with the factors that dictate its T_2 relaxation time that are responsible for this apparent trend. The lack of correlation of the OH component in raw rice grains is expected to arise from two major factors, being the convolution of OH arising from water and starch making it unclear, as well as the likelihood of the majority of OH groups participating in dipolar coupling as a result of double helix structures. Given the disruption of helical structure during cooking, it would not be expected to be factor in the digestibility of cooked rice grains.

Interestingly, no link between the T_2 of the CH_x in cooked rice grains the digestibility was observed. The contributions of the OH and CH_x signals in the CPMG of cooked rice represented ≈90 % of the total sample, highlighting the impacts of gelatinisation in increasing the total mobility within the sample. Given the strong "normalisation" of the underlying starch structure to an apparently amorphous state as a result of gelatinisation, it is expected that any smaller contributions of other structures may be dominated by the other major CH_x and OH components. This was likely compounded further by the high moisture content, with water become the major component of the rice grain after cooking. Thus, further work would be required to assess if different regions of structures can still be observed in cooked rice grains, with possible avenues including investigations of shorter time scale FID relaxation analysis or water suppression protocols. Due to the use of static measurements for NMR experiments, the methodology and outcomes are also transferable to benchtop NMR instrumentation, an important aspect in making this a usable tool for rice researchers. Specific NMR relaxometer instruments are available, providing faster CPMG acquisitions along with access to shorter T_2 times; however, these instruments would also require a different data analysis process to that discussed here. Relaxometers are a platform that should be explored in transferring the outcomes of this study to a more accessible platform.

Given the apparent link between molecular dynamics, it would be interesting to assess the strength of this trend on a larger sample set, given the small sample size here no strong conclusions could be drawn. Further to this, if the trend can be confirmed by further testing, the link to *in vivo* digestion would be another interesting avenue to explore in understanding the role of starch structures in digestibility. While this study focussed solely on the starch hydrolysed after 60 minutes as an assessment of digestibility, this is an arbitrary measure. The digestion of rice is complex involving multiple enzymes and stages; thus, it would be interesting to evaluate the role of molecular dynamics on the kinetics of digestion as an additional avenue in understanding digestibility.

5.5 Supporting Information

S 5.5.1 Determination of minimum cooking time and assessing degree of cooking

The cooking time of all varieties with the excess water method was tested by a staggered sequence cooking trial where 5 grains were tested using the squash test every 30 seconds over a period of time. The squash test involves placing the rice grains between two transparent glass slides and applying pressure to 'squash' to rice grains (Figure S 5-1). The presence of small white dots, or non-gel-like material, in the centre of the grain indicates that the grain is not completely cooked. This is clearly visible from 14-17 minutes in Figure S 5-1. Once cooking is complete, the

embryo of the rice grain can sometimes still be visible on the periphery of the cooked grain, this is not considered a factor in the cooking of the grain. The minimum cooking time was determined as the time it takes for 5 grains to be completely cooking as confirmed by the squash test.

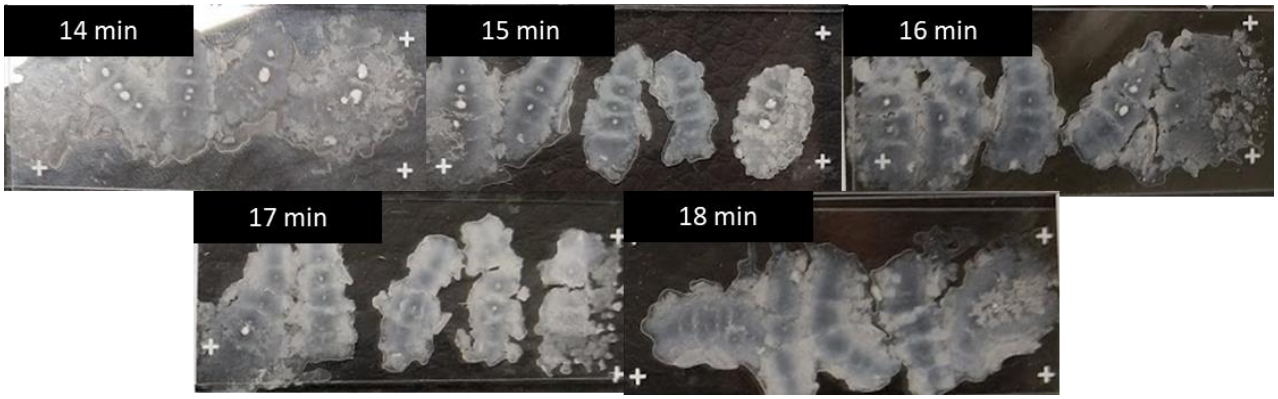

Figure S 5-1 Example of the "squash" test, showing rice grains cooked for different lengths of time in boiling water and compressed by hand between two glass microscope slides

The minimum cooking times determined were then used as a guide for experiments involving cooked grains, with the degree of cooking confirm for each variety via the squash test before experiments were performed. If the grain was undercooked, it was left to cook for longer in the boiling water. The average cooking times reported in Table S 5-1, represent multiple cooking experiments on the same samples in this study but for unrelated studies. The statistics indicate a standard deviation in cooking time of approximately 1 minute for most varieties, highlighting the importance of checking via the squash test before analysis.

Table S 5-1 The average cooking times of commercial rice varieties using the excess water method

Variety	Repeats	Average Cooking time (min)	Std Dev (min)	Std Err (min)
Doongara	9	18.5	0.9	0.3
Koshihikari	7	17.6	1.0	0.3
Topaz	6	15.2	0.9	0.3
Opus	3	17.5	1.2	0.5
Reiziq	3	18.0	1.3	0.5
Sherpa	3	19.2	0.4	0.2

S 5.5.2 Determination of T_2 components for cooked rice grains

A partial experimental set of spectra for a cooked rice grain showing the signal decay using the CPMG sequence with a spin-echo delay ranging from an initial delay of ~1.2 ms to a final delay of ~500 ms is shown in Figure S 5-2. Compared to the CPMG decay of the raw rice grain spectra

(Figure 2), the OH (4.8 ppm) and CH (3.8 ppm) signals are not clearly resolved in the CPMG decay of cooked rice grains, with both appearing to decay at a similar rate. This poor resolution is likely a result of the higher water content of the cooked grain (≈70 % moisture content) resulting in water becoming the dominating source of protons in the sample. Closer visual inspection at higher delay times indicates the CH shoulder at 3.8 ppm is still present with the OH signal. Therefore, assignment of the relaxing components was not possible by visual means.

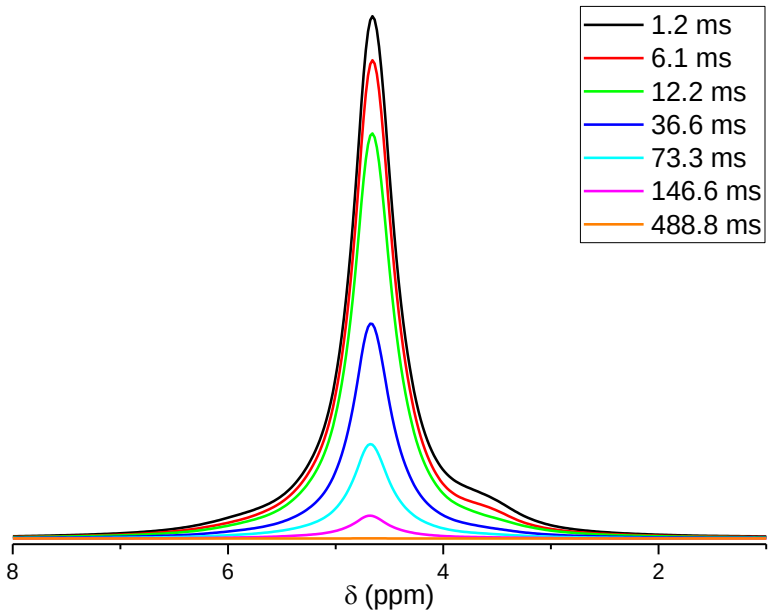

Figure S 5-2 Spectra with increasing echo delay from Carr-Purcell-Meiboom-Gill experiment on cooked rice grain showing the evolution of the signal with increasing number of repeat cycles. Echo delay lengths are as follows 1.2 (black), 6.1 (red), 12.2 (green), 36.6 (dark blue), 73.3 (light blue), 146.6 (pink) and 488.8 (orange) ms. Covers the range of ~ 1 to 500 ms echo delay

An example experimental exponential decay of peak area for a cooked rice grain is shown in Figure S 5-3A, where the majority of signal can be seen to have completely relaxed by the 250 ms

echo delay stage of the sequence. Similar, to the observations for the raw rice grains (Figure 5-3B), multiple components were observed for the cooked rice grains (Figure S 5-3B).

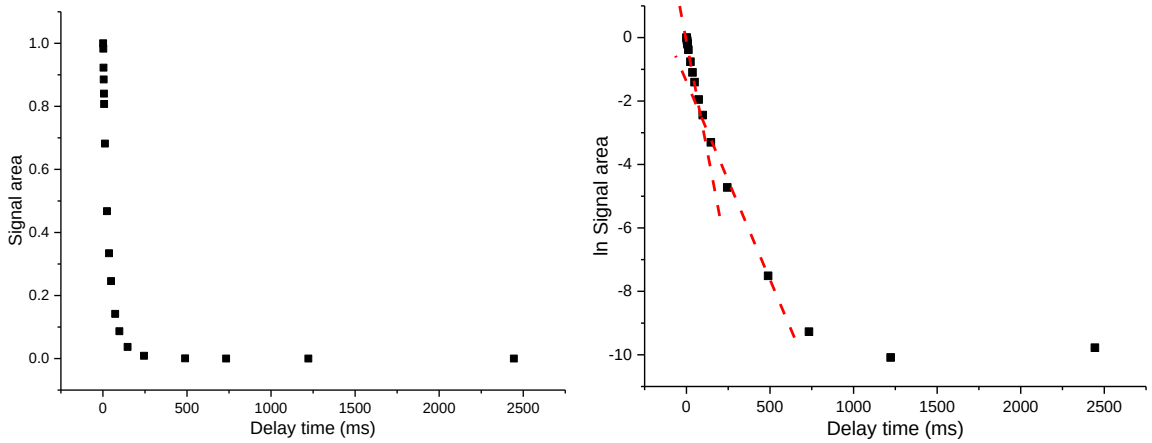

Figure S 5-3 A) Exponetial decay of signal area with increasing echo delay time and B) Natural logarithm of signal area for each spectrum of CPMG sequence plotted against the calculated delay time from a CPMG experiment on a raw rice grain. Dotted red lines show the presence of multiple slopes, representing multiple T_2 relaxation times in the decay profile

The two observed decaying components were then fitted using the same approach described in Section 5.3.2. Example fits for both components are shown in Figure S 5-4.

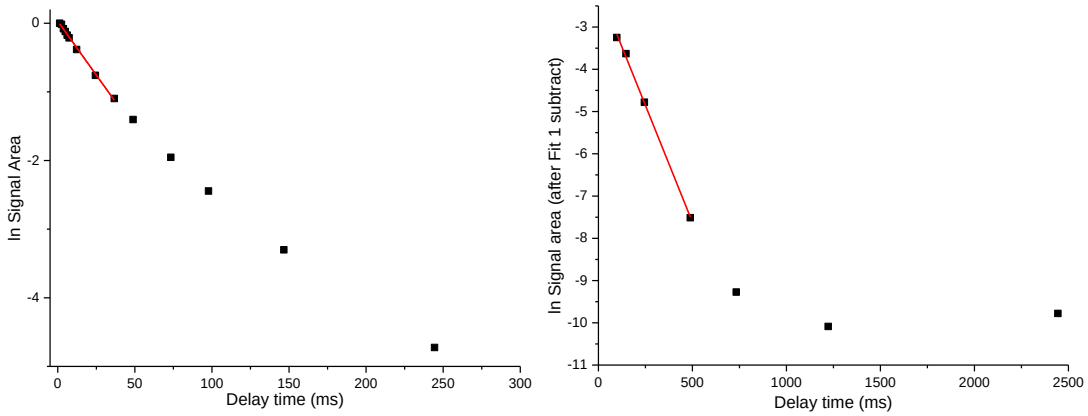

Figure S 5-4 Linear fits of transformed data in Figure S 5-3A for a) the first relaxing component of Figure S2 (n= 9 and adjusted R^2 = 0.99) and b) the second relaxing component of Figure S2 after subtraction of the initial linear fit (n = 4 and adjusted R^2 = 0.99)

S 5.5.3 Example overlay of the decays of different rice varieties

The T_2 relaxation times of the first component in the CPMG sequence of the raw rice grains were similar, while the second component displayed substantial differences in T_2 between varieties. A visual observation of the difference is shown in Figure S 5-5, where the apparent slopes of Doongara (red line) and waxy (blue line) are shown to differ significantly. The remaining varieties appear to have an average slope somewhere between that of the Doongara and Waxy varieties, in line with the intermediate T_2 values that were determined for their second component decays.

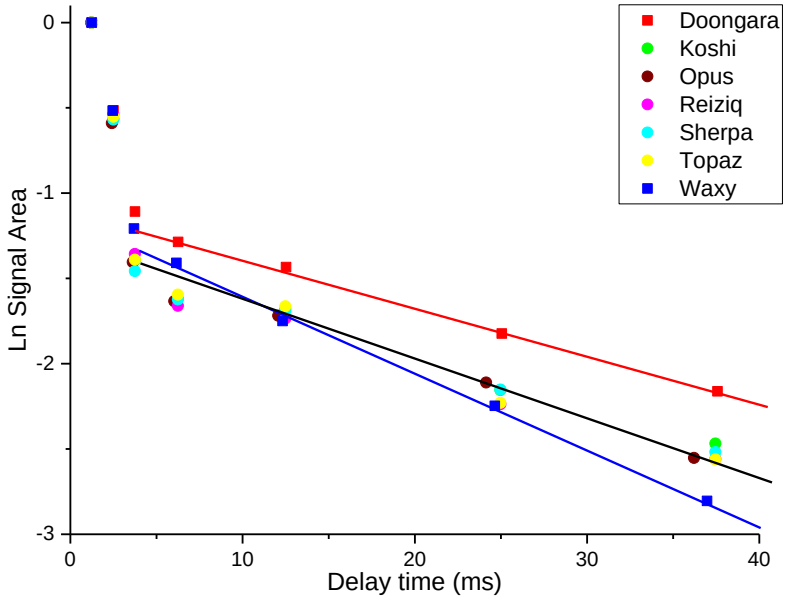

Figure S 5-5 The natural log of the signal area plotted against delay time for spectra of the CPMG experiment up to ≈40 ms. The apparent slopes of the second relaxing component of Doongara (red) and Waxy (blue) are shown, along with a general apparent slope for the remaining overlapping varieties (black)

S 5.5.4 Moisture contents of rice samples

The moisture content of raw rice flours and cooked rice grains measured by thermogravimetric analysis is shown in Table S 5-2 and

Table S 5-3. Moisture content was measured on a TGA/DSC- Netzsch STA449C Jupiter using an argon atmosphere (25 mL·min^{-1}). Temperature was ramped from 25 to 120 °C at a rate of 10 K·min^{-1}, and held at 120 °C until constant mass (approx. 2 hours) and moisture determined from the difference of initial and final mass. A pre-run measurement of an empty crucible was used as a baseline. Flour samples were weighed directly into crucibles, while cooked rice grains were cut lengthways and placed flat side down in the crucible.

Table S 5-2 Moisture contents of raw rice flours and starches determined by thermogravimetric analysis.
[a] Sample equilibrated at 44 % relative humidity

Variety	Moisture Content (% w/w)
Amorphous Doongara flour [a]	11.12
Amorphous Doongara flour [a] in rotor for 12 days	10.52
Raw Doongara flour [a]	12.88
Waxy Maize [a]	11.67
Waxy Maize (after NMR)	12.25
Amorphous Waxy Maize [a]	10.54
Amorphous Waxy Maize (after NMR)	10.96
Gelose 80 [a]	12.63
Gelose 80 (after NMR)	13.32
Amorphous Gelose 80 (after NMR)	12.07
Regular Maize [a]	12.75
Regular Maize (after NMR)	12.52
Amorphous Regular Maize [a]	11.29
Amorphous Regular Maize (after NMR)	11.83

Table S 5-3 Moisture contents of cooked rice grains determined by thermogravimetric analysis

Variety	Moisture Content (% w/w)
Cooked Doongara	75.82
Cooked Doongara rice grain (24 hours in sealed rotor)	67.42
Cooked Koshihikari	70.10
Overcooked Koshihikari	74.38
Cooked Koshihikari (2 hours in sealed rotor)	68.94

S 5.5.5 T_2 values and fitting statistics for raw and cooked rice grains

The T_2 values and linear fitting statistics are shown for raw rice (Table S 5-4 and Table S 5-5) and cooked rice (Table S 5-6).

Table S 5-4 T_2 and linear fit statistics from triplicate measurement of T_2 for raw rice grains of each variety for the first component of the CPMG decay

Variety	Rep 1			Rep 2			Rep 3		
	T_2 (ms)	Points	r^2	T_2 (ms)	Points	r^2	T_2 (ms)	Points	r^2
Doongara	2.45	3	0.998	2.12	3	1.000	2.78	3	0.965
Koshihikari	1.74	3	1.000	1.77	3	0.987	1.79	3	0.977
Opus	1.72	3	0.983	2.09	3	0.989	1.85	3	0.984
Reiziq	1.40	3	0.994	1.84	3	0.971	1.64	3	0.970
Sherpa	1.86	3	0.997	1.71	3	0.969	1.71	3	0.998
Topaz	1.71	3	0.988	1.72	3	0.979	1.80	3	0.972
Waxy	2.04	3	0.986	2.24	3	0.991	1.87	3	0.991

Table S 5-5 T_2 and linear fit statistics from triplicate measurement of T_2 for raw rice grains of each variety for the second component of the CPMG decay

Variety	Rep 1			Rep 2			Rep 3		
	T_2 (ms)	Points	r^2	T_2 (ms)	Points	r^2	T_2 (ms)	Points	r^2
Doongara	48.53	4	0.996	38.85	5	0.996	44.16	5	0.977
Koshihikari	36.66	5	0.992	35.92	5	0.981	34.49	5	0.986
Opus	33.87	5	0.983	34.33	5	0.989	33.46	5	0.995
Reiziq	29.71	5	0.972	32.54	5	0.989	33.09	5	0.989
Sherpa	32.29	5	0.988	33.14	5	0.978	33.86	5	0.982
Topaz	29.43	5	0.966	29.37	5	0.991	29.56	5	0.983
Waxy	24.25	4	0.998	24.65	4	0.995	24.05	4	0.996

Table S 5-6 T_2 and linear fit statistics from a single measurement of T_2 for cooked rice grains of each variety for the first and second components of the CPMG decay

Variety	Component 1			Component 2		
	T_2	Points	r^2	T_2	Points	r^2
Doongara	31.85	8	0.998	90.36	4	0.995
Koshihikari	36.00	9	0.996	85.59	4	0.995
Opus	27.80	8	0.998	64.12	4	0.999
Reiziq	31.45	8	0.993	77.75	4	0.999
Sherpa	24.09	8	0.997	61.35	4	0.996
Topaz	28.79	8	0.991	68.33	4	1.000
Waxy						

S 5.5.6 Signal assignment in raw starches

Two waxy maize samples were prepared, one deuterated (d-waxy) by suspension in D_2O and freeze drying twice and one unmodified (h-waxy), with both stored in a desiccator over a saturated aqueous solution of K_2CO_3 in D_2O. An aliquot of each sample (d-waxy-FD and h-waxy-FD) was also freeze dried overnight shortly before measurement (rotor packed within 1 hour).

^{1}H NMR spectra were recorded on Bruker DRX700 spectrometer with low-range [N-C] probe, 2.5 mm rotors, at 700 MHz, 25 kHz MAS.

S 5.5.6.1 Effect of deuteration and freeze drying on ^{1}H SPE spectrum

The ^{1}H NMR spectrum of the unmodified waxy maize starch shows a sharp peak at ≈4.3 ppm (Figure S 5-6, black), likely to be attributed to the OH peak of water and possibly starch. This was confirmed by the spectrum recorded for the waxy maize immediately after freeze drying, where the sharp signal is no longer observed at 4.3 ppm, leaving only a broad signal (Figure S 5-6, green). The maximum of this broad underlying signal lined up with the shoulder of the unmodified trace (Figure S 5-6), and is expected to be attributed to non-exchangeable protons of CH_x groups of starch.

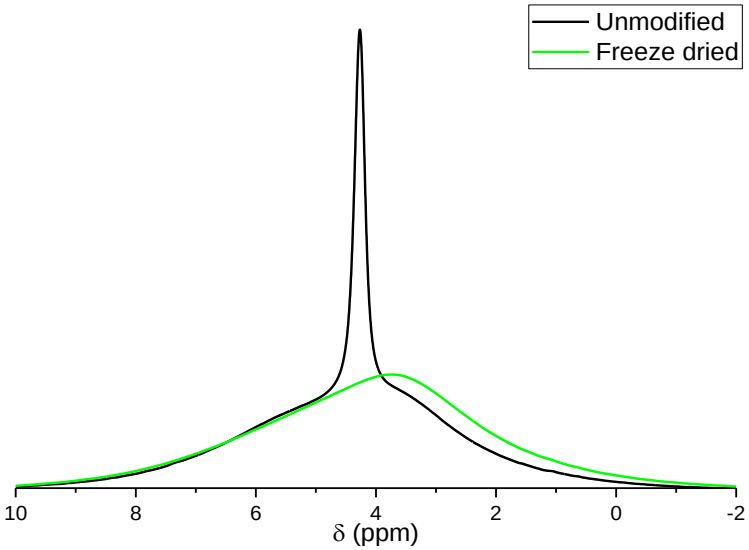

Figure S 5-6 ^{1}H SPE NMR spectrum of waxy maize (h-waxy) before (black) and immediately after (green) freeze drying

The ^{1}H NMR spectrum of the deuterated waxy maize starch also displayed a sharp signal at ≈4.3 ppm (Figure S 5-7, black), and given the previous assignment in Figure S 5-6, this is likely to be attributed to the residual OH of water. This was confirmed by the spectrum recorded for the deuterated waxy maize immediately after freeze drying, where the sharp signal is no longer observed at 4.3 ppm, leaving only a broad signal (Figure S 5-7, green). The maximum of this broad underlying signal lined up with the shoulder of the unmodified trace (Figure S 5-7), and is expected to be attributed to non-exchangeable protons of CH_x groups of starch.

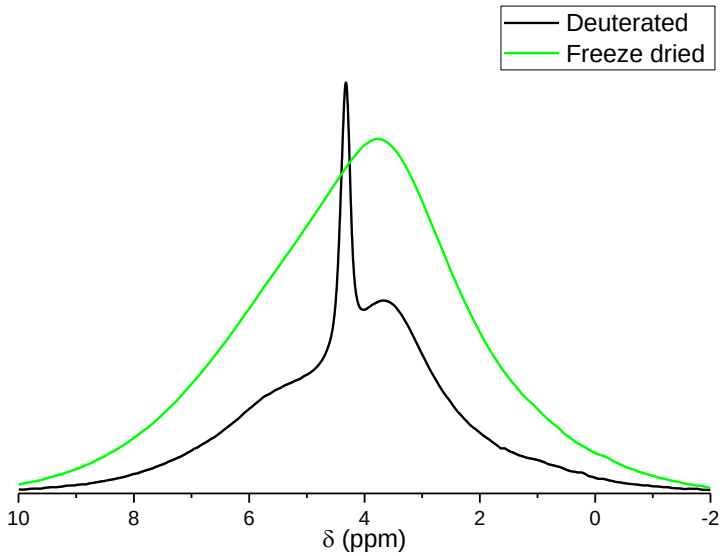

Figure S 5-7 ^{1}H SPE NMR spectrum of deuterated waxy maize (d-waxy) before (black) and immediately after (green) freeze drying

S 5.5.7 Examples of TopSpin fitting functions

The extraction of T_2 values from CPMG experiments on rice grains was first explored through the use of the built-in TopSpin dynamics centre, where a variety of functions are available to assess various aspects of the dynamics of a system. The functions of interest for T_2 relaxation times are "uxnmrt2" and "expdec", both of which were assessed. The first, "uxnmrt2" is the most common function to extract T_2 values; however, the software allows for only one value to be determined from the data. The resulting fit was of poor quality (Figure S 5-8), and therefore was not deemed to be useful in the multi-component systems being examined.

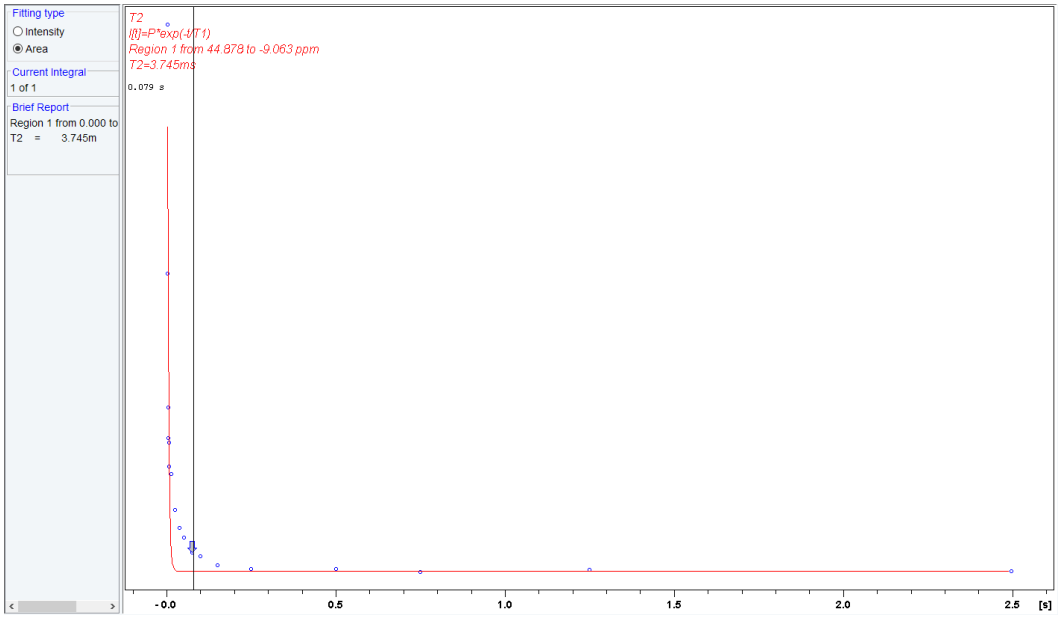

Figure S 5-8 Fit of a single relaxing component using the "uxnmrt2' function on the exponential decay of signal area with increasing echo delay time from a CPMG experiment on a raw rice grain

The second function "expdec", allowed for the fitting of multiple components, resulting in a much better fit of the data and thus improved determination of individual T_2 values. Though the fit was improved, the lack of control over the fitting process resulting in poor repeatability of the fitting process across samples. In addition, the fitting of more than 3 components at once resulted in poor fits, even in samples where more than 2 decaying components were observed in the linearized exponential (not shown).

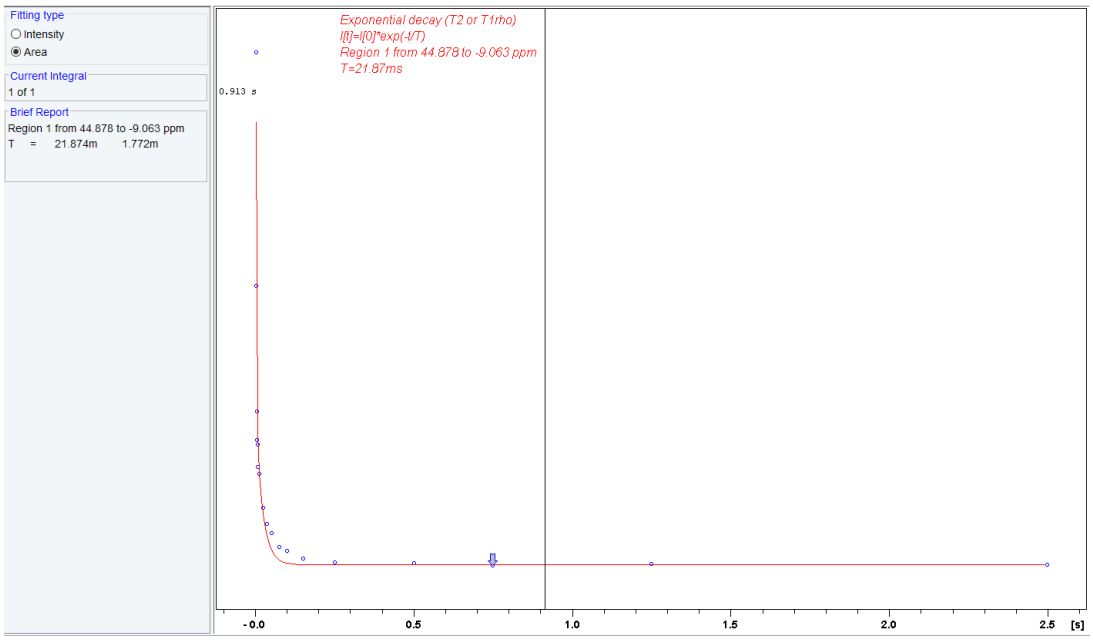

Figure S 5-9 Fit of two relaxing components using the "expdec' function on the exponential decay of signal area with increasing echo delay time from a CPMG experiment on a raw rice grain

An example of the T_2 values obtained by each of the methods is shown in Table S 5-7 for 3 repeats of a single variety of rice. The limitations of the "uxnmrt2" function are clear only allowing determination of a single T_2 and displayed little consistency between repeats. The "expdec" and iterative manual approach that was used in this study yielded similar values; however, the manual approach yielded a greater consistency across experimental repeats, and allowed for visualisation of the components present in each sample through the log transformations.

Table S 5-7 Relaxation times of both components observed in CPMG experiments of raw Koshihikari rice grains using different T_2 extraction methods

Run	Manual Approach (5.3.2)		"uxnmrt2"	"expdec"	
	Comp. 1	Comp. 2		Comp. 1	Comp. 2
1	1.741	36.664	3.617	0.998	36.159
2	1.771	35.9151	3.411	1.296	37.268
3	1.793	34.494	3.745	1.772	21.874

Chapter 6 Conclusions and future work

6.1 Fulfilled aims

The overall aim of this work was to determine what features of starch structure are capable of distinguishing different rice cultivars and better understand their digestibility. Starch is a natural polymer with a complex multi-level hierarchical structure ranging from molecular to supramolecular. Knowing the starch structures that best describes functional properties is useful for many purposes and research fields. While the methods in the literature for characterisation of supramolecular structures are well researched, current methods to analyse the molecular structures do not allow a complete characterisation of the molecular structures. This especially applies to analysis of native starch as present in rice flours.

At the molecular level, methods including capillary electrophoresis in the critical conditions (CE-CC and) and nuclear magnetic resonance (NMR) spectroscopy were used to explore the dissolution conditions of starch, finding that commonly used solvents such as DMSO/water mixtures and aqueous NaOH are not appropriate for accurate characterisation due to incomplete dissolution or potential sample degradation. In addition, it was determined that filtration significantly degrades the fragile branching structure of amylopectin, an important factor that should be considered in separation methods where stationary phases are employed. It was determined that anhydrous DMSO with some proportion of LiBr (0.5 to 5.0 %) resulted in faster and greater extent of dissolution, with the absence of water reported to result in an altered dissolution mechanism [78]. Further modifications in CE-CC experiments, including the use of lower concentrations (1 $g.L^{-1}$) than in the literature (>10 $g.L^{-1}$), as well as the maintenance of high dissolution temperatures (80 °C) resulted in minimised aggregation, greater extent of dissolution and greater dissolution stability.

With reliable dissolution conditions determined, the accurate characterisation of the branching structures in starch was achieved by NMR spectroscopy and CE-CC. The average DB was determined by NMR spectroscopy; however, the nature of this measurement does not allow for individual assessments of the distributions of *DB*s of amylose and amylopectin. Average *DB* was observed to be proportional with *AAC*, a result of the bimodal nature of the branching structure in starch, where increasing proportion of the less branched population appears to have dominating effect of decreasing the average *DB*. Therefore, it was determined that average *DB* by NMR spectroscopy did not provide significant additional value in comparison to the already well-established measurement of *AAC*.

The assessment of branching structures was undertaken through the characterisation of distributions of electrophoretic mobility distributions by CE-CC. Successful separation of the two branching populations, amylose and amylopectin, in native, unmodified rice flours allowed for individual assessment of their branching structures. A third, intermediate branching population, between amylopectin and amylose, was also observed in some rice cultivars, assigned to the theoretical third type of starch mentioned in literature [255], and assumed to be amylopectin with long chain branching due to the correlation of its average mobility with the double helix content. By relation to other structural factors, the mobility ranges of amylopectin and amylose were defined allowing for a reliable interpretation of analysis results. Weight-average mobilities revealed that rice cultivars exhibit different branching structures for amylopectin; this was also observed for amylose. The width of the distributions of electrophoretic mobility was found to vary between varieties, indicating differences in heterogeneity of branching structures. These outcomes highlighted the potential to broaden thinking around diversity of amylose and amylopectin structures and invites a revision of relationships between AAC and functional characteristics such as digestibility and texture. The ability for automation and parallelisation (multi-capillary operation) of the method have the potential to minimise labour costs associated with measurement and increase throughput. Initial setup costs are moderate ($70,000+), though running costs are relatively low with the major costs being consumables including vials and solvent (≈$1/sample) and reusable capillaries (≈$6/capillary). Current data analysis protocols have also largely automated processing; however, manual inputs are still required at some stages. Given the current costs and throughput of the methodology, if the data obtained proves meaningful it has promise as a potential candidate in routine analysis.

Further characterisation at the molecular level was through the measurement of the molecular dynamics by solid-state NMR spectroscopy, a property that is influenced by the supramolecular structures in starch. Multiple spin-spin relaxation components were observed for whole rice grains in the range of 1 – 1000 ms. The first two components were assigned to OH and CH_x protons within the sample. For the raw rice grains, the OH component was determined to be dominated by a convolution of starch and water, exhibiting low spin-spin relaxation times, at the limit of the CPMG sequence and similar between varieties. The T_2 relaxation times of the CH_x component were found to differ between the raw grains and display an apparent relationship with the cooked *in vitro* digestibility. The raw grains of the commercial low GI Doongara, and high GI waxy varieties displayed significantly different CH_x T_2 relaxation times. Interestingly, these relaxing components represented a very small percentage of the total hydrogen containing structures within sample despite their apparent relationship with digestibility.

Similar work on the cooked grains noted higher T_2 relaxation times, likely a direct result of the increased molecular mobility due to disruption of ordered structure as a result of gelatinisation;

however, no correlation with digestibility was found. In the cooked varieties, the relaxing components represented a large proportion of the total sample, and so it is likely that as a result of gelatinisation the majority of structure has somewhat normalised, potentially hiding the contribution of the relevant component observed in the raw grains. Despite this, the assessment of molecular mobility in raw rice grains by solid-state NMR spectroscopy shows promise as a tool in the prediction of digestibility. Significant costs would arise from instrumentation ($100,000 - $1,000,000+), with consumable costs much lower (reusable sample rotors, $500 each) and no sample preparation required. Automation of sample measurement is currently very cost prohibitive, increasing labour requirements, while data processing itself can be largely automated in software resulting in a current sample throughput of ≈10 samples/day. The potential for application on benchtop instrumentation (>$100,000) increases the accessibility of the methodology, aligning it well as a potential candidate for routine analysis. While current benchtop instrumentation does not allow for sample measurement at the magic angle, the relaxometry work in this thesis was done with a static sample, therefore the angle at which it is placed is irrelevant. In addition to this, specific relaxometry instrumentation is commercially available, offering faster acquisitions and access to a wider range of relaxation times than was possible with instrumentation in this study.

The results from this thesis also identified key areas requiring further study, including additional assessment of the iodine binding conditions of the CE-CC method, as well as confirmation of dissolution conditions in high amylose (>30% AAC) rice flours. In the measurement of molecular mobility, future work is needed to explore the potential of extracting additional components of the CPMG relaxation sequence for a complete analysis of the relaxing components on this time scale, as well as an investigation into faster decaying components (<1 ms).

6.2 Further investigation of starch structure and relation to digestibility

The previous chapters of this study explored the accurate analysis of molecular starch structure in rice. And while correlations of molecular structure were observed with the digestibility, the supramolecular structures are also a major component of the starch structure. Therefore, in the exploring the aims of this thesis, the supramolecular structure must also be assessed to obtain a more thorough assessment of the role of starch structure in rice digestibility. From the assessment of multiple levels of starch structure, a wider range of potential tools to predict digestibility could be explored, with the potential for translation to other rice grain properties. The link between AAC and digestibility is currently the only published link available

with which researchers can predict digestibility characteristics of a given rice sample [26]. A major study including over 200 unique rice cultivars, reported a negative apparent correlation with r^2 of 0.73, while much smaller studies with a limited range of *AAC* observed an r^2 of 0.92 (n= 8) [170], or no link at all (n=8) [311], indicating the likelihood of additional drivers at play. *In vitro* digestion and AAC data for a diverse set of 10 raw rice flours (*AAC* of 10 – 35 %) was provided by The University of Sydney and NSW DPI. While no clear link has been reported between digestibility of raw and cooked rice, an assessment of the impact of starch structure on enzymatic digestion can still be made. A preliminary investigation of the role of supramolecular structures of starch in raw rice grains with the digestibility was undertaken.

6.2.1 Short-range molecular order

The short-range molecular order was assessed through the determination of double and single helix content by solid-state ^{13}C NMR spectroscopy [118]. The arrangement of double helices arises from highly branched amylopectin molecules, and single helices from less branched amylose molecules. Single helices typically form in the presence of lipids or other suitable inclusions, so their abundance depends on several factors. The helices represent the smallest unit of molecular organisation in starch structure and are the building blocks of the higher levels of organisation.

No clear correlation between the glucose concentration and either double helix (Figure 6-1A) or single helix (Figure 6-1B) contents was observed. The lack of correlation with double helix content is interesting; however, given the size scale of helical structure (4-6 nm) it is possible that it is rather the spatial distribution and packing of helices that is a more important factor than the helix content itself. The weakly trending increase in digestibility with increasing single-helix content was counterintuitive, as single helix content for these varieties was positively correlated with *AAC* (data not shown). However, it has been suggested that rearrangements of amylose into helices during digestion are responsible for its apparent rate limiting behaviour [161], though this does not appear to be linked to the initial single helix content (Figure 6-1B).

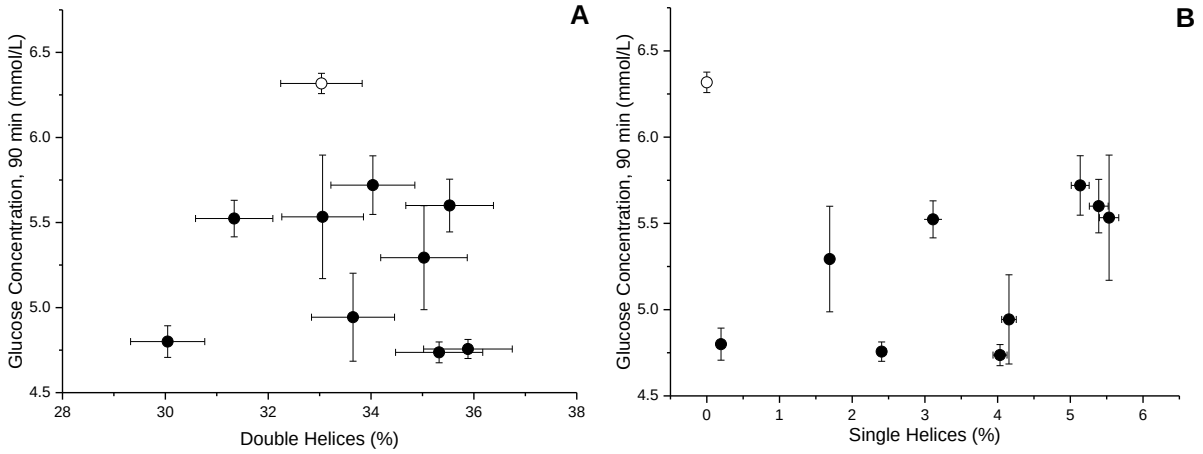

Figure 6-1 Glucose concentration after 90 minutes of enzymatic digestion of raw rice flour plotted against A) Double helix content and B) Single helix content for different rice flours. Error bars for glucose concentration are the standard error of 4 repeat digestions. Error bars for helix content are an estimated relative standard deviation of 2.4% [118]. Solid circles are non-waxy and open circles waxy varieties

Despite a lack of ability in predicting the digestibility, the double and single helix content was capable of distinguishing varieties, potentially a descriptor or factor influencing properties of rice other than digestibility. It would be interesting to further explore if the initial concentration of single helices is a factor in the apparent rate limiting effect of amylose chains on digestion in cooked rice. In contrast, the phase transformations of amylopectin and double helix structure during gelatinisation suggest that initial double helix content is likely not a strong driver of cooked rice properties, but the individual characteristics of the helices may be [312].

6.2.2 Long-range molecular order

The long-range molecular order was assessed through the determination of the extent of A-type and V-type crystalline structure by powder X-ray diffraction [131]. This long-range A-type crystalline order arises from the packing of double helices while the V-type polymorph is analogous to single helix content, though only those arranged in crystalline form. The remaining structure is typically deemed to be amorphous, though can still include single and double helix content.

The relation of digestibility to A-type crystallinity provided an interesting observation, indicating that increasing crystallinity of the starch resulted in decrease susceptibility to digestion of the raw rice flours (Figure 6-2A). However, a waxy variety goes against this apparent trend, by displaying the highest crystallinity and highest digestibility. This may be an outlier, potentially a result of significant differences in enzyme accessibility on the macroscopic scale compared to the other varieties, resulting in greater accessibility and thus greater digestibility. However, data on the macroscopic scale was not obtained and so this cannot be confirmed. The V-type crystalline structure also yielded an interesting observation, with digestibility apparently increasing with the concentration of V-type polymorph (Figure 6-2B). This relationship was similar to observations

on single helix content (Figure 6-1B), and again the opposite of the expected trend, given the positive correlation of V-type crystallinity with *AAC* (data not shown). Again, factors such as lipid content and spatial distribution, or branching structures may be factor in this. The highly digestible waxy variety appeared to go against this trend, indicating that this level of structure is likely not a sole factor in explaining its high digestibility.

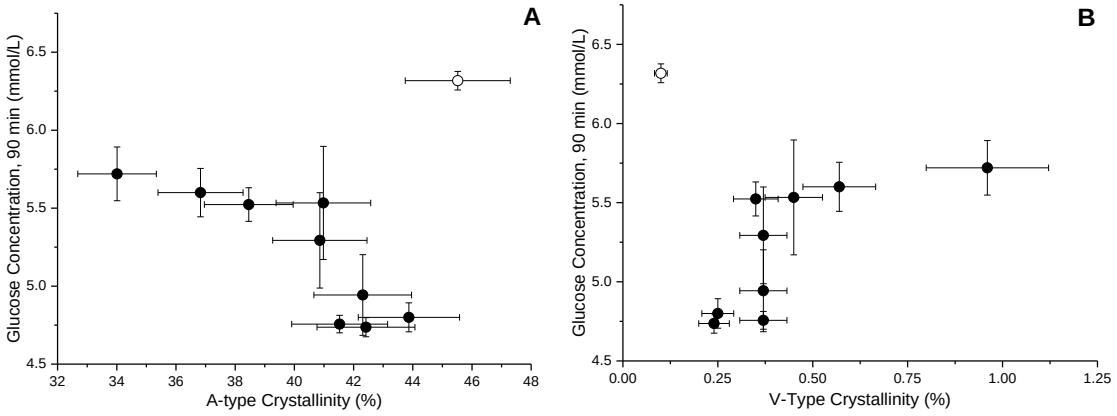

Figure 6-2 Glucose concentration after 90 minutes of enzymatic digestion of raw rice flour plotted against extent of A) A-type crystallinity and B) V-type crystallinity for different rice flours. Error bars for glucose concentration are the standard error of 4 repeat digestions. Error bars for helix content are an estimated relative standard deviation of 3.9% for A-type and 16.8 % for V-type [131]. Solid circles are non-waxy and open circles waxy varieties

While some link of the long-range crystalline order with the digestibility was observed, this did not hold true for all varieties, with the waxy variety exhibiting an apparently opposite behaviour. Despite this, the long-range crystalline structure was still capable of distinguishing varieties and may be relevant to properties other than digestibility. It would also be interesting to explore the role of these structures in cooked rice, as while long-range order will likely be mostly gelatinised, the V-type crystalline structure may in fact serve as a seed in the formation of resistant starches observed through cooking [31].

6.2.3 Semi-crystalline lamellar structure

The features of the semi-crystalline lamellar structure of starch were assessed by small angle X-ray scattering. The semi-crystalline structure of starch is composed of repeating rings of semi-crystalline and amorphous lamellae that form the starch granule. These semi-crystalline lamellae are then comprised of repeating crystalline and amorphous lamellae. Through fitting of the SAXS lamellar peak of starch, the relative extent of semi-crystalline structure, lamellar repeat thickness and heterogeneity of lamellar spacing was assessed.

The relative intensity of the SAXS lamellar peak serves as an indicator of the extent of semi-crystalline structure in the starch, with higher intensity indicative of a greater extent of semi-crystalline structure. Due to the influence of packing densities on the relative intensity in SAXS care must be taken in packing and hydration of samples. Unfortunately, consistent packing can be

difficult to perform, and in these measurements the error in relative intensities was quite high. Regardless, an apparent decrease in the digestibility was seen at higher peak intensities (Figure 6-3), similar to observations of increased crystallinity (Figure 6-2A) and in line with the relationship of peak intensity with *AAC* (Chapter 2). The waxy variety was an outlier again, exhibiting the highest extent of semi-crystalline structure and the highest digestibility, highlighting that there are clearly additional factors affecting digestibility.

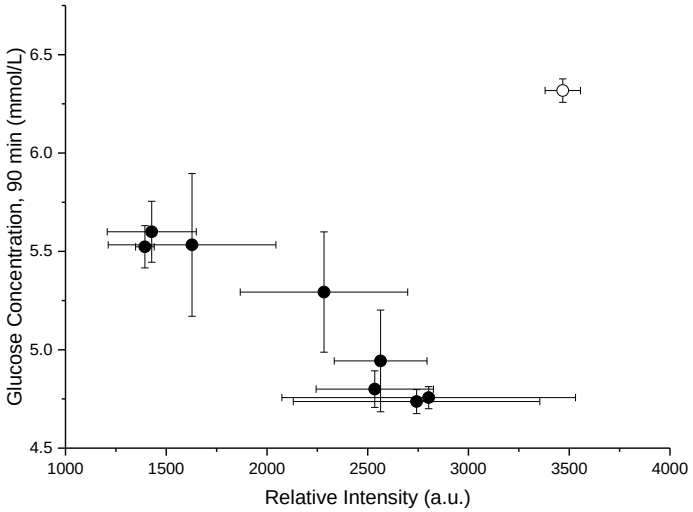

Figure 6-3 Glucose concentration after 90 minutes of enzymatic digestion of raw rice flour plotted against the relative intensity of the SAXS lamellar peak of starch for rice flours. Error bars for glucose concentration are the standard error of 4 repeat digestions. Error bars for relative intensity are the standard error of 3 repeats. Solid circles are non-waxy and open circles waxy samples

From the lamellar peak position and peak width, the lamellar repeat thickness and the uniformity of the lamellar repeat thickness could be determined. The lamellar repeat thickness refers to the length of one crystalline plus one amorphous lamella within the semi-crystalline lamellae and is typically confined to the range of 9-10 nm in starch. The rice varieties exhibited lamellar repeat thicknesses within this range which also clearly differed between varieties (Figure 6-4A). A smaller lamellar repeat thickness appeared to be linked with a lower digestibility in non-waxy varieties, with a plateau of the increasing glucose concentrations after 9.4 nm. The exception to this was the waxy variety, displaying a higher digestibility, above the range of the plateau. It appears that the lamellar repeat thickness plays some role in digestibility, but is not a sole driver, likely a result of the very small differences in size (<1 nm) playing a smaller role in the grand scheme of the semi-crystalline structure. The uniformity of the lamellae was assessed by the half-width at half-maximum (HWHM) of the lamellar peak (Figure 6-4B). Given the close relationship of lamellar repeat length with HWHM, similar trends were observed as were for lamellar repeat length. Digestibility was observed to increase between a HWHM of 1.6 to 2.0, before plateauing, while the waxy variety did not follow this trend again reporting much higher digestibility despite similar lamellar structure (Figure 6-4B).

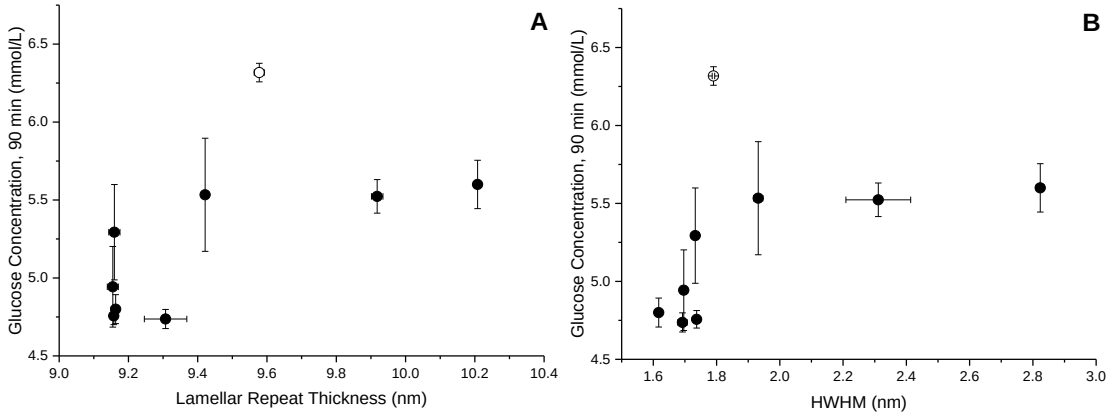

Figure 6-4 Glucose concentration after 90 minutes of enzymatic digestion of raw rice flour plotted against A) Average lamellar repeat thickness and B) Average HWHM of the SAXS lamellar peak for rice flours. Error bars for glucose concentration are the standard error of 4 repeat digestions. Error bars for lamellar repeat thickness and HWHM are the standard error of 3 repeats. Solid circles are non-waxy and open circles waxy varieties

6.2.4 Future assessment of supramolecular structures role in digestibility of rice grains

A clear role of the investigated levels of crystalline structure as rate defining factors in the digestibility of rice flour was not observed for the rice varieties measured, with the waxy variety always yielding the opposite behaviour to the non-waxy varieties. This could arise from differences in waxy varieties that are separate from the starch structures in this preliminary work. This raises the question of whether waxy samples should be treated as a separate class of grains in analysis, though further work would be required. It is possible that these structures have some role in the digestibility but is clear that no one level of structure is a definitive driver for digestibility. For example, the act of digestion itself changes the structure in some way that is not directly linked to the initial structures present but may be influenced by them. It is then necessary to expand the study of these structures to a greater range of rice varieties to confidently assess their role, whether significant or not. It should be noted that the opportunity to perform this study on non-commercial breeding samples provides a unique opportunity to analyse a very diverse sample set not available with commercial varieties. So, while only 10 varieties were analysed in this preliminary study, the high diversity still allows for valuable insights to be gained on the influence of starch structure on digestibility. This diversity is highlighted by the broad range of *AAC* (10 to 35 %), in addition to the clear ability to distinguish varieties by their crystalline structures, both areas where commercial samples typically show much less diversity. As a result, the relationship of these structures on other properties of rice may also be confidently explored.

Future directions for this data could also explore its relation to the digestibility of cooked rice grains, determining if some pre-existing factors of the supramolecular structure are catalysts for the differences in digestibility after cooking. This is supported by the knowledge that, above the

gelatinisation temperature, the rate of water ingress into the grain becomes the limiting factor [313]. This means that physical grain dimensions and porosity are likely to be the more dominant factors in cooking time when gelatinisation temperature is exceeded, properties that may be a product of the supramolecular starch structure. The topic of cooking is an issue that is present in many studies of starch and starchy cereal digestion, as realistically, the sample matrix should mimic what is native to the *in vivo* mechanism. This is further complicated by the variability observed *in vivo* as well as the attempts to develop a proxy for *in vivo* using *in vitro* methods. For direct assessments of human digestion, *in vivo* digestion studies would be most appropriate; however, *in vitro* studies offer some valuable insight in initial investigations [26]. The challenge for the field of research then becomes defining appropriate cooking protocols that standardise the method of cooking and clearly define a point at which cooking is complete. These two factors can be difficult to reconcile, as differences between varieties such as physical size and gelatinisation temperature can result in variability in minimum cooking times. Avoiding this could be achieved by overcooking all samples; however, the impacts of this on digestibility are not clear. This is further complicated by the decisions and requirements of manufacturers, especially when considering labelling which would require not only determination of individual cooking recommendations but also assessments of consistency and adherence to allowed variations. This is a huge undertaking, and an important aspect of the rice research field that needs to be addressed.

Therefore, in assessing the relationships of supramolecular structures, and indeed of molecular structures to digestibility in cooked rice grains, further research in the field needs to be undertaken in defining consistent conditions in which the digestibility can be assessed. This is a significant undertaking, requiring extensive study of the effects of cooking on starch structure and clear definitions of what constitutes as “cooked” for rice grains.

6.3 A brief discussion on development of tools for use in routine testing

A wide array of tools is already employed in the routine testing of rice grains, yielding important information on parameters relevant to the grain quality. The scope of breeding programs is broad, with development of new varieties taking up to 10 years and involving the assessment of thousands of candidates every year. This time span can be impacted by factors such as the limitations of seasonal growing cycles, especially where glasshouses are not available or are not appropriate, as well as throughput of phenotyping capabilities. While glasshouses can provide greater throughput in early stages, greater space requirements in later stages as well as the necessity of testing local growing conditions make them unfeasible. As a result, the parameters

measured as part of routine testing need to be high quality, provide meaningful and useful data relevant to the goals of the breeding program, as well as be high throughput to allow multiple traits to be measured and analysed before the next sowing date. Therefore, the inclusion of new parameters as part of routine testing must then be thoroughly assessed in its value relative to the tools already available and to the desired outcomes.

The determination of factors of starch structure relevant to digestibility here was intended to better understand the drivers of digestibility in rice grains. This is not intended to replace direct measurements of digestibility, but rather act as a tool with which to assess samples likely to exhibit a higher or lower digestibility, allowing a better selectivity in breeding where certain digestibility characteristics are a grain quality goal. The assessment of branching structures by CE-CC provides an abundance of information on the amylose and amylopectin molecules in starch. The differences observed between varieties on the molecular level show promise in defining the role of different branching structures in digestibility, expected to be a complementary factor with *AAC*. The use of CE-CC as a tool for routine testing shows promise due to the potential for not only automation, but also parallelisation given recent advances in instrumentation, allowing for high throughput operation. Using the same CE instrumentation, Taylor Dispersion Analysis could also be employed in further characterisation of starch molecules, allowing for a size-based characterisation of starch molecules [277].

Additionally, the apparent link between molecular dynamics in NMR spectroscopy and digestibility provides a simple method with which digestibility could be predicted. While measurements in this work were performed on large and expensive spectrometers, the method is also applicable on smaller and cheaper benchtop spectrometers, increasing accessibility to instrumentation. While assessments of molecular mobility are simple and can be optimised for higher throughput, there does not yet exist methods to allow for parallelisation. Automation is possible but is generally not a time saver in the case of this method.

The methods employed in the measurement of supramolecular structures as discussed in Section 2 yield an abundance of information on the large-scale structural differences between starch in rices. However, with current instrumentation, these approaches are unsuitable for most routine testing programs as a result of limitations of access to instrumentation, of their high costs and associated expertise required for operation and maintenance. In addition, data analysis can be highly time consuming and its reliability heavily depends on the skills of the operator. Thus, while supramolecular structure may be found in the future to be a strong driver in the digestibility of cooked rice grains, it is not expected that the methods employed will be appropriate in routine testing with the current climate of instrumentation and analysis, serving more as a fundamental analysis in understanding digestibility rather than a predictive tool.

6.4 Future possibilities: Incorporation of structural characterisation in other aspects of rice grain quality

Given the high starch content of most rices (≈90 %) the impact of starch structure on digestibility was a strong starting point for understanding how digestibility can vary. In addition, the protein and lipid contents of rice need to be considered, as they are known to influence properties such as texture. While starch structure was found to differ substantially between rice varieties, not all types of structure could explain differences in digestibility. Given the complexity of starch structure, and indeed of rice grain properties, it is likely that differences in starch structure can also impact on the other important properties of rice such as texture. Therefore, future work could involve the assessment of the multiple levels of structural with respect to other facets of rice besides digestibility. Crystalline structures are especially expected play a role in many of the textural and cooking properties, given their positioning as a factor controlling water ingress into the starch.

Beyond the relation to other properties of rice grains, the structural characterisation of starch may also be applied to other starchy cereals and grains, especially in cases where the starch content is lower. Such a cross-species assessment would provide further insight into the role of starch structure for cereal/grain properties in general. It is expected that the methodologies applied in this work are applicable to other types of cereals/grains with minimal to no modification, a predetermined goal in the selection and development of methods employed in this work.

References

1. Juliano BO. Rice: Overview. In: Faubion J, Seetharaman K, Wrigley C, Corke H, editors. Encyclopedia of Food Grains (Second Edition). 1. 2nd ed. Oxford: Academic Press; 2016. p. 125-9.
2. Bhattacharya KR, Ali SZ. Agronomy, production and trade of rice. In: Bhattacharya KR, Ali SZ, editors. An Introduction to Rice-grain Technology. Woodhead Publishing India in Food Science, Technology and Nutrition: WPI Publishing; 2015. p. 10-37.
3. Sun Rice. Australian Rice Varieties: Sun Rice; 2020; Accessed: 18/04/2020. Available: https://www2.sunrice.com.au/media/6661/australian_rice_varieties_v2.pdf.
4. Ward RM. Quality parameters and testing methods in rice cultivation. In: Sasaki T, Kumar A, Pereira A, Angleles-Shim RB, Ashikari M, editors. Achieving Sustainable Cultivation of Rice. 1. Great Britain: Burleigh Dodds; 2017.
5. Fitzgerald MA, Reinke RF. Rice grain quality III. Australia: Rural Industries Research and Development Corporation; 2006. RIRDC Publication: 06/056, ISSN: 1440-6845.
6. Guimarães EP. Rice Breeding. In: Carena MJ, editor. Cereals. New York, NY: Springer US; 2009. p. 99-126.
7. Concepcion JCT, Ouk M, Zhao D, Fitzgerald MA. The need for new tools and investment to improve the accuracy of selecting for grain quality in rice. Field Crops Research. 2015;182:60-7.
8. Balindong JL, Ward RM, Liu L, Rose TJ, Pallas LA, Ovenden BW, Snell PJ, Waters DLE. Rice grain protein composition influences instrumental measures of rice cooking and eating quality. Journal of Cereal Science. 2018;79(Supplement C):35-42.
9. Misra G, Cuevas RP, Anacleto R, Butardo VM, Jr, Sreenivasulu N, Kavi Kishor PB. Designing climate-resilient rice with ideal grain quality suited for high-temperature stress. Journal of Experimental Botany. 2015;66(7):1737-48.
10. Ward RM. Potential impact of temperature and carbon dioxide levels on rice quality [PhD thesis]. Sydney, Australia: The University of Sydney; 2007.
11. Jiang H, Dian W, Wu P. Effect of high temperature on fine structure of amylopectin in rice endosperm by reducing the activity of the starch branching enzyme. Phytochemistry. 2003;63(1):53-9.
12. Commonwealth Scientific and Industrial Research Organisation, Australian Government Bureau of Meteorology. State of the Climate 2018. Australia; 2018. ISBN: 978-1-925315-97-4.
13. Gross LS, Li L, Ford ES, Liu S. Increased consumption of refined carbohydrates and the epidemic of type 2 diabetes in the United States: an ecologic assessment. The American Journal of Clinical Nutrition. 2004;79(5):774-9.
14. Australian Bureau of Statistics. Australian Health Survey: First Results, 2014-15. Commonwealth of Australia; 2015. Report No.: Catalogue No.: 4364.0.55.001.
15. The Organisation for Economic Co-operation and Development (OECD). Obesity Update 2017; Accessed: 29/04/2020. Available: http://www.oecd.org/health/obesity-update.htm.
16. World Health Organisation. Obesity: preventing and managing the global epidemic. Geneva; 2000. Report No.: 0512-3054.
17. Hill JO, Melanson EL. Overview of the determinants of overweight and obesity: current evidence and research issues. Medicine & Science in Sports & Exercise. 1999;31(11):S515.
18. Markwald RR, Melanson EL, Smith MR, Higgins J, Perreault L, Eckel RH, Wright KP. Impact of insufficient sleep on total daily energy expenditure, food intake, and weight gain. Proceedings of the National Academy of Sciences. 2013;110(14):5695-700.
19. Wolever TMS. Dietary carbohydrates and insulin action in humans. British Journal of Nutrition. 2000;83(S1):S97-S102.
20. Bessesen DH. The Role of Carbohydrates in Insulin Resistance. The Journal of Nutrition. 2001;131(10):2782S-6S.
21. Arendt E, Zannini E. Rice. In: Cereal Grains for the Food and Beverage Industries. 248. Cambridge, Sawston: Woodhead Publishing; 2013.

22. Buléon A, Colonna P, Planchot V, Ball S. Starch granules: structure and biosynthesis. International Journal of Biological Macromolecules. 1998;23(2):85-112.
23. Waters DLE, Henry RJ, Reinke RF, Fitzgerald MA. Gelatinization temperature of rice explained by polymorphisms in starch synthase. Plant Biotechnology Journal. 2006;4(1):115-22.
24. Zhou Z, Robards K, Helliwell S, Blanchard C, Baxter G. Rice Ageing. I. Effect of Changes in Protein on Starch Behaviour. Starch - Stärke. 2003;55(3-4):162-9.
25. Zhou Z, Robards K, Helliwell S, Blanchard C. Effect of the addition of fatty acids on rice starch properties. Food Research International. 2007;40(2):209-14.
26. Fitzgerald MA, Rahman S, Resurreccion AP, Concepcion J, Daygon VD, Dipti SS, Kabir KA, Klingner B, Morell MK, Bird AR. Identification of a Major Genetic Determinant of Glycaemic Index in Rice. Rice. 2011;4(2):66-74.
27. Sowbhagya CM, Ramesh BS, Bhattacharya KR. The relationship between cooked-rice texture and the physicochemical characteristics of rice. Journal of Cereal Science. 1987;5(3):287-97.
28. Strocchi A, Levitt MD. Measurement of starch absorption in humans. Canadian Journal of Physiology and Pharmacology. 1991;69(1):108-10.
29. Tamura M, Singh J, Kaur L, Ogawa Y. Impact of the degree of cooking on starch digestibility of rice – An in vitro study. Food Chemistry. 2016;191:98-104.
30. Rashmi S, Urooj A. Effect of processing on nutritionally important starch fractions in rice varieties. International Journal of Food Sciences and Nutrition. 2003;54(1):27-36.
31. Chiu Y-T, Steward ML. Effect of variety and cooking method on resistant starch content of white rice and subsequent postprandial glucose response and appetite in humans. Asia Pacific Journal of Clinical Nutrition. 2013;22(3):372-9.
32. Rewthong O, Soponronnarit S, Taechapairoj C, Tungtrakul P, Prachayawarakorn S. Effects of cooking, drying and pretreatment methods on texture and starch digestibility of instant rice. Journal of Food Engineering. 2011;103(3):258-64.
33. Li H, Fitzgerald MA, Prakash S, Nicholson TM, Gilbert RG. The molecular structural features controlling stickiness in cooked rice, a major palatability determinant. Scientific Reports. 2017;7:43713.
34. Baxter G, Zhao J, Blanchard C. Salinity alters the protein composition of rice endosperm and the physicochemical properties of rice flour. Journal of the Science of Food and Agriculture. 2011;91(12):2292-7.
35. Zhou Z, Robards K, Helliwell S, Blanchard C. Composition and functional properties of rice. International Journal of Food Science & Technology. 2002;37(8):849-68.
36. Zhou Z, Robards K, Helliwell S, Blanchard C. Effect of storage temperature on cooking behaviour of rice. Food Chemistry. 2007;105(2):491-7.
37. Zhou Z, Robards K, Helliwell S, Blanchard C. Effect of storage temperature on rice thermal properties. Food Research International. 2010;43(3):709-15.
38. Gaborieau M, Castignolles P. Caractérisation de l'amidon et de ses matériaux composites. Les Annales des falsifications de l'expertise chimique et toxicologique (Société des Experts Chimistes de France). 2009;9710:23-32.
39. Blazek J, Gilbert EP. Effect of enzymatic hydrolysis on native starch granule structure. Biomacromolecules. 2010;11(12):3275-89.
40. Englyst HN, Kingman SM, Cummings JH. Classification and measurement of nutritionally important starch fractions. European Journal of Clinical Nutrition. 1992;46(S2):S33-50.
41. Wolever TMS. Glycaemic Index : A Physiological Classification of Dietary Carbohydrate. Wallingford, Oxfordshire, GBR: CABI Publishing; 2006.
42. Englyst HN, Hudson GJ. The classification and measurement of dietary carbohydrates. Food Chemistry. 1996;57(1):15-21.
43. Bornhorst GM, Singh RP. Gastric Digestion In Vivo and In Vitro: How the Structural Aspects of Food Influence the Digestion Process. Annual Review of Food Science and Technology. 2014;5(1):111-32.

44. Minekus M, Alminger M, Alvito P, Ballance S, Bohn T, Bourlieu C, Carriere F, Boutrou R, Corredig M, Dupont D, Dufour C, Egger L, Golding M, Karakaya S, Kirkhus B, Le Feunteun S, Lesmes U, Macierzanka A, Mackie A, Marze S, McClements DJ, Menard O, Recio I, Santos CN, Singh RP, Vegarud GE, Wickham MSJ, Weitschies W, Brodkorb A. A standardised static in vitro digestion method suitable for food - an international consensus. Food & Function. 2014;5(6):1113-24.
45. Jenkins DJ, Wolever TM, Taylor RH, Barker H, Fielden H, Baldwin JM, Bowling AC, Newman HC, Jenkins AL, Goff DV. Glycemic index of foods: a physiological basis for carbohydrate exchange. The American Journal of Clinical Nutrition. 1981;34(3):362-6.
46. Salmeron J, Ascherio A, Rimm EB, Colditz GA, Spiegelman D, Jenkins DJ, Stampfer MJ, Wing AL, Willett WC. Dietary fiber, glycemic load, and risk of NIDDM in men. Diabetes Care. 1997;20(4):545-50.
47. Liu S, Willett WC, Stampfer MJ, Hu FB, Franz M, Sampson L, Hennekens CH, Manson JE. A prospective study of dietary glycemic load, carbohydrate intake, and risk of coronary heart disease in US women. The American Journal of Clinical Nutrition. 2000;71(6):1455-61.
48. Englyst K, Goux A, Meynier A, Quigley M, Englyst H, Brack O, Vinoy S. Inter-laboratory validation of the starch digestibility method for determination of rapidly digestible and slowly digestible starch. Food Chemistry. 2018;245:1183-9.
49. Benelam B. Satiation, satiety and their effects on eating behaviour. Nutrition Bulletin. 2009;34(2):126-73.
50. Mayer J, Vitale JJ, Bates MW. Mechanism of the Regulation of Food Intake. Nature. 1951;167(4249):562-3.
51. Bray GA. Static Theories in a Dynamic World: A Glucodynamic Theory of Food Intake. Obesity Research. 1996;4(5):489-92.
52. Chaput JP, Tremblay A. The glucostatic theory of appetite control and the risk of obesity and diabetes. International Journal of Obesity. 2009;33(1):46-53.
53. Feskens EJM, Du H. Dietary glycaemic index from an epidemiological point of view. International Journal of Obesity. 2006;30(S3):S66-71.
54. Lehmann U, Robin F. Slowly digestible starch – its structure and health implications: a review. Trends in Food Science & Technology. 2007;18(7):346-55.
55. Brand-Miller JC, Holt SH, Pawlak DB, McMillan J. Glycemic index and obesity. The American Journal of Clinical Nutrition. 2002;76(1):281S-5S.
56. Byrnes SE, Brand-Miller JC, Denyer GS. Amylopectin starch promotes the development of insulin resistance in rats. The Journal of Nutrition. 1995;125(6):1430-7.
57. Pawlak DB, Kushner JA, Ludwig DS. Effects of dietary glycaemic index on adiposity, glucose homoeostasis, and plasma lipids in animals. The Lancet. 2004;364(9436):778-85.
58. Wolever TM, Jenkins DJ, Ocana AM, Rao VA, Collier GR. Second-meal effect: low-glycemic-index foods eaten at dinner improve subsequent breakfast glycemic response. The American Journal of Clinical Nutrition. 1988;48(4):1041-7.
59. Wolever TM, Mehling C. Long-term effect of varying the source or amount of dietary carbohydrate on postprandial plasma glucose, insulin, triacylglycerol, and free fatty acid concentrations in subjects with impaired glucose tolerance. The American Journal of Clinical Nutrition. 2003;77(3):612-21.
60. Slavin J, Green H. Dietary fibre and satiety. Nutrition Bulletin. 2007;32:32-42.
61. Ordonio RL, Matsuoka M. Increasing resistant starch content in rice for better consumer health. Proceedings of the National Academy of Sciences of the United States of America. 2016;113(45):12616-8.
62. Willis HJ, Eldridge AL, Beiseigel J, Thomas W, Slavin JL. Greater satiety response with resistant starch and corn bran in human subjects. Nutrition Research. 2009;29(2):100-5.
63. Nilsson AC, Östman EM, Holst JJ, Björck IME. Including indigestible carbohydrates in the evening meal of healthy subjects improves glucose tolerance, lowers inflammatory markers, and increases satiety after a subsequent standardized breakfast. The Journal of Nutrition. 2008;138(4):732-9.

64. Kaur B, Ranawana V, Henry J. The Glycemic Index of Rice and Rice Products: A Review, and Table of GI Values. Critical Reviews in Food Science and Nutrition. 2016;56(2):215-36.
65. Mohan V, Spiegelman D, Sudha V, Gayathri R, Hong B, Praseena K, Anjana RM, Wedick NM, Arumugam K, Malik V, Ramachandran S, Bai MR, Henry JK, Hu FB, Willett W, Krishnaswamy K. Effect of Brown Rice, White Rice, and Brown Rice with Legumes on Blood Glucose and Insulin Responses in Overweight Asian Indians: A Randomized Controlled Trial. Diabetes Technology & Therapeutics. 2014;16(5):317-25.
66. Wang SJ, Li PY, Zhang T, Yu JL, Wang S, Copeland L. In vitro starch digestibility of rice flour is not affected by method of cooking. Lwt-Food Science and Technology. 2017;84:536-43.
67. Ward R. Quality parameters and testing methods in rice cultivation. In: Sasaki T, editor. Achieving sustainable cultivation of rice. 1: Burleigh Dodds Science Publishing Limited; 2017. p. 237-52.
68. Misra G, Badoni S, Domingo CJ, Cuevas RPO, Llorente C, Mbanjo EGN, Sreenivasulu N. Deciphering the Genetic Architecture of Cooked Rice Texture. 2018;9(1405).
69. Jane J, Chen YY, Lee LF, McPherson AE, Wong KS, Radosavljevic M, Kasemsuwan T. Effects of Amylopectin Branch Chain Length and Amylose Content on the Gelatinization and Pasting Properties of Starch. Cereal Chemistry Journal. 1999;76(5):629-37.
70. Sulaiman R, Dolan KD. Effect of amylose content on estimated kinetic parameters for a starch viscosity model. Journal of Food Engineering. 2013;114(1):75-82.
71. Knutson CA. A simplified colorimetric procedure for determination of amylose in maize starches. Cereal Chemistry. 1986;63(2):89-92.
72. Knutson CA. Evaluation of variations in amylose-iodine absorbance spectra. Carbohydrate Polymers. 1999;42:65-72.
73. Fitzgerald MA, Bergman CJ, Resurreccion AP, Moller J, Jimenez R, Reinke RF, Martin M, Blanco P, Molina F, Chen MH, Kuri V, Romero MV, Habibi F, Umemoto T, Jongde S, Graterol E, Reddy KR, Bassinello PZ, Sivakami R, Rani NS, Das S, Wang YJ, Indrasari SD, Ramli A, Ahmad R, Dipti SS, Xie LH, Lang NT, Singh P, Toro DC, Tavasoli F, Mestres C. Addressing the Dilemmas of Measuring Amylose in Rice. Cereal Chemistry. 2009;86(5):492-8.
74. AACCI. Approved Methods of Analysis. 11th ed. Method 61-03.01, Amylose Content of Milled Rice. St. Paul, MN, U.S.A.: AACC International; 2011.
75. Zhu T, Jackson DS, Wehling RL, Geera B. Comparison of amylose determination methods and the development of a dual wavelength iodine binding technique. Cereal Chemistry. 2008;85(1):51-8.
76. Nollet LML. Liquid chromatography in food analysis. In: Encyclopedia of Analytical Chemistry: John Wiley & Sons, Ltd; 2006.
77. Kärkkäinen J, Lappalainen K, Joensuu P, Lajunen M. HPLC-ELSD analysis of six starch species heat-dispersed in [BMIM]Cl ionic liquid. Carbohydrate Polymers. 2011;84(1):509-16.
78. Dona A, Yuen C-WW, Peate J, Gilbert RG, Castignolles P, Gaborieau M. A new NMR method for directly monitoring and quantifying the dissolution kinetics of starch in DMSO. Carbohydrate Research. 2007;342(17):2604-10.
79. Schmitz S, Dona AC, Castignolles P, Gilbert RG, Gaborieau M. Assessment of the Extent of Starch Dissolution in Dimethyl Sulfoxide by 1H NMR Spectroscopy. Macromolecular Bioscience. 2009;9(5):506-14.
80. Gérard C, Barron C, Colonna P, Planchot V. Amylose determination in genetically modified starches. Carbohydrate Polymers. 2001;44(1):19-27.
81. Oliver JD, Gaborieau M, Hilder EF, Castignolles P. Simple and robust determination of monosaccharides in plant fibers in complex mixtures by capillary electrophoresis and high performance liquid chromatography. Journal of Chromatography A. 2013;1291:179-86.
82. Hoang N-L, Landolfi A, Kravchuk A, Girard E, Peate J, Hernandez JM, Gaborieau M, Kravchuk O, Gilbert RG, Guillaneuf Y, Castignolles P. Toward a full characterization of native starch: Separation and detection by size-exclusion chromatography. Journal of Chromatography A. 2008;1205(1–2):60-70.

83. Cave RA, Seabrook SA, Gidley MJ, Gilbert RG. Characterization of Starch by Size-Exclusion Chromatography: The Limitations Imposed by Shear Scission. Biomacromolecules. 2009;10(8):2245-53.
84. Langhorst MA, Stanley FW, Cutie SS, Sugarman JH, Wilson LR, Hoagland DA, Prud'homme RK. Determination of nonionic and partially hydrolyzed polyacrylamide molecular weight distributions using hydrodynamic chromatography. Analytical chemistry. 1986;58(11):2242-7.
85. You S, Lim S-T. Molecular characterization of corn starch using an aqueous HPSEC-MALLS-RI system under various dissolution and analytical conditions. Cereal Chemistry. 2000;77(3):303-8.
86. Roger P, Tran V, Lesec J, Colonna P. Isolation and characterisation of single chain amylose. Journal of Cereal Science. 1996;24(3):247-62.
87. Uliyanchenko E, van der Wal S, Schoenmakers PJ. Deformation and degradation of polymers in ultra-high-pressure liquid chromatography. Journal of Chromatography A. 2011;1218(39):6930-42.
88. Gidley MJ, Hanashiro I, Hani NM, Hill SE, Huber A, Jane J-L, Liu Q, Morris GA, Rolland-Sabaté A, Striegel AM, Gilbert RG. Reliable measurements of the size distributions of starch molecules in solution: Current dilemmas and recommendations. Carbohydrate Polymers. 2010;79(2):255-61.
89. Hanashiro I, Tagawa M, Shibahara S, Iwata K, Takeda Y. Examination of molar-based distribution of A, B and C chains of amylopectin by fluorescent labeling with 2-aminopyridine. Carbohydrate Research. 2002;337(13):1211-5.
90. Gaborieau M, Castignolles P. Size-exclusion chromatography (SEC) of branched polymers and polysaccharides. Analytical and Bioanalytical Chemistry. 2011;399(4):1413-23.
91. Berek D. Size exclusion chromatography – A blessing and a curse of science and technology of synthetic polymers. Journal of Separation Science. 2010;33(3):315-35.
92. Wong K-S, Jane J-L. Chapter 12 Starch chain length analysis by using an anion-exchange chromatography system equipped with an enzyme reactor and a PAD detector. In: Rassi ZE, editor. Journal of Chromatography Library. 66: Elsevier; 2002. p. 403-22.
93. Suortti T, Gorenstein MV, Roger P. Determination of the molecular mass of amylose. Journal of Chromatography A. 1998;828(1–2):515-21.
94. Charoenkul N, Uttapap D, Pathipanawat W, Takeda Y. Simultaneous determination of amylose content & unit chain distribution of amylopectins of cassava starches by fluorescent labeling/HPSEC. Carbohydrate Polymers. 2006;65(1):102-8.
95. Grant LA, Ostenson AM, Rayas-Duarte P. Determination of amylose and amylopectin of wheat starch using high performance size-exclusion chromatography (HPSEC). Cereal Chemistry. 2002;79(6):771-3.
96. Kobayashi S, Schwartz SJ, Lineback DR. Rapid analysis of starch, amylose and amylopectin by high-performance size-exclusion chromatography. Journal of Chromatography A. 1985;319:205-14.
97. Suortti T, Pessa E. Gel permeation chromatographic determination of starches using alkaline eluents. Journal of Chromatography A. 1991;536:251-4.
98. Roger P, Baud B, Colonna P. Characterization of starch polysaccharides by flow field-flow fractionation–multi-angle laser light scattering–differential refractometer index. Journal of Chromatography A. 2001;917(1–2):179-85.
99. Nilsson L. Starch and other polysaccharides. In: Williams RSK, Caldwell DK, editors. Field-Flow Fractionation in Biopolymer Analysis. Vienna: Springer; 2012. p. 165-85.
100. Wahlund K-G, Leeman M, Santacruz S. Size separations of starch of different botanical origin studied by asymmetrical-flow field-flow fractionation and multiangle light scattering. Analytical and Bioanalytical Chemistry. 2011;399(4):1455-65.
101. Foret F, Krivankova L, Bocek P. Capillary zone electrophoresis. Weinheim and New York: VCH; 1993.
102. Toutounji MR, Van Leeuwen MP, Oliver JD, Shrestha AK, Castignolles P, Gaborieau M. Quantification of sugars in breakfast cereals using capillary electrophoresis. Carbohydrate Research. 2015;408:134-41.

103. Kalsoom U, Guijt RM, Boyce MC, Townsend AT, Haselberg R, Breadmore MC. Direct electrokinetic injection of inorganic cations from whole fruits and vegetables for capillary electrophoresis analysis. Journal of Chromatography A. 2016;1428:346-51.
104. Thevarajah JJ, Gaborieau M, Castignolles P. Separation and Characterization of Synthetic Polyelectrolytes and Polysaccharides with Capillary Electrophoresis. Advances in Chemistry. 2014;2014:Article ID 798503.
105. Oliver JD, Sutton AT, Karu N, Phillips M, Markham J, Peiris P, Hilder EF, Castignolles P. Simple and robust monitoring of ethanol fermentations by capillary electrophoresis. Biotechnology and Applied Biochemistry. 2015;62(3):329-42.
106. Bosserhoff A, Hellerbrand C. Chapter 5 - Capillary Electrophoresis. In: Patrinos GP, Ansorge WJ, editors. Molecular Diagnostics (Second Edition). San Diego: Academic Press; 2010. p. 59-73.
107. Zhang Z, Zhang F, Liu Y. Recent Advances in Enhancing the Sensitivity and Resolution of Capillary Electrophoresis. Journal of Chromatographic Science. 2013;51(7):666-83.
108. Breadmore MC, Tubaon RM, Shallan AI, Phung SC, Abdul Keyon AS, Gstoettenmayr D, Prapatpong P, Alhusban AA, Ranjbar L, See HH, Dawod M, Quirino JP. Recent advances in enhancing the sensitivity of electrophoresis and electrochromatography in capillaries and microchips (2012-2014). Electrophoresis. 2015;36(1):36-61.
109. Herrero-Martínez JM, Schoenmakers PJ, Kok WT. Determination of the amylose–amylopectin ratio of starches by iodine-affinity capillary electrophoresis. Journal of Chromatography A. 2004;1053(1–2):227-34.
110. Van Leeuwen MP. Relating starch structure in breakfast cereals and rice to digestibility [Master of Science (Honours) Medicine]. Parramatta, Australia: Western Sydney University; 2016.
111. Stellwagen NC, Gelfi C, Righetti PG. The free solution mobility of DNA. Biopolymers. 1997;42(6):687-703.
112. Cottet H, Gareil P, Theodoly O, Williams CE. A semi-empirical approach to the modeling of the electrophoretic mobility in free solution: application to polystyrenesulfonates of various sulfonation rates. Electrophoresis. 2000;21(17):3529-40.
113. Gaborieau M, Causon TJ, Guillaneuf Y, Hilder EF, Castignolles P. Molecular weight and tacticity of oligoacrylates by capillary electrophoresis–mass spectrometry. Australian Journal of Chemistry. 2010;63(8):1219-26.
114. Maniego AR, Ang D, Guillaneuf Y, Lefay C, Gigmes D, Aldrich-Wright JR, Gaborieau M, Castignolles P. Separation of poly(acrylic acid) salts according to topology using capillary electrophoresis in the critical conditions. Analytical and Bioanalytical Chemistry. 2013;405(28):9009-20.
115. Gilbert RG, Hess M, Jenkins AL, Jones GR, Kratochvil P, Stepto RFT. Dispersity in Polymer Science. Pure and Applied Chemistry. 2009;81(2):351-3.
116. Thevarajah JJ, Sutton AT, Maniego AR, Whitty EG, Cottet H, Castignolles P, Gaborieau M. Quantifying the heterogeneity of chemical structures in complex charged polymers through the dispersity of their distributions of electrophoretic mobilities or of compositions. Analytical chemistry. 2016;88(3):1674-81.
117. Waigh TA, Kato KL, Donald AM, Gidley MJ, Clarke CJ, Riekel C. Side-chain liquid-crystalline model for starch. Starch - Stärke. 2000;52(12):450-60.
118. Tan I, Flanagan BM, Halley PJ, Whittaker AK, Gidley MJ. A Method for Estimating the Nature and Relative Proportions of Amorphous, Single, and Double-Helical Components in Starch Granules by 13C CP/MAS NMR. Biomacromolecules. 2007;8(3):885-91.
119. Spiess HW. Interplay of Structure and Dynamics in Macromolecular and Supramolecular Systems. Macromolecules. 2010;43(13):5479-91.
120. Zhu F. NMR spectroscopy of starch systems. Food Hydrocolloids. 2017;63:611-24.
121. Claridge TDW. Chapter 1 - Introduction. In: High-Resolution NMR Techniques in Organic Chemistry: Elsevier; 2009. p. 1-10.
122. Schmidt-Rohr K, Spiess HW. Chapter Three - High-Resolution NMR Techniques for Solids. In: Multidimensional Solid-State NMR and Polymers. San Diego: Academic Press; 1994. p. 69-134.

123. Claridge TDW. Chapter 2 - Introducing high-resolution NMR. In: High-Resolution NMR Techniques in Organic Chemistry: Elsevier; 2009. p. 11-34.
124. Carr HY, Purcell EM. Effects of Diffusion on Free Precession in Nuclear Magnetic Resonance Experiments. Physical Review. 1954;94(3):630-8.
125. Meiboom S, Gill D. Modified Spin-Echo Method for Measuring Nuclear Relaxation Times. Review of Scientific Instruments. 1958;29(8):688-91.
126. Andrew ER. Magic Angle Spinning. In: Encyclopedia of Magnetic Resonance: John Wiley & Sons, Ltd; 2007.
127. Bruker. Very High Speed MAS.; Accessed: 03/08/2016. Available: https://www.bruker.com/products/mr/nmr/probes/probes/solids/very-fast-mas/07-mm/overview.html.
128. Gaborieau M. Solid-state NMR investigation of spatial and dynamic heterogeneity in acrylic pressure sensitive adhesives (PSAs) compared to model poly(n-alkyl acrylates) and poly(n-alkyl methacrylates) [PhD thesis]. Strasbourg, France: University Louis Pasteur; 2005.
129. Gidley MJ, Bociek SM. Molecular organisation in starches: a 13C CP/MAS NMR study. Journal of the American Chemistry Society. 1985;107:7040-4.
130. Flanagan BM, Gidley MJ, Warren FJ. Rapid quantification of starch molecular order through multivariate modelling of 13C CP/MAS NMR spectra. Chemical Communications. 2015;51(80):14856-8.
131. Lopez-Rubio A, Flanagan BM, Gilbert EP, Gidley MJ. A novel approach for calculating starch crystallinity and its correlation with double helix content: A combined XRD and NMR study. Biopolymers. 2008;89(9):761-8.
132. Farhat IA. Applications of NMR in the Studies of Starch Systems. In: Webb GA, editor. Modern Magnetic Resonance. Dordrecht: Springer Netherlands; 2006. p. 1899-907.
133. Gidley MJ. Quantification of the structural features of starch polysaccharides by n.m.r. spectroscopy. Carbohydrate Research. 1985;139(0):85-93.
134. Morrison WR, Law RV, Snape CE. Evidence for inclusion complexes of lipids with v-amylose in maize, rice and oat starches. Journal of Cereal Science. 1993;18(2):107-9.
135. Stanjek H, Häusler W. Basics of X-ray Diffraction. Hyperfine Interactions. 2004;154(1-4):107-19.
136. Ji Y, Zhu K, Zhou H, Qian H. Study of the retrogradation behaviour of rice cake using rapid visco analyser, Fourier transform infrared spectroscopy and X-ray analysis. International Journal of Food Science & Technology. 2010;45(5):871-6.
137. Lionetto F, Maffezzoli A, Ottenhof M-A, Farhat IA, Mitchell JR. The Retrogradation of Concentrated Wheat Starch Systems. Starch - Stärke. 2005;57(1):16-24.
138. Shrestha AK, Blazek J, Flanagan BM, Dhital S, Larroque O, Morell MK, Gilbert EP, Gidley MJ. Molecular, mesoscopic and microscopic structure evolution during amylase digestion of maize starch granules. Carbohydrate Polymers. 2012;90(1):23-33.
139. Shrestha AK, Ng CS, Lopez-Rubio A, Blazek J, Gilbert EP, Gidley MJ. Enzyme resistance and structural organization in extruded high amylose maize starch. Carbohydrate Polymers. 2010;80(3):699-710.
140. Purohit SR, Rao PS. Optimization of paddy parboiling process for higher starch crystallinity by response surface methodology. International Journal of Biological Macromolecules. 2017;104(Part A):1091-8.
141. Wang S, Zhang X, Wang S, Copeland L. Changes of multi-scale structure during mimicked DSC heating reveal the nature of starch gelatinization. Scientific Reports. 2016;6:28271.
142. Nara S, Mori A, Komiya T. Study on relative crystallinity of moist potato starch. Starch - Stärke. 1978;30(4):111-4.
143. Chung H-J, Liu Q, Lee L, Wei D. Relationship between the structure, physicochemical properties and in vitro digestibility of rice starches with different amylose contents. Food Hydrocolloids. 2011;25(5):968-75.

144. Warren FJ, Gidley MJ, Flanagan BM. Infrared spectroscopy as a tool to characterise starch ordered structure—a joint FTIR–ATR, NMR, XRD and DSC study. Carbohydrate Polymers. 2016;139:35-42.
145. Teng A, Witt T, Wang K, Li M, Hasjim J. Molecular rearrangement of waxy and normal maize starch granules during in vitro digestion. Carbohydrate Polymers. 2016;139:10-9.
146. Cardoso MB, Westfahl H. On the lamellar width distributions of starch. Carbohydrate Polymers. 2010;81(1):21-8.
147. Zhang B, Chen L, Li X, Li L, Zhang H. Understanding the multi-scale structure and functional properties of starch modulated by glow-plasma: A structure-functionality relationship. Food Hydrocolloids. 2015;50:228-36.
148. Blazek J, Gilbert EP. Application of small-angle X-ray and neutron scattering techniques to the characterisation of starch structure: A review. Carbohydrate Polymers. 2011;85(2):281-93.
149. Cameron RE, Donald AM. A small-angle X-ray scattering study of the annealing and gelatinization of starch. Polymer. 1992;33(12):2628-35.
150. Waigh TA, Jenkins PJ, Donald AM. Quantification of water in carbohydrate lamellae using SANS. Faraday Discussions. 1996;103:325-37.
151. Witt T, Doutch J, Gilbert EP, Gilbert RG. Relations between Molecular, Crystalline, and Lamellar Structures of Amylopectin. Biomacromolecules. 2012;13(12):4273-82.
152. Wang H, Liu Y, Chen L, Li X, Wang J, Xie F. Insights into the multi-scale structure and digestibility of heat-moisture treated rice starch. Food Chemistry. 2018;242(Supplement C):323-9.
153. Daniels DR, Donald AM. Soft Material Characterization of the Lamellar Properties of Starch: Smectic Side-Chain Liquid-Crystalline Polymeric Approach. Macromolecules. 2004;37(4):1312-8.
154. Agamalyan MM, Evmenenko GA, Vilesov AD, Frenkel SY, Zgonnik VN, Vinogradova LV, Melenevskaya EY. Small-angle neutron diffraction study of block copolymer superstructure. Polymer. 1992;33(12):2542-7.
155. Schmidt-Rohr K. Simulation of small-angle scattering curves by numerical Fourier transformation. Journal of Applied Crystallography. 2007;40(1):16-25.
156. Verma R, Marand H, Hsiao B. Morphological changes during secondary crystallization and subsequent melting in poly(ether ether ketone) as studied by real time small angle X-ray scattering. Macromolecules. 1996;29(24):7767-75.
157. Vonk C. Investigation of non-ideal two-phase polymer structures by small-angle X-ray scattering. Journal of Applied Crystallography. 1973;6(2):81-6.
158. Wang Z-G, Hsiao BS, Murthy NS. Comparison of intensity profile analysis and correlation function methods for studying the lamellar structures of semi-crystalline polymers using small-angle X-ray scattering. Journal of Applied Crystallography. 2000;33(3 Part 1):690-4.
159. Yuryev VP, Krivandin AV, Kiseleva VI, Wasserman LA, Genkina NK, Fornal J, Blaszczak W, Schiraldi A. Structural parameters of amylopectin clusters and semi-crystalline growth rings in wheat starches with different amylose content. Carbohydrate Research. 2004;339(16):2683-91.
160. Chanvrier H, Uthayakumaran S, Appelqvist IA, Gidley MJ, Gilbert EP, Lopez-Rubio A. Influence of storage conditions on the structure, thermal behavior, and formation of enzyme-resistant starch in extruded starches. Journal of Agricultural and Food Chemistry. 2007;55(24):9883-90.
161. Lopez-Rubio A, Flanagan BM, Shrestha AK, Gidley MJ, Gilbert EP. Molecular rearrangement of starch during in vitro digestion: Toward a better understanding of enzyme resistant starch formation in processed starches. Biomacromolecules. 2008;9(7):1951-8.
162. Zhang B, Xie F, Wang DK, Zhao S, Niu M, Qiao D, Xiong S, Jiang F, Zhu J, Yu L. An improved approach for evaluating the semicrystalline lamellae of starch granules by synchrotron SAXS. Carbohydrate Polymers. 2017;158:29-36.
163. Donald AM, Kato KL, Perry PA, Waigh TA. Scattering Studies of the Internal Structure of Starch Granules. Starch - Stärke. 2001;53(10):504-12.
164. Blanshard JMV, Bates DR, Muhr AH, Worcester DL, Higgins JS. Small-angle neutron scattering studies of starch granule structure. Carbohydrate Polymers. 1984;4(6):427-42.

165. Perry PA, Donald AM. SANS study of the distribution of water within starch granules. International Journal of Biological Macromolecules. 2000;28(1):31-9.
166. Doutch J, Bason M, Franceschini F, James K, Clowes D, Gilbert EP. Structural changes during starch pasting using simultaneous Rapid Visco Analysis and small-angle neutron scattering. Carbohydrate Polymers. 2012;88(3):1061-71.
167. Brewster JD, Fishman ML. Capillary electrophoresis of plant starches as the iodine complexes. Journal of Chromatography A. 1995;693(2):382-7.
168. Tang HR, Brun A, Hills B. A proton NMR relaxation study of the gelatinisation and acid hydrolysis of native potato starch. Carbohydrate Polymers. 2001;46(1):7-18.
169. Thevarajah JJ, Van Leeuwen MP, Cottet H, Castignolles P, Gaborieau M. Determination of the distributions of the degrees of acetylation of chitosan. International Journal of Biological Macromolecules. 2017;95:40-8.
170. Toutounji MR, Butardo VM, Zou W, Farahnaky A, Pallas L, Oli P, Blanchard CL. A High-Throughput In Vitro Assay for Screening Rice Starch Digestibility. Foods. 2019;8(12):601.
171. Ayres NM, McClung AM, Larkin PD, Bligh HFJ, Jones CA, Park WD. Microsatellites and a single-nucleotide polymorphism differentiate apparentamylose classes in an extended pedigree of US rice germ plasm. Theoretical and Applied Genetics. 1997;94(6):773-81.
172. Krishnan P, Ramakrishnan B, Reddy KR, Reddy VR. Chapter three - High-Temperature Effects on Rice Growth, Yield, and Grain Quality. In: Sparks DL, editor. Advances in Agronomy. 111: Academic Press; 2011. p. 87-206.
173. Pallas L. Rice Processing: Beyond the Farm Gate. In: Reference Module in Food Science: Elsevier; 2016.
174. Perez S, Bertoft E. The molecular structures of starch components and their contribution to the architecture of starch granules: A comprehensive review. Starch-Starke. 2010;62(8):389-420.
175. De Bruyn H, Sprong E, Gaborieau M, David G, Roper III JA, Gilbert RG. Starch-graft-copolymer latexes initiated and stabilized by ozonolyzed amylopectin. Journal of Polymer Science Part A Polymer Chemistry. 2006;44(20):5832-45.
176. AACCI. Approved Methods of Analysis 11th ed. Amylose Content of Milled Rice Method 61-0301. St. Paul, MN, U.S.A.: AACC International; 2011.
177. Gartner C, López BL, Sierra L, Graf R, Spiess HW, Gaborieau M. Interplay between Structure and Dynamics in Chitosan Films Investigated with Solid-State NMR, Dynamic Mechanical Analysis, and X-ray Diffraction. Biomacromolecules. 2011;12(4):1380-6.
178. Usui T, Yokoyama M, Yamaoka N, Matsuda K, Tuzimura K, Sugiyama H, Seto S. Proton magnetic-resonance spectra of d-gluco-oligosaccharides and d-glucans. Carbohydrate Research. 1974;33(1):105-16.
179. Gaborieau M, De Bruyn H, Mange S, Castignolles P, Brockmeyer A, Gilbert RG. Synthesis and characterization of synthetic polymer colloids colloidally stabilized by cationized starch oligomers. Journal of Polymer Science Part A: Polymer Chemistry. 2009;47(7):1836-52.
180. Hernández JM, Gaborieau M, Castignolles P, Gidley MJ, Myers AM, Gilbert RG. Mechanistic Investigation of a Starch-Branching Enzyme Using Hydrodynamic Volume SEC Analysis. Biomacromolecules. 2008;9(3):954-65.
181. Castro JV, Ward RM, Gilbert RG, Fitzgerald MA. Measurement of the molecular weight distribution of debranched starch. Biomacromolecules. 2005;6(4):2260-70.
182. Koch K, Andersson R, Aman P. Quantitative analysis of amylopectin unit chains by means of high-performance anion-exchange chromatography with pulsed amperometric detection. Journal of Chromatography A. 1998;800(2):199-206.
183. Kazarian AA, Smith JA, Hilder EF, Breadmore MC, Quirino JP, Suttil J. Development of a novel fluorescent tag O-2- aminoethyl fluorescein for the electrophoretic separation of oligosaccharides. Analytica Chimica Acta. 2010;662(2):206-13.
184. van Soest JJG, Tournois H, de Wit D, Vliegenthart JFG. Short-range structure in (partially) crystalline potato starch determined with attenuated total reflectance Fourier-transform IR spectroscopy. Carbohydrate Research. 1995;279:201-14.

185. Capron I, Robert P, Colonna P, Brogly M, Planchot V. Starch in rubbery and glassy states by FTIR spectroscopy. Carbohydrate Polymers. 2007;68(2):249-59.
186. Liu F, Romanova N, Lee Elizabeth A, Ahmed R, Evans M, Gilbert Elliot P, Morell Matthew K, Emes Michael J, Tetlow Ian J. Glucan affinity of starch synthase IIa determines binding of starch synthase I and starch-branching enzyme IIb to starch granules. Biochemical Journal. 2012;448(3):373.
187. Aravind N, Sissons M, Fellows CM, Blazek J, Gilbert EP. Optimisation of resistant starch II and III levels in durum wheat pasta to reduce in vitro digestibility while maintaining processing and sensory characteristics. Food Chemistry. 2013;136(2):1100-9.
188. Salman H, Blazek J, Lopez-Rubio A, Gilbert EP, Hanley T, Copeland L. Structure–function relationships in A and B granules from wheat starches of similar amylose content. Carbohydrate Polymers. 2009;75(3):420-7.
189. Vermeylen R, Goderis B, Reynaers H, Delcour JA. Gelatinisation related structural aspects of small and large wheat starch granules. Carbohydrate Polymers. 2005;62(2):170-81.
190. Bayer RK, Baltá-Calleja FJ. Nanostructure of Potato Starch, Part I: Early Stages of Retrogradation of Amorphous Starch in Humid Atmosphere as Revealed by Simultaneous SAXS and WAXS. International Journal of Polymeric Materials and Polymeric Biomaterials. 2006;55(10):773-88.
191. Vermeylen R, Goderis B, Delcour JA. An X-ray study of hydrothermally treated potato starch. Carbohydrate Polymers. 2006;64(2):364-75.
192. Tyburn J-M. Variable temperature unit user manual version 001. Wissembourg, France: Bruker; 1998. Report No.: DWG-Nr: Drw / 1185001 Z31482.
193. Hoffman RE. Standardization of chemical shifts of TMS and solvent signals in NMR solvents. Magnetic Resonance in Chemistry. 2006;44(6):606-16.
194. Manelius R, Maaheimo H, Nurmi K, Bertoft E. Characterisation of Fractions Obtained by Isoamylolysis and Ion-exchange Chromatography of Cationic Waxy Maize Starch. Starch - Stärke. 2002;54(2):58-65.
195. Nilsson GS, Gorton L, Bergquist K-E, Nilsson U. Determination of the Degree of Branching in Normal and Amylopectin Type Potato Starch with 1H-NMR Spectroscopy Improved resolution and two-dimensional spectroscopy. Starch - Stärke. 1996;48(10):352-7.
196. Petoukhov MV, Franke D, Shkumatov AV, Tria G, Kikhney AG, Gajda M, Gorba C, Mertens HDT, Konarev PV, Svergun DI. New developments in the ATSAS program package for small-angle scattering data analysis. Journal of Applied Crystallography. 2012;45(2):342-50.
197. WaveMetrics Inc. Igor Pro 6.37. 6.3.7.2 ed. Lake Oswego, OR, USA.
198. Kline S. Reduction and analysis of SANS and USANS data using IGOR Pro. Journal of Applied Crystallography. 2006;39(6):895-900.
199. Striegel A. Advances in the understanding of the dissolution mechanism of cellulose in DMAc/LiCl. Journal of The Chilean Chemical Society - J CHIL CHEM SOC. 2003;48.
200. Singh J, McCarthy OJ, Singh H. Physico-chemical and morphological characteristics of New Zealand Taewa (Maori potato) starches. Carbohydrate Polymers. 2006;64(4):569-81.
201. Castignolles P, Graf R, Parkinson M, Wilhelm M, Gaborieau M. Detection and quantification of branching in polyacrylates by size-exclusion chromatography (SEC) and melt-state 13C NMR spectroscopy. Polymer. 2009;50(11):2373-83.
202. Maniego AR, Sutton AT, Gaborieau M, Castignolles P. Assessment of the Branching Quantification in Poly(acrylic acid): Is It as Easy as It Seems? Macromolecules. 2017;50(22):9032-41.
203. Thevarajah JJ, Bulanadi JC, Wagner M, Gaborieau M, Castignolles P. Towards a less biased dissolution of chitosan. Analytica Chimica Acta. 2016;935:258-68.
204. The International Organization for Standardization. Rice - Determination of amylose content - Part 1: Reference Method ISO 6647-1:2015. The International Organization for Standardization; 2015.
205. Hirano HY, Eiguchi M, Sano Y. A single base change altered the regulation of the Waxy gene at the posttranscriptional level during the domestication of rice. Molecular Biology and Evolution. 1998;15(8):978-87.

206. Larkin PD, Park WD. Transcript accumulation and utilization of alternate and non-consensus splice sites in rice granule-bound starch synthase are temperature-sensitive and controlled by a single-nucleotide polymorphism. Plant molecular biology. 1999;40(4):719-27.
207. Chen M-H, Bergman C, Pinson S, Fjellstrom R. Waxy gene haplotypes: Associations with apparent amylose content and the effect by the environment in an international rice germplasm collection. Journal of Cereal Science. 2008;47(3):536-45.
208. Sano Y, Hirano HY, Nishimura M. Evolutionary significance of differential regulation at the wx locus of rice. In: Rice Genetics II. Rice Genetics Collection. Volume 2: World Scientific Publishing Company; 2008. p. 11-20.
209. Wang TL, Bogracheva TY, Hedley CL. Review article. Starch: as simple as A, B, C? Journal of Experimental Botany. 1998;49(320):481-502.
210. Hermann TS, Harvey SR. Infrared spectroscopy at sub-ambient temperatures: I. Literature review. Applied Spectroscopy. 1969;23(5):435-50.
211. Tyburn J-M. Variable temperature unit user manual version 001. Bruker, editor. Wissembourg (France): Bruker; 1998. 37 (97) p.
212. Elfstrand L, Frigård T, Andersson R, Eliasson A-C, Jönsson M, Reslow M, Wahlgren M. Recrystallisation behaviour of native and processed waxy maize starch in relation to the molecular characteristics. Carbohydrate Polymers. 2004;57(4):389-400.
213. Dunn Jr. LB, Krueger WJ. Branching ratios of starch via proton nuclear magnetic resonance and their use in determining amylose/amylopectin content: Evidence for three types of amylopectin. Macromolecular Symposia. 1999;140(1):179-86.
214. McIntyre DD, Ho C, Vogel HJ. One-Dimensional Nuclear Magnetic Resonance Studies of Starch and Starch Products. Starch - Stärke. 1990;42(7):260-7.
215. Greenspan L. Humidity fixed points of binary saturated aqueous solutions. Journal of Research of the National Bureau of Standards - A Physics and Chemistry. 1977;81A(1):89-96.
216. Bruker Optik GmbH. Opus 7.5. 7.5 ed. Rudolf-Plank-Straße, Ettlingen, Germany.
217. Caspary R. Infrared spectroscopy at low temperature for the improved resolution of spectra. Applied Spectroscopy. 1968;22(6):694-6.
218. Stuart B. Infrared Spectroscopy : Fundamentals and Applications. Hoboken, NJ, USA: Wiley; 2004.
219. Holland-moritz K, Siesler HW. Infrared spectroscopy of polymers. Applied Spectroscopy Reviews. 1976;11(1):1-55.
220. Hermann TS, Harvey SR, Honts CN. Infrared spectroscopy at sub-ambient temperatures: II. Pure molecules. Applied Spectroscopy. 1969;23(5):451-60.
221. Li H, Qi Y, Zhao Y, Chi J, Cheng S. Starch and its derivatives for paper coatings: A review. Progress in Organic Coatings. 2019;135:213-27.
222. Avérous L, Halley PJ. Chapter 1 - Starch Polymers: From the Field to Industrial Products. In: Avérous L, Halley PJ, editors. Starch Polymers. Amsterdam: Elsevier; 2014. p. 3-10.
223. Zhong F, Yokoyama W, Wang Q, Shoemaker CF. Rice starch, amylopectin, and amylose: Molecular weight and solubility in dimethyl sulfoxide-based solvents. Journal of Agricultural and Food Chemistry. 2006;54(6):2320-6.
224. Leloup VM, Colonna P, Buleon A. Influence of amylose-amylopectin ratio on gel properties. Journal of Cereal Science. 1991;13(1):1-13.
225. Ong MH, Blanshard JMV. Texture determinants in cooked, parboiled rice. I: Rice starch amylose and the fine stucture of amylopectin. Journal of Cereal Science. 1995;21(3):251-60.
226. Matsunaga K, Kawasaki S, Takeda Y. Influence of physicochemical properties of starch on crispness of tempura fried batter. Cereal Chemistry. 2003;80(3):339-45.
227. Copeland L, Blazek J, Salman H, Tang MC. Form and functionality of starch. Food Hydrocolloids. 2009;23(6):1527-34.
228. Mahmood T, Turner MA, Stoddard FL. Comparison of Methods for Colorimetric Amylose Determination in Cereal Grains. Starch - Stärke. 2007;59(8):357-65.

229. Takeda Y, Hizukuri S, Juliano BO. Structures of rice amylopectins with low and high affinities for iodine. Carbohydrate Research. 1987;168(1):79-88.
230. Striegel AM, Kirkland JJ, Yau WW, Bly DD. 7.11.2 Sample Solution Filtration. In: Modern Size Exclusion Chromatography. 2nd ed. Hoboken: Wiley; 2009. p. 185-6.
231. Chen Y, Fringant C, Rinaudo M. Molecular characterization of starch by SEC: dependance of the performances on the amylopectin content. Carbohydrate Polymers. 1997;33(1):73-8.
232. You S, Stevenson SG, Izydorczyk MS, Preston KR. Separation and Characterization of Barley Starch Polymers by a Flow Field-Flow Fractionation Technique in Combination with Multiangle Light Scattering and Differential Refractive Index Detection. Cereal Chemistry. 2002;79(5):624-30.
233. Castignolles P, Gaborieau M, Hilder EF, Sprong E, Ferguson CJ, Gilbert RG. High-resolution separation of oligo(acrylic acid) by capillary zone electrophoresis. Macromolecular Rapid Communications. 2006;27(1):42-6.
234. Sutton AT, Arrua RD, Gaborieau M, Castignolles P, Hilder EF. Characterization of oligo(acrylic acid)s and their block co-oligomers. Analytica Chimica Acta. 2018;1032:163-77.
235. de Gennes P-G. Scaling Concepts in Polymer Physics. 1st ed. Ithaca, United States: Cornell University Press; 1979 30 November 1979. 319 p.
236. Taylor DL, Ferris CJ, Maniego AR, Castignolles P, in het Panhuis M, Gaborieau M. Characterization of Gellan Gum by Capillary Electrophoresis. Australian Journal of Chemistry. 2012;65(8):1156-64.
237. Aust N, Parth M, Lederer K. SEC of ultra-high molar mass polymers: Optimization of experimental conditions to avoid molecular degradation in the case of narrow polystyrene standards. International Journal of Polymer Analysis and Characterization. 2001;6(3-4):245-60.
238. Han J-A, Lim S-T. Structural changes of corn starches by heating and stirring in DMSO measured by SEC-MALLS-RI system. Carbohydrate Polymers. 2004;55(3):265-72.
239. Camilleri P. History and Development of Capillary Electrophoresis. In: Camilleri P, editor. Capillary Electrophoresis: Theory and Practice. 2nd ed: CRC Press; 2005. p. 1-22.
240. Cherney LT, Petrov AP, Krylov SN. One-dimensional approach to study kinetics of reversible binding of protein on capillary walls. Analytical chemistry. 2015;87(2):1219-25.
241. Pei L, Lucy CA. Insight into the stability of poly(diallydimethylammoniumchloride) and polybrene poly cationic coatings in capillary electrophoresis. Journal of Chromatography A. 2014;1365:226-33.
242. Pei L, Lucy CA. Polymerized phospholipid bilayers as permanent coatings for small amine separations using mixed aqueous/organic capillary zone electrophoresis. Journal of Chromatography A. 2012;1267:80-8.
243. Sutton AT, Read E, Maniego AR, Thevarajah JJ, Marty J-D, Destarac M, Gaborieau M, Castignolles P. Purity of double hydrophilic block copolymers revealed by capillary electrophoresis in the critical conditions. Journal of Chromatography A. 2014;1372:187-95.
244. Le Saux T, Cottet H. Size-based characterization by the coupling of capillary electrophoresis to Taylor dispersion analysis. Analytical chemistry. 2008;80(5):1829-32.
245. Chamieh J, Martin M, Cottet H. Quantitative analysis in capillary electrophoresis: Transformation of raw electropherograms into continuous distributions. Analytical chemistry. 2015;87(2):1050-7.
246. Ludwig DS, Hu FB, Tappy L, Brand-Miller J. Dietary carbohydrates: role of quality and quantity in chronic disease. 2018;361:k2340.
247. James MG, Denyer K, Myers AM. Starch synthesis in the cereal endosperm. Current Opinion in Plant Biology. 2003;6(3):215-22.
248. Hirose T, Terao T. A comprehensive expression analysis of the starch synthase gene family in rice (Oryza sativa L.). Planta. 2004;220(1):9-16.
249. Fujita N, Yoshida M, Asakura N, Ohdan T, Miyao A, Hirochika H, Nakamura Y. Function and Characterization of Starch Synthase I Using Mutants in Rice. 2006;140(3):1070-84.
250. Smith AM, Denyer K, Martin C. The synthesis of the starch granule. Annual Review of Plant Physiology and Plant Molecular Biology. 1997;48(1):67-87.

251. Nakamura Y, Francisco PB, Hosaka Y, Sato A, Sawada T, Kubo A, Fujita N. Essential amino acids of starch synthase IIa differentiate amylopectin structure and starch quality between japonica and indica rice varieties. Plant molecular biology. 2005;58(2):213-27.
252. Flipse E, Keetels CJAM, Jacobsen E, Visser RGF. The dosage effect of the wildtype GBSS allele is linear for GBSS activity but not for amylose content: absence of amylose has a distinct influence on the physico-chemical properties of starch. Theoretical and Applied Genetics. 1996;92(1):121-7.
253. Martin C, Smith AM. Starch biosynthesis. The Plant Cell. 1995;7(7):971-85.
254. Denyer K, Barber LM, Burton R, Hedley CL, Hylton CM, Johnson S, Jones DA, Marshall J, Smith AM, Tatge H, Tomlinson K, Wang TL. The isolation and characterization of novel low-amylose mutants of Pisum sativum L. Plant, Cell and Environment. 1995;18(9):1019-26.
255. Nishi A, Nakamura Y, Tanaka N, Satoh H. Biochemical and genetic analysis of the effects of amylose-extender mutation in rice endosperm. Plant Physiology. 2001;127(2):459-72.
256. Liu F, Zhao Q, Mano N, Ahmed Z, Nitschke F, Cai Y, Chapman KD, Steup M, Tetlow IJ, Emes MJ. Modification of starch metabolism in transgenic Arabidopsis thaliana increases plant biomass and triples oilseed production. Plant Biotechnology Journal. 2016;14(3):976-85.
257. Burton RA, Bewley JD, Smith AM, Bhattacharyya MK, Tatge H, Ring S, Bull V, Hamilton WDO, Martin C. Starch branching enzymes belonging to distinct enzyme families are differentially expressed during pea embryo development. The Plant Journal. 1995;7(1):3-15.
258. Guan HP, Preiss J. Differentiation of the Properties of the Branching Isozymes from Maize (Zea mays). Plant Physiology. 1993;102(4):1269-73.
259. Takeda Y, Guan H-P, Preiss J. Branching of amylose by the branching isoenzymes of maize endosperm. Carbohydrate Research. 1993;240:253-63.
260. Bertoft E. Understanding Starch Structure: Recent Progress. Agronomy. 2017;7(3):56.
261. Ball S, Guan H-P, James M, Myers A, Keeling P, Mouille G, Buléon A, Colonna P, Preiss J. From Glycogen to Amylopectin: A Model for the Biogenesis of the Plant Starch Granule. Cell. 1996;86(3):349-52.
262. Tian Z, Qian Q, Liu Q, Yan M, Liu X, Yan C, Liu G, Gao Z, Tang S, Zeng D, Wang Y, Yu J, Gu M, Li J. Allelic diversities in rice starch biosynthesis lead to a diverse array of rice eating and cooking qualities. Proceedings of the National Academy of Sciences of the United States of America. 2009;106(51):21760-5.
263. He Y, Han Y, Jiang L, Xu C, Lu J, Xu M. Functional analysis of starch-synthesis genes in determining rice eating and cooking qualities. Molecular Breeding. 2006;18(4):277-90.
264. Liu H, Yu L, Xie F, Chen L. Gelatinization of cornstarch with different amylose/amylopectin content. Carbohydrate Polymers. 2006;65(3):357-63.
265. Rindlav-Westling Å, Stading M, Hermansson A-M, Gatenholm P. Structure, mechanical and barrier properties of amylose and amylopectin films. Carbohydrate Polymers. 1998;36(2–3):217-24.
266. Castro JV, Dumas C, Chiou H, Fitzgerald MA, Gilbert RG. Mechanistic information from analysis of molecular weight distributions of starch. Biomacromolecules. 2005;6(4):2248-59.
267. Schmid T, Himmelsbach M, Oliver JD, Gaborieau M, Castignolles P, Buchberger WW. Investigation of photochemical reaction products of glucose formed during direct UV detection in capillary electrophoresis. Journal of Chromatography A. 2015;1388:259-66.
268. Chiou H, Martin M, Fitzgerald M. Effect of Purification Methods on Rice Starch Structure. Starch - Stärke. 2002;54(9):415-20.
269. Arendt E, Zannini E. Rice. In: Cereal Grains for the Food and Beverage Industries. Volume 248. Cambridge, Sawston: Woodhead Publishing; 2013.
270. Snape CE, Morrison WR, Maroto-Valer MM, Karkalas J, Pethrick RA. Solid state ^{13}C NMR investigation of lipid ligands in V-amylose inclusion complexes. Carbohydrate Polymers. 1998;36(2–3):225-37.
271. Moulay S. Molecular iodine/polymer complexes. Journal of Polymer Engineering. 2013;33(5):389.

272. Ahn J, Chang T, Wang X, Limpouchová Z, Procházka K. Influence of the Chain Architecture and the Presence of End-Groups or Branching Units Chemically Different from Repeating Structural Units on the Critical Adsorption Point in Liquid Chromatography. Macromolecules. 2017;50(21):8720-30.
273. Gilbert RG, Gidley MJ, Hill S, Kilz P, Rolland-Sabaté A, Stevenson DG, Cave RA. Characterizing the size and molecular weight distribution of starch: Why it is important and why it is hard. Cereal Foods World. 2010;55(3):139-43.
274. Harrisson S. The downside of dispersity: why the standard deviation is a better measure of dispersion in precision polymerization. Polymer Chemistry. 2018;9(12):1366-70.
275. Takeda Y, Hizukuri S, Juliano BO. Purification and structure of amylose from rice starch. Carbohydrate Research. 1986;148(2):299-308.
276. Juliano BO. Structure chemistry and function of the rice grain and its fraction. Cereal Foods World. 1992;37:772-4.
277. Leclercq L, Saetear P, Rolland-Sabaté A, Biron J-P, Chamieh J, Cipelletti L, Bornhop DJ, Cottet H. Size-Based Characterization of Polysaccharides by Taylor Dispersion Analysis with Photochemical Oxidation or Backscattering Interferometry Detections. Macromolecules. 2019;52(12):4421-31.
278. Cameron RE, Donald AM. A small-angle x-ray scattering study of starch gelatinization in excess and limiting water. Journal of Polymer Science Part B: Polymer Physics. 1993;31(9):1197-203.
279. Cameron RE, Donald AM. A small-angle X-ray scattering study of the absorption of water into the starch granule. Carbohydrate Research. 1993;244(2):225-36.
280. Chang Y-H, Lin J-H. Effects of molecular size and structure of amylopectin on the retrogradation thermal properties of waxy rice and waxy cornstarches. Food Hydrocolloids. 2007;21(4):645-53.
281. Duer MJ. NMR Techniques for Studying Molecular Motion in Solids. In: Solid-State NMR Spectroscopy Principles and Applications 2002. p. 237-79.
282. Spiess HW. 50th Anniversary Perspective: The Importance of NMR Spectroscopy to Macromolecular Science. Macromolecules. 2017;50(5):1761-77.
283. Fattori J, Rodrigues FHS, Pontes JGM, Paula Espíndola A, Tasic L. Chapter 6 - Monitoring Intermolecular and Intramolecular Interactions by NMR Spectroscopy. In: ur-Rahman A, Choudhary MI, editors. Applications of NMR Spectroscopy: Volume 3: Bentham Science Publishers; 2015. p. 180-266.
284. McIntosh LP. CPMG. In: Roberts GCK, editor. Encyclopedia of Biophysics. Berlin, Heidelberg: Springer Berlin Heidelberg; 2013. p. 386.
285. Froix MF, Nelson R. The Interaction of Water with Cellulose from Nuclear Magnetic Resonance Relaxation Times. Macromolecules. 1975;8(6):726-30.
286. Garvey Christopher J, Parker Ian H, Simon George P, Whittaker Andrew K. The hydration of paper studied with solid-state magnetisation-exchange 1H NMR spectroscopy. Holzforschung2006. p. 409.
287. Collison R, McDonald M. Broadening of the Water Proton Line in High-Resolution Nuclear Magnetic Resonance Spectra of Starch Gels. Nature. 1960;186:548-9.
288. Jaska E. Starch Gelatinization as Detected by Proton Magentic Resonance. Cereal Chemistry. 1971;48(4):437-44.
289. Hennig HJ, Lechert H, Goemann W. Untersuchung des Quellverhaltens von Stärke mit Hilfe der Kernresonanz-Impuls-Spektroskopie (Examination of the Swelling Mechanism of Starch by Pulsed NMR-Method). Die Staerke - Starch. 1976;28(11):10-3.
290. Lechert H. Möglichkeiten und Grenzen der Kernresonanz-lmpuls-Spektroskopie in der Anwendung auf Probleme der Stärkeforschung und Stärketechnologie (Possibilities and Limits of Pulsed NMR Spectroscopy for the Investigation of Problems of Starch-Research and Starch Technology). Die Staerke - Starch. 1976;28(11):369-73.
291. Basler W, Lechert H. Kernresonanzuntersuchungen an Wasser in Staerkegelen bei 295 K (Wide-Line NMR of Water in Starch Gels at 295 K). Die Staerke - Starch. 1973;25(9):289-92.
292. Lelievre J, Mitchell JR. A Pulsed NMR Study of Some Aspects of Starch Gelatinization. Die Staerke - Starch. 1975;27(4):113-5.

293. Tang HR, Godward J, Hills B. The distribution of water in native starch granules—a multinuclear NMR study. Carbohydrate Polymers. 2000;43(4):375-87.
294. Ritota M, Gianferri R, Bucci R, Brosio E. Proton NMR relaxation study of swelling and gelatinisation process in rice starch–water samples. Food Chemistry. 2008;110(1):14-22.
295. Engelsen SB, Jensen MK, Pedersen HT, Nørgaard L, Munck L. NMR-baking and Multivariate Prediction of Instrumental Texture Parameters in Bread. Journal of Cereal Science. 2001;33(1):59-69.
296. Partanen R, Marie V, MacNaughtan W, Forssell P, Farhat I. 1H NMR study of amylose films plasticised by glycerol and water. Carbohydrate Polymers. 2004;56(2):147-55.
297. Hills BP, Godward J, Manning CE, Biechlin JL, Wright KM. Microstructural characterization of starch systems by NMR relaxation and q-space microscopy. Magnetic Resonance Imaging. 1998;16(5):557-64.
298. Hills BP, Le Floc'h G. NMR studies of non-freezing water in cellular plant tissue. Food Chemistry. 1994;51(3):331-6.
299. Flibotte S, Menon RS, MacKay AL, Hailey JRT. Proton magnetic resonance of western red cedar. Wood and Fiber Science. 1990;4:362-76.
300. Vodovotz Y, Vittadini E, Sachleben JR. Use of 1H cross-relaxation nuclear magnetic resonance spectroscopy to probe the changes in bread and its components during aging. Carbohydrate Research. 2002;337(2):147-53.
301. Teo CH, Seow CC. A Pulsed NMR Method for the Study of Starch Retrogradation. Starch - Stärke. 1992;44(8):288-92.
302. Berger A. Magnetic resonance imaging. BMJ. 2002;324(7328):35.
303. Takeuchi S, Maeda M, Gomi Y-i, Fukuoka M, Watanabe H. The change of moisture distribution in a rice grain during boiling as observed by NMR imaging. Journal of Food Engineering. 1997;33(3):281-97.
304. Stapley AGF, Hyde TM, Gladden LF, Fryer PJ. NMR imaging of the wheat grain cooking process. International Journal of Food Science & Technology. 1997;32(5):355-75.
305. Kratzer A, Handschin S, Lehmann V, Gross D, Escher F, Conde-Petit B. Hydration Dynamics of Durum Wheat Endosperm as Studied by Magnetic Resonance Imaging and Soaking Experiments. Cereal Chemistry. 2008;85(5):660-6.
306. Ali TS, Prasadam I, Xiao Y, Momot KI. Progression of Post-Traumatic Osteoarthritis in rat meniscectomy models: Comprehensive monitoring using MRI. Scientific Reports. 2018;8(1):6861.
307. Ali TS, Thibbotuwawa N, Gu Y, Momot KI. MRI magic-angle effect in femorotibial cartilages of the red kangaroo. Magnetic Resonance Imaging. 2017;43:66-73.
308. Ali TS, Tourell MC, Hugo HJ, Pyke C, Yang S, Lloyd T, Thompson EW, Momot KI. Transverse relaxation-based assessment of mammographic density and breast tissue composition by single-sided portable NMR. Magnetic Resonance in Medicine. 2019;82(3):1199-213.
309. McBrierty VJ, Keely CM, Coyle FM, Xu H, Vij JK. Hydration and plasticization effects in cellulose acetate: molecular motion and relaxation. Faraday Discussions. 1996;103(0):255-68.
310. Díez-Peña E, Quijada-Garrido I, Barrales-Rienda JM, Schnell I, Spiess HW. Advanced 1H Solid-State NMR Spectroscopy on Hydrogels, 1. Macromolecular Chemistry and Physics. 2004;205(4):430-7.
311. Dhital S, Dabit L, Zhang B, Flanagan B, Shrestha AK. In vitro digestibility and physicochemical properties of milled rice. Food Chemistry. 2015;172:757-65.
312. Waigh TA, Gidley MJ, Komanshek BU, Donald AM. The phase transformations in starch during gelatinisation: a liquid crystalline approach. Carbohydrate Research. 2000;328(2):165-76.
313. Mohorič A, Vergeldt F, Gerkema E, de Jager A, van Duynhoven J, van Dalen G, Van As H. Magnetic resonance imaging of single rice kernels during cooking. Journal of Magnetic Resonance. 2004;171(1):157-62.